Assessing the Osteology of *Notropis* (Cypriniformes: Leuciscidae)

by

Erika Kiel Jessen

A thesis submitted in partial fulfillment of the requirements for the degree of

Master of Science

in
Systematics and Evolution

Department of Biological Sciences
University of Alberta

Abstract

The genus *Notropis* (Cypriniformes: Leuciscidae) represents one of the largest genera of freshwater fishes in North America. The osteology of *Notropis* and closely associated genera including *Cyprinella*, *Luxilus* and *Lythrurus*, has been the subject of two primary areas of research. First is research examining a specific region of the skeleton including, but not limited to, the cranium, pharyngeal teeth and dental formulae, and the caudal skeleton. Second is research examining and comparing osteological characters to determine the evolutionary relationship within and between *Notropis* and its allies, sometimes termed 'notropin fishes'. However, no research has been done to assess the osteological variation of a single *Notropis* species. Furthermore, no research has assessed and compared notropin osteology in the context of recent molecular phylogenies. Therefore, this thesis had two objectives: (1) describe and analyse the osteology of *Notropis hudsonius* within and between different populations, and (2) compare the osteology of 11 different *Notropis* species, which according to recent molecular studies represent four subgenera as well as two species of unclear placement. In the first part of this thesis, I describe the osteology of *N. hudsonius* and outline key osteological differences within and among 15 populations from Alberta, Northwest Territories, Manitoba and Ontario. Specific focus is placed on the elements of the oral jaws, suspensorium, opercular series, branchial apparatus, hyoid region, circumorbital series, pectoral girdle, pelvic girdle, caudal skeleton and skull. The second part of this thesis builds on my description of *N. hudsonius* and compares the osteological characteristics of *Notropis atherinoides*, *N. blennius*, *N. buchanani*, *N. dorsalis*, *N. heterodon*, *N. heterolepis*, *N. hudsonius*, *N percobromus*, *N. stramineus*, *N. texanus* and *N. volucellus*. According to recent molecular studies, nine of these species are classified in four subgenera while two (*N. dorsalis* and *N. heterolepis*) are of unclear placement. My analysis of the osteology of *N. hudsonius* reveals variation in all examined regions except the pelvic girdle. Regional differentiation between eastern and western populations is especially evident in the degree of fusion of the pectoral girdle, fusion of the parhypural and first hypural of the caudal skeleton, and shape of the urohyal. In comparing the osteology of 11 *Notropis* species, I found that interspecific differences are not usually restricted to specific subgenera. Some traits, such as those of the palatine and pharyngeal teeth, are reinterpreted as convergent rather than synapomorphic based on recent molecular phylogenies. These findings provide insight into the intraspecific variation of *N. hudsonius* and help reinterpret osteological traits in notropin evolution, distinguishing between synapomorphies and convergent traits.

Preface

This thesis is an original work by Erika Kiel Jessen. No part of this thesis has been previously published.

Acknowledgements

I am forever grateful to the many people who have substantially contributed to my thesis, education and continual development as a scientist.

1. Dr. Alison Murray for her support, patience and attentiveness as a supervisor and mentor.
2. Dr. Margaret Docker and Jesse Ogden for so generously loaning me specimens from the University of Manitoba's collections for this thesis.
3. Taia Wyenberg-Henzler for her help with navigating the challenges of R studio and PCA.
4. Dr. Mrinal Das for getting me engaged with the field of ichthyology
5. Dr. Corwin Sullivan for his insights and outsider's perspective on this thesis.
6. Dr. Robert Holmes for his kindness and input on my specimen drawings.
7. The faculty and staff at MacEwan University for providing be with the foundation to advance and succeed in graduate work.
8. The faculty and staff from the Department of Biological Sciences at the University of Alberta including Dr. Braden Barr, John Acorn, Christianne Nylund, Shelley Scott, Dr. Eva Koppelhus, Dr. Heather Proctor Dr. Mike Caldwell and many more.
9. My fellow graduate students including Meghan Dueck, Luke Nelson, Mark Powers, Colton Coppock, Annie McIntosh, Mori Chida, Jasdeep Kaur, Christiana Garros, Henry Sharpe, Brandon Theurer and many more.
10. My family for their love and support.

Table of Contents

List of Tables

List of Figures

List of Abbreviations

AAC	Anterior angle of fifth ceratobranchial
AAT	Anterior arm of the tripus
ACH	Anterior ceratohyal
ANL	Anterior limb of fifth ceratobranchial
ART	Anguloarticular
ASL	Ascending limb of fifth ceratobranchial
AWH	Anterior wing of hyomandibular
BB	Basibranchial
BHY	Basihyal
BHYP	Basihyal projection
BOC	Basioccipital
BOPA	Proatlas of basioccipital
BOPP	Pharyngeal process of basioccipital
BPT	Basipterygium
BSR	Branchiostegal rays
CBR	Ceratobranchial
CC	Compound centrum
CL	Cleithrum
CLA	Claustrum
CM	Coronomeckelian
COR	Coracoid
CSI	Cavum sinus impar
DE	Dentary
DS	Dermosphenoitc
EB	Epibranchial
ECPT	Ectopterygoid
ENPT	Endopterygoid
EP	Epural
EPO	Epiotic
EX	Exoccipital

FIII	Oculomotor foramen
FIV	Trochlear nerve
FV	Trigeminal foramen
FVS	Ophthalmic branch of trigeminal nerve
FVII	Facial foramen
FVIIS	Foramen of superficial branch of facial nerve
FX	Vagal foramen
FBON	Foramen for branch of orbitonasal vein
FIC	Foramen of internal carotid artery
FM	Foramen magnum
FR	Frontal
H	Hypural
HB	Hypobranchial
HHD	Dorsal hypohyal
HHV	Ventral hypohyal
HS	Hemal spine
HYO	Hyomandibular
HYP	Hypurapophysis
IC	Intercalarium
IHY	Interhyal
INT	Intercalar
IO	Infraorbital
IOC	Infraorbital canal
IOP	Interoperculum
ISC	Ischiac process of basipterygium
K	Kinethmoid
LA	lacrimal
LE	Lateral ethmoid
LP1	Lateral process, vertebrae 1
LP2	Lateral process vertebrae 2
LPP	Lateral process of the palatine

M	Mentomeckelian
MC	Mesocoracoid
ME	Mesethmoid portion of ethmoid block
MK	Meckel’s cartilage
MP	Masticatory plate of basioccipital
MPT	Metapterygoid
MX	Maxilla
N	Nasal
NA	Neural arch
NA2	Neural arch, vertebrae 2
NA3	Neural arch, vertebrae 3
NA4	Neural arch, vertebrae 4
NC	Neural complex
NS	Neural spine
NS4	Neural spine, vertebrae 4
OF	Olfactory foramen
OP	Operculum
OPM	Posterior myodome opening
ORS	Orbitosphenoid
OS	Os suspensorium
PA	Parietal
PAC	Posterior angle of fifth ceratobranchial
PAL	Palatine
PAT	Posterior arm of the tripus
PBR	Pharyngobranchial
PCH	Posterior ceratohyal
PCL	Postcleithrum
PDB	Predorsal bones
PE	Preethmoid
PH	Parhypural
PL	Pleurostyle

PLS	Pelvic splint
PMP	Premaxillary process of the maxilla
PMX	Premaxilla
POC	Postorbital commissure
POM	Preopercularmandibular canal
POP	Preoperculum
POPS	Postorbital process of the sphenotic
PRO	Prootic
PS	Parasphenoid
PTE	Pterotic
PTF	Posttemporal fossa
PTS	Pterosphenoid
PTT	Posttemporal
PU	Preural centrum
QA	Quadrate
R	Rib
RA	Retroarticular
RAD	Radial
RP	Rostral process of the maxilla
SC	Scaphium
SCL	Supracleithrum
SC	Scapula
SE	Supraethmoid portion of ethmoid block
SOB	Supraorbital
SOC	Supraoccipital
SO	Supraorbital canal
SOP	Suboperculum
SPH	Sphenotic
SS	Sphenotic spine
STC	Supratemporal canal
STF	Subtemporal fossa

SY	Symplectic
TR	Tripus
UN	Uroneural
VF	Ventral flange of fifth ceratobranchial
VO	Vomer

Chapter 1: Introduction

1.1 General Introduction

The teleost ostariophysan order Cypriniformes represents at least 489 genera and 4025 species of freshwater fishes native to Eurasia, Africa and North America (Nelson et al., 2016). As a member of series Otophysi, the Cypriniformes are characterized in part by their possession of a Weberian apparatus, a modification of the elements associated with four or five of the anteriormost vertebrae (Fink and Fink, 1981; Chardon and Vandewalle, 1996; Nelson et al., 2016). The Weberian apparatus functions by amplifying sound waves, enhancing the fish's hearing ability (Chardon and Vandewalle, 1996; Nelson et al., 2016), which has no doubt contributed to the evolutionary success and diversity of all four otophysan lineages, including Cypriniformes (Fink and Fink, 1981; Chardon and Vandewalle, 1996; Gidmark and Simons, 2014). Unlike other ostariophysans, cypriniforms lack an adipose fin (Nelson et al., 2016). They have scaleless heads and possess a kinethmoid, a sesamoid bone exclusive to their order that helps with jaw protrusion (Gidmark and Simons, 2014; Nelson et al., 2016). Most distinctly, all cypriniforms have pharyngeal teeth attached to the fifth ceratobranchial arch to process food items in lacking oral teeth altogether (Pasco-Viel et al., 2010; Gidmark and Simons, 2014).

Due to the great diversity observed in Cypriniformes, several reclassifications of its families and subfamilies have recently been made (Schönhuth et al., 2018). Based on recent research on the phylogenetic relationships among Cypriniform clades (Stout et al., 2016; Schönhuth et al., 2018; Tan and Armbruster, 2018), the family Cyprinidae, traditionally regarded as the largest family of freshwater fishes (Chen and Mayden, 2009; Nelson et al., 2016), is now classified as the suborder Cyprinoidei Rafinesque, 1815. Its eleven subfamilies, including Cyprininae, Gobioninae and Leuciscinae (Tan and Armbruster, 2018) have also been elevated to the family and family level (Schönhuth et al., 2018; Tan and Armbruster, 2018; Froese and Pauly, 2023). Leuciscidae, formerly Leuciscinae (Nelson et al., 2016; Schönhuth et al., 2018), is one of the larger families within Cyprinoidei, with about 683 species (Fricke et al., 2022). Commonly called 'minnows,' the leuciscids are distributed across North America and most of Eurasia (Nelson et al., 2016). Subfamily Pogonichthyinae represents one of the family's North American clades (Schönhuth et al., 2018) with approximately 27 genera and 257 species (Fricke et al., 2022). Of these 27 genera, the one of the most speciose is *Notropis* Rafinesque, 1818.

1.2 Genus *Notropis*

Notropis represents one of North America's largest genera of freshwater fish (Page and Burr, 2011). Colloquially referred to as 'shiners,' members of *Notropis* are found across the continent from northern Canada to Mexico (Page and Burr, 2011). Rafinesque (1818) was the first to name and describe *Notropis* as a genus. At the same time, he described *Notropis atherinoides* Rafinesque 1818, establishing it as the type species for the genus (Coburn, 1982; Bielawski and Gold, 2001). Characteristics Rafinesque (1818) highlighted in *N.atherinoides* included a total length of 1 to 2 inches (about 25-51 mm), a compressed body, very large eyes, a lateral band and a large mouth lacking teeth (Rafinesque, 1818). He also described the back as 'carinated' or 'keeled,' hence the generic name, which is derived from the Greek word 'noton' or 'back keel' (Rafinesque, 1818; Etnier and Starnes, 1993; Froese and Pauly, 2023). However, Rafinesque (1818) based his original description on preserved, shrivelled specimens, meaning the 'keels' he observed were specific to his specimens rather than a trait of taxonomic significance (Froese and Pauly, 2023). Thus, the name *Notropis* is itself a misnomer (Froese and Pauly, 2023).

Presently, 91 different species are classified within *Notropis* (Froese and Pauly, 2023). Traditionally, several traits have been used as diagnostic characteristics of the genus: one or two rows of pharyngeal teeth, with no more than four teeth in the major row; typically eight dorsal fin rays; absence of maxillary barbels; short gut; large scales that number no more the 55 along the lateral line, but are usually fewer than 40; small body size with a standard length (SL) that is generally less than 100 mm but never more than 175mm (Gilbert, 1978). Still, exceptions have been made for most of these traits when describing new *Notropis* species (Gilbert, 1978). For example, Gilbert and Bailey (1972) included *Opsopoeodus emiliae* Hay, 1881 in *Notropis* despite it having nine dorsal fin rays and five pharyngeal teeth in the major row. Similarly, *Notropis mekistocholas* Snelson, 1971 is placed within *Notropis* despite it having an elongated gut (Snelson, 1971). Only lateral line scale counts and a small body size remain constants in descriptions of *Notropis* species (Snelson, 1971; Gilbert and Bailey, 1972; Gilbert, 1978; Coburn, 1982; Bortone, 1989).

Despite having diagnostic characters for the genus having been identified by Gilbert (1978), subsequent authors have assigned species to *Notropis* that lack these characters, creating a history of reclassification, addition and removal of members over the last several decades. In

September 1977, 131 valid species were classified within *Notropis* (Gilbert, 1978), 40 more than the 91 currently listed (Froese and Pauly, 2023). This is partly because species such as *Opsopoeodus emiliae* and *Aztecula sallaei* Günter, 1868 have been initially described in different genera, reassigned to *Notropis*, then subsequently removed from *Notropis* later on because they do not possess a specific trait or traits traditionally attributed to the genus (Gilbert and Bailey, 1972; Chernoff and Miller, 1981; Fricke et al., 2022). Another reason for multiple reclassifications has been the elevation of certain subgenera traditionally placed within *Notropis*. Notably, Mayden's (1989) work on subgenus *Cyprinella* Girard, 1856 resulted in its elevation to the generic level based on behavioural and physical characteristics. A total of 27 species were removed from Notropis by Mayden (1989).

Since the work of Mayden (1989), molecular data has emerged as a different way to assess relationships within *Notropis* and among *Notropis* and closely related taxa (Mayden et al., 2006; Schönhuth et al., 2018; Stout et al., 2022). This has led to more reclassifications of *Notropis* and the genera and subgenera traditionally associated with it.

1.3 Phylogenetic Relationships of *Notropis*

Over the past thirty years, research has focused on deciphering the evolutionary relationships between *Notropis* and closely related cyprinoid and leuciscid groups. Apart from elevating *Cyprinella* to the generic level, Mayden (1989) was the first to specifically examine the relationships between North American Cyprinoids based on morphological data. Most notably, he proposed that a subset of North American Cyprinoids could be categorized around the possession of an opening in the floor of the posterior myodome surrounded by the parasphenoid and basioccipital. This opening had previously been documented by Coburn (1982) and was suggested to be a synapomorphy (Coburn, 1982; Simons and Mayden, 1999). This led to the formation of the open posterior myodome (OPM) clade, which included *Notropis* (s.l) alongside many eastern North American genera and a handful of Pacific coastal genera such as *Richardsonius* Girard, 1856 and *Oregonichthys* Hubbs, 1929 (Mayden, 1989; Gidmark and Simons, 2014). However, the validity and monophyly of the OPM clade has been questioned.

Using morphological data, Coburn and Cavender (1992) examined the relationships of North American cyprinoid genera. They recognized three major clades: 1) the western clade, 2) the chub clade, and 3) the shiner clade, with *Notropis* placed in the shiner clade with the genera *Richardsonius*, *Clinostomus* Girard, 1856*, Oregonichthys, Luxilus* Rafinesque, 1820, *Lythrurus*

Jordan, 1876, *Cyprinella, Pimephales* Rafinesque, 1820 and *Opsopoedus* Hay, 1881 (Coburn and Cavender, 1992). Members of Mayden's (1989) OPM group were distributed across these three clades, suggesting the OPM clade was a polyphyletic grouping (Coburn and Cavender, 1992). This discrepancy was partly attributed to the use of different characteristics and differences in how Mayden (1989) and Coburn and Cavender (1992) interpreted specific features, including the OPM.

The use of molecular data to analyze the relationships of the North American cyprinoids (Simons and Mayden, 1999; Simons et al., 2003; Schönhuth and Mayden, 2009) has more consistently identified three clades that combine elements of Mayden (1989) and Coburn and Cavender's (1992) phylogenies: the creek chub clade, western clade and OPM clade. Simons and Mayden 1999 and Simons et al. (2003) specifically described several more subclades within the OPM clade, including a shiner clade to which the genus *Notropis* belongs. Schönhuth et al. (2018) more recently also supported the idea of a shiner clade, which again included *Notropis.* However, the evolutionary relationships of North American cyprinoids, and by extension, the placement of *Notropis* amongst the other genera, remains unclear (Gidmark and Simons, 2014).

Much focus has also been placed on understanding the evolutionary relationships within *Notropis* (s.l). Previous authors have divided *Notropis* into several different subgenera, including but not limited to *Alburnops* Girard, 1856*, Graodus,* Günther 1868*, Hudsonius* Girard, 1856*, Miniellus* Jordan, 1882*, Aztecula* Jordan and Everman, 1896 *Ericymba* Cope, 1865*, Hydrophlox* Jordan and Brayton, 1878*, Cyprinella, Luxilus, Lythrurus* and *Notropis* (Snelson, 1968; Mayden, 1989; Cashner et al., 2011; Schönhuth et al., 2018; Tan and Armbruster, 2018). Some authors have also designated species groups, for example, the *Notropis dorsalis* Agassiz, 1854 and *Notropis procne* Cope, 1865 species groups (Warren et al., 1994; Raley and Wood, 2001). Another research focus has therefore been on the evolutionary relationships among and within these subgenera and species groupings (Coburn, 1982; Warren et al., 1994; Bielawski, 2000; Bielawski and Gold, 2001; Raley and Wood, 2001). In a few studies, research has also focused on the evolutionary relationships of *Notropis* species from a specific geographic region (Schönhuth and Doadrio, 2003). In assessing the evolutionary relationships within *Notropis* and other cyprinoids and leuciscids and the evolutionary relationships within *Notropis* itself, the monophyly of *Notropis* has been consistently unsupported. Mayden (1989) concluded that

Notropis as a taxon was artificial, supported only in phenetic classifications using convergent characteristics.

Mayden et al. (2006) conducted one of the most comprehensive analyses of the relationships of what they termed the 'notropin' shiners and minnows. The term itself does not refer to a taxonomic rank but has been used as a broad term for *Notropis* species plus taxa that have been closely associated and allied with them (Coburn and Cavender, 1992; Mayden et al., 2006; Stout et al., 2022). Mayden et al. (2006) used the sequences of the mitochondrial cytochrome b gene of 168 notropin species to construct a phylogeny and ultimately concluded that *Notropis* as a taxon is polyphyletic. More recently, Stout et al. (2022) examined the relationships within the shiner clade proposed by Schönhuth et al. (2018) using a combination of nuclear and mitochondrial DNA sequences. Unsurprisingly, their results corroborated those of Mayden (1989) and Mayden et al. (2006) by suggesting that *Notropis* is an artificial, nonmonophyletic genus.

The results of Mayden et al.'s (2006) study have led to more proposed taxonomic reclassifications. Following the recommendations of Mayden et al. (2006), Gidmark and Simons (2014) further split *Notropis*, elevating the subgenera *Alburnops, Aztecula, Ericymba, Graodus, Hudsonius* and *Miniellus* to the generic level. However, many species remain left by default in '*Notropis*' (using single quotes to indicate non-monophyly) due to the uncertain placement and unclear relationships, meaning that even with the elevation of these subgenera, *Notropis* (s.s) remains nonmonophyletic. Furthermore, while some authors have accepted the elevations of these subgenera as proposed by Mayden et al. (2006) and Gidmark and Simons (2014) (e.g., Schönhuth et al., 2018; Tan and Armbruster, 2018; Stout et al., 2022), these reclassifications have been slow to be widely adopted (Page and Burr, 2011; Munno et al, 2022; Chappell, 2023). As such, *Notropis* (s.s) will likely remain a polyphyletic "bin for species of questionable affinity" (Martin and Bonett, 2015: 20) for the foreseeable future.

1.4 *Notropis* Osteology

The osteology of *Notropis* (both s.l. and s.s) has also been a research focus. Part of the interest in the osteology of *Notropis* is tied to discerning its phylogenetic relationships. Cavender and Coburn (1992) examined the relationships of North American cyprinoids, including a handful of *Notropis* (s.l) species, compared to other members of Cyprinoidei. Their study included osteological characteristics of the cranium, pelvic girdle, pectoral girdle and Weberian apparatus as part of their data matrix (Cavender and Coburn, 1992). Coburn and Cavender (1992) looked at a similar set of traits in a select number of Notropis (s.l) species to discern the relationships of North American cyprinoids. Coburn (1982) and Mayden (1989) focused more exclusively on the osteological characteristics of *Notropis* to determine the relationships within genera and between subgenera. Their focus was primarily on cranial elements and the branchial apparatus.

A few authors have focused on the osteology of *Notropis* for other reasons. Harrington (1955) described the osteocranium of *Notropis bifrenatus* Cope, 1867 to better understand the skull morphology of cyprinoids and teleosts. Reno (1966) looked at the infraorbital series of *Notropis volucellus* Cope, 1865 and *Notropis buchanani* Meek, 1896 as part of his examination and comparison of the infraorbital canals of the two species. Eastman and Underhill (1973) examined the pharyngeal teeth of seventeen *Notropis* species as part of a broader study on the intraspecific variation of pharyngeal teeth formulae in cyprinoids. In his description of *Notropis melanostomus* Bortone, 1989, Bortone (1989) included the morphology of the pharyngeal teeth. In his study of North American cyprinoid tail osteology, Buhan (1972) examined the caudal skeleton of several *Notropis* species to determine if any characteristics could help delineate relationships. More recently, Conway and Kim (2016) reviewed and compared the shape of the metapterygoid and fifth ceratobranchial arch as part of their justification to remove *Notropis megalops* Girard, 1856 from synonymy with *Notropis amabilis* Girard, 1856.

To date, one of the most comprehensive osteological descriptions of any *Notropis* species is that of Coburn (1982). Coburn (1982) described the morphology and osteology of *Notropis atherinoides* as part of his research on *Notropis* osteology and phylogenetic relationships. His reasoning for choosing *N.atherinoides* out of the 122 then recognized *Notropis* species was because of its generalized morphology and its status as the type species for the genus (Coburn, 1982; Bielawski and Gold, 2001). By describing the type species, Coburn (1982) aimed to identify plesiomorphic and apomorphic characteristics and establish a baseline of traits that could define *Notropis* as a genus (Coburn, 1982). His description of the osteology of *N.atherinoides* included the pectoral and pelvic girdles, Weberian apparatus, transitional vertebrae, caudal skeleton, dorsal and anal fin supports, branchial apparatus, fifth branchial arch and cranium (Coburn, 1982). In the same study, Coburn (1982) examined specific osteological features of 77 *Notropis* (s.l.) species. He included species from *Cyprinella, Luxilus, Lythrurus* and

Pteronotropis Fowler, 1935*,* which were considered subgenera at the time. The features he focused on centred primarily around the ethmoid, orbital, postorbital, basicranial, suspensorial and hyoid regions (Coburn, 1982).

Coburn (1982) noted that he failed to find any osteological characteristics that could be used to consistently define *Notropis* as a genus and clade. Nonetheless, his research was crucial in establishing a base understanding of the osteology of *Notropis* and identified characteristics that later authors would use in the study of North American cyprinoid evolution and systematics (Mayden, 1989; Coburn and Cavender, 1992; Bielawski and Gold, 2001; Stout et al., 2022). However, more needs to be done to document the osteology of *Notropis* species across subgenera. Furthermore, no work has been done to assess possible intraspecific osteological variation between populations of a single species. My thesis will, therefore, aim not only to survey and document the osteology of *Notropis* species from several subgenera but also to explore the degree of intraspecific osteological variation among populations of a single species, specifically *Notropis hudsonius* Clinton, 1824 .

1.5 Thesis Objectives

This thesis has two objectives:

1. The first objective is to document and describe the osteology of *Notropis hudsonius* and survey 15 different populations for osteological variability. I will look at *N. hudsonius* populations predominantly from Alberta, as well as one from the Northwest Territories, two from Manitoba and one from western Ontario. This will involve descriptions and comparisons of elements from the cranial, branchial, pectoral, pelvic and caudal regions.

2. The second objective is to examine and compare the osteology of the species *Notropis atherinoides, Notropis blennius* Girard, 1856, *Notropis buchanani*, *Notropis dorsalis*, *Notropis heterodon* Cope 1865, *Notropis heterolepis* Eigenmann and Eigenmann, 1893, *Notropis hudsonius*, *Notropis percobromus* Cope, 1871, *Notropis stramineus* Cope, 1865, *Notropis texanus* Girard, 1865 and *Notropis volucellus.* All of these species are endemic to the Canadian provinces of Alberta, Saskatchewan and Manitoba (Page and Burr, 2011), except *N.buchanani* which has a limited range in south-western Ontario (Holm and Houston, 1993). Nine of these species are classified into four separate subgenera *sensu* Mayden et al. (2006). *Notropis atherinoides, N. buchanani, N. percobromus* and *N. vollucellus* are placed within subgenus *Notropis (Notropis)* Rafinesque 1818, *N. heterodon* and *N. stramineus* in *Notropis* (*Miniellus),*

N. blennius and *N. texanus* in *Notropis (Alburnops)* and *N. hudsonius* in *Notropis (Hudsonius)* (Mayden et al., 2006). The remaining species, *N.dorsalis* and *N. heterolepis* are not presently assigned to any particular subgenus (Mayden et al., 2006). Building on my osteological description of *N.hudsonius,* I will compare the osteological characteristics of these eleven species, also focusing on elements of the cranial, branchial, pectoral, pelvic and caudal regions. However, the focus will instead be on determining major interspecific differences instead of intraspecific variants.

For this thesis, I do not intend to propose any new reclassifications within *Notropis*. The purpose, instead, is to first assess the degree of osteological variability among populations of *Notropis hudsonius* and determine which traits are more plastic and, therefore, unreliable for use in species identification and research. I will also explore and reassess the osteology of this artificial genus in the context of the molecular based phylogenies and subgenera established by Mayden et al. (2006). Ultimately, this thesis will establish a better understanding of the osteology of four different subgenera of *Notropis* and two species of uncertain placement and the nature of intraspecific variability. More broadly, this thesis will have implications for understanding the process of evolution and speciation of North American leuciscids.

1.6 Figures

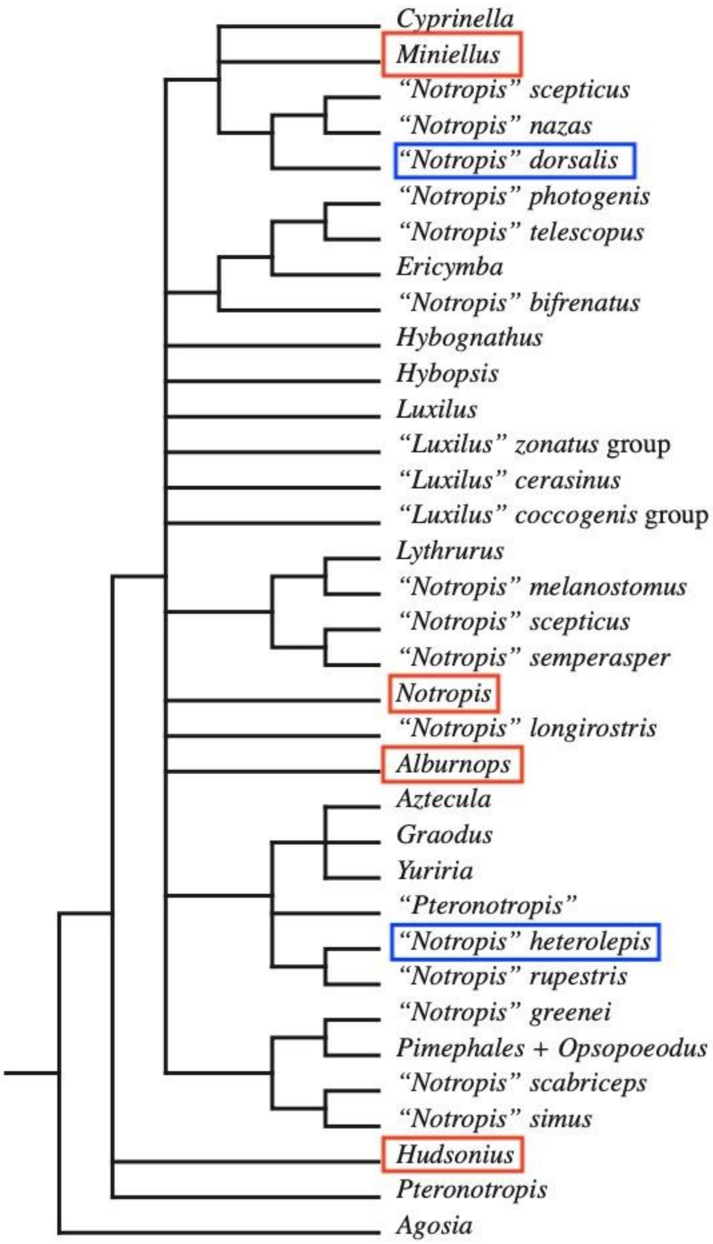

Figure 1.1. Hypotheses of relationships of *Notropis* and its allies redrawn from Mayden et al. (2006) (Gidmark and Simons, 2014, figure 12.62). The subgenera (red) and species of unclear placement (blue) examined in this thesis are highlighted.

1.7 Literature Cited

Agassiz, L. 1854. Notice of a collection of fishes from the southern bend of the Tennessee River, in the State of Alabama. American Journal of Science and Arts 17:297–308, 353–365.

Bielawski, J. P. 2000. Molecular phylogenetics and evolution of subgenus *Notropis*. PhD dissertation, Texas A&M University, 144 pp.

Bielawski, J. P., and J. R. Gold. 2001. Phylogenetic relationships of cyprinid fishes in subgenus *Notropis* inferred from nucleotide sequences of the mitochondrially encoded cytochrome b gene. Copeia 2001:656–667.

Bonaparte, C. L. 1835. Prodromus systematis ichthyologiae. Nuovi Annali Delle Scienze Naturali Bologna 2:181-196,272-277.

Bortone, S. A. 1989. *Notropis melanostomus*, a New Species of Cyprinid Fish from the Blackwater-Yellow River Drainage of Northwest Florida. Copeia 1989:737.

Buhan, P. J. 1972. The comparative osteology of the caudal skeleton of some North American minnows (Cyprinidae). American Midland Naturalist 88:484–490.

Cashner, M. F., K. R. Piller, and H. L. Bart. 2011. Phylogenetic relationships of the North American cyprinid subgenus *Hydrophlox*. Molecular Phylogenetics and Evolution 59:725–735.

Cavender, T. M., and M. M. Coburn. 1992. Interrelationships of North American Cyprinid Fishes; pp. 328–373 in Systematics, historical ecology, and North American freshwater fishes. Stanford University Press, Stanford, California.

Chappell, L. E. 2023. Hydrology and geology as structuring mechanisms of semi-arid fish communities. Master's Thesis, Texas State University, 33 pp.

Chardon, M., and P. Vandewalle. 1996. Evolutionary trends and possible origin of the Weberian apparatus. Netherlands Journal of Zoology 47:383–403.

Chen, W.-J., and R. L. Mayden. 2009. Molecular systematics of the Cyprinoidea (Teleostei: Cypriniformes), the world's largest clade of freshwater fishes: Further evidence from six nuclear genes. Molecular Phylogenetics and Evolution 52:544–549.

Chernoff, B., and R. R. Miller. 1981. Systematics and variation of the aztec shiner, *Notropis sallei*, a cyprinid fish from central Mexico. Proceedings of the Biological Society of Washington 94:18–36.

Clinton, D. 1824. Description of a new species of fish, from the Hudson River. Annals of the Lyceum of Natural History of New York 1:49–50.

Coburn, M. M. 1982. Anatomy and relationships of *Notropis atherinoides*. PhD dissertation, Ohio State University, 384 pp.

Coburn, M. M., and T. M. Cavender. 1992. Phylogenetic relationships of North American Cyprinidae; pp. 328–373 in Systematics, historical ecology, and North American freshwater fishes. Stanford University Press, Stanford, California.

Conway, K. W., and D. Kim. 2015. Redescription of the Texas Shiner *Notropis amabilis* from the southwestern United States and northern Mexico with the reinstatement of *N. megalops*(Teleostei: Cyprinidae). Ichthyological Exploration of Freshwaters 26:305–340.

Cope, E. D. 1865. Partial catalogue of the cold-blooded Vertebrata of Michigan. Pt. I. Proceedings of the Academy of Natural Sciences of Philadelphia 16:276–285.

Cope, E. D. 1867. Synopsis of the Cyprinidae of Pennsylvania. Transactions of the American Philosophical Society 13:351–410.

Cope, E. D. 1871. Recent reptiles and fishes. Report on the reptiles and fishes obtained by the naturalists of the expedition; pp. 432–442 in Preliminary report of the United States Geological Survey of Wyoming and portions of contiguous territories. vol. 4. Government Printing Office, Washington D.C.

Eigenmann, C. H., and R. S. Eigenmann. 1893. Preliminary descriptions of new fishes from the northwest. American Naturalist 27:151–154.

Etnier, D. A., and W. C. Starnes. 1993. The Fishes of Tennessee. The University of Tennessee Press, Knoxville, Tennessee, 689 pp.

Fink, S. V., and W. L. Fink. 1981. Interrelationships of the ostariophysan fishes (Teleostei). Zoological Journal of the Linnean Society 72:297–353.

Fricke, R., W. N. Eschmeyer, and J. D. Fong. 2024. Eschmeyer's Catalog of Fishes: Genera/Species By Family/Subfamily. Available at https://researcharchive.calacademy.org/research/ichthyology/catalog/SpeciesByFamily.asp. Accessed December 1, 2022.

Froese, R., and D. Pauly. 2023. FishBase.World Wide Web electronic publication. Available at www.fishbase.org. Accessed April 21, 2024.

Gidmark, N. J., and A. M. Simons. 2014. Cyprinidae: carps and minnows; pp. 334–450 in Freshwater Fishes of North America. Johns Hopkins University Press, Baltimore, Maryland.

Gilbert, C. R. 1978. Type catalogue of the North American cyprinid fish genus *Notropis*. Bulletin of the Florida Museum of Natural History 23:1–104.

Gilbert, C. R., and R. M. Bailey. 1962. Synonymy, characters, and distribution of the American cyprinid Fish *Notropis shumardi*. Copeia 1962:807.

Gilbert, C. R., and R. M. Bailey. 1972. Systematics and zoogeography of the American cyprinid fish *Notropis (Opsopoeodus) emiliae*. Occasional Papers of the Museum of Zoology, University of Michigan 664:1–35.

Girard, C. F. 1856. Research upon the cyprinoid fishes inhabiting the fresh waters of the United States, west of the Mississippi Valley, from specimens in the museum of the Smithsonian Institution. Proceedings of the Academy of Natural Sciences of Philadelphia 2:165–213.

Girard, C. F. 1858. General report upon zoology of the several Pacific railroad routes; pp. in Reports of explorations and surveys, to ascertain the most practicable and economical route for a railroad from the Mississippi River to the Pacific Ocean. vol. 10. Beverly Tucker, Washington D.C.

Günther, A. 1868. Catalogue of the Physostomi, containing the families Heteropygii, Cyprinidæ, Gonorhynchiidæ, Hypodontidæ, Osteoglossidæ, Clupeidæ, Chirocentridæ, Alepochephalidæ, Notopteridæ, Halosauridæ, in the collection of the British Museum. Catalogue of the Fishes in the British Museum 7:1–512.

Harrington, R. W. 1955. The Osteocranium of the American Cyprinid Fish, *Notropis bifrenatus*, with an Annotated Synonymy of Teleost Skull Bones. Copeia 1955:267–290.

Hay, O. P. 1881. On a collection of fishes from eastern Mississippi. Proceedings of the United States National Museum 3:488–515.

Holm, E., and J. Houston. 1993. Status of the ghost shiner, *Notropis buchanani*, in Canada. Canadian Field-Naturalist 107:440–445.

Jordan, D. S. 1876. Class V.--Pisces; pp. 199–362 in Manual of the vertebrates of the northern United States, including the district east of the Mississippi River and north of North Carolina and Tennessee, exclusive of marine species. Jansen, McClurg & Co, Chicago, Illinois.

Jordan, D. S. 1882. Report on the fishes of Ohio; pp. 735–1002 in Report of the Geological Survey of Ohio. vol. 4. Columbus, Nevins & Myers, state printers, Columbus,Ohio.

Jordan, D. S., and A. W. Brayton. 1878. Contributions to North American ichthyology. No. 3. A. On the distribution of the fishes of the Alleghany region of South Carolina, Georgia, and Tennessee, with descriptions of new or little known species. Bulletin of the United States National Museum 3–95.

Jordan, D. S., and B. W. Evermann. 1896. The Fishes of North and Middle America : A Descriptive Catalogue of the Species of Fish-like Vertebrates Found in the Waters of North America, North of the Isthmus of Panama. United States National Museum, Washington, Smithsonian Institution, 1240 pp.

Martin, S. D., and R. M. Bonett. 2015. Biogeography and divergent patterns of body size disparification in North American minnows. Molecular Phylogenetics and Evolution 93:17–28.

Mayden, R. L. 1989. Phylogenetic studies of North American minnows, with emphasis on genus *Cyprinella*. Miscellaneous Publication University of Kansas Publications, Museum of Natural History 80:1–189.

Mayden, R. L., A. M. Simons, R. M. Wood, P. M. Harris, and B. R. Kuhajda. 2006. Molecular systematics and classification of North American notropin shiners and minnows (Cypriniformes: Cyprinidae); pp. 72–101 in In Studies of North American Desert Fishes in Honor of EP (Phil) Pister, Conservationist. Universidad Autonoma de Nuevo Leon, Mexico.

Meek, S. E. 1896. A list of fishes and mollusks collected in Arkansas and Indian Territory in 1894. Bulletin of the U. S. Fish Commission 15:341–349.

Munno, K., P. A. Helm, C. Rochman, T. George, and D. A. Jackson. 2022. Microplastic contamination in Great Lakes fish. Conservation Biology 36:e13794.

Nelson, J. S., T. C. Grande, and M. V. H. Wilson. 2016. Fishes of the World, 5th ed. John Wiley & Sons, Inc, Hoboken, New Jersey, 707 pp.

Page, L. M., and B. M. Burr. 2011. A Field Guide to Freshwater Fishes: North America North of Mexico, 2nd ed. Houghton Mifflin Harcourt Publishing Company, New York, New York, 663 pp.

Pasco-Viel, E., C. Charles, P. Chevret, M. Semon, P. Tafforeau, L. Viriot, and V. Laudet. 2010. Evolutionary trends of the pharyngeal dentition in Cypriniformes (Actinopterygii: Ostariophysi). PLoS ONE 5:1–15.

Rafinesque, C. S. 1815. Analyse de La Nature, Ou Tableau de l'univers et Des Corps Organises. Aux dépens de l'auteur, Palerme, 224 pp.

Rafinesque, C. S. 1818. Descriptions of two new genera of North American fishes, Opsanus and Notropis. American Monthly Magazine and Critical Review 2:203–204.

Rafinesque, C. S. 1820. Fishes of the Ohio River. Western Review and Miscellaneous Magazine: A Monthly Publ., Devoted to Literature and Science 2:235–242.

Raley, M. E., and R. M. Wood. 2001. Molecular systematics of members of the *Notropis dorsalis* species group (Actinopterygii: Cyprinidae. Copeia 2001:638–645.

Reno, H. W. 1966. The infraorbital canal, its lateral-line ossicles and neuromasts, in the minnows *Notropis volucellus* and *N. buchanani*. Copeia 1966:403–413.

Schönhuth, S., and I. Doadrio. 2003. Phylogenetic relationships of Mexican minnows of the genus *Notropis* (Actinopterygii, Cyprinidae). Biological Journal of the Linnean Society 80:323–337.

Schönhuth, S., and R. L. Mayden. 2009. Phylogenetic relationships in the genus *Cyprinella* (Actinopterygii: Cyprinidae) based on mitochondrial and nuclear gene sequences. Molecular Phylogenetics and Evolution 55:77–98.

Schönhuth, S., J. Vukić, R. Šanda, L. Yang, and R. L. Mayden. 2018. Phylogenetic relationships and classification of the Holarctic family Leuciscidae (Cypriniformes: Cyprinoidei). Molecular Phylogenetics and Evolution 127:781–799.

Schultz, L. P. 1929. Check-list of the fresh-water fishes of Oregon and Washington; pp. 43–50 in Check-list of the fresh-water fishes of Oregon and Washington. vol. 2. Publications in Fisheries, Seattle, Washington.

Simons, A. M., and R. L. Mayden. 1999. Phylogenetic Relationships of North American Cyprinids and Assessment of Homology of the Open Posterior Myodome. Copeia 1999:13–21.

Simons, A. M., P. B. Berendzen, and R. L. Mayden. 2003. Molecular systematics of North American phoxinin genera (Actinopterygii: Cyprinidae) inferred from mitochondrial 12S and 16S ribosomal RNA sequences. Zoological Journal of the Linnean Society 139:63–80.

Snelson, F. F. 1968. Systematics of the Cyprinid Fish *Notropis amoenus*, with Comments on the Subgenus Notropis. Copeia 1968:776.

Snelson, F. F. 1971. *Notropis mekistocholas*, a New Herbivorous Cyprinid Fish Endemic to the Cape Fear River Basin, North Carolina. Copeia 1971:449–462.

Stout, C., S. Schonhuth, R. Mayden, N. L. Garrison, and J. W. Armbruster. 2022. Phylogenomics and classification of *Notropis* and related shiners (Cypriniformes: Leuciscidae) and the utility of exon capture on lower taxonomic groups. PeerJ 10:e14072.

Stout, C. C., M. Tan, A. R. Lemmon, E. M. Lemmon, and J. W. Armbruster. 2016. Resolving Cypriniformes relationships using an anchored enrichment approach. BMC Evolutionary Biology 16:244.

Tan, M., and J. W. Armbruster. 2018. Phylogenetic classification of extant genera of fishes of the order Cypriniformes (Teleostei: Ostariophysi). Zootaxa 4476:6–39.

Warren, M. L., B. M. Burr, and J. M. Grady. 1994. *Notropis albizonatus*, a new cyprinid fish endemic to the Tennessee and Cumberland River drainages, with a phylogeny of the *Notropis procne* species group. Copeia 1994:868–886.

Chapter 2: Assessing the Intraspecific Osteological Variation of *Notropis hudsonius* (Cypriniformes: Leuciscidae)

2.1 Introduction

Notropis hudsonius Clinton, 1824, commonly known as the spottail shiner, is a cyprinoid fish species native to North America. It is widely distributed from the eastern United States and as far north as the Northwest Territories in Canada (Page and Burr, 2011; Froese and Pauly, 2023). They are small fish, reaching no more than 147 mm in total length (Gidmark and Simons, 2014). *Notropis hudsonius* is found in various freshwater habitats including lakes, streams and rivers, and has an omnivorous diet (Nelson and Paetz, 1992; Gidmark and Simons, 2014). Distinguishing features of *Notropis hudsonius* include a moderately compressed body with blue-green colouring dorsally and silver colouring laterally. Preserved specimens have a dark lateral stripe not seen in living fish (Nelson and Paetz, 1992). The most distinct marking is a large black dot at the base of the caudal fin (Page and Burr, 2011).

Notropis hudsonius has been regarded as one of the most plesiomorphic and basal species placed within the genus *Notropis* Rafinesque, 1818 (s.s.). In his analysis of the osteology of *Notropis atherinoides* Rafinesque, 1818 and 77 different *Notropis* (s.l.) species, Coburn (1982) considered *N. hudsonius* to be one of the most plesiomorphic species within the genus. This conclusion was made based on its anal ray count, dorsal fin position, body size, egg size, tuberculation, spawning behaviour, and scale morphology. *N. atherinoides*, the type species for the genus, was found to be plesiomorphic in many respects. However, Coburn (1982) noted that it had several derived characteristics commonly found in pelagic fishes, including mouth position, colouration and gill raker count. *N. hudsonius,* meanwhile, has a more generalist lifestyle. Coburn (1982) was, therefore, of the opinion that *N. hudsonius* was among the most plesiomorphic *Notropis* species and would be useful in determining character states for *Notropis* as a genus. Over the past two decades, molecular studies have given further phylogenetic support for the basal nature of *Notropis hudsonius*. Using sequences from the mitochondrial cytochrome b gene, Mayden et al. (2006) assessed the phylogenetic relationships of 168 different notropin shiner species. The resulting analysis placed *N. hudsonius* within the basal, monophyletic *Notropis (Hudsonius)* Girard, 1856 clade wherein *N. hudsonius* was sister to a clade containing *Notropis altipinnis* Cope, 1870 and *Notropis cummingsae* Meyers, 1925. *Notropis (Hudsonius)* formed a trichotomy with a grouping of three species from the polyphyletic genus *Pteronotropis*

Fowler, 1935 and a large group the authors dubbed the ‘notropin clade’ encompassing a vast majority of genera species traditionally placed within *Notropis* (s.l.).

However, the presumed monophyly of Mayden et al.’s (2006) *Hudsonius* clade has faced some challenges, specifically when nuclear DNA has been used alongside mitochondrial DNA in subsequent phylogenetic analyses. For example, Schönhuth et al. (2018) found a *Hudsonius* clade containing *Notropis hudsonius, Notropis altipinnis* and *Notropis cummingsae* to be polyphyletic. Stout et al. (2022) came to a similar conclusion through phylogenomic analysis. That said, the polyphyly of the *Hudsonius* clade in both studies resulted from an unclear placement for *N. cumingisi*. Schönhuth et al. (2018) and Stout et al. (2022) specifically found that the polyphyly of *Hudsonius* resulted from *N. cumingisi* being more closely related to *Pteronotropis.* However, the placement of *N. hudsonius* itself has remained consistent among all three authors in that it is always in the same clade as *N. altipinnis*. The consensus is that *N. hudsonius* has a basal relationship to the other species currently and traditionally placed within *Notropis* (s.l.).

Past research on the osteology of *Notropis hudsonius* has been in the context of wider phylogenetic studies (Coburn, 1982; Mayden, 1989) or studies focusing on a specific osteological characteristic amongst other North American cyprinoids, like the caudal skeleton or pharyngeal teeth (Buhan, 1972; Eastman and Underhill, 1973). Despite the basal nature of *N. hudsonius*, research has yet to focus specifically on the osteology of the whole skeleton. Furthermore, research has yet to focus on the osteological variation of *N. hudsonius* or other *Notropis* species.

In this chapter, I will describe the osteology of *Notropis hudsonius* to identify and illustrate osteological features subject to variability. This description will focus on the elements of the cranial, branchial, pectoral, pelvic, and caudal regions. By describing the osteology of this taxon, I will not only outline the osteology of a basal, plesiomorphic *Notropis* species but also determine what parts of the skeleton of *N. hudsonius* are subject to variability and reveal any patterns of this variation that may exist among different populations. The osteological description of *N. hudsonius* provided in this chapter will also act as a base for comparison of the ten other species analyzed in Chapter 3 and provide insight into what osteological characteristics are more variable and thus unreliable in distinguishing among different *Notropis* species and subgenera. More broadly, the results of this chapter will provide important insight into the osteology and evolution of *Notropis* and North American leuciscids as a whole.

2.2 Materials and Methods

2.2.1 Materials

The *Notropis hudsonius* specimens used in this study are cataloged in the University of Alberta Museum of Zoology Ichthyology Collection, Edmonton, Canada and the University of Manitoba Ichthyology Collection, Winnipeg, Canada (Appendix A). I used a total of 72 specimens sampled from 15 different populations in Alberta (11), Manitoba (2), western Ontario (1) and the Northwest Territories (1). Four population samples from the University of Alberta's collections were cleared and stained prior to this study and stored in 100% glycerin. All remaining specimens were initially preserved in alcohol that then were cleared and stained following the protocols of Taylor and Van Dyke (1985). Specimen numbers correspond to different populations. For more details on the specimens used, please consult Appendix A.

2.2.2 Measurements and Statistical Analysis

Measurements (n = 54), meristic counts (n = 54), and dental formulas (n = 43) were documented according to Hubbs and Lagler (2004). Scale counts were collected according to Armbruster (2012), while preanal, prepectoral and prepelvic length follow Habib et al. (2019). Definitions for these measurements and meristic counts can be found in Appendix B. An explanation on how the dental formulas were counted is seen in Figure 2.1. Vertebral counts (n = 42) included the four Weberian centra and the compound centrum of the caudal skeleton (Fink and Fink, 1981). Pore counts (n = 24) of the supraorbital, supratemporal, infraorbital, preopercular mandibular and postocular commissure sensory canals were taken from cleared and stained specimens and counted according to Illick (1956). Measurements and meristic counts (including vertebral counts) were further analyzed using principal component analysis (PCA). These analyses were done to determine if and how osteological related measurements and meristic counts, namely from the fins, gill rakers and vertebral counts, tie into the intraspecific variation on *Notropis hudsonius.* The PCA was completed using R Studio version 4.2.2, using "princomp" function of pcaMethods package. To account for size, measurements were analyzed as a proportion of standard length (SL).

A total of 50 cleared and stained specimens were analyzed. Photographs for osteological drawings were taken with a Zeiss Stereo Discovery.V8 stereomicroscope with a Carl Zeiss

44403 6-9000 eyepiece (8x) and a variety of lenses (Zeiss Achromat S 0.3x FWD 236 mm, Zeiss Plan Apo S 0.63x FWD 81 mm, and Zeiss Plan Apo S 1.0x FWD 60 mm), with NIS-Elements F package 2.20, version 5.03. Osteological terminology generally follows Coburn (1982) and Conway (2011) unless otherwise specified. Terminology relating to the sensory canal system follows Reno (1966). 20 cleared and stained specimens were further dissected, having their branchial apparatuses removed. My analysis focused on the oral jaws ($n = 45$), suspensorium ($n = 45$), opercular series ($n = 39$), branchial apparatus ($n = 22$), hyoid region ($n = 46$), circumorbital series ($n = 39$), Weberian apparatus ($n = 49$), pectoral girdle ($n = 45$), pelvic girdle ($n = 45$) and caudal skeleton ($n = 50$). I also analyzed the elements of the skull, breaking my analysis into an ethmoid region ($n = 49$), orbital region ($n = 49$), otic and occipital region ($n = 20$) and basicranial region ($n = 20$). My analysis of the branchial apparatus, otic, occipital and basicranial regions was limited by the number of specimens I was able to dissect.

2.3 Results

2.3.1 Statistical Analysis

The PCA conducted on the measurements of 54 *Notropis hudsonius* specimens standardized as ratios of standard length (Table 2.1) showed that a vast majority of the explained variance was captured in the first, second, third and fourth principal components (Fig. 2.2). For PC1, the largest loadings are from body depth, prepectoral length, prepelvic length and preanal length, all of which are positively correlated with PC1. For PC2, the largest loadings are from preanal length, predorsal length and prepelvic length, all positively correlated with PC2. For PC3, body depth and peduncle length had the highest loadings, and are both positively correlated with PC3, followed by prepelvic length ad pectoral fin length, which are negatively correlated (Fig. 2.3). For PC4, the largest loadings are from body depth and dorsal fin length, which are positively correlated, and prepectoral and head length, which are negatively correlated. When PC1 was plotted against PC2 (Fig. 2.4) four samples were distinctly separate from the others along the lower ends of PC1 and PC2. Three of these samples are from Manitoba and western Ontario, while one is from central Alberta.

2.3.2 Osteology

2.3.2.1 Ethmoid Region

The ethmoid block or complex is a single, median element that makes up the anterior portion of the nasal cavity. According to Conway (2011), the ethmoid block has a fused mesethmoid and supraethmoid portion. It has a deep anterior notch that accommodates the kinethmoid and an expanded base that sits on a cartilage strip, the planum ethmoidale (Harrington, 1955), separating it from the vomer. The mesethmoid portion forms the ventral part of the ethmoid complex. It is oval and constricted in the middle, forming a nasal septum. The supraethmoid portion forms the dorsal region of the ethmoid complex, roofing the nasal cavity. It is dorsally flattened and, in dorsal view, is constricted towards the posterior end (Fig. 2.5).

The lateral ethmoids rim the anterior region of the orbit and form the posterior portion of the nasal cavity. They articulate with the ethmoid block anteriorly, the frontals dorsally, the orbitosphenoid posteriorly and the vomer and parasphenoid ventrally. In ventral view (Fig. 2.6), they have a thick median margin that narrows into a set of broad, flat, lateral wings. The ventral surface is concave anteriorly, and the posterior margin forms a ridge. When viewed laterally, the lateral ethmoids narrow towards the ventral region (Fig. 2.7). The ventral part of the anterior margin of the lateral ethmoid forms an anteriorly directed shelf while the anterodorsal corner is separated from the mesethmoid portion of the ethmoid complex by cartilage. The lateral ethmoids form the posterior margin of the olfactory foramen, while the nasal septum of the ethmoid block forms the anterior margin. In four specimens examined, the olfactory foramen was encompassed entirely within the lateral ethmoids (Fig. 2.8). The orbitonasal foramen is observed just below the olfactory foramen, along its posterior margin

The preethmoids sit between the vomer and ethmoid complex. They are round, ossified nodules surrounded by cartilage and are directed laterally. The vomer is a flat dermal bone located ventral to the parasphenoid and ethmoid complex. It is broadest anteriorly with round lateral edges and a single, pointed posterior process that sits between the lateral ethmoids. Its anterior end has a deep, round notch. The nasals are tubular bones that lie lateral to the supraethmoid portion of the ethmoid block. They each have three pores (Fig. 2.5).

2.3.2.2 Orbital Region

The orbitosphenoid is a single median bone that articulates with the frontals dorsally, the lateral ethmoids anteriorly and the pterosphenoids posteriorly (Fig. 2.7). Its dorsal margin is divided into left and right lamellae that join in a single median ridge extending ventrally to the parasphenoid. The anteroventral corner of the medial ridge rests on a cartilage extension from the lateral ethmoids. In three specimens, the posteroventral corner is fused with the parasphenoid (Fig. 2.7). The posterior edge of the orbitosphenoid forms an oval foramen with the lateral ethmoid. This foramen was absent in three of the specimens examined. The orbitosphenoid forms the anterior margin of the optic foramen.

The pterosphenoid is a ventrally concave endochondral element that makes up the posterior region of the orbit (Fig. 2.7). It articulates with the orbitosphenoid anteriorly, the frontal and sphenotic dorsolaterally, and the prootic posteriorly. The pterosphenoids do not articulate with one another medially but instead, form the posterior margins of the optic foramen and the anterior portion of the hypophyseal foramen. The posteroventral corner of the pterosphenoid forms the front edge of the anterior hyomandibular fossa. In *Notropis hudsonius*, there are four foramen in the pterosphenoid, accommodating a branch of the orbitonasal vein, the trochlear nerve, the superficial ophthalmic branch of the facial nerve and the ophthalmic branch of the trigeminal nerve (Fig. 2.6).

The frontal is the largest bone of the cranium, either overlapping or underlapping the its opposite medially (Fig. 2.12). It articulates with the supraethmoid portion of the ethmoid block, supraorbital and lateral ethmoids anteriorly and the orbitosphenoids and pterosphenoids ventrally (Fig. 2.10). Its posterolateral margin articulates with the sphenotic, and the posterior margin overlaps the parietals. When viewed dorsally (Fig. 2.9), it narrows anteriorly, with the widest point being where the frontal contacts the sphenotic. The frontal has a ventrally placed, laterally projecting orbital shelf that lies over and follows the curve of the orbit, narrowing anteriorly. The orbital shelf articulates posteriorly with the postorbital process of the sphenotic (Fig. 2.6).

2.3.2.3 Otic and Occipital Regions

The sphenotic is a paired endochondral bone. It articulates with the pterosphenoid anteriorly, the frontal dorsally, the parietal posterodorsally, the pterotic posteriorly, and the prootic ventrally. The ventral border of the sphenotic makes up half of the anterior hyomandibular facet and a portion of the posterior facet. Dorsolateral to the anterior facet is an obliquely oriented postorbital process. The posterior tip of this process is drawn out into a blunt, short and posteriorly curved sphenotic spine (Fig. 2.6). In one specimen, the sphenotic spine is sharp and elongate (Fig. 2.10)

The prootic is a large endochondral bone with a hexagonal shape. It articulates with the pterosphenoid anteriorly and the basioccipital posteriorly (Fig. 2.6). It contacts the sphenotic and pterotic laterodorsally, contributing to the anterior and posterior hyomandibular facets. It forms the anterior wall of the subtemporal fossa, articulating with the epiotic and exoccipital within the fossa (Fig. 2.6). The prootic splits into two lamellae along the medial margin. The dorsal lamella meets its opposite medially and diverges anteriorly to form the posterior portion of the hypophyseal foramen. The ventral lamella forms part of the wall of a posterior myodome, with the medial margins articulating with the parasphenoid. The posterior portion is enlarged into a capsule. The trigeminal foramen is usually bordered by the prootic posteriorly and the pterosphenoid anteriorly; however, the trigeminal foramen is fully encompassed within the prootic in one specimen. In three specimens, the trigeminal foramen is fully encompassed within the prootic on one side, and shared with the pterotic on the other (Fig. 2.6). In seven specimens, I also observed a bony strut that forms over the trigeminal foramen, just lateral to the wings of the parasphenoid, on at least one side (Fig. 2.10).

The oculomotor foramen is found in the anteromedial corner of the prootic (Fig. 2.10). Of the specimens whose occipital region I was able to examine, the oculomotor foramen was most commonly bordered by both the prootic and pterosphenoid, in about two fifths of the specimens. In five specimens, the oculomotor foramen was fully encompassed within the prootic on one side, and shared with the pterotic on the other. In another five specimens, the oculomotor foramen was encompassed within the prootics only.

The pterotic is a large element that overlaps the sphenotic anteriorly and is overlapped by the parietal dorsally (Fig. 2.9). It forms the lateral wall of the subtemporal fossa (Fig. 2.6), articulating with the epiotic and exoccipital within the fossa. Ventrolaterally, the pterotic forms the posterior hyomandibular facet. A short spine protrudes from the posterolateral margin of the pterotic, which is joined ligamentously to the posttemporal and supracleithrum.

The parietal is a rectangular dermal bone on the dorsal surface of the skull (Fig. 2.9). It overlaps the supraoccipital and epiotic posteriorly, the sphenotic and pterotic laterally and is overlapped by the frontal anteriorly.

The exoccipital is a large endochondral bone that articulates with the basioccipital medially, pterotic laterally, epiotic dorsolaterally, supraoccipital dorsally and prootic anteriorly (Figs. 2.6 and 2.11). In ventral view, it forms the medial portion of the subtemporal fossa (Fig. 2.6). In posterior view, it forms the ventromedial wall of the posttemporal fossa (Fig. 2.11). The most prominent feature of the exoccipital is a bony ring that arches posteriorly and encloses a large lateral occipital foramen. The ring has a pointed process on its posterior margin directed towards the notch formed in the neural spine of the second Weberian vertebra. These rings converge posteromedially, almost touching to form a round, roughly triangular foramen magnum. The exoccipitals join medially to form the roof of the-cavum sinus impar and the floor of the foramen magnum (Fig. 2.11). The vagal foramina, seen ventrally, are very small. In posterior view, the exoccipital forms the base of a bulge formed by the semicircular canals that continue to the epiotic and terminate along the lateral margin of the supraoccipital.

The epiotic is a paired endochondral bone that articulates with the supraoccipital medially, exoccipital ventrally and parietal dorsally (Fig. 2.11). Its lamellae contribute to the lateral portion of the subtemporal fossa. In posterior view, it forms the dorsomedial wall of the posttemporal fossa. It has a prominent bulge formed by the semicircular canal along its posterior surface (Fig. 2.11). A laterally facing shelf is formed along the dorsolateral margin of this bulge for the posttemporal to articulate and form the roof of the posttemporal fossa (Fig. 2.11). A weak tubercle is also observed on the medial margin of the bulge.

The supraoccipital is a median endochondral bone that articulates epiotics laterally and exoccipitals ventrally (Fig. 2.11), while the parietals overlap its anterodorsal margin (Fig 2.9). In dorsal view, the supraoccipital has a triangular shape and is anteriorly convex and dorsomedially concave with a small sagittal crest. The supraoccipital forms the dorsal margin of the foramen magnum. Its posterolateral surface has a bulge formed by the semicircular canal on either side that terminates before the sagittal crest.

The intercalars are paired dermal ossifications. They are crescentic and lie along the posterior margin of the pterotic, close to the pterotic-exoccipital suture (Figs. 2.6 and 2.11). They are small in *Notropis hudsonius*.

2.3.2.4 Basicranial Region

The basioccipital is a single posteroventrally positioned element (Figs. 2.9 and 2.11). It articulates with the exoccipitals dorsally, prootics anteriorly and parasphenoid ventrally (Figs. 2.6 and 2.11). Posteriorly, it articulates with the first vertebral centrum. The pharyngeal process is found ventrally and is directed posteriorly (Fig. 2.7). It is laterally compressed, widens posteriorly and had an almost rectangular shape with a round posterior end that does not quite reach the os suspensorium. Anterior to the pharyngeal process is a concave, anteroventrally facing masticatory plate with squared, ventrolaterally projecting wings, a narrow posterior margin, and a notched anterior margin (Fig. 2.6). Dorsal to the plate are supporting arches that connect the pharyngeal process and plate to the ventrolateral portion of the basioccipital (Fig.

2.11). A large canal is formed between the arches. The anteroventral margin of the basioccipital is notched, forming a portion of the walls and roof of the posterior myodome. Two ventral lamellae extend over the anterior edge of the basioccipital and dorsal margins of the prootics (Fig. 2.6). These lamellae overlap the posterior end of the parasphenoid to create a ventral floor that helps to close the posterior myodome along with the parasphenoid. In one of the specimens examined, the ventral lamellae are absent, but this closure of the posterior myodome is still observed.

The parasphenoid is a single bone and the longest of the cranium. It can be divided into three parts. First is the anterior shaft, which passes between the left and right orbits and terminates dorsal to the vomer (Fig. 2.7). Second, are two dorsally directed ascending wings that suture to the anteromedial margins of the prootics and form the anterior margin of the foramen for the internal carotid artery. Third is the forked posterior end. The medial margins of the fork abut and create a portion of the roof of the closed posterior myodome (Fig. 2.6).

2.3.2.5 Branchial Apparatus

The pharyngobranchials are the dorsal most elements of the branchial apparatus (Fig. 2.12); there are only two pairs of pharyngobranchials, representing pharyngobranchials two and three. These are small bones with irregular edges. The second pharyngobranchial has a roughly subcircular shape and is joined by cartilage to the first epibranchial along its anterolateral margin and the second epibranchial along the posteromedial margin. The third pharyngobranchial is more elongate than the second, overlying a quarter of the posterodorsal end of the second pharyngobranchial, and is of similar width. Its median edge is sigmoidal, while the lateral edge is semicircular. In four of the branchial apparatuses examined, the medial edge has a deep notch (Fig. 2.13). The second and third pharyngobranchials are connected medially by cartilage. The posterolateral edge of the third pharyngobranchial is joined by cartilage to the third epibranchial, while its posterior edge joins to the fourth epibranchial, also by cartilage.

Four pairs of epibranchials are present, attaching to the ceratobranchials at their distal ends. All the epibranchials are slightly concave dorsally and have a shallow notch and a posteriorly projecting uncinate process along the posterior margin. The first three epibranchials are constricted towards their dorsal ends next to the uncinate process. The first epibranchial is narrower than the second or third, and its anterior margin is gently convex. Its posterior notch and uncinate process are weakly developed. The second epibranchial has a straight anterior margin, with a better-developed posterior notch and uncinate process. The third epibranchial is shorter than the first and second epibranchials. Its distal end is wider than its proximal end, with a pronounced posterior notch and a long, slender, uncinate process that overlaps the fourth epibranchial. A thin, broad process is found on the dorsal surface of the third epibranchial, originating lateral to the uncinate process. In four of the branchial apparatuses examined, this dorsal process is present on only one side. The fourth epibranchial is more slender than the others, and its distal end is narrower. A thin, medially directed dorsal process of varied size and position can sometimes be found in close proximity to the uncinate process of the third epibranchial (Fig. 2.14). This dorsal process was seen on only one epibranchial in 11 of the examined specimens and was either present on both or entirely absent in six. The uncinate process of the fourth epibranchial is broad, flat and round, positioned closer to the distal end, and directed posterodorsally. Unlike the other epibranchials, it is constricted in the middle.

The ceratobranchials are the largest elements of the gill arches. The first four are ventrally concave, narrow and elongate, contacting their respective epibranchials at their distal ends. The first ceratobranchial is the longest, while the second, third and fourth ceratobranchials get progressively shorter. The proximal end is narrower than the distal end for the first and third ceratobranchials and wider for the second ceratobranchial. Both ends are equal for the fourth ceratobranchial. The proximal portion of the first ceratobranchial is slightly constricted for about one-third of the bone before widening distally.

The pharyngeal teeth are supported on the fifth ceratobranchial (Fig. 2.15). This bone can be divided into two limbs: the anterior (ventral) limb and the ascending (posterior) limb. The anterior limb runs parallel to the other ceratobranchials but is more ventrally positioned. When viewed laterally, the anterior limb narrows anteriorly into a blunt point with a ventral flange that runs along the lateral margin and tapers ventrally. The ascending limb is broader and curves dorsally. The two limbs meet in an acute, blunt anterior angle,. The ascending limb is weakly arched, with a weak, undeveloped posterior angle. In one set of pharyngeal arches examined, the anterior angle of the ascending limb was broad and round (Fig. 2.16).

The pharyngeal teeth are long and conical with hooked ends. The majority of specimens had a dental formula of 1,4-4,1 (Table 2.3), which was counted on 25 of the sets of ceratobranchial arches. The most common dental formula that deviated from 1,4-4,1 was 2,4-4,2 (five sets) followed by 0,4-4,0 and 2,4-4,1 (both four sets) and 1,4-4,0 (three sets). The formulae

1,4-4,2 and 0,3-4,0 were observed only once each. In one of the sets examined, there appeared to be three rows of teeth instead of two on the left arch. However, this is likely due to a failure of some functional teeth, in this case, the first and fourth tooth on the major row, to fall out when its replacement ankylosed with the arch (Evans and Deubler, 1955).

Three pairs of nodular, irregularly shaped bones, the hypobranchials, are located between the first three ceratobranchials and basibranchials. The first pair is the largest, followed by the second and third. The first and second pairs have short, blunt ventral processes. The third pair of hypobranchials have a set of long, slender ventral processes that hook out anteriorly.

The three basibranchials are unpaired bones found along the midline of the branchial apparatus. The first basibranchial is the shortest and tapers posteriorly in dorsal view. In lateral view, it has a triangular shape and a constricted anterior end. A notch on either side at the midsection of the bone accommodates the articulation of the first pair of hypobranchials. The second and third basibranchials are rod-shaped. The second basibranchial is constricted in the middle, and the anterior and posterior ends are equal in width. The third basibranchial is the longest and slender, tapering posteriorly.

The basihyal is a long, unpaired bone and the anteriormost element of the branchial apparatus. It curves up dorsally and has an anterior cartilaginous tip. The deepest point of the curve is towards the anterior end, about one-third of the way down, with a ventral ridge. The posterior end of the basihyal articulates with the first basibranchial and has two tubercles on either side for ligaments to anchor it to the ventral hypohyals. The shaft of the basihyal narrows posteriorly. The posterior end is bulbous and wider than the narrowest point of the bone but still narrower than the anterior portion.

In one of the branchial apparatuses I examined (MZF 680), there are four basibranchials instead of three (Fig. 2.13). In this specimen, the fourth, posterior-most basibranchial is the longest, followed by the second, third and first. The hypobranchials lie between the first and second, third, and fourth basibranchials and at the end of the fourth basibranchial. The first basibranchial is essentially the same as described above. The second basibranchial is widest at the anterior end, tapering posteriorly. The anterior and posterior ends of the third basibranchial are equal, and the middle is constricted. The fourth basibranchial is uniform in overall shape, and the anterior end is slightly wider.

2.3.2.6 Hyoid Region

The interhyal is a small, cylindrical bone that attaches to the medial surface of the hyomandibula-symplectic junction with cartilage at one end, with the other articulating in a divot found on the posterodorsal margin of the posterior ceratohyal (Fig 2.17).

The posterior ceratohyal (Fig. 2.18) is triangular. It has two superficial foramina on its dorsal edge that are connected under a bridge of bone. The anterior opening is larger than the posterior opening. Posterior to the foramina is a notch where the interhyal articulates. This notch is noticeably deeper in five of the specimens examined (Fig 2.17).

The anterior ceratohyal is widest at its edge that contacts the posterior ceratohyal. It is tapered in the middle, then widens into a slightly twisted head at its anterior end. The anterodorsal portion articulates with the dorsal hypohyal, while the anteroventral portion articulates with the ventral hypohyal. A small notch is found on the medial side at the narrowest point of the anterior ceratohyal where the anteriormost branchiostegal ray articulates.

The ventral hypohyal is larger than the dorsal hypohyal. The dorsal hypohyal is an angular bone articulating with the ventral and the anterior ceratohyal along its ventral surface. The posterior portion of the basihyal rests between the right and left dorsal hypohyals and is ligamentously attached to each element. A tubercle is observed along the dorsomedial margin of the dorsal hypohyal. The ventral hypohyal is triangular, articulating with the anterior ceratohyal and dorsal hypohyal. A small tubercle is observed on its anterolateral surface.

The anterior ceratohyal and the dorsal and ventral hypohyals variably form the hypohyal foramen (Fig. 2.19). In 18 of the hyoid bars examined, the hypohyal foramen is encompassed within the dorsal and ventral hypohyals, but the anterior ceratohyal does not contribute. In 26 rest of the hyoid bars examined, the hypohyal foramen is formed by all three elements, giving the anterior ceratohyal a shallowly forked appearance. In two of the hyoid bars examined, the hypohyal foramen is encompassed only within the ventral hypohyal.

The three branchiostegal rays (Fig. 2.18) are all similar in shape. The first branchiostegal is the smallest and slenderest, tapering anteriorly into a short, blunt head that articulates with the medial surface of the anterior ceratohyal. In 16 of the hyoid bars examined, the head is elongate. The base ventral to this head is expanded with a broad, round anterior margin, the clupeoid projection (McAllister, 1968). The heads of the second and third branchiostegals are much broader than the first, while the head of the second branchiostegal is the largest. The second branchiostegal articulates with the lateral side of the anterior ceratohyal, while the third articulates with the lateral side of the posterior ceratohyal. The third branchiostegal ray is the broadest.

The urohyal has two horizontal ventral wings and a single vertical dorsal wing. All three wings taper together anteriorly into a constricted, cylindrical neck, bifurcating into two processes separated by a distinct notch. These processes attach to the ventral hypohyals via ligaments. In 27 of the hyoid bars examined, the dorsal wing is slightly longer than the ventral wings and has a broad, semicircular posterior margin (Fig. 2.20). In 19 of the hyoid bars examined, the ventral wings are longer than the dorsal wings, and the dorsal wing itself has a triangular shape with a round posterodorsal corner (Fig 2.21). One urohyal has a distinct shape: the ventral wings were much longer than the dorsal wing, and the posterior margin of the dorsal wing was almost straight (Fig 2.22)

2.3.2.7 Opercular Series

Four bones make up the opercular series (Fig. 2.23). The opercle is the largest bone. It is concave medially and the anterodorsal corner is drawn into a short, blunt arm, the opercular process, that overlaps the posterior margin of the hyomandibula. The anteroventral edge of the opercle is convex and is overlapped by the preopercle. The anterodorsal edge is shallowly concave and shorter than the posteroventral edge. The posterodorsal edge is also sigmoidal with a distinct posterodorsal corner. The opercular facet is found just beneath the anterodorsal process on the lateral side. It is a deep socket that joins the opercle to the hyomandibular.

The subopercle is crescentic with a straight, anterodorsal edge while the posteroventral edge is convex. The anterodorsal corner of the subopercle, is drawn into a short anterodorsal process that articulates with the medial side of the interopercle. The branchiostegal rays lie along the medial side of the subopercle when they are at rest.

The interopercle is a wedge-shaped bone with a concave dorsal margin that underlies the preopercle. The posterior margin of the interopercle is convex. The interopercle is widest at its posterior end, tapering anteriorly into a fine point that ligamentously attaches to the retroarticular. Medially, it contacts the interhyal and posterior ceratohyal, overlapping dorsolateral margin of the interopercle.

The preopercle is a curved bone with distinct vertical and horizontal limbs; the vertical limb is slightly longer. The hyomandibula-symplectic-interhyal junction lies along the lateral margin of the vertical limb. The posterior flange of the hyomandibula overlaps the anterodorsal margin of the vertical limb. The anterodorsal margin of the horizontal limb articulates underneath the ventral groove of the quadrate.

2.3.2.8 Suspensorium

The hyomandibula (Fig. 2.23) is the posterior-most element of the suspensorium. It is widest at its dorsal end, forming a head with anterior and posterior condyles, which articulate with the skull in corresponding anterior and posterior fossae formed by the sphenotic, pterosphenoid and prootic. The hyomandibula tapers ventrally, ending in a cartilaginous cap that articulates and forms a junction with the metapterygoid, symplectic and interhyal. The anteroventral margin of the hyomandibula articulates with the metapterygoid at two points, the ventral point being part of the junction with the symplectic and interhyal, and the dorsal point articulating with the hyomandibula just ventral to the termination of the anterior wing. The anterior wing originates at the anterior margin of the head of the hyomandibula and extends roughly two-thirds of the length of the bone. In 17 of the suspensoria examined, the anterior wing is constricted towards the ventral end and drawn into a distinct anteroventral point (Fig. 2.24). The posterior wing starts below the posterior margin of the head and terminates towards the ventral end of the bone, overlapping the vertical arm of the preopercle. The opercular condyle protrudes posteriorly, articulating with the opercle. In four of the specimens examined, a weak adductor ridge is present at the level of the opercular condyle (Fig. 2.24), while in one, the adductor ridge is developed into a distinct flange.

The symplectic (Fig. 2.23) is a compressed, rod-shaped, dorsally curved bone with round cartilaginous anteroventral and posterodorsal ends. The posterodorsal end is part of the hyomandibula-symplectic-interhyal junction. The dorsal edge of the anteroventral end inserts beneath a groove formed by the quadrate. Usually, the dorsal edge of the symplectic is separate does not articulate with the metapterygoid. However, in 19 of the suspensoria examined, the dorsal edge of the symplectic does articulate with the metapterygoid.

The metapterygoid is a broad bone that curves dorsomedially. It typically overlaps the anterior margin of the endopterygoid completely (Figs 2.23 and 2.25). In 11 of the suspensoria examined, the metapterygoid partially overlaps the endopterygoid, covering only the posteroventral corner (Fig. 2.26). The posterior margin of the metapterygoid has two distinct cartilaginous heads. The smaller one articulates with the junction formed by the symplectic, hyomandibula and interhyal, while the larger one articulates with the anterior margin of the hyomandibula. The dorsal edge is concave, while the anterodorsal corner is drawn into a process that is level with the dorsal edge of the ectopterygoid. The anterodorsal process typically has a broad, square shape (Fig. 2.25). In seven of the suspensoria examined, the anterodorsal process has a round shape (Fig. 2.26), while in another seven, the anterodorsal process has a thin, pointed shape (Fig. 2.27). In one specimen, the anterodorsal process is indistinct (Fig. 2.23). A weakly developed process is found at the posterodorsal corner of the metapterygoid.

The quadrate has a dorsal semicircular blade whose anterior and dorsal margins overlap the ectopterygoid and endopterygoid (Fig. 2.23). The anteroventral corner forms a round condyle that articulates with the anguloarticular. Ventral to the blade is a long, ventrally grooved posterior process that accommodates the symplectic and articulates with the dorsal edge of the horizontal limb of the preopercle (Fig. 2.23). The ventral base of the quadrate has a medially placed fossa.

The endopterygoid is larger than the metapterygoid. It curves medially. The lateral side of is overlapped by the ectopterygoid anteriorly, the quadrate ventrally and the metapterygoid posteriorly (Fig. 2.23). The anterodorsal corner of the endopterygoid has a socket that articulates with the posterior end of the palatine. Dorsal to the facet is a pointed, medially directed anterior process extending over the palatine. Another ventrally placed socket is present posterior to this process, which accommodates the posterior margin of the lateral ethmoid. In one specimen, the anterior process is reduced and rudimentary. A flange forms the lateral margin of this socket and extends posteroventrally along the lateral side of the endopterygoid. The dorsal edge of the endopterygoid is roughly straight, and the posterior edge aligns with the posterior most corner of the quadrate blade (Fig. 2.23).

The ectopterygoid overlaps the endopterygoid along its dorsomedial margin and is overlapped by the quadrate posterolaterally. It has a roughly oval shape. (Fig. 2.23)

The palatine is the anterior-most bone of the suspensorium. Its shaft is cylindrical, and its posterior end has a cartilaginous cap that articulates with the endopterygoid. A dorsolateral tubercle is positioned just anterior to the cartilaginous cap. The anterior end trifurcates into three processes directed dorsally, ventrally and laterally (Figs. 2.5 and 2.23). The dorsal process is on the medial margin, and narrows into a long, fine, dorsally directed tip. The ventral process is also medially positioned and is shorter and broader than the dorsal process, with a pointed shape. The dorsal and ventral processes form a deep groove over the posterolateral portion of the preethmoid. The lateral process is laterally positioned and drawn into a broad, flat, wing that braces against the rostral process of the premaxilla.

2.3.2.9 Oral Jaws

The dentary (Fig. 2.23) is the largest bone of the lower jaw. Its anterior end curves medially to meet with its opposite. Its posterodorsal margin broadens into the flat, round, coronoid process. In nine sets of oral jaws examined, the coronoid process is narrower and more elongate than in the others (Fig. 2.28). The posterior margin of the dentary tapers to a point that terminates anterior to the retroarticular. The anteromedial margin is fused to the mentomeckelian, an ossification at the anterior end of the Meckel's cartilage. The entire anterior end of the anguloarticular slots into the posterior end of the dentary, with the Meckel's cartilage overlying the medial surfaces of both elements (Fig. 2.23).

The anguloarticular (Fig. 2.23) articulates with the retroarticular along its ventral margin. It has a deep socket at its posterior end, where the quadrate articulates. The posteroventral corner forms a blunt posterior process that extends under the anteroventral margin of the quadrate. The retroarticular is a small bone articulating with the anguloarticular along its dorsal margin. It has an irregular, elongate shape.

The coronomeckelian is found on the medial margin of the anguloarticular (Fig. 2.23). It is the extension of the ossification of the posterior end of the Meckel's cartilage. The coronomeckelian has a deep anterior notch and a central, medially directed flange.

The premaxilla is slender, laterally curved and L-shaped bone. It forms the entire gape of the upper jaw. A long, posteriorly concave ascending process contacts its opposite in the midline. The ascending process is broad at the base and tapers into a blunt point. The premaxilla tapers posteriorly into a laterally flattened shaft with a round end that curves ventrally.

The maxilla (Fig. 2.23) is a laterally curved bone that overlaps and supports the premaxilla, acting as a lever to push the premaxilla as the mouth opens. The anterior end of the maxilla has two processes: the premaxillary process and the rostral process posterior to it (Fig. 2.5). The premaxillary process is short, flat and curves medially, overlapping the ascending process of the premaxilla when the mouth is closed. The rostral process is long and hook-like, and curves in medially where it is ligamentously joined to its opposite. Posterior to the rostral and premaxillary processes are two condyles, which serve as pivot points about which the maxilla rotates. When the mouth opens, the medial condyle braces against the preethmoid, while the lateral condyle braces against the lateral process of the palatine (not illustrated in Figure 2.5). A small, pointed tubercle is observed along the anterolateral margin of the maxilla, just posterior to the premaxillary process for the insertion of the adductor mandibulae. Posterior to the premaxillary process, the dorsal margin of the maxilla is deeply notched, creating a neck that leads to the ascending process. The ascending process of the maxilla is broad and flat with a round and anterodorsally oriented corner (Fig. 2.28). In 11 of the oral jaws examined, the ascending process is squared and drawn into a distinct, anterodorsal point (Fig. 2.28). In two sets of oral jaws examined, the ascending process is broadened and rectangular, while in one, the ascending process is broad and round with a hooked anterodorsal corner. The posterior end of the maxilla tapers into a blunt end with a round posterior flange on the ventral margin. This posterior flange is overlapped by the posterior end of the premaxilla.

The kinethmoid (Fig. 2.29) is a single, median endochondral element. When the mouth is closed, it lies between the maxillae, posterior to the premaxillae and anterior to the ethmoid block. The kinethmoid is roughly three times as tall as it is wide. The kinethmoid is constricted between dorsal and ventral portions. The dorsal portion of the kinethmoid is forked and curves anteriorly while the ventral portion has a laterally positioned tubercle on either side and a posteriorly placed fossa that leads into a single, blunted, anteriorly positioned ventral process.

2.3.2.10 Circumorbital Series

The circumorbital series surround the eye and include the supraorbital and the five infraorbitals. The supraorbital is an ovular, dorsally curved element that lies along the dorsal margin of the eye (Figs. 2.6 and 2.9). Its medial margin is convex, and its lateral margin is straight. In dorsal view, it is widest in the middle, narrowing posteriorly into a blunted end (Fig. 2.9)

The infraorbitals are a series of five flat, plate-like bones that surround the ventral and posterior margin of the orbit (Fig. 2.30). The lacrimal is the first and largest element of the infraorbital series. It covers part of the nasal capsule and maxilla and is braced by the palatine. It is roughly as tall as it is wide, with five edges: dorsal, orbital, ventral, posterior and anterior. Overall, the lacrimal is roughly squared, but round anteriorly. In 14 of the specimens examined, the anterior edge is deepened. The ventral edge is convex and longer than the anterior edge. The posterior edge is short, abutting the second infraorbital

The second infraorbital is elongate. The third infraorbital is longer and broader than the second, with a curved, crescentic shape. The fourth infraorbital lies along the posterior edge of the orbit and overlaps the anterior portion of the hyomandibula. The fifth infraorbital, or dermosphenotic (Coburn, 1982), overlies the sphenotic spine and is reduced to a bony tube.

2.3.2.11 Sensory Canal System

The sensory canals extend along and are present on some bones of the skull, oral jaws, opercular series and circumorbital series (Fig. 2.30). The supraorbital canal extend through the nasal and is enclosed in the frontal, extending along the dorsal margin of the orbit. The nasal portion usually has three pores, and the total number of pores is typically eight, but numbers nine in five specimens (Table 2.4). However, in three specimens, all from the same sample (MZF 2506), the nasal portion was absent, and the supraorbital portion had only six pores. The postocular commissure, sometimes called the lateral temporal canal (Coburn, 1982), is enclosed in the pterotic and has a single pore. In one specimen, there is two pores instead of one (Table 2.4).

The supratemporal canal is present along the posteromedial margin of the parietal, extends to the pterotic and always has three pores. The preopercular mandibular canal is enclosed in and extends along the dentary, anguloarticular and preopercle. It typically has ten pores, four from the dentary portion and six along the preopercular portion. The total number can be as low as nine (four specimens) and as high as 11(five specimens) (Table 2.4). Pores along the dentary portion were observed to be as low as three (one specimen) and up to five (two specimens), and pores along the preopercular portion range from as low as five (four specimens) to as high as seven (four specimens) (Table 2.4).

The infraorbital extends along the infraorbital series. There are typically seven pores: four on the lacrimal, one on the second infraorbital and two on the third infraorbital. The number of infraorbital pores can be as low as six (one specimen) and as high as eight (two specimens) (Table 2.4). One specimen has three pores on the lacrimal instead of four, while two specimens have three pores on the third infraorbital instead of the usual two.

2.3.2.12 Weberian Apparatus

The Weberian apparatus (Fig. 2.31) can be divided into two components: the pars sustentaculum and the pars auditum (Coburn, 1982; Bird and Hernandez, 2007; Bird et al., 2020). The pars sustentaculum is derived from the first four vertebrae, which have been modified to support the four Weberian ossicles, which form the pars auditum (Coburn, 1982).

2.3.2.12.1 Pars sustentaculum

The first vertebra is a centrum with a transverse process on either side projecting horizontally from the ventrolateral surface. The anterior face of the centrum articulates with the basioccipital.

The second vertebra is slightly smaller than the first. It has an amphicoelous centrum with large, blade-like transverse processes that project anterolaterally and extend under the anterior end of the transverse process of the first vertebrae. Its neural arch is modified into a saddle-shaped element that curves over the neural canal and has an anterior notch that the exoccipital fits into.

The third vertebra is the largest of the pars sustentaculum. It has an amphicoelous centrum with a small ventral lip that projects under the second vertebrae. The posterolateral surface is grooved to support the foot of the tripus. This groove is directed posterodorsally and develops into a ridge that extends slightly beyond the centrum. The neural arch is modified and can be broken down into three components. First is the base, which rests on the dorsal surface of the centrum. It is broader than the neck but narrower than the dorsal flange. The second is the neck, which is constricted and has its own expanded flange at its base. Third, the dorsal flange extends over the second vertebra, articulating anteriorly with the second neural arch, with the neural complex dorsally, and with the fourth neural arch posteriorly.

The neural complex comprises a broad base, a constricted neck and a divided dorsal crest. The base of the neural complex articulates with the second neural arch anteriorly, the third neural arch ventrally, and the fourth neural spine posteriorly. The crest of the neural complex extends dorsally over the second vertebral centrum and the posterior portion of the second neural arch. In 20 of the Weberian apparatuses examined, the dorsal crest is elongate, projecting over more than half of the second neural arch. The double crest of the neural complex is reduced and shortened in 10 of the Weberian apparatuses examined.

Five flat predorsal bones lie dorsal to vertebrae 3 to 9. They are all irregularly shaped and become smaller posteriorly. The first predorsal bone lies dorsal to the third, fourth and fifth vertebrae, above the dorsal crest of the neural complex. The second predorsal bone is found above the sixth vertebra, the third is found above the seventh, the fourth is found above the eighth, and the fifth is found above the ninth. In five of the Weberian apparatuses examined, the first predorsal bone fit between the left and right sides of the double crest of the neural complex (Fig. 2.32).

The fourth vertebrae has an amphicoelous centrum with a modified neural arch and neural spine. The neural arch is autogenous with an expanded base and a deep, lateral groove that penetrates towards the base. It articulates with the third neural arch anteriorly, and the neural complex dorsally. The neural spine is shorter than those of the succeeding vertebrae and is directed anteriorly. The fourth vertebral centrum supports the os suspensorium, which comprises two arms. The outer arm is autogenous of the vertebral centrum and articulates with the fourth vertebral centrum via an expanded head, widens posterolaterally, before tapering back anteriorly. The posterior most corner of the outer arm lies under the fifth rib. The inner arm of the os suspensorium is fused to the medial margin of the outer arm. It starts with a broad base that tapers and curves in medially, running in parallel, but not articulating with, its opposite. The fifth vertebrae is much like the other post-Weberian vertebrae and differs only in its larger parapohysis and a thicker rib.

2.3.2.12.2 Pars auditum

The claustrum lies dorsal to the first vertebra and is overlapped by the scaphium laterally. The claustrum can be divided into a lower facet and an upper crest. The upper crest has a triangular shape, and the posterior edge is connected to the anteroventral edge of the second neural arch.

The scaphium rests along the posterolateral region of the first vertebra. It comprises a 'cupped' portion and separate, posteriorly placed dorsal and ventral processes. The cupped portion is the largest, with the opening on the medial side and a small tubercle on the middle of the lateral side. The dorsal process is dorsally directed with a thin, pointed end. The ventral process is anteriorly directed, is shorter than the ascending arm and attaches cartilageously to the first vertebral centrum.

The intercalarium is a Y-shaped ossicle with a single anterior arm and posterior articulating and ascending processes. The anterior arm is blunted, curving anterodorsally and positioned lateral to the scaphium. The posterior end branches into the ascending and articulating processes. The ascending process is the longer of the two and is directed dorsally. The articulating arm is directed ventrally and articulates with the lateral surface of the second vertebral centrum.

The tripus is the largest Weberian ossicle. It has a dorsally concave shape. The tripus can be divided into a body with anterior and posterior arms. The body is triangular with a posterodorsally directed process. The tripus is positioned along the lateral side of the third vertebral centrum. The arms of the tripus are flattened. The anterior arm is shorter and broader, curving dorsomedially and terminating dorsal to the transverse process of the second vertebra and lateral to the anterior end of the intercalarium, to which it is ligamentously connected. A dorsal ridge originates from the medial edge of the anterior arm and runs dorsomedially to meet the dorsoposterior corner of the body. This ridge is absent in two of the Weberian apparatuses examined. The posterior arm runs posteroventrally, curling in medially and terminating between the inner and outer arms of the os suspensorium, connecting to the swim bladder.

2.3.2.13 Pectoral Girdle

The posttemporal is a flat element that overlaps the supracleithrum ventrally. It is roughly tear-dropped shaped, narrowing dorsally into a pointed end (Figs. 2.33 and 2.35). Its anterodorsal margin contacts the pterotic, forming much of the roof and lateral margin of the posttemporal fossa.

The supracleithrum is a flat element overlapped by the posttemporal dorsally and overlapping the cleithrum ventrally (Figs. 2.33 and 2.34). The dorsal margin has a blunt, hooked dorsal process. In five of the pectoral girdles examined, the dorsal process was straight, lacking the hook. The supracleithrum is widest at the base of the dorsal process and tapers into a blunt, round, ventral end. The posterodorsal corner of the opercle overlaps the anterodorsal margin of the supracleithrum.

The cleithrum is the largest bone of the pectoral girdle, with a vertical and horizontal limb of equal length that meet at an obtuse angle (Fig. 2.33). The anterior margin of the horizontal limb meets its opposite in the midline. The midpoint of the horizontal limb is narrowed, while the anterior and posterior margins broaden, and both articulate with the coracoid medially to create a large foramen. A distinct ridge runs along the medial surface of the horizontal limb, tapering posteriorly and terminating at the base of the vertical limb. When viewed dorsally, the anterolateral edge of the horizontal limb is shallowly concave (Fig 2.35). The vertical limb of the cleithrum consisted of a broad, triangular, lateral plate that starts along the anterior end of the horizontal limb and terminates at the end of the vertical limb in a blunt spine, and a medial ridge that widens dorsally and terminates into a moderately developed flange just before the dorsal spine of the lateral plate (Figs. 2.33 and 2.34). The lateral plate of the vertical limb articulates with the lateral margin of the scapula, while the mesocoracoid articulates with the anterior margin of the medial ridge (Fig.2.34).

The coracoid widens posteriorly, articulating with the cleithrum at its anterior and posterior ends, forming sutures. The posterior point of articulation is larger than the anterior. Where it articulates with the cleithrum, a large, foramen is formed. The posterior end of the coracoid articulates with the scapula, while the posteromedial margin forms a bony shelf that articulates with the mesocoracoid. In one specimen, a unique pathology is observed in which the cleithrum and coracoid together a second, anteriorly placed foramen (Fig. 2.36) .

The mesocoracoid (Fig. 2.34) is a triangular element that narrows dorsally. Its ventral margin articulates with the scapula posteriorly and the coracoid anteriorly. It has a round process along the anterodorsal margin that articulates with the median ridge of the ascending arm of the cleithrum.

The scapular foramen is large and positioned anterodorsally. In one of the pectoral girdles examined, the scapular foramen of the left scapula is divided into two by a bony strut (Fig. 2.37). The dorsal margin of the scapula is round, articulating with the medial surface of the cleithrum. The posterior edge has a facet that articulates with the first pectoral fin ray. The posterodorsal corner of the scapula is developed into a weak, round flange that articulates with the medial surface of the cleithrum. In three of the pectoral girdles examined, the posterodorsal flange was strongly developed.

A total of four radials support the rays of the pectoral fin. Counting dorsal to ventral, the first (dorsal most), radial is the shortest. It has a round shape, and overlaps the posterolateral margin of the scapula. The second radial is broad and slightly shorter than the first and overlaps the medial margin of the scapula. The third radial is the longest, while the fourth is the thinnest.

In about 11 of the pectoral girdles I examined, there was complete fusion of the cleithrum, scapula, coracoid and mesocoracoid into a single element (Figs. 2.38 and 2.39).These specimens, including the one that remained unfused, also have an enlarged dorsal flange on the medial ridge of the cleithrum (Fig. 2.39). The dorsal spine of the lateral plate of the cleithrum was also noticeably shortened in these specimens (Fig. 2.39).

2.3.2.14 Pelvic Girdle

The pelvic girdle (Figs. 2.40 and 2.41) consists of two basipterygia that are joined by cartilage along their medial edges. Both basipterygia are dorsally concave and have forked anterior ends, producing two anteriorly projecting processes. The lateral process is longer and narrower than the medial process. In dorsal view, two shallow ridges run along the lateral and medial processes. The ridge of the lateral process extends farther up its length. A round tuberosity is observed at the base of the ridge of the medial process. When viewed ventrally, a weak tuberosity is observed at the posterior end of each basipterygia.

Each basipterygium has a broad, blunt, laterally curving ischiac process found posterior to the point where the left and right sides are joined. Three radials support the rays of each pelvic fin. The medial-most radial is a large, hooked element that curves medially and has an expanded base that is overlapped by the basipterygia ventrally. The middle and lateral radials are smaller, articulating along the posterolateral margin of the basipterygium. The lateral radial is larger than the middle radial.

2.3.2.15 Caudal Skeleton

As with other cyprinoids, the last four vertebrae of *Notropis hudsonius* (Fig. 2.42) support the rays of the caudal fin (Buhan, 1972). The first preural vertebra is the compound centrum which supports an epural, uroneural, pleurostyle, six hypurals and a parhypural. The compound centrum has a single, blunt, short neural spine. In one of the caudal skeletons examined, there are two neural spines on the compound centrum (Fig. 2.43). The following three vertebrae are preural centra, each with a single neural and hemal spine. In seven of the caudal skeletons examined, there are two neural spines on the second preural centrum (Fig. 2.44), while in three more caudal skeletons, there were two neural spines on the third preural centrum. In one caudal skeleton, there were two hemal spines on the third preural centrum while in another, the neural spine of the second preural centrum was divided distally (Fig. 2.45). In another specimen, the neural spines of the second and third preural centra are fused together at the base (Fig. 2.46).

In one specimen, the third and fourth preural centra appears to be fused together, giving the appearance of an enlarged vertebra with two neural and hemal spines (Fig. 2.47).

The elements supporting the rays of the lower lobe of the caudal fin are comprised of the hemal spines of the second, third and fourth preural centra, the parhypural and the first and second hypurals. The hemal spine of the second preural centrum is autogenous. The parhypural and first hypural are fused together proximally and are together separate from the compound centrum. In 16 of the caudal skeletons examined, the parhypural and first hypural were partly fused together proximally (Fig. 2.48), while the parhypural and first hypural abutted but were not fused (Fig. 2.47) in eight. The first hypural has a thin, tapered base and widens distally. The parhypural bears a hypurapophysis. The second hypural is roughly rectangular and fused to the compound centrum. The hypurals and parhypural support the principal rays of the lower lobe of the caudal fin, while the ventral procurrent rays are supported by the hemal spines of the second, third and fourth preural vertebrae.

The elements supporting the rays of the upper lobe of the caudal fin are comprised of the neural spines of the three preural centra plus the epural, pleurostyle, uroneurals and the third, fourth, fifth and sixth hypurals, with the sixth hypural always being the smallest. In one specimen, the sixth hypural is absent and the fifth hypural is enlarged (Fig. 2.49). The epural is a slender, elongate element that is almost always unfused to the compound centrum. In four of the caudal skeletons examined, the epural abutted but did not fuse with the compound centrum. In another two, the epural was fused to the compound centrum (Fig. 2.49). The pleurostyle is broad and roughly squared, and is firmly fused to the compound centrum. The uroneural is slender, and is longer than the sixth hypural. The hypurals support the principal rays of the upper lobe, while the procurrent rays are supported by the uroneurals, epural, and neural spines of the second, third and fourth preural vertebrae. There are consistently 19 caudal fin rays, 10 in the upper lobe and 9 in the lower lobe.

2.4 Discussion

2.4.1 Measurements, Meristics and Statistical Analysis

There is large degree of variation in the measurements and corresponding proportions for the *Notropis hudsonius* specimens used in this study. This variability can be observed both within and between *N. hudsonius* populations. In some samples, (UAMZ 213, 214, 220 and 1525) there is a high degree of variability in measurements relating to population-level variability in peduncle length, predorsal length and body depth. In the results of the PCA conducted on these measurements, the variability within these samples is particularly notable along PC1 and PC3. When PC1 and PC2 are plotted against each other in a PCA plot, four samples, one from central Alberta, one from Ontario, and two from Manitoba (UAMZ F9126, MZF 680,2506 and 2507) group together along the lower ends of both principal components. These samples all have similar proportional body depth as well as preanal, predorsal and prepelvic lengths, which, in comparison to the other *N. hudsonius* specimens examined are generally lower. The results of this PCA also suggest that overall, there is some degree morphometric divergence between western *N. hudsonius* populations in Alberta and the Northwest Territories, and eastern populations in Manitoba and Ontario. However, the results also suggest that there can be a large degree of morphometric variation within populations as well.

Of the meristic counts taken on the *Notropis hudsonius* specimens used in this study, the lateral line, predorsal scales and postdorsal scales had, by far, the largest ranges. The Circumferential scale count likewise has a larger range than most other meristic counts. The lateral line scale count of *N. hudsonius* has been reported to range from 38 to 42 (Scott and Crossman, 1973), 36 to 42 (Page and Burr, 2011) and 36 to 40 (Nelson and Paetz, 1992). However, the range of lateral line scales reported in this study (35 to 43), is still unprecedented. Overall, the lateral line scale can count vary as much within populations as it does between them. For example, in two samples, the lateral line scale count varied from 36 to 43 (UAMZ 214) and 37 to 42 (UMAZ 3215). Critically, there is no clear regional distinction between eastern populations in Manitoba and Ontario, and western populations in Alberta and the Northwest Territories. A similar pattern is observed with respect to the circumferential, predorsal and post dorsal scale counts, reflecting a high degree of variability both between and within *N. hudsonius* populations. The range and frequency of the other meristic counts are generally follow the observations of past researchers (Scott and Crossman, 1973; Nelson and Paetz, 1992). However, the gill raker counts that I took typically ranged from three to six, contrasting the range reported by Nelson and Paetz (1992) (four to nine). In one sample (UAMZ 1525) a single specimen had no gill rakers at all.

2.4.2 Intraspecific Osteological Variation of *Notropis hudsonius*

From this study, it is clear that *Notropis hudsonius* shows a high degree of osteological variability. With the exception of the pelvic girdle, I observed some form of intraspecific variation in all regions examined, though to varying degrees. I observed variations in the sensory canal system, hyoid bar, branchial apparatus, pectoral girdle, oral jaws, suspensorium, opercular series, Weberian apparatus, skull, infraorbital series and caudal skeleton.

For the most part, the sensory canal system of *Notropis hudsonius* is in agreement with the descriptions of both Illick (1956) and Coburn (1982) in regards to both structure and pore count (Table 2.3). However, the specimens from one sample (MZF 2506) showed a slight reduction in the sensory canal system, specifically in the supraorbital and infraorbital canals. In all three specimens examined, the nasal portion of the infraorbital canal and the nasal bones themselves were absent. In one specimen, the infraorbital pore count was also reduced, with three lacrimal pores instead of the usual four. A reduction in the sensory canal system has been reported for other *Notropis* (s.l.) species as an adaptation to calm, low-turbidity environments (Reno, 1966; Swift, 1970). This reduction is often observed in the supraorbital and infraorbital canals, as seen here. However, when the supraorbital canal is reduced, the nasal portion is retained in these other species (Reno, 1966; Swift, 1970), contrary to what I observed with these *Notropis hudsonius* specimens, which were sampled from a lake environment. However, I did not see the same sensory reduction in specimens from other lakes. The loss of the nasal portion of the supraorbital canal is a phenomenon that will require further study.

The positioning of the hypohyal foramen and the shape of urohyal are both variable in *Notropis hudsonius*. Uyeno (1961) used the positioning of the hypohyal foramen, relative to the hypohyals and anterior ceratohyal as a systematic character to distinguish different cyprinoid genera. The position and shape of the hypohyal foramen have also been featured in the descriptions of notropin species and genera (Coburn, 1982; Mayden, 1989) and in phylogenetic studies of North American cyprinoids (Coburn and Cavender, 1992). However, my analysis of *Notropis hudsonius* suggests that the exact position of the hypohyal foramen is variable. While it is usually formed by the anterior ceratohyals and the dorsal and ventral hypohyals, it is also restricted to the last two elements represents a sizable minority, being observed in 18 of the 46 sets of hyoid bars examined . Rarely, the hypohyal foramen is formed only by the ventral hypohyal. Both character states are found in specimens from western and eastern populations. I frequently noted both character states in specimens from the same sample. The position of the hypohyal foramen is clearly variable within *N. hudsonius*. This variability should be considered when analyzing other notropin species.

The urohyal shows two distinct variants in regard to overall shape and wing proportion. One of these variants, in which the dorsal wing has a rounded, semicircular posterior edge that extends beyond the ventral wings, was observed only in specimens sampled from Alberta and the Northwest Territories. The other variant, where the dorsal wing is triangular and shorter than the ventral wings, is observed in specimens sampled from both Alberta, the Northwest Territories , Manitoba and Ontario. While the second variant was by far the most common in western populations, a mixture of both variants is often observed in specimens from a single sample. The second variant was prevalent in the three samples collected from Manitoba and western Ontario. However, one urohyal is a specimen sampled from Ontario had a distinct shape: the ventral wings were much longer than the dorsal wing, and the posterior margin of the dorsal wing was almost straight. In his study on the evolutionary relationships of North American cyprinoids, Mayden (1989) noted that roughly 40% of the *Notropis hudsonius* specimens examined had a pair of lateral processes at the base of the neck of the urohyal. However, I did no observe this specific variant in the *N. hudsonius* specimens that I examined.

The branchial apparatus of *Notropis hudsonius* is unique in that the third epibranchial has a dorsal process, a trait that is not described in any other notropin species (Coburn, 1982; Mayden, 1989). Similarly, the variable presence and absence of the dorsal process on the fourth epibranchial contradicts the descriptions of other notropin species as well in which the dorsal process is always present (Coburn, 1982; Mayden, 1989). Although documented in only one specimen, the presence of four basibranchials instead of three is a unique variant not previously reported in the literature. Given the rarity of this variant, it is likely either a pathology or perhaps is a morphological variation that evolved only in the population from which the specimen was sampled (MZF 680). The usual dental formula (1,4-4,1) that I observed in *N. hudsonius* contrasts with Eastman and Underhill (1973) and Hubbs and Lagler (2004) who found the usual formula to either be 2,4-4,2 and Peer (1961) and Nelson and Paetz (1991) reported the dental formula of *N. husdonius* to be variable between 1,4-4,1 and 2,4-4,2. However, Eastman and Underhill (1973) observed the same variety of dental formulas in *N. hudsonius* that I observed myself (Table 2.3), with the exception of 0,3-4,0.

In their analysis of 42 notropin species native to Minnesota, Eastman and Underhill (1973) noted that the dental formula of *Notropis hudsonius* was, by far, the most variable of all the species studied. Most of this variation was because of a missing tooth on the minor row of one arch. The authors concluded that *Notropis hudsonius* was evolving towards a 1,4-4,1 condition. The results of my own analysis may be a reflection of this trend. However, it should be noted that the *N. hudsonius* specimens used by Eastman and Underhill (1973) were sampled in Minnesota and South Dakota. By comparison, mine were sampled in Alberta, Manitoba, Ontario and the Northwest Territories. Thus, this difference in dental formula could also reflect regional differences among *N. hudsonius* populations.

The pelvic girdle shows no notable variants beyond pelvic fin ray count. In contrast, the pectoral girdle shows a few notable variations. The fusion of the coracoid, mesocoracoid, cleithrum and scapula into a single element is a novel variant not previously reported by other researchers. This fused variant was predominant in specimens sampled from Manitoba and western Ontario, with eight out of nine specimens showing this variant. This fusion is almost always accompanied by an enlarged dorsal flange on the medial ridge of the cleithrum and a shortened dorsal spine of the lateral plate of the cleithrum. Excluding specimens sampled from Manitoba and Ontario, I observed the fused variant only three times in specimens from Alberta. Two of these specimens also exhibited an enlarged dorsal flange on the medial ridge of the cleithrum as well as a shortened dorsal spine. Three other specimens showed partial fusion of the pectoral girdle, one from Alberta and the other two from the Northwest Territories and also had an enlarged dorsal flange and shortened dorsal spine. In another specimen, also from Alberta, the pectoral girdle was unfused, but the cleithrum had the same enlarged flange and dorsal spine typically observed in fused pectoral girdles. In yet another specimen, the pectoral girdle was fused, but the dorsal flange was reduced, and the dorsal spine elongate, as typically seen in unfused pectoral girdles. My results suggest that this fused variant is much more prevalent in eastern *N. hudsonius* populations, but not isolated to them. However, the frequency of this fused variant clearly differs between eastern and western regions.

Notropis hudsonius consistently has 19 caudal fin rays, 10 in the upper lobe and 9 in the lower, a plesiomorphic condition in ostariophysians and common amongst Cypriniformes (Lundberg and Baskin, 1969; Coburn, 1982). However, the caudal skeleton itself shows variability. The most notable variant is the fusion of the parhypural with the first hypural distally.

In one specimen there is a loss of the sixth hypural and an enlarged fifth hypural. Fusion and loss of the hypurals have been noted in North American cyprinoids, usually as a species specific trait (Buhan, 1972; Mayden, 1989). However, the fusion of the first hypural and parhypural seems to be unique to *N. hudsonius* (Buhan, 1972). Of the caudal skeletons I examined, fusion of the parhypural and first hypural was the most common variation compared to the majority of specimens in which these two bones are only fused proximally at the base. However, it is not uncommon to have the parhypural and first hypural abut distally, but not fuse. All specimens sampled from Manitoba and Ontario show either fusion or abutting of the parhypural and first hypural. These specimens were also on the larger side, ranging between 63.2 - 75.5 mm in standard length. However, I also observed the unfused state in specimens of similar size sampled from western populations. To add, I also noted fusion of the parhypural and first hypural in smaller specimens that were under 60 mm in standard length. Thus, I suspect the fusion of the parhypural and first hypural to be linked to population and region rather than body size. Other variations of the caudal skeleton that I observed, including two neural or hemal spines on a preural centrum, division of a neural spine, and fusion of two preural centra are, based on their rarity, most likely individual variants that are of no taxonomic significance.

Variations observed in the suspensorium, oral jaws, and infraorbital series, specifically the lacrimal, relate to the shape of a feature for a few specific elements. For the suspensorium, it is the shape of the anterodorsal process of the metapterygoid and the anterior wing of the hyomandibula. Past descriptions of other notropin, and indeed cyprinoid, species always mention a distinct, well developed adductor ride is present on the lateral side of the hyomandibula, at the level of the opercular condyle (Uyeno, 1961; Buhan, 1970; Coburn, 1982; Mayden, 1989). However, I observed found a weakly developed adductor ridge in only four of the suspensoria examined, and a well-developed adductor ridge in only one specimen. For the oral jaws variation is observed in the shape of the ascending process of the maxilla and coronoid process of the dentary. For the infraorbital series it is the anterior edge of the lacrimal. These variants are not isolated to any one population or region. However, the fact that these kinds of variations can exist should be acknowledged when examining and comparing other notropin species.

For the Weberian apparatus, specimens sampled from the Northwest Territories specifically consistently have an elongate dorsal crest that projecting over more than half of the second neural arch. However, this variant is observed in other populations, though less frequently. In samples taken from two populations in east central Alberta (UAMZ 213,4950) the first predorsal bone fits between the left and right sides of the double crest of the neural complex in five specimens. Otherwise, variations of the Weberian apparatus are not generally associated with a specific population or region.

Coburn (1982) noted four foramina in the pterosphenoid, in contrast with Harrington (1955), who reported only two. My own observations align with those of Coburn (1982).Coburn (1982) noted that the foramen for the opthamalic branch of the trigeminal nerve was often continuous with the trigeminal foramen instead of separated. However, I did not observe this variant in *N. hudsonius*. However, I did observe that the position of the olfactory, trigeminal and oculomotor foramina appears to be variable. Though rare, the olfactory foramen was sometimes formed exclusively within the lateral ethmoid instead of being formed by the mesethmoid anteriorly and the lateral ethmoids posteriorly as is common in the specimens that I analysed. Similarly, the trigeminal foramen, while usually formed by both the pterosphenoid and prootic, is, in one instance formed only by the prootic. In three other instances, it is formed by the prootic on only one side and the pterosphenoid and prootic on the other. The oculomotor foramen is more variable, forming between the prootics and pterosphenoids in some specimens, or only the prootics in other specimens. These variants are also not restricted to any single population or region. However, these types of variants should also be kept in mind when examining and comparing other notropin species.

Coburn (1982) and Mayden (1989) described what has since been termed the open posterior myodome, or OPM. The OPM is an opening bounded by the parasphenoid anteriorly and the basioccipital posteriorly. Coburn (1982) was the first to describe the OPM. Mayden (1989) went further by suggesting that the OPM was a synapomorphy shared by all North American cyprinoids. He also noted a secondary closure in the genera *Nocomis* Girard, 1856, *Campostoma* Agassiz, 1855 and *Dionda* Girard, 1856 and the species *Playygobio gracilis* Richardson, 1836, *Notropis boucardi* Günther 1868, and *Notropis bifrenatus* Cope 1867. In these taxa, Mayden (1989) observed that the OPM was present in juveniles but fused shut in adults. He considered this secondary closure to be a derived trait. All other North American cyprinoids examined by Mayden (1989) lacked this secondary closure, including *Notropis hudsonius*. Contrary to Mayden (1989) I did not observe an OPM in any of the *N. hudsonius* specimens examined. Instead, I observed a secondary closure (Figure 2.12), the closed posterior myodome (CPM).

2.4.2 Conclusions

From this analysis, it is clear that *Notropis hudsonius* is a species with a high degree of intraspecific variation. The PCA conducted on both the meristic counts of the *N. hudsonius* used in this study indicate a that there is as much variation within populations as there is between them, mostly in relation to lateral line, predorsal and postdorsal scale counts. The PCA conducted on the measurements from the same specimens indicate some possible morphometric divergent between eastern and western populations (Fig. 2.50), but also indicated that there can be morphometric variation between members of the same population.

Some osteological variants are observed in only a few specimens, while others are observed more frequently in individuals from the 15 populations I examined. A few variants seem to reflect regional differentiation based on what variants are most common in specimens from different regions. Overall, three osteological characteristics appear vary in frequency between western populations in Alberta and the Northwest Territories and eastern populations in Manitoba and Ontario. First is the fusion of the cleithrum, coracoid, mesocoracoid and scapula into a single element, accompanied by presence of an enlarged dorsal flange on the medial ridge of the cleithrum and a shortened dorsal spine, which is found predominantly in eastern populations, and rarely observed in western populations. Second is the dorsal wing of the urohyal which, in lateral view is usually triangular and shorter than the ventral wings. However, it can also be rounded and slightly longer than the ventral wings in western populations. Third is the caudal skeleton. In western populations, the parhypural and first hypural are usually fused proximally at the base. Rarely, there is fusion or abutting of the parhypural and first hypural distally. In contrast, the fusion or abutting of the parhypural and first hypural is consistently observed in eastern populations.

These variation in the osteological characters examined raise further questions about the regional differentiation within *N. hudsonius* as a species. Furthermore, I would suggest that these findings indicate that there may be specific or subspecific differences among these populations and regions. However, the specimens examined in this study are from the western portion of the range traditionally attributed to *N. hudsonius* (Page and Burr, 2011). In order to determine if these populations should be recognized as distinct species or subspecies, more research will need to be done. This might include a study that focuses on the osteology of *N. hudsonius* populations in eastern Canada and the US. Further research will also need to focus on the genetic diversity of *N. hudsonius*, to see if genetic differences between eastern and western populations correlate with the osteological differences I have observed. Genetic based research should more broadly focus on potential genetic differences of *N. hudsonius* throughout its native range. Both osteological and genetic analyses will be necessary to understand the evolution and regional diversity of *N. hudsonius* and whether this species, as it is currently classified, can be further divided into subspecies or even species.

2.5 Tables

Table 2.1. Measurements and ratios taken for *Notropis hudsonius* ($n = 54$). Measurements are in millimeters.

Measurement	**Minimum**	**Maximum**	**Mean**	**SD**
Standard length (SL)	31.26	75.5	58.21	10.58
Preanal length SL^{-1}	0.63	0.77	0.7	0.03
Predorsal length SL^{-1}	0.47	0.56	0.52	0.03
Prepelvic length SL^{-1}	0.46	0.56	0.52	0.03
Prepectoral length SL^{-1}	0.23	0.35	0.27	0.02
Head length (HL) SL^{-1}	0.27	0.34	0.26	0.02
Snout length SL^{-1}	0.03	0.15	0.07	0.02
Snout length HL^{-1}	0.59	0.14	0.26	0.07
Postorbital length SL^{-1}	0.08	0.14	0.11	0.01
Postorbital length HL^{-1}	0.33	0.49	0.43	0.04
Dorsal fin base SL^{-1}	0.10	0.18	0.14	0.02
Anal fin base SL^{-1}	0.08	0.17	0.12	0.02
Peduncle length SL^{-1}	0.17	0.30	0.23	0.03
Interorbital width SL^{-1}	0.06	0.12	0.09	0.01
Interorbital width HL^{-1}	0.23	0.43	0.35	0.05
Eye diameter SL^{-1}	0.04	0.10	0.08	0.01
Eye diameter HL^{-1}	0.18	0.39	0.30	0.05
Body depth SL^{-1}	0.18	0.34	0.24	0.03
Caudal peduncle depth SL^{-1}	0.06	0.13	0.10	0.01
Dorsal fin length SL^{-1}	0.15	0.27	0.22	0.02
Anal fin length SL^{-1}	0.11	0.21	0.18	0.02
Pectoral fin length SL^{-1}	0.13	0.23	0.18	0.02
Pelvic fin length SL^{-1}	0.11	0.19	0.16	0.02

Table 2.2. Meristics for *Notropis hudsonius* (*n* = 54) unless otherwise stated). The number of specimens for each count is in brackets.

Number of									
Dorsal fin rays	7 (3)	8 (41)	9 (10)						
Anal fin rays	7 (3)	8 (45)	9 (6)						
Pelvic fin rays	7 (3)	8 (22)	9 (29)						
Pectoral fin rays (*n* = 53)	12 (2)	13 (6)	14 (28)	15 (12)	16 (5)				
Lateral line scales	35 (1)	36 (3)	37 (5)	38 (10)	39 (15)	40 (9)	41 (5)	42(3)	43(3)
Predorsal scales	12 (1)	13 (2)	14 (11)	15 (11)	16 (11)	17 (13)	18 (3)	19 (1)	20(1)
Postdorsal scales	13 (1)	14 (3)	15 (4)	16 (8)	17 (13)	18 (12)	19 (11)	20 (1)	21(1)
Scales above lateral line	4 (2)	5 (12)	6 (30)	7 (10)					
Scales below lateral line	4 (9)	5 (43)	6 (2)						
Circumferential scales	24 (2)	25 (9)	26 (18)	27 (11)	28 (8)	29 (6)			
Peduncle scales	10 (16)	11 (23)	12 (15)						
Gill rakers	0 (1)	3 (3)	4 (10)	5 (32)	6 (8)				
Predorsal vertebrae (*n* = 42)	10 (2)	11 (21)	12 (19)						
Total number of vertebrae (*n* = 42)	37(5)	38(22)	39(10)	40(4)	41(1)				

Table 2. 3. Dental formulae taken for *Notropis hudsonius* (*n* = 43).

Dental formula	**Number observed**
1,4-4,1	25
2,4-4,2	5
2,4-4,1	4
1,4-4,2	1
1,4-4,0	3
0,4-4,0	4
0,3-4,0	1

Table 2. 4. Sensory canal pore counts taken for *Notropis hudsonius* (n = 24). The number of specimens that showed each count is in brackets.

Sensory canal			
Supraorbital	6(3)	8(16)	9(5)
Supratemporal	3(24)		
Postocular commissure	1(23)	2(1)	
Preopercularmandibular	9(4)	10(15)	11(5)
Infraorbital	6(1)	7(21)	8(2)

2.6 Figures

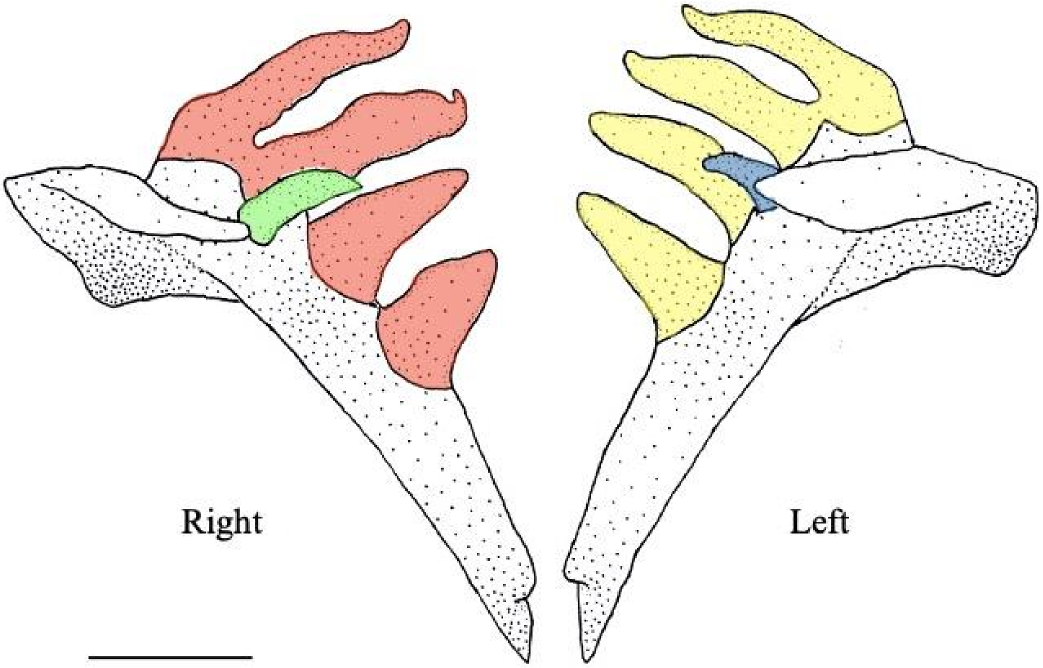

Figure 2.1. Illustration of the pharyngeal arches of *Notropis hudsonius* UAMZ F1258, specimen 1, in dorsal view, anterior to bottom of the page. The dental formula is counted from left to right, starting with the teeth on the minor (blue) and major (yellow) rows of t on the minor (blue) and major (yellow) rows of the left arch, followed by the teeth of the major (red) and minor (green) rows of the right arch. The corresponding dental formula of this specimen is thus 1,4-4,1. Scale bar = 1 mm.

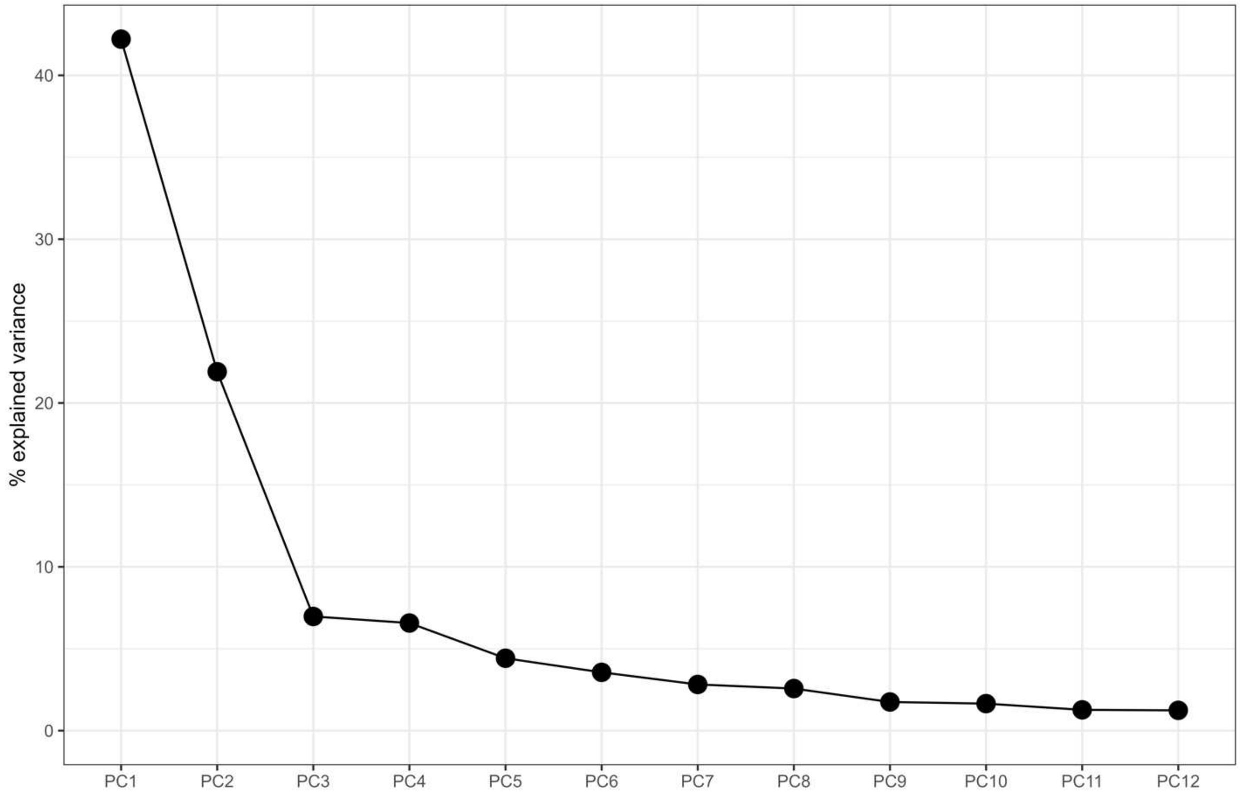

Figure 2.2. Scree plot for first ten principal components for PCA conducted on measurements of 54 *Notropis hudsonius* specimens. Measurements were analyzed as ratios of standard length.

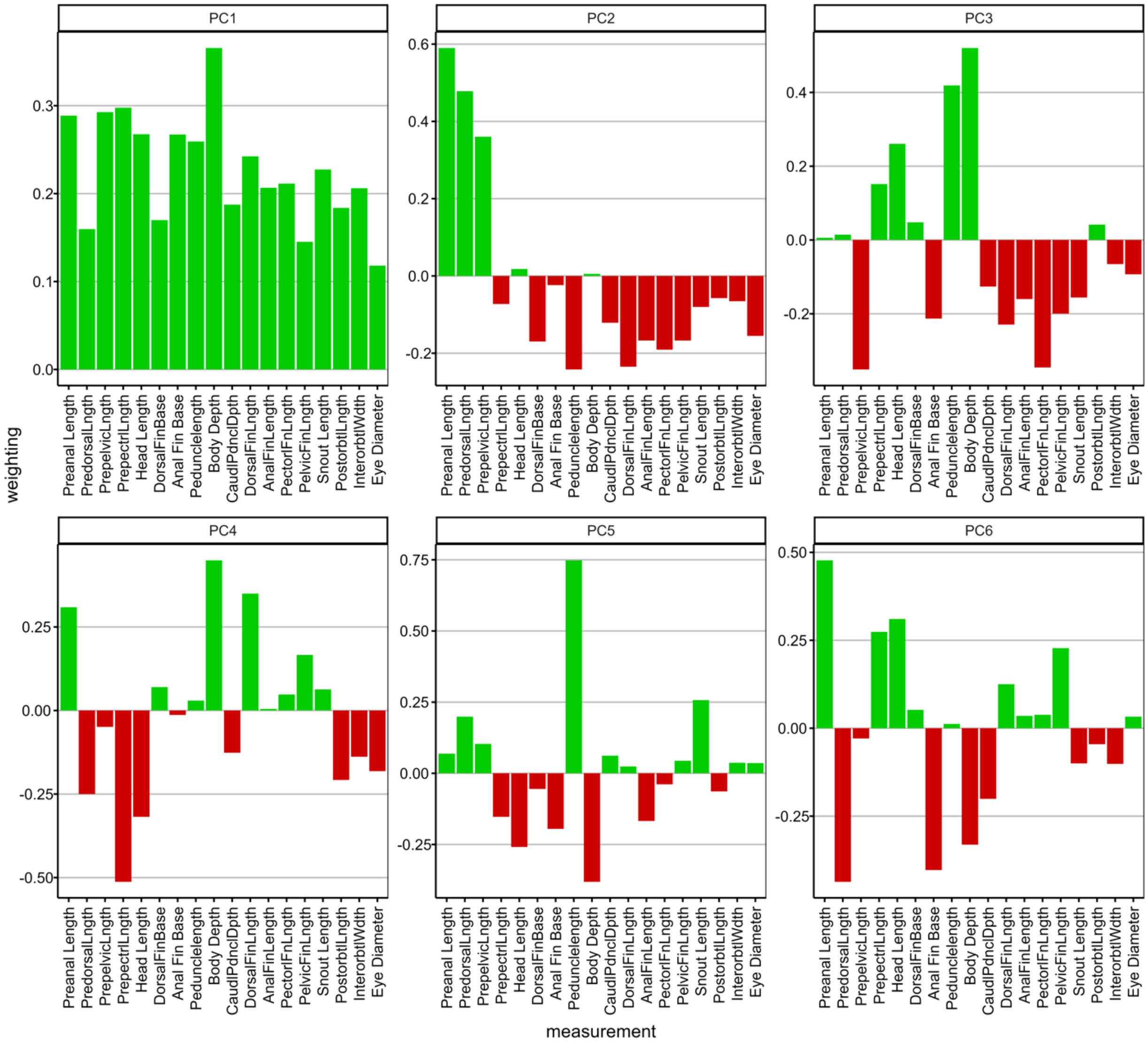

Figure 2.3. Loading plot for first ten principal components for PCA conducted on measurements of 54 *Notropis hudsonius* specimens. Measurements were analyzed as ratios of standard length.

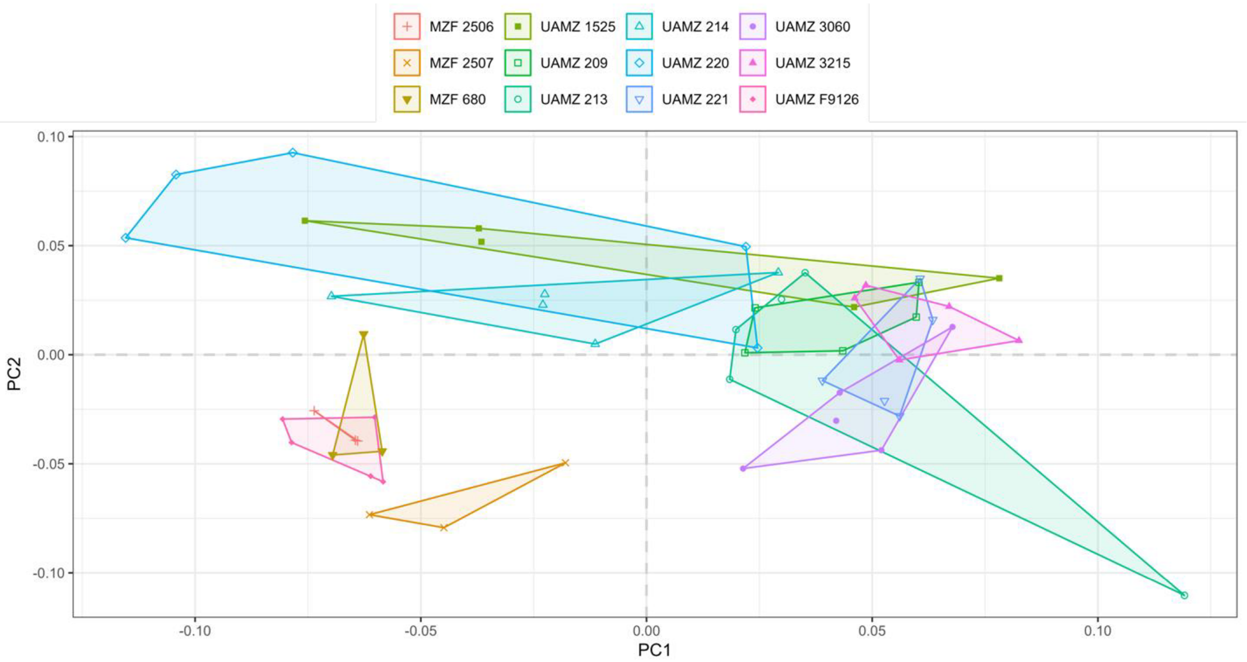

Figure 2.4. PCA scatter plot of measurements for 54 *Notropis hudsonius* specimens. PC2 is plotted against PC1. Measurements were analyzed as ratios of standard length. Sample numbers correspond to different populations in Alberta (UAMZ 209, 213,214, 220, 221, 1525, 3215 and F9126), Northwest Territories (UAMZ 3060), Manitoba (MZF 680 and 2507) and Ontario (MZF 2506). Details of collections are in Appendix A.

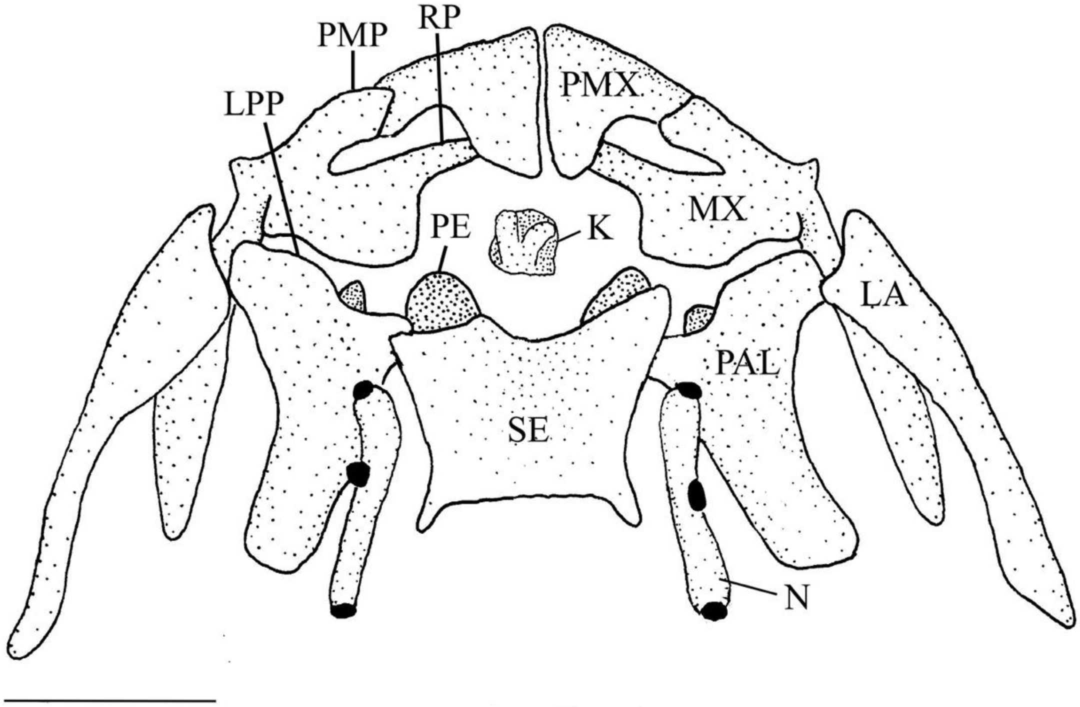

Figure 2.5. Illustration of the supraethmoid, nasals, maxillae, premaxillae and kinethmoid of *Notropis hudsonius* UAMZ F1258, specimen 1, in dorsal view, anterior to top of the page. The mouth is closed in this illustration. Scale bar = 1 mm.

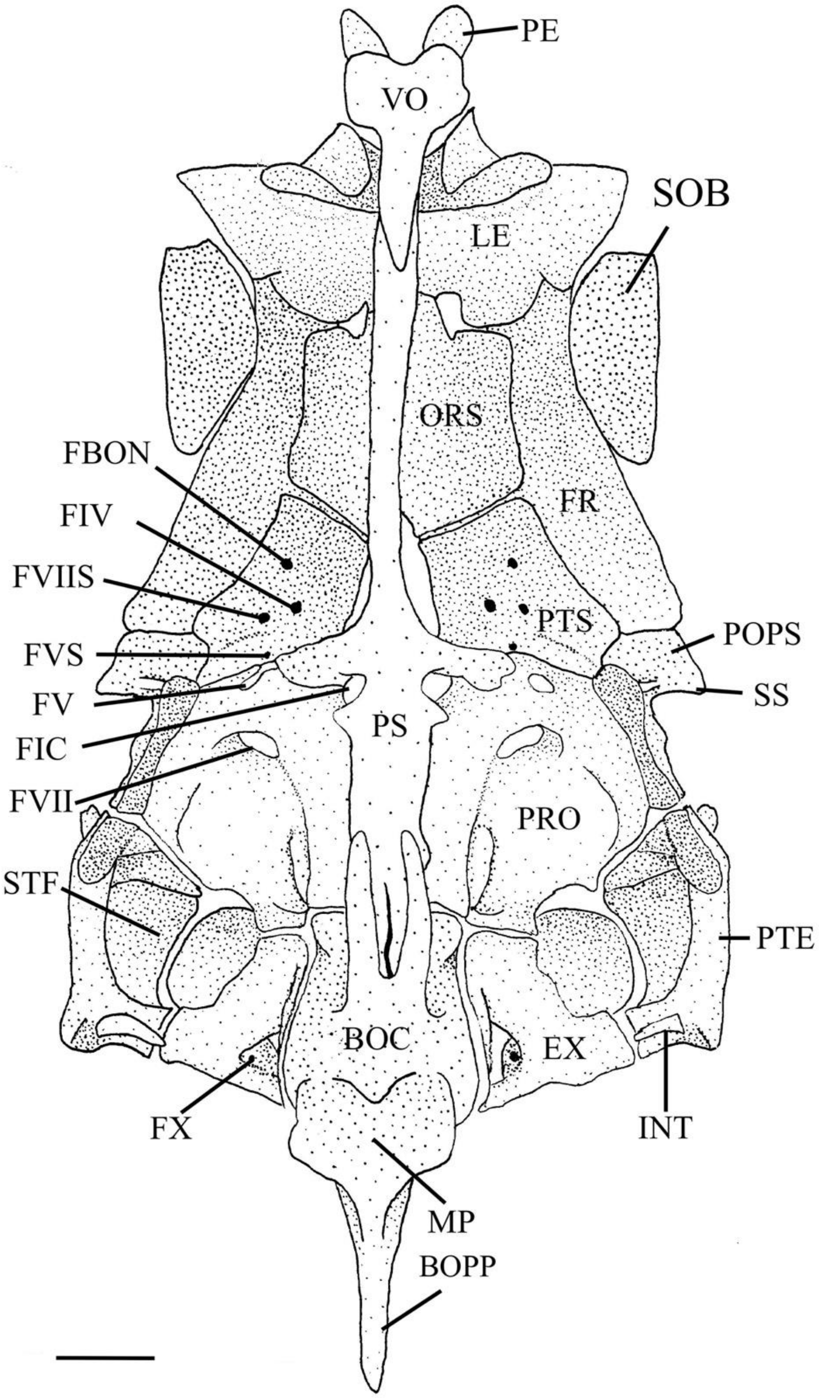

Figure 2.6. Illustration of the skull of *Notropis hudsonius* UAMZ F1258, specimen 1, in ventral view, anterior to top of the page. Scale bar = 1 mm.

.

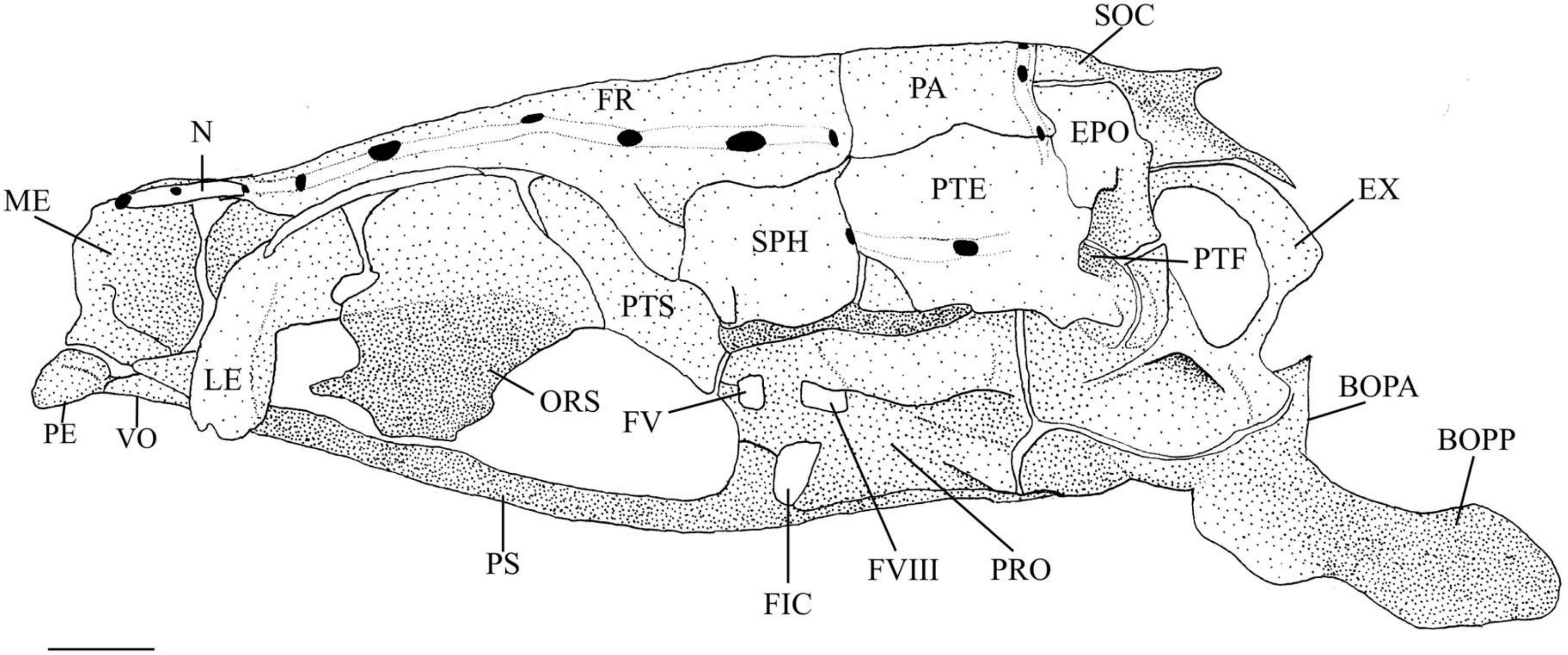

Figure 2.7. Illustration of the skull of *Notropis hudsonius* UAMZ F1258, specimen 1, in left lateral view, anterior to left. Scale bar = 1 mm.

Figure 2.8. The ethmoid and orbital regions of *Notropis hudsonius* MZF 2507, specimen 2, in lateral view, anterior to left. Specimen shows olfactory foramen encompassed only within the lateral ethmoids, and fusion of the orbitosphenoid to the parasphenoid. Scale bar = 2 mm.

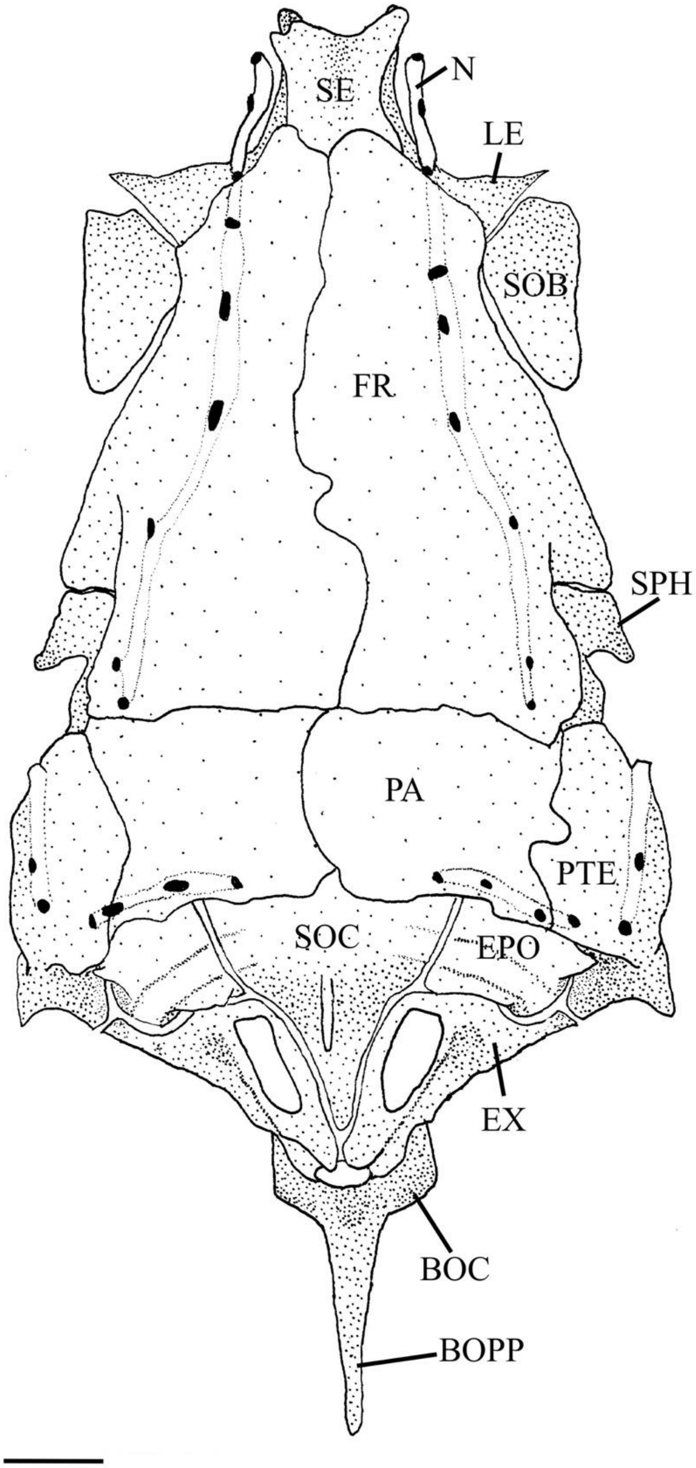

Figure 2.9. Illustration of the skull of *Notropis hudsonius* UAMZ F1258, specimen 1, in dorsal view, anterior to top of the page. Scale bar = 1 mm.

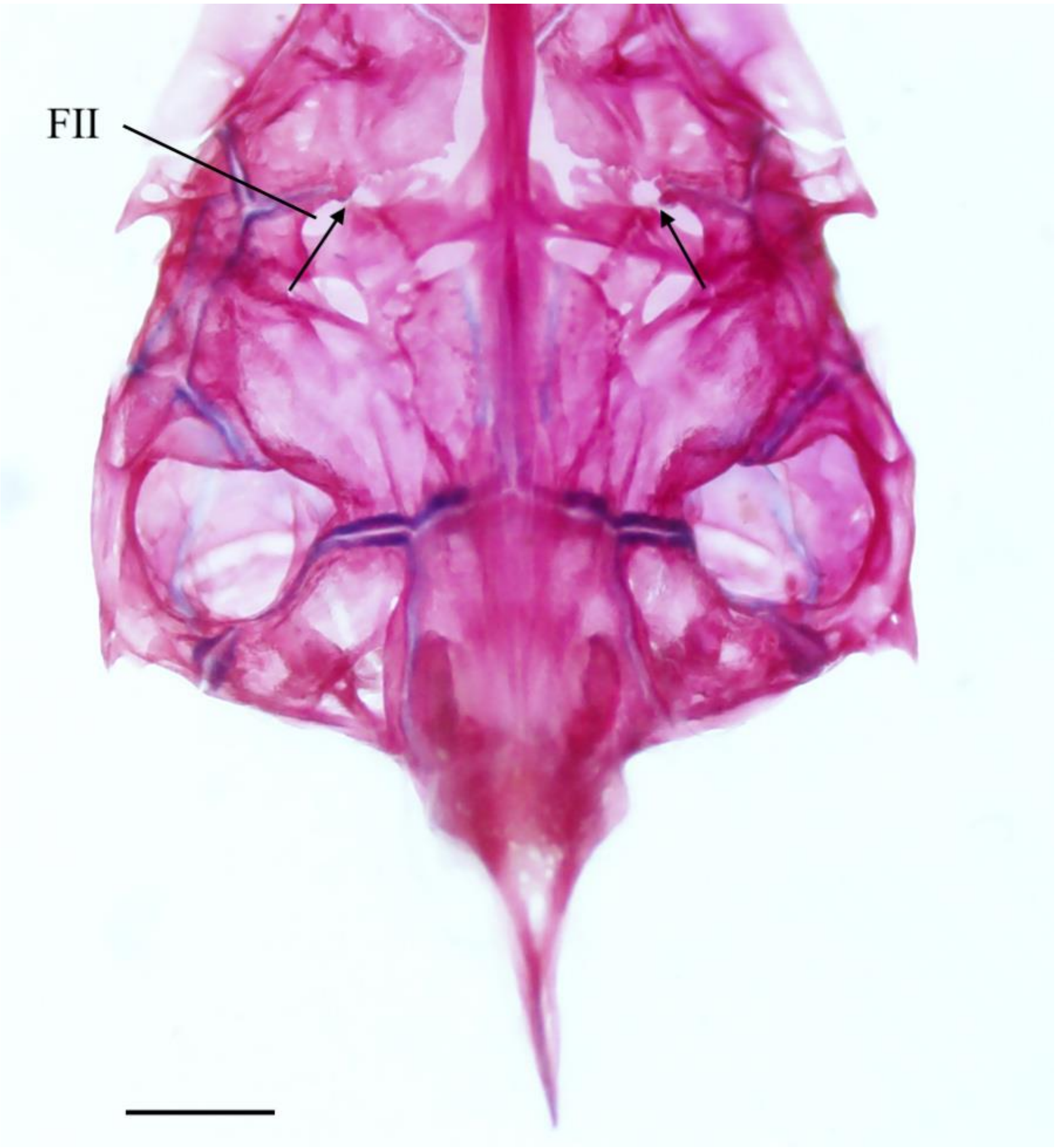

Figure 2.10. The otic, occipital and basicranial region of the skull of *Notropis hudsonius* UAMZ 209, specimen 2, in ventral view, anterior to top of the page. Specimen shows bony struts formed over the trigeminal foramina (indicated by arrows). Scale bar = 1 mm.

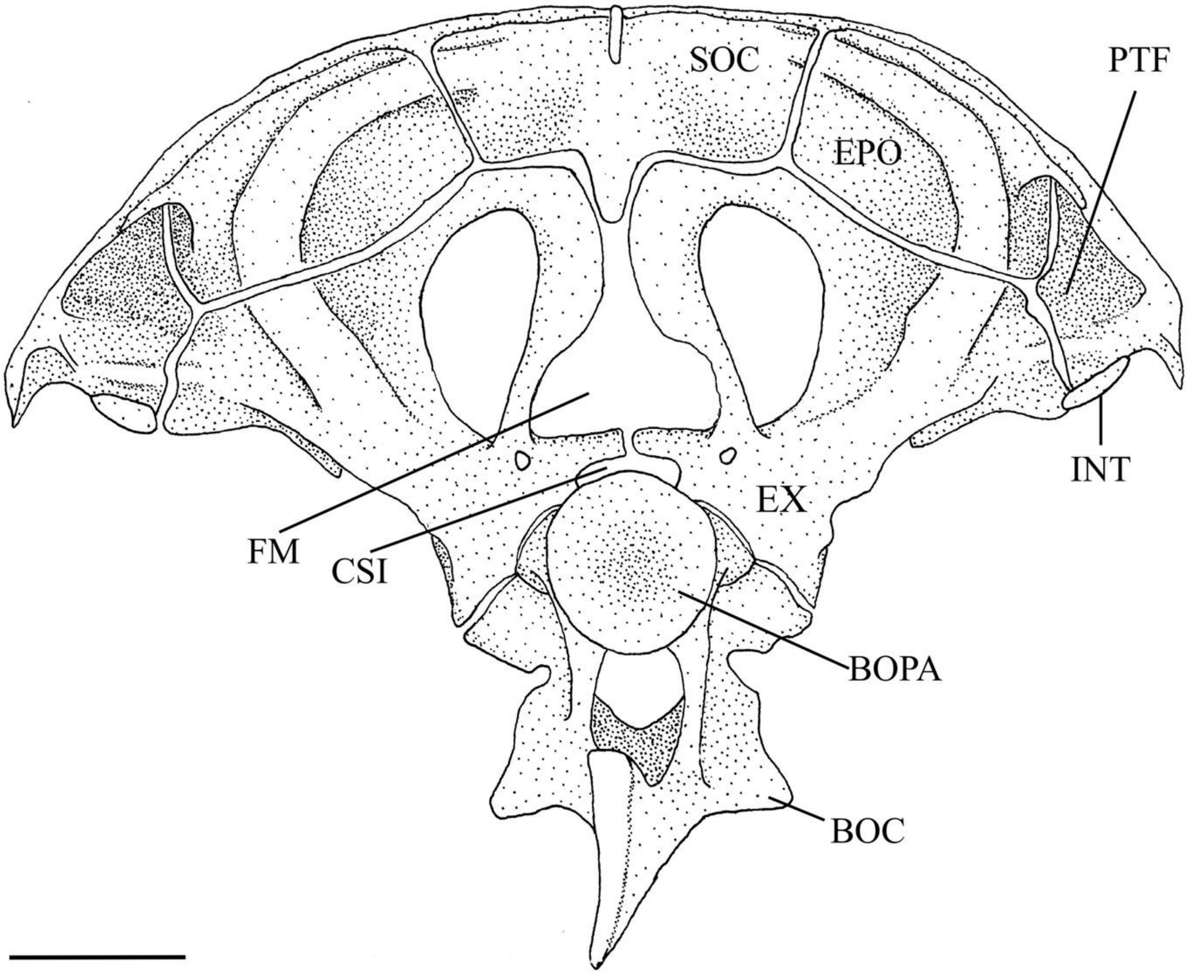

Figure 2.11. Illustration of the skull of *Notropis hudsonius* UAMZ 4950, specimen 1, in posterior view, dorsal to top of the page. Scale bar = 1 mm.

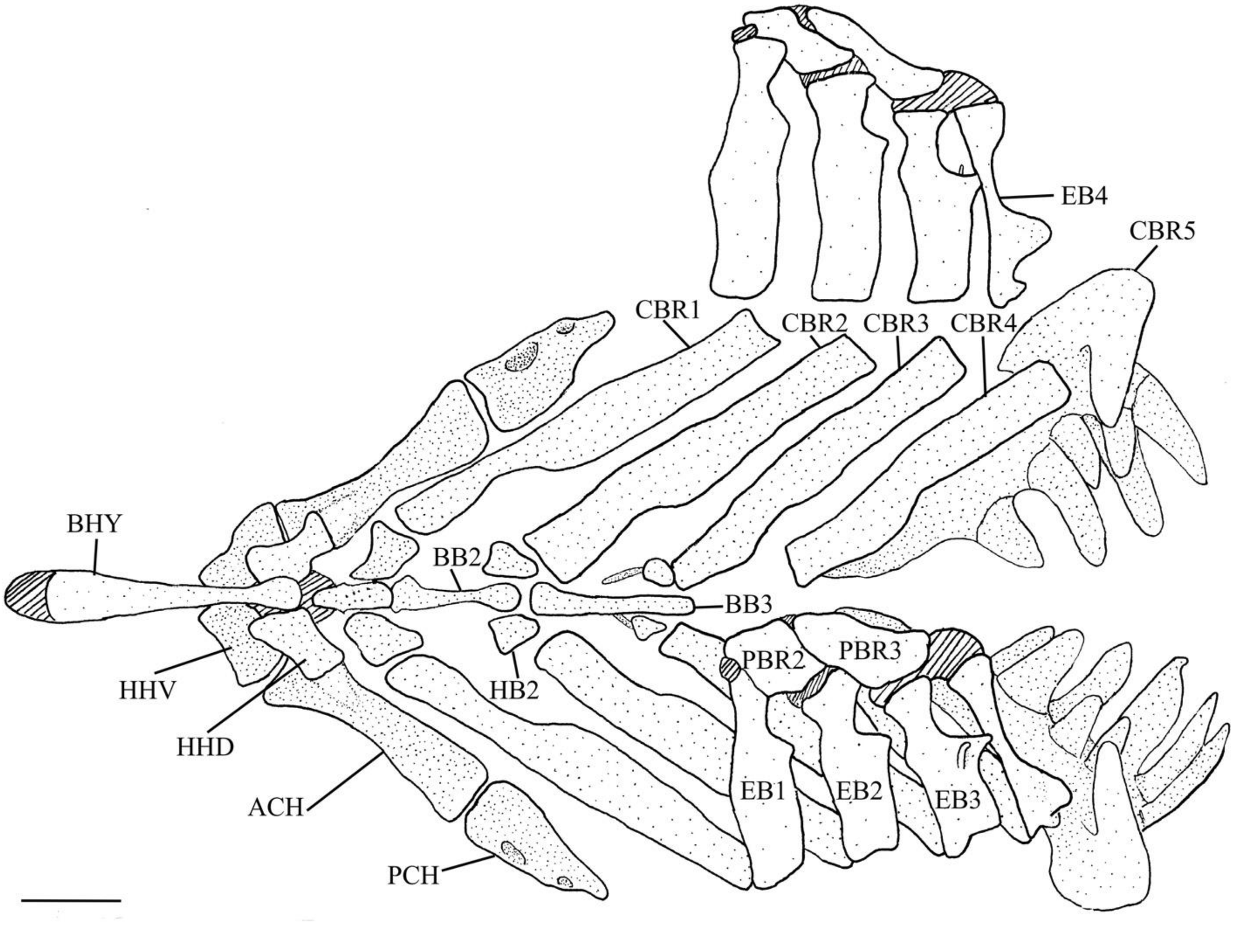

Figure 2.12. Illustration of the branchial apparatus and hyoid bars of *Notropis hudsonius* UAMZ 4950, specimen 1, in dorsal view, anterior to left. Upper elements on the right side are reflected away and are in ventral view. Hatching represents cartilage. Scale bar = 1 mm

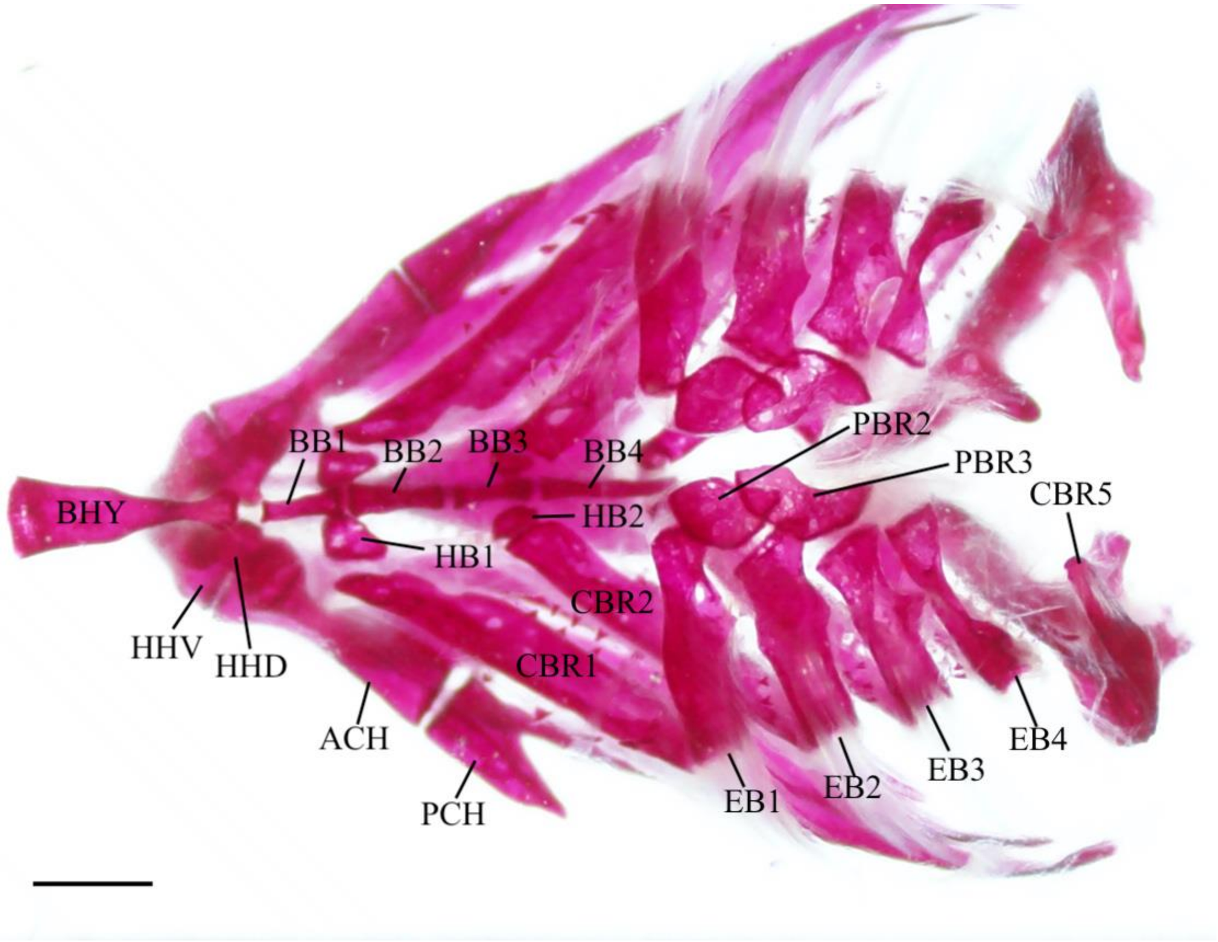

Figure 2.13. The branchial apparatus of *Notropis hudsonius* MZF 680, specimen 3, in dorsal view, anterior to left. Specimen has a fourth basibranchial that is not present in any of the other branchial apparatuses examined. Scale bar = 1 mm.

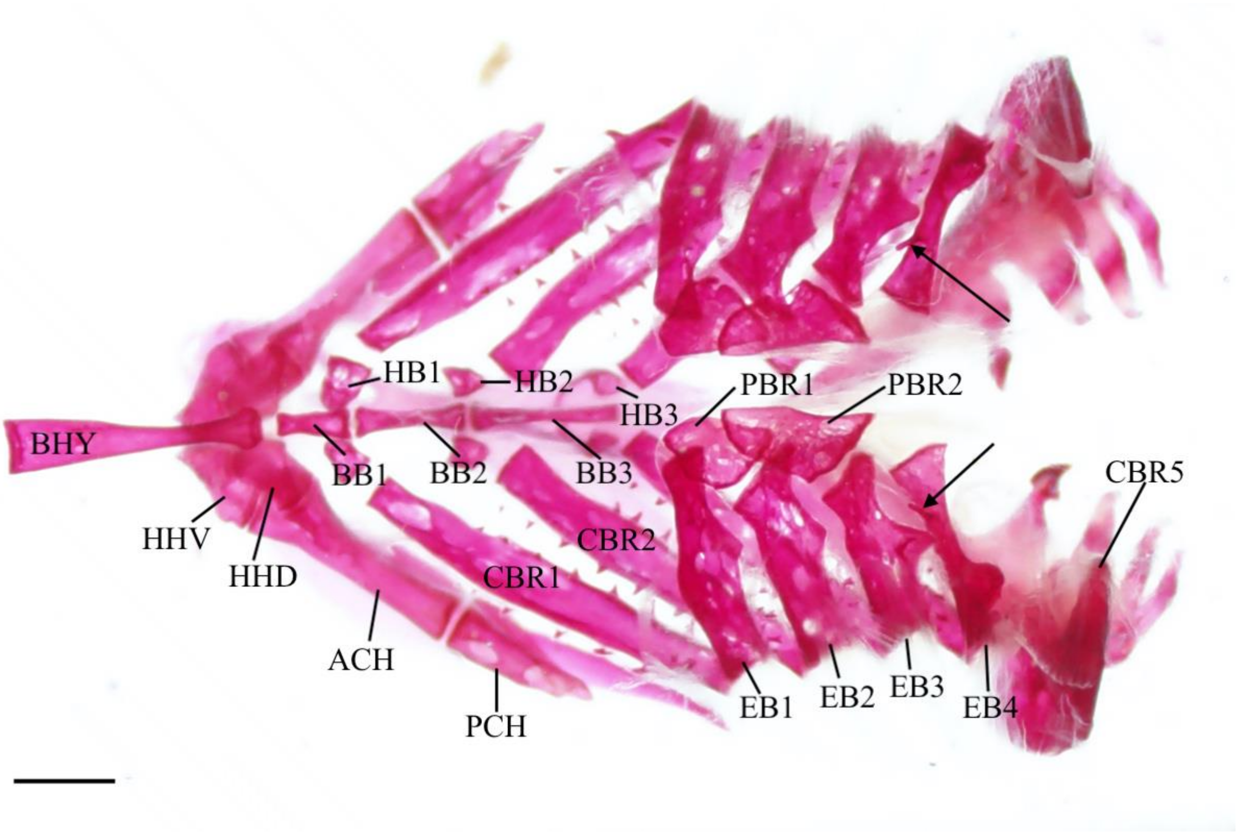

Figure 2.14. The branchial apparatus of *Notropis hudsonius* MZF 2506, specimen 1, in dorsal view, anterior to left. Arrows point to dorsal processes on the fourth epibranchials. Scale bar = 1 mm.

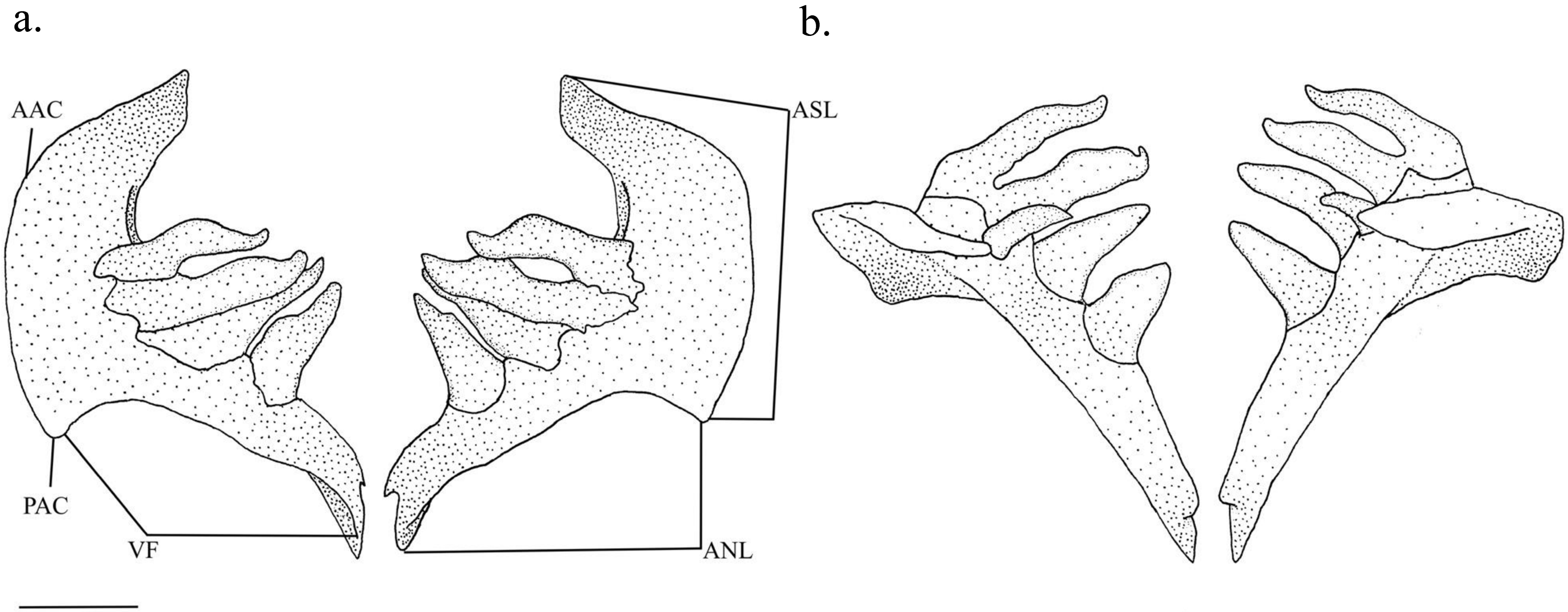

Figure 2.15. Illustration of the pharyngeal arched of *Notropis hudsonius* UAMZ F1258, specimen 1, in (a) posteroventral view, dorsal to top of the page and (b) dorsal view, anterior to bottom of the page. Scale bar = 1 mm.

Figure 2.16. The pharyngeal arches of *Notropis hudsonius* UAMZ 4950, specimen 1, in posteroventral view, dorsal to top of the page. Specimen shows broadened posterior angle (indicated by arrow). Scale bar = 1 mm.

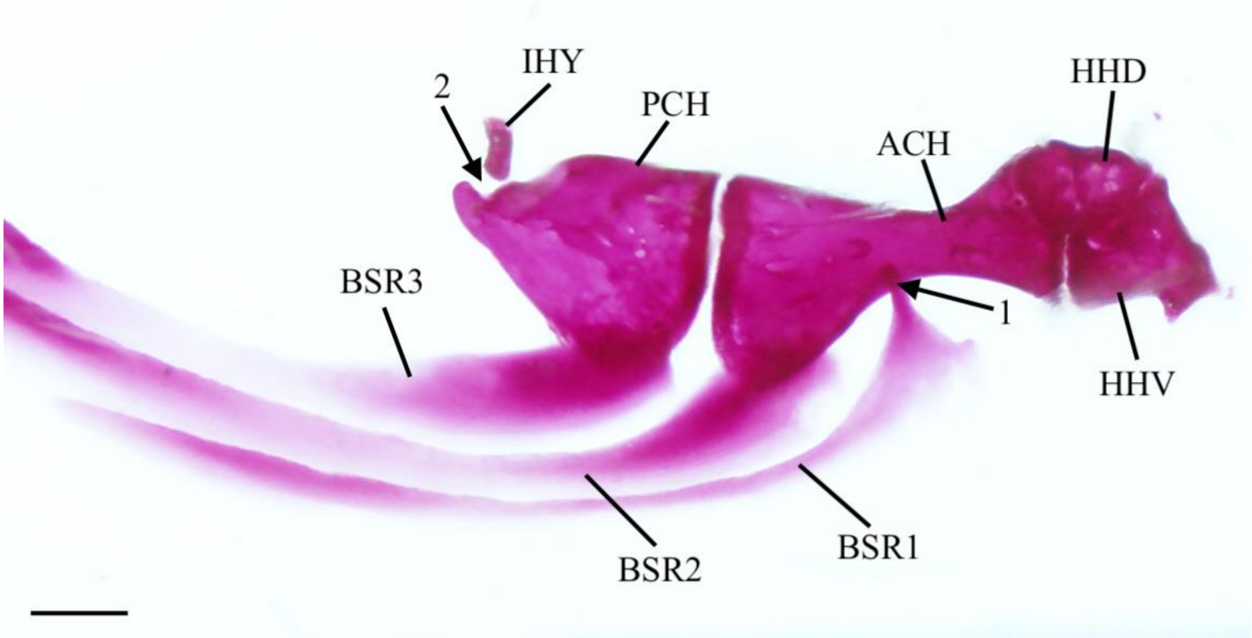

Figure 2.17. The hyoid bar or *Notropis hudsonius* UAMZ F9126, specimen 2, in medial view, anterior to right. Specimen shows an elongate head on the first branchiostegal ray (indicated by arrow 1) and a deepened posterior notch on the posterior ceratohyal (indicated by arrow 2). Scale bar = 0.5 mm.

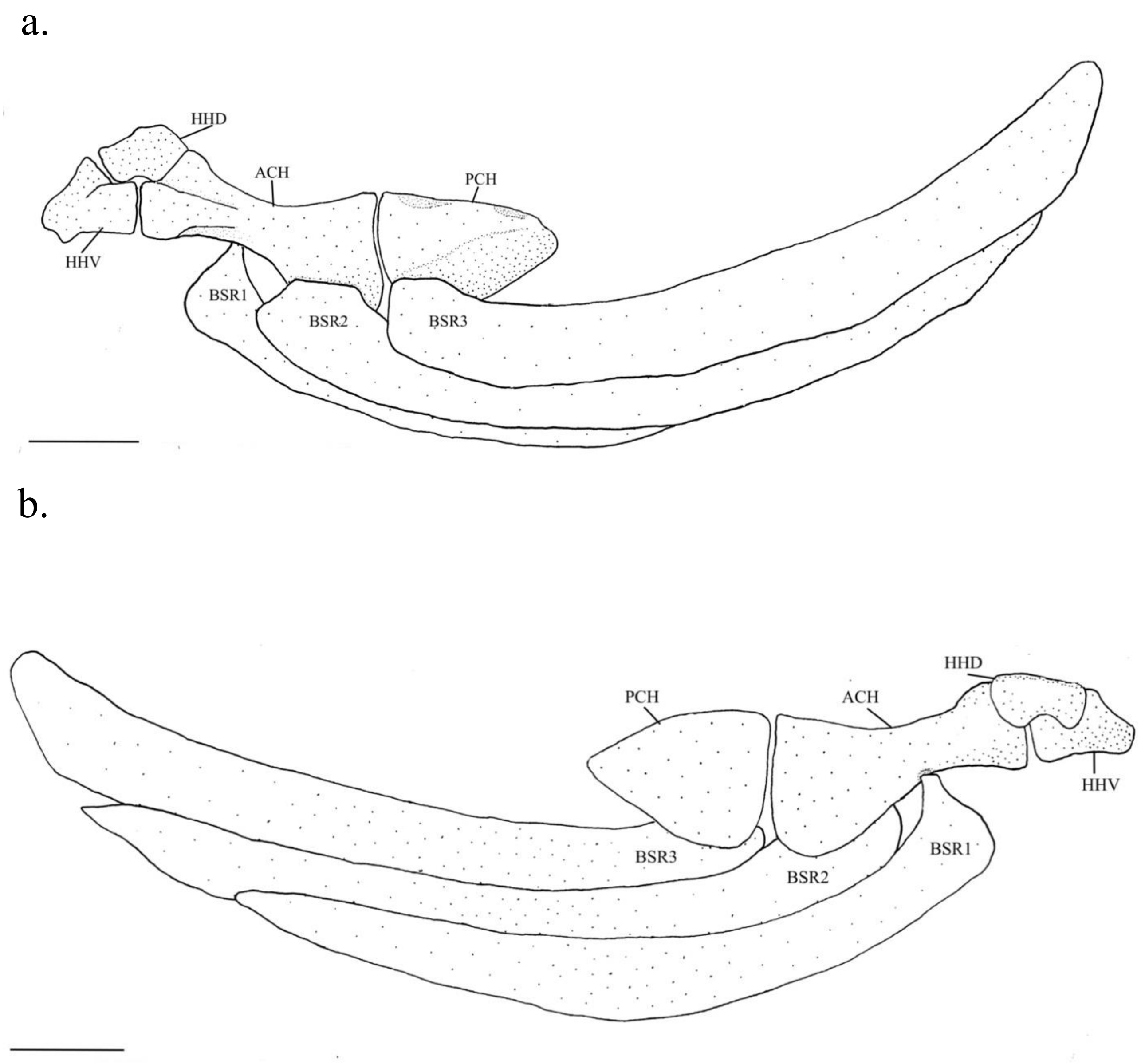

Figure 2.18. Illustration of the left hyoid bar of *Notropis hudsonius* UAMZ 4950, specimen 1, in (a) lateral view, anterior to left and (b) medial view, anterior to right. Scale bars = 1 mm.

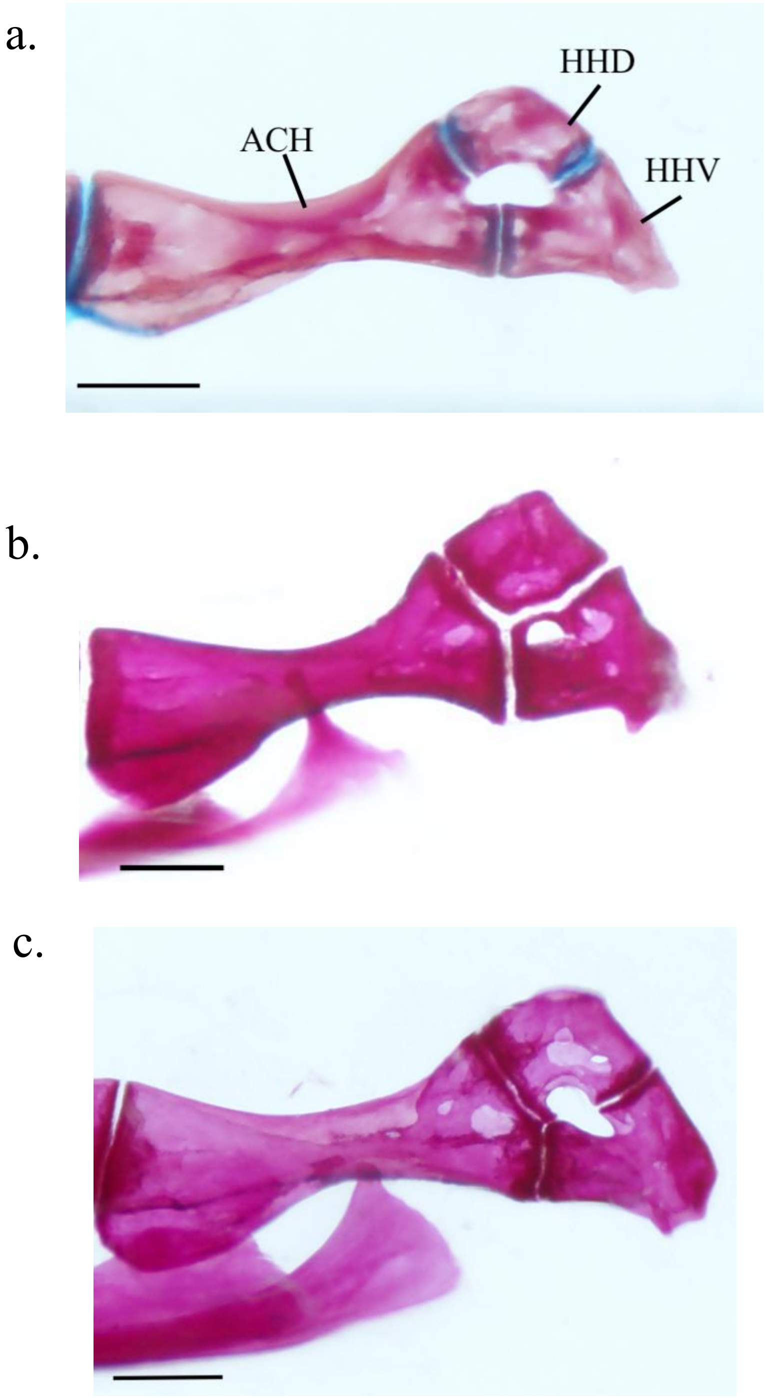

Figure 2.19. The left hypohyal foramen of *Notropis hudsonius* UAMZ 209, specimen 1, (a), UAMZ F9126, specimen 2, (b), UAMZ 4950, specimen 1, (c) in medial view, anterior to right. The hypohyal foramen can be partly formed by the anterior ceratohyal (a), formed only in the ventral hypohyal (b) or formed by only the dorsal and ventral hypohyals (c). Scale bars = 0.5 mm.

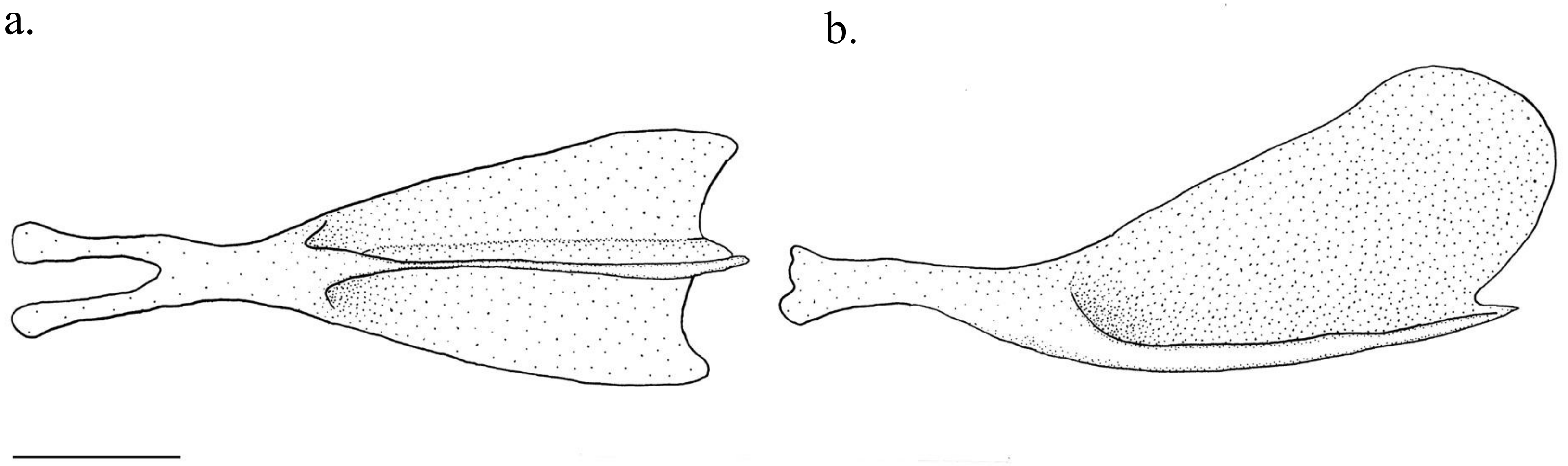

Figure 2.20. Illustration of the urohyal of *Notropis hudsonius* UAMZ 1525, specimen 3, in (a) dorsal and (b) lateral view. Anterior to left. Scale bar = 1 mm.

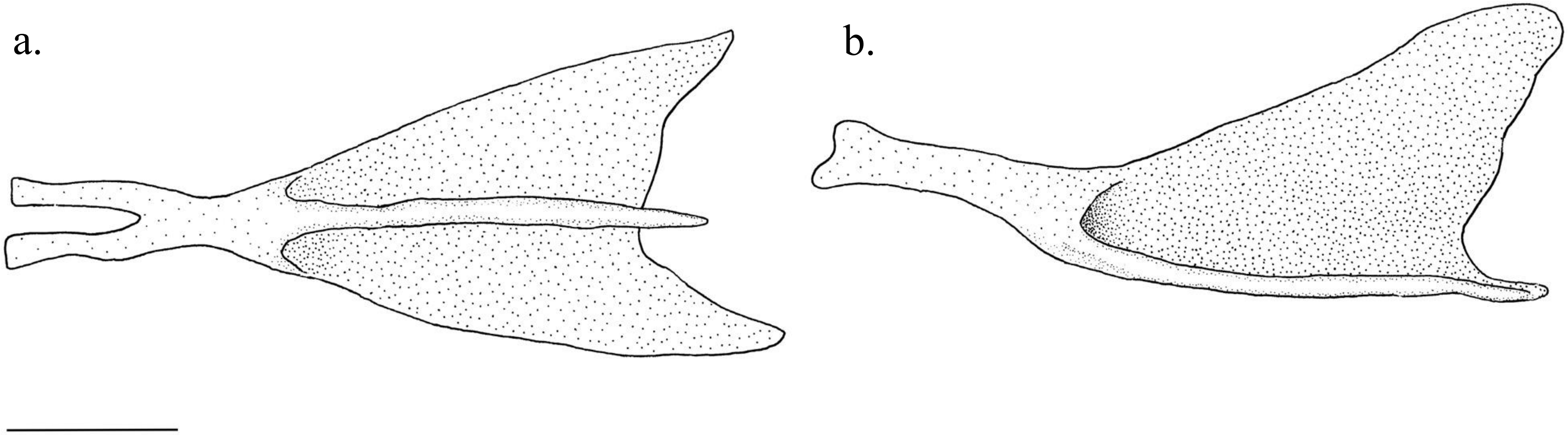

Figure 2.21. Illustration of the urohyal of *Notropis hudsonius* UAMZ 4950, specimen 1, in (a) dorsal and (b) lateral view, anterior to left. Scale bar = 1 mm.

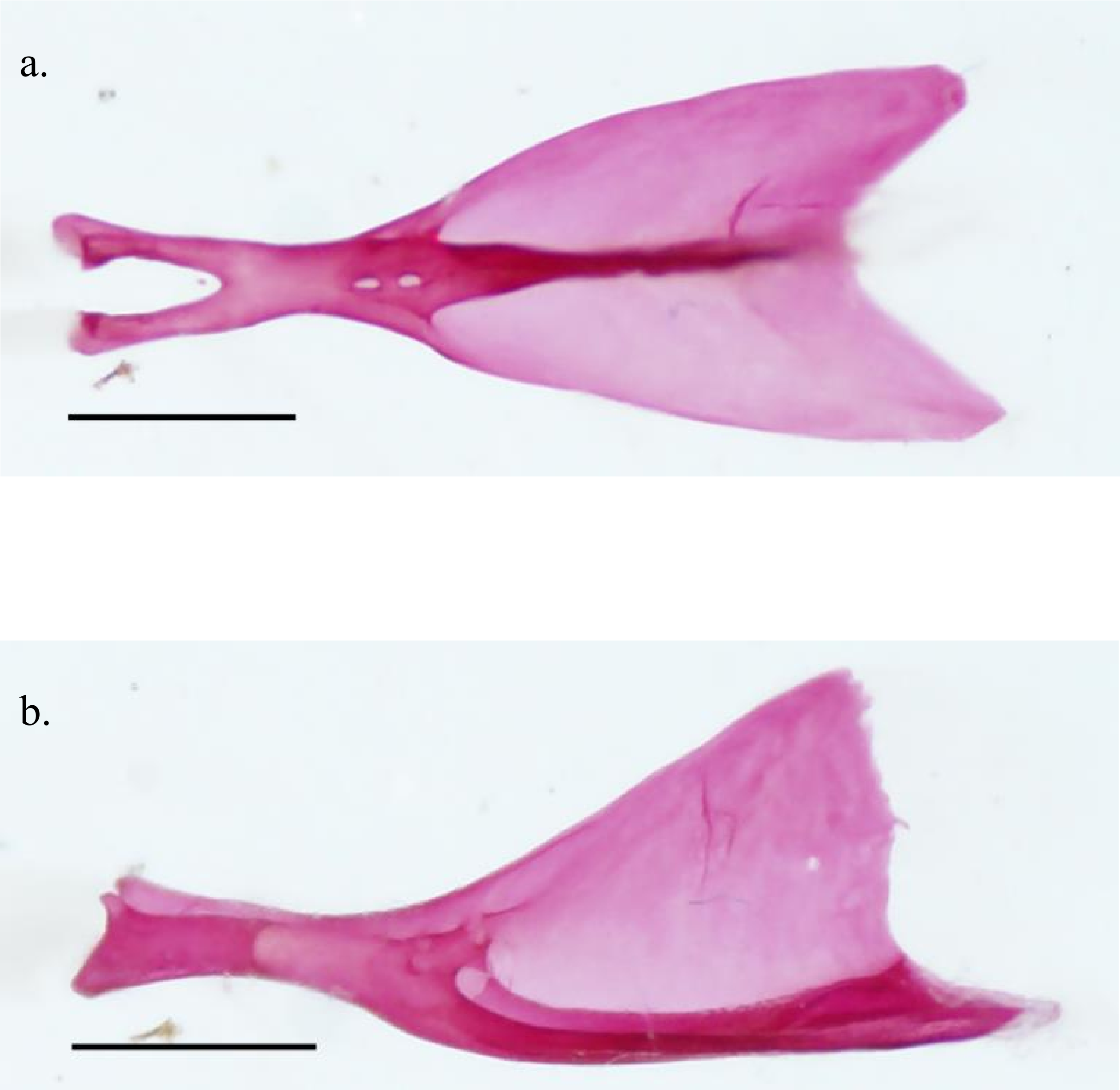

Figure 2.22. The urohyal of Notropis hudsonius MZF 2506, specimen 1, in (a) dorsal and (b) lateral view, anterior to left. Scale bar = 1 mm.

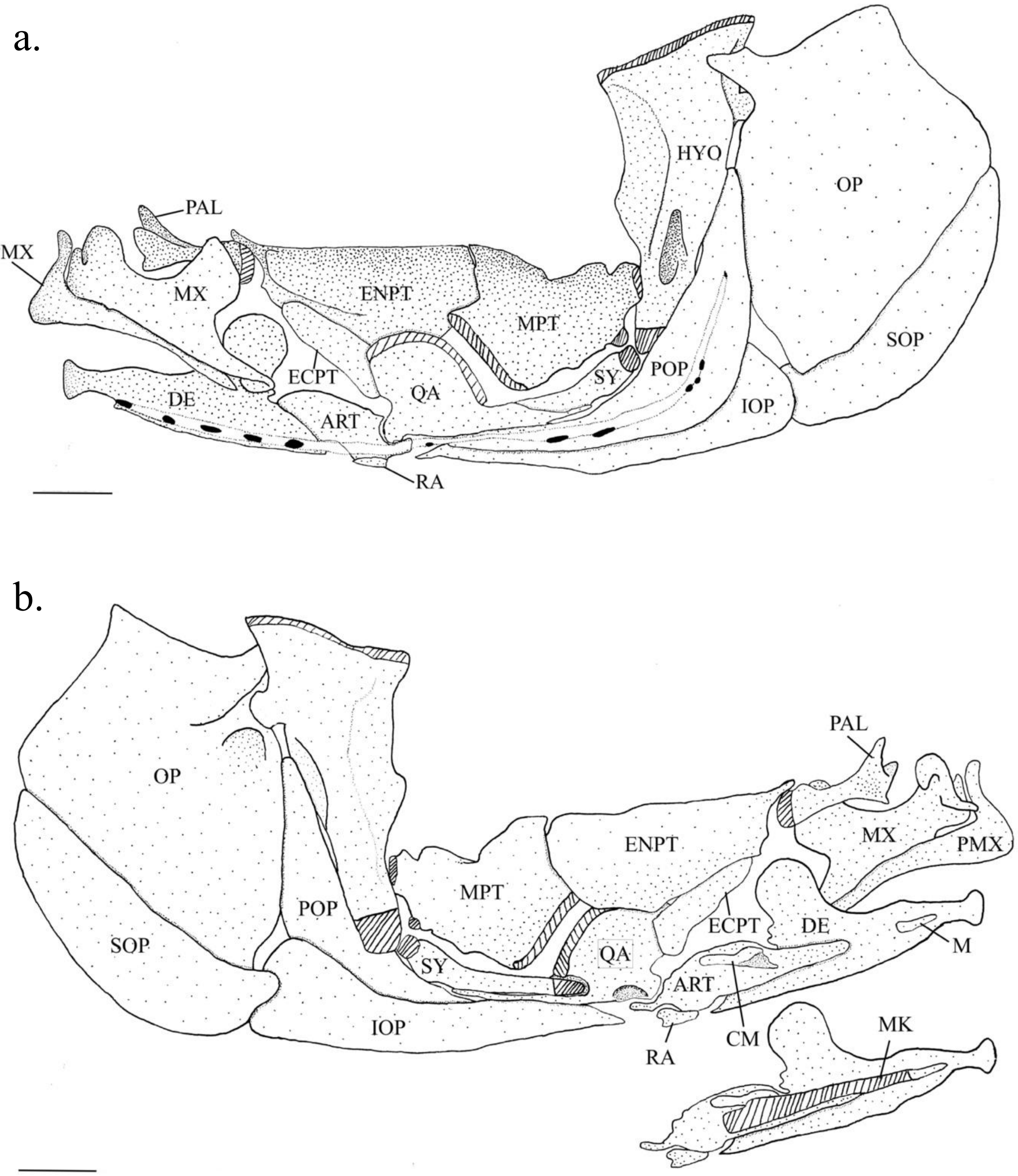

Figure 2.23. Illustration of the left opercular series, suspensorium and oral jaws of *Notropis hudsonius* UAMZ 3215, specimen 1, in (a) lateral view, anterior to left and (b) medial view, anterior to right. Hatching represents cartilage. Scale bars = 1 mm.

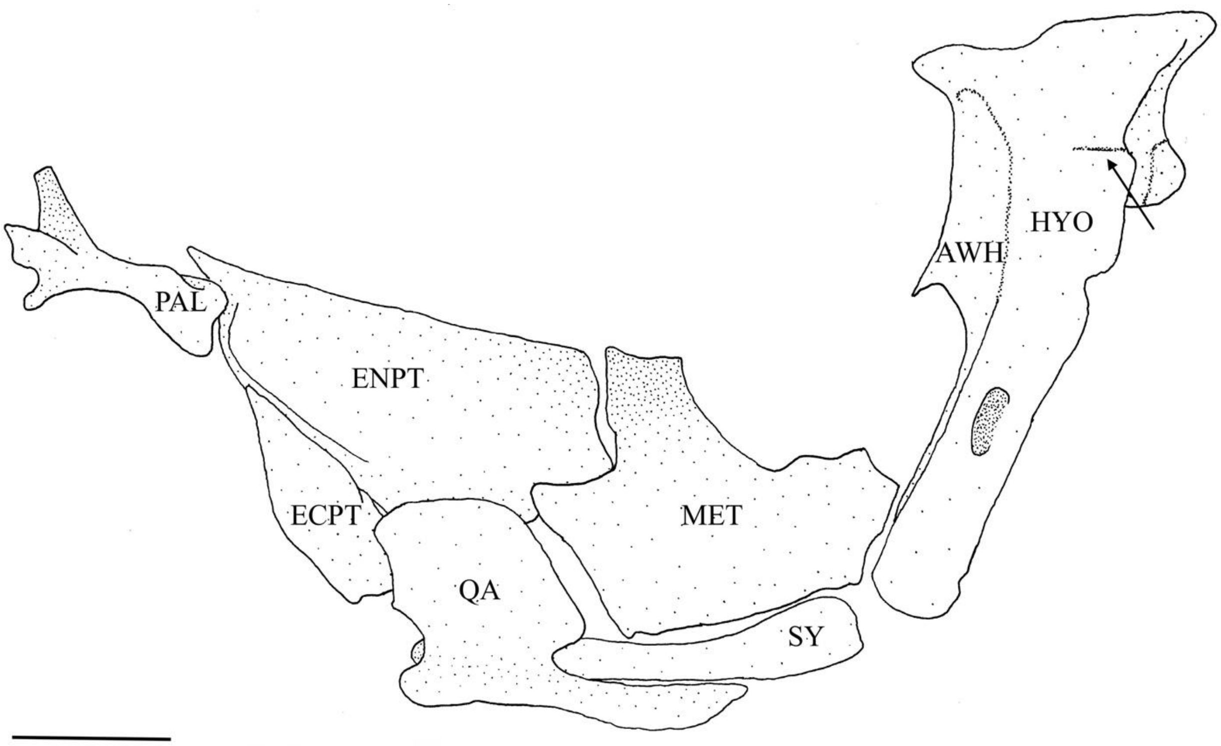

Figure 2.24. Illustration of the left suspensorium of *Notropis hudsonius* MZF 2605, specimen 1 in lateral view, anterior to left. The anterior wing of the hyomandibula is constricted towards the ventral end and drawn into an anteroventral point. Adductor ridge of the hyomandibula is well-developed (indicated by arrow). Scale bar = 1 mm.

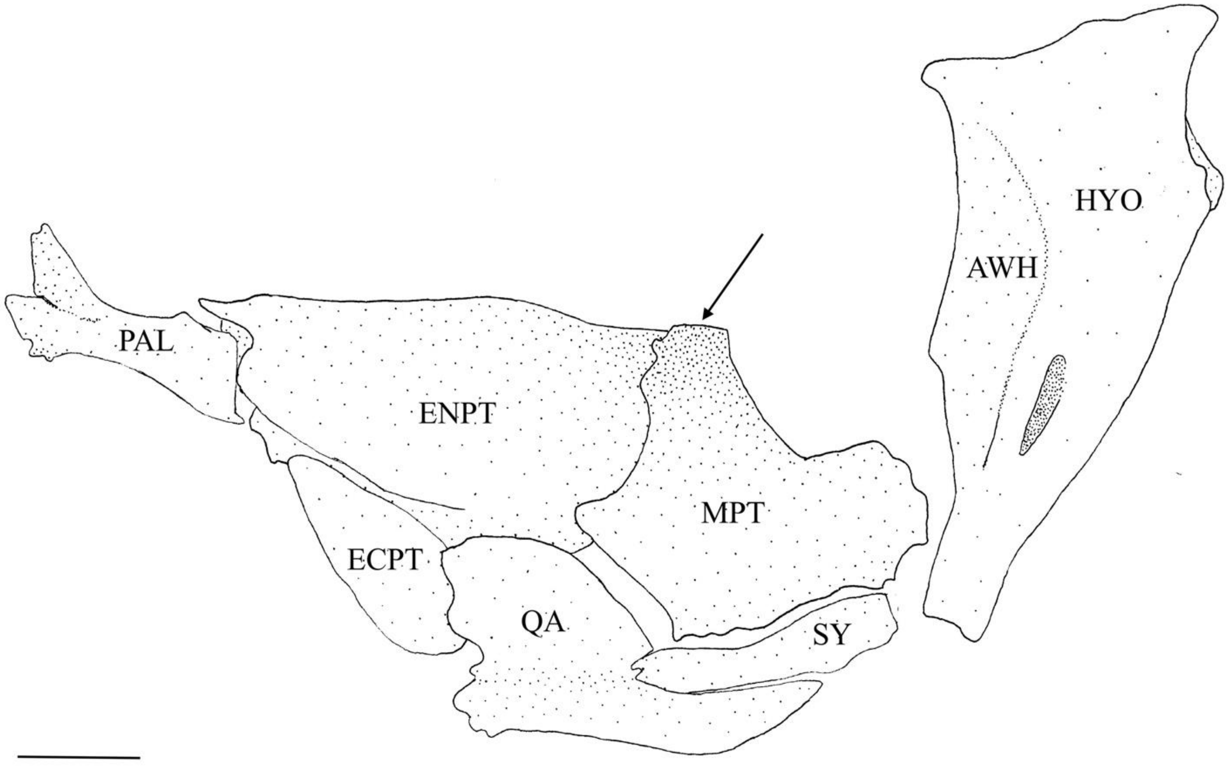

Figure 2.25. Illustration of the left suspensorium of *Notropis hudsonius* MZF 2605, specimen 1 in lateral view, anterior to left. Arrow points to the anterodorsal process of the metapterygoid. Scale bar = 1 mm.

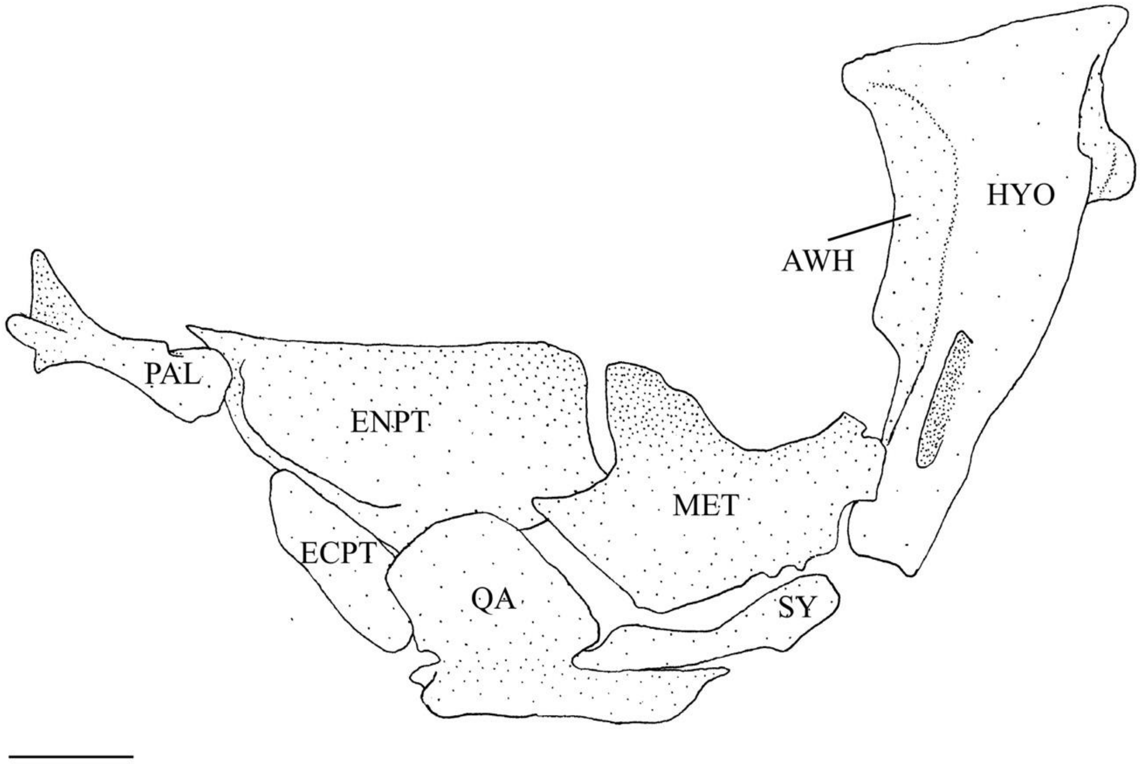

Figure 2.26. Illustration of the left suspensorium of *Notropis hudsonius* UAMZ 4950, specimen 1 in lateral view, anterior to left. Specimen shows rounded anterodorsal process of the hyomandibula. Scale bar = 1 mm.

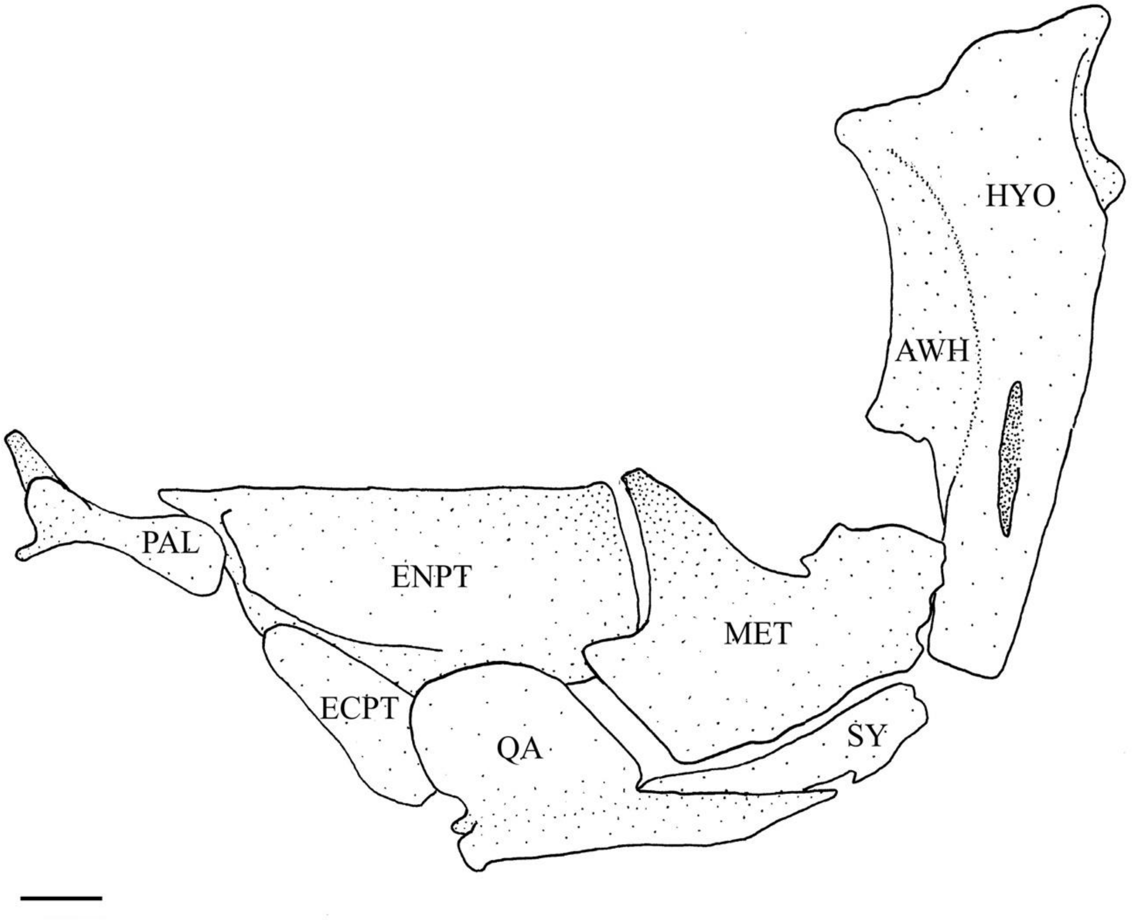

Figure 2.27. Illustration of the suspensorium of *Notropis hudsonius* UAMZ 1525, specimen 3 in lateral view, anterior to left. Specimen has a pointed anterodorsal process of the hyomandibula. Scale bar = 1 mm.

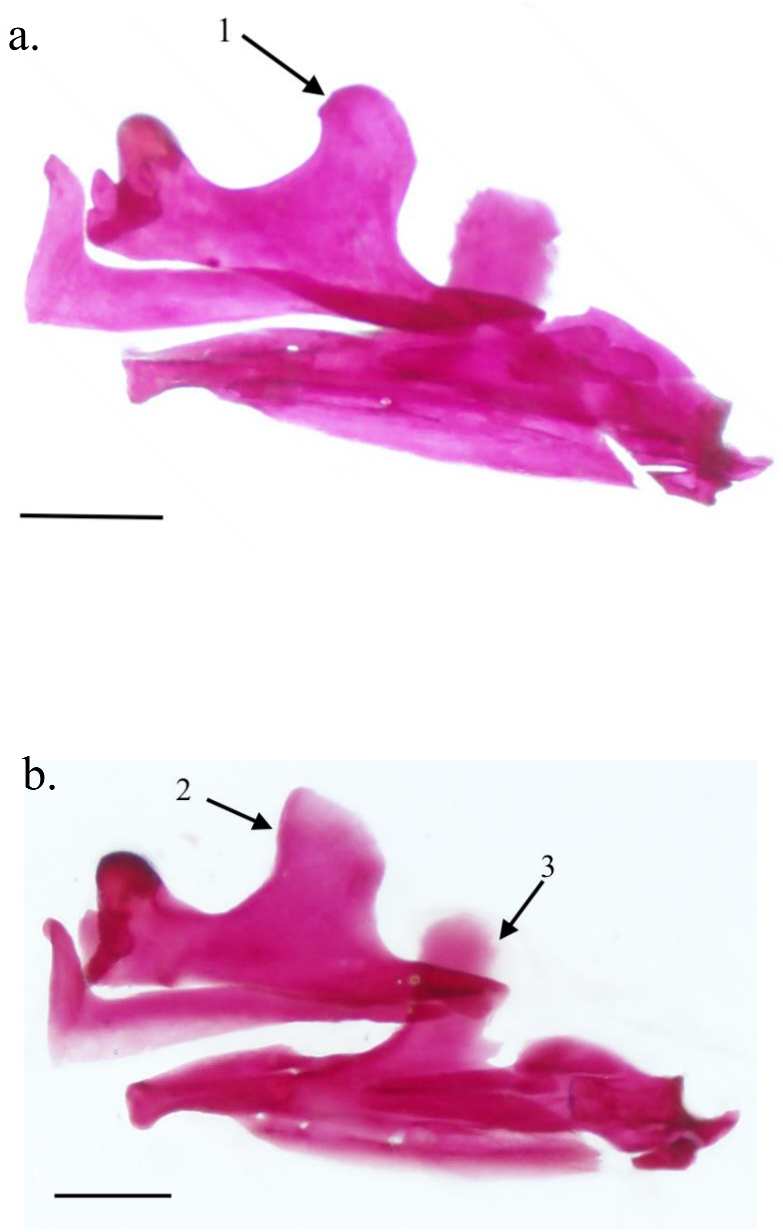

Figure 2.28. The left oral jaws of *Notropis hudsonius* MZF 680, specimen 3, from Manitoba (a), UAMZ 213, specimen 5, from Alberta (b). Arrow 1 points to the rounded ascending process of the maxilla found in some specimens. Arrow 2 points to the squared, pointed morphology of the ascending process of the maxilla found in other specimens. Arrow 3 points to an elongate variant of the coronoid process of the dentary (compare with more robust coronoid process of the dentary in upper photograph. Specimens are in lateral view, anterior to left. Scale bars = 1 mm.

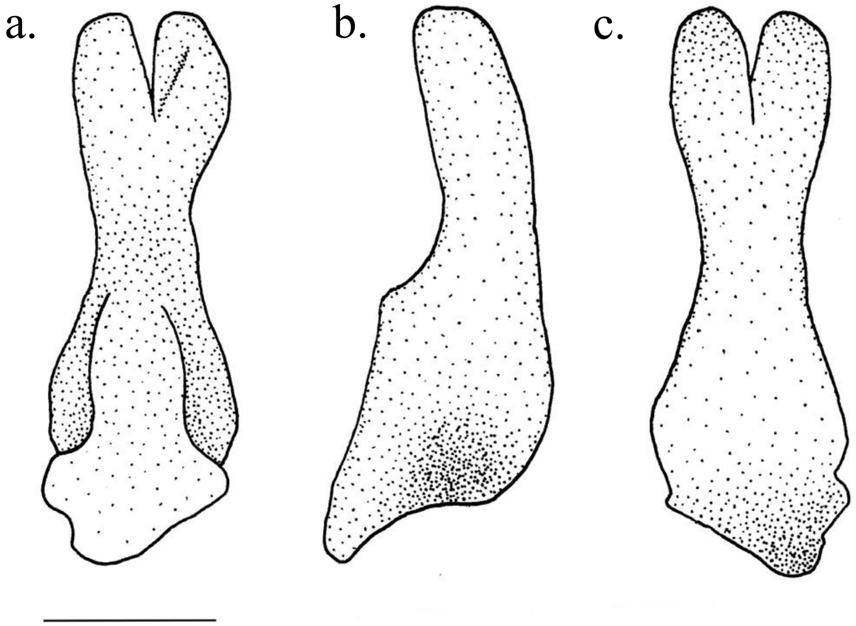

Figure 2.29. Illustration of the kinethmoid of *Notropis hudsonius* MZF 3215, specimen 1, in (a) anterior, (b) lateral and (c) posterior view when the mouth is closed, dorsal region to top of the page. Scale bar = 0.25 mm.

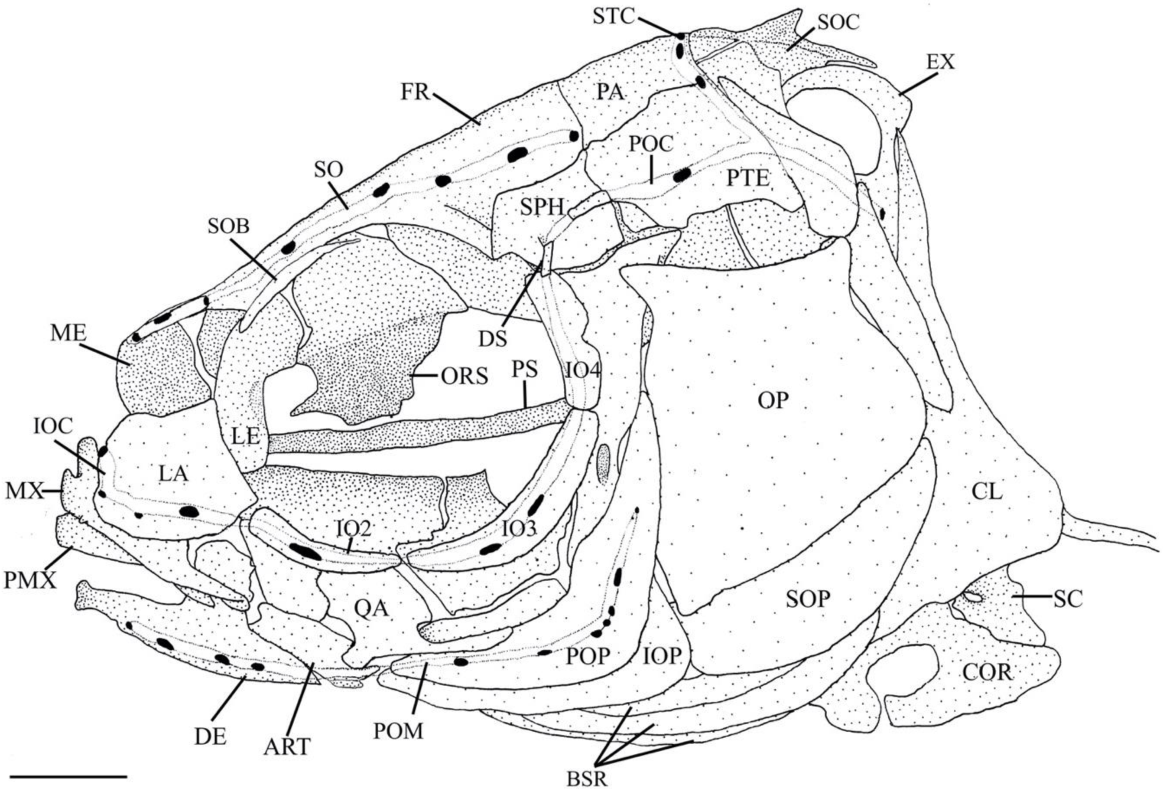

Figure 2.30. Illustration of the skull and sensory canal system of *Notropis hudsonius* UAMZ F1258, specimen 1, in left lateral view, anterior to left. Scale bar = 1 mm.

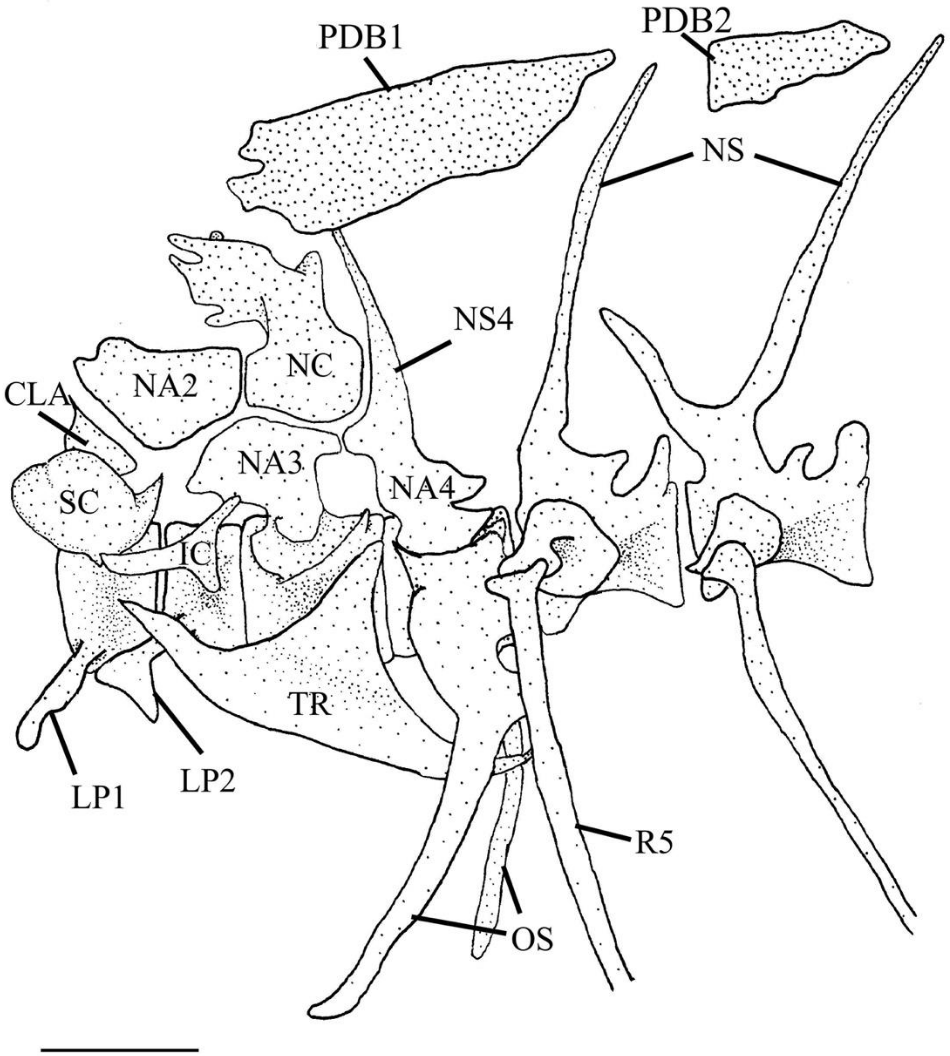

Figure 2.31. Illustration of the Weberian apparatus of *Notropis hudsonius* UAMZ 1258, specimen 1, in lateral view, anterior to left. Scale bar = 1 mm.

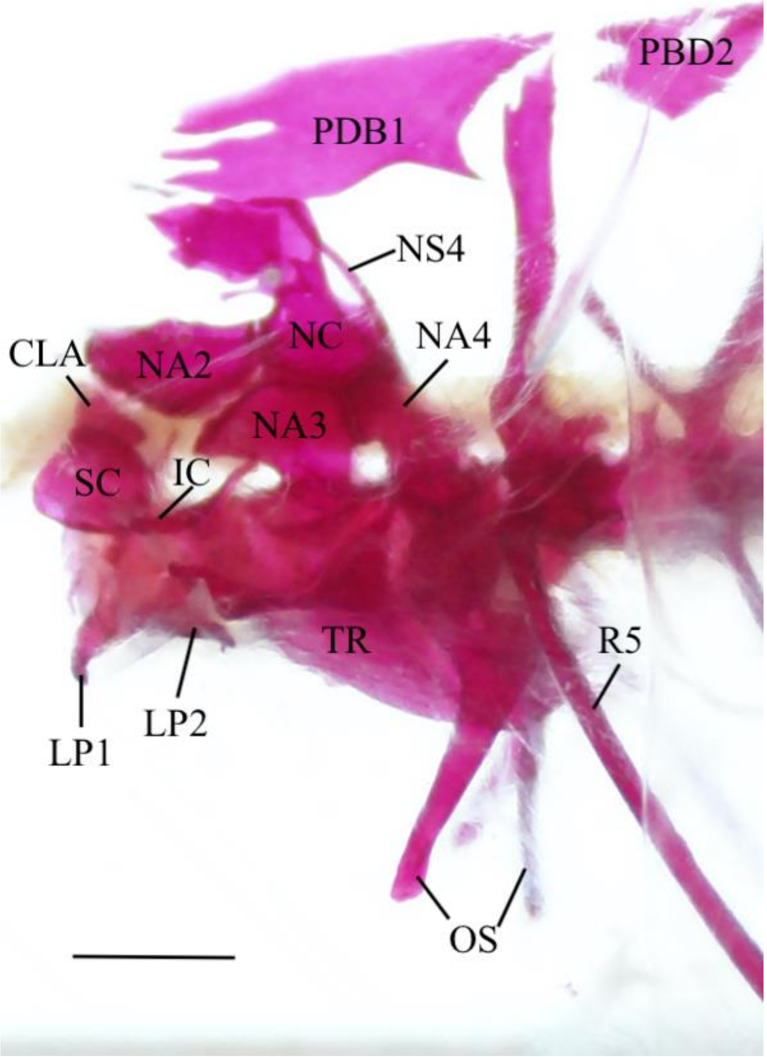

Figure 2.32. The Weberian apparatus of *Notropis hudsonius* UAMZ 4950, specimen 1, in lateral view, anterior to right. The first predorsal bone (add arrow) slots within the neural crest. Scale bar = 1 mm.

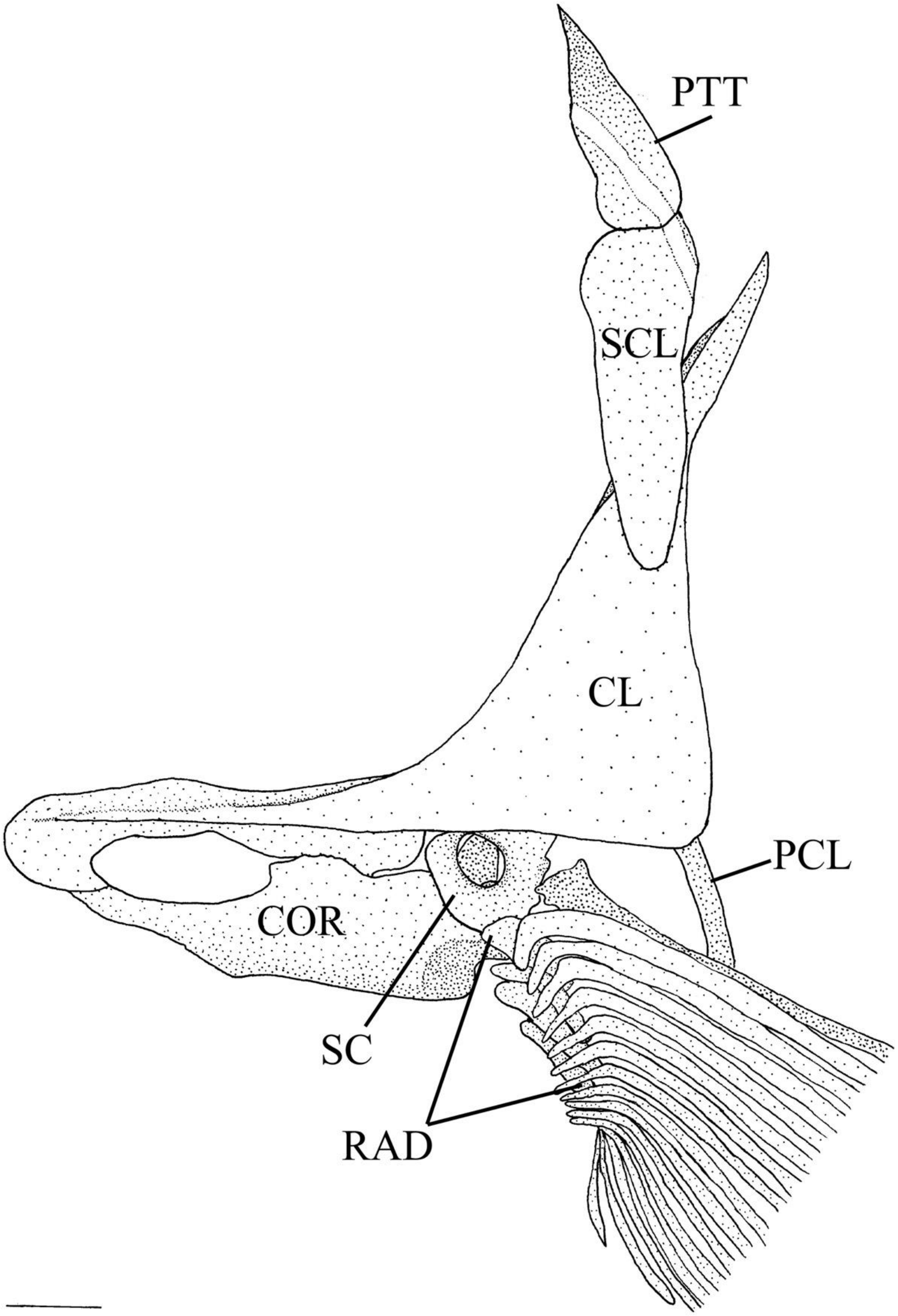

Figure 2.33. Illustration of the pectoral girdle of *Notropis hudsonius* UAMZ 5644.1, specimen 1, in lateral view, anterior to left. Scale bar = 1 mm.

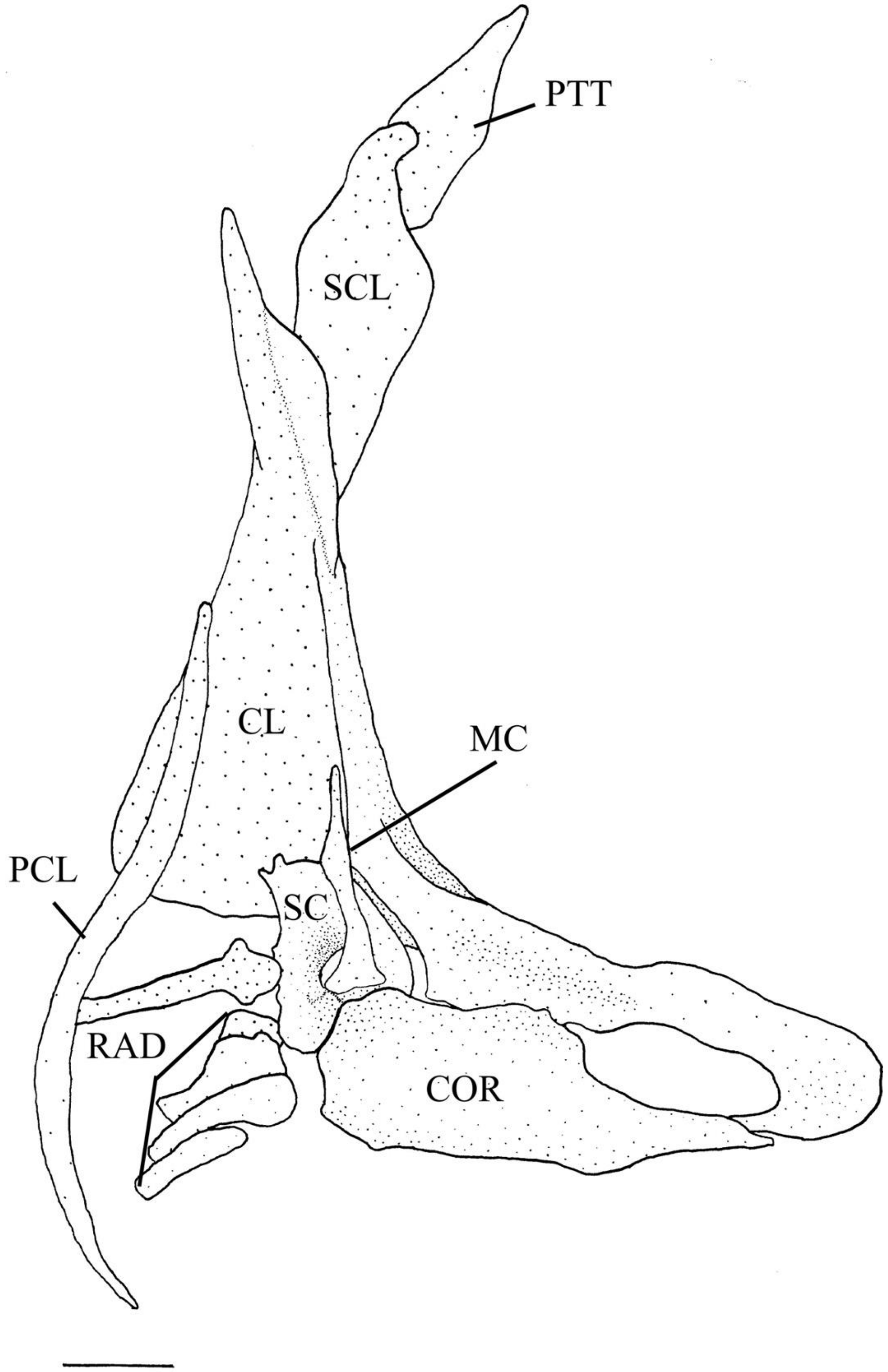

Figure 2.34. Illustration of the pectoral girdle *of Notropis hudsonius* UAMZ 5644.1, specimen 1, in medial view, anterior to right. Scale bar = 1 mm.

Figure 2.35. The horizontal arm of the cleithrum of *Notropis hudsonius* UAMZ 5644.1, specimen 1, in dorsal view, anterior to top of the page. Scale bar = 1 mm.

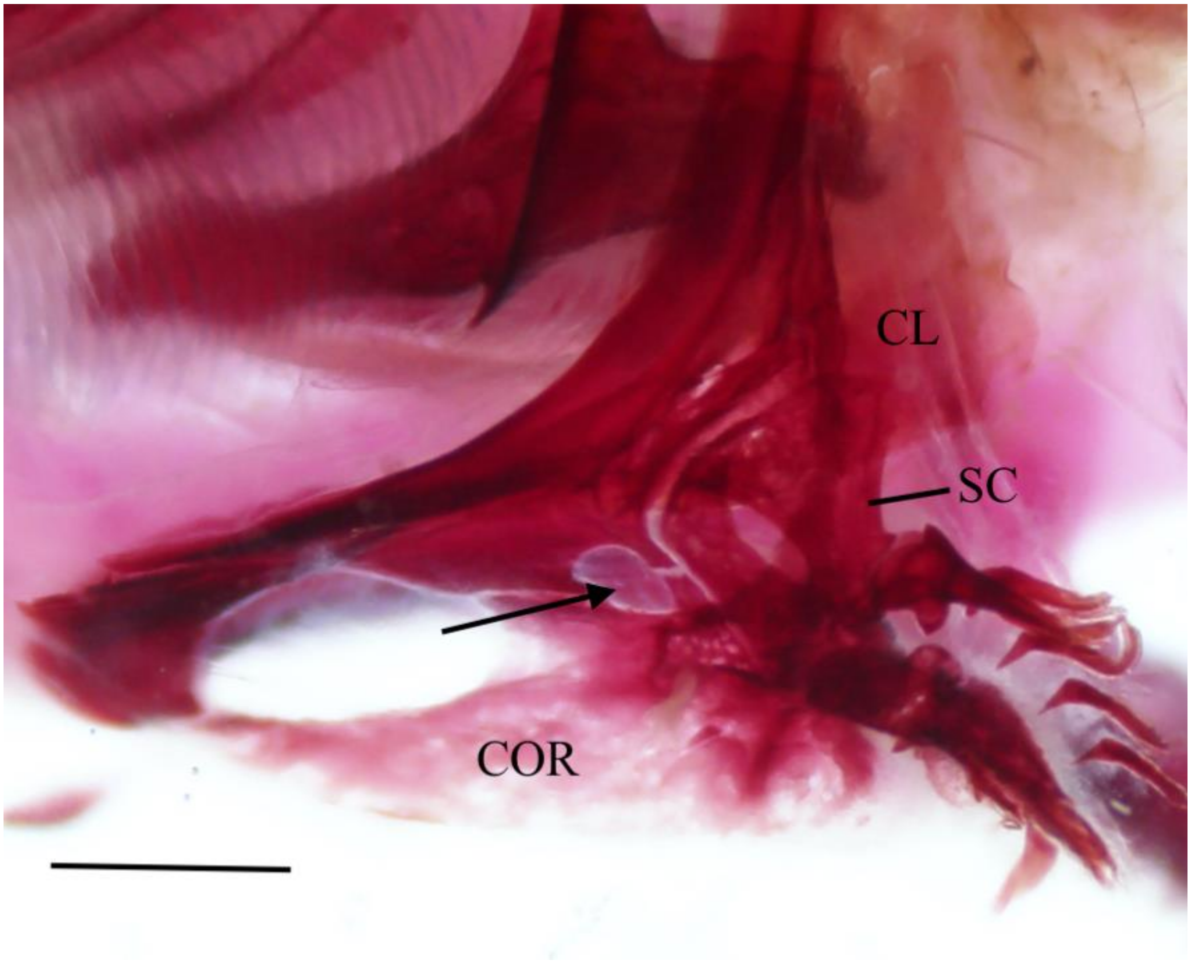

Figure 2.36. The left pectoral girdle of *Notropis hudsonius* UAMZ 221, specimen 4, in lateral view, anterior to left. Specimen shows secondary foramen formed by the coracoid and cleithrum (indicated by arrow). Scale bar = 1 mm.

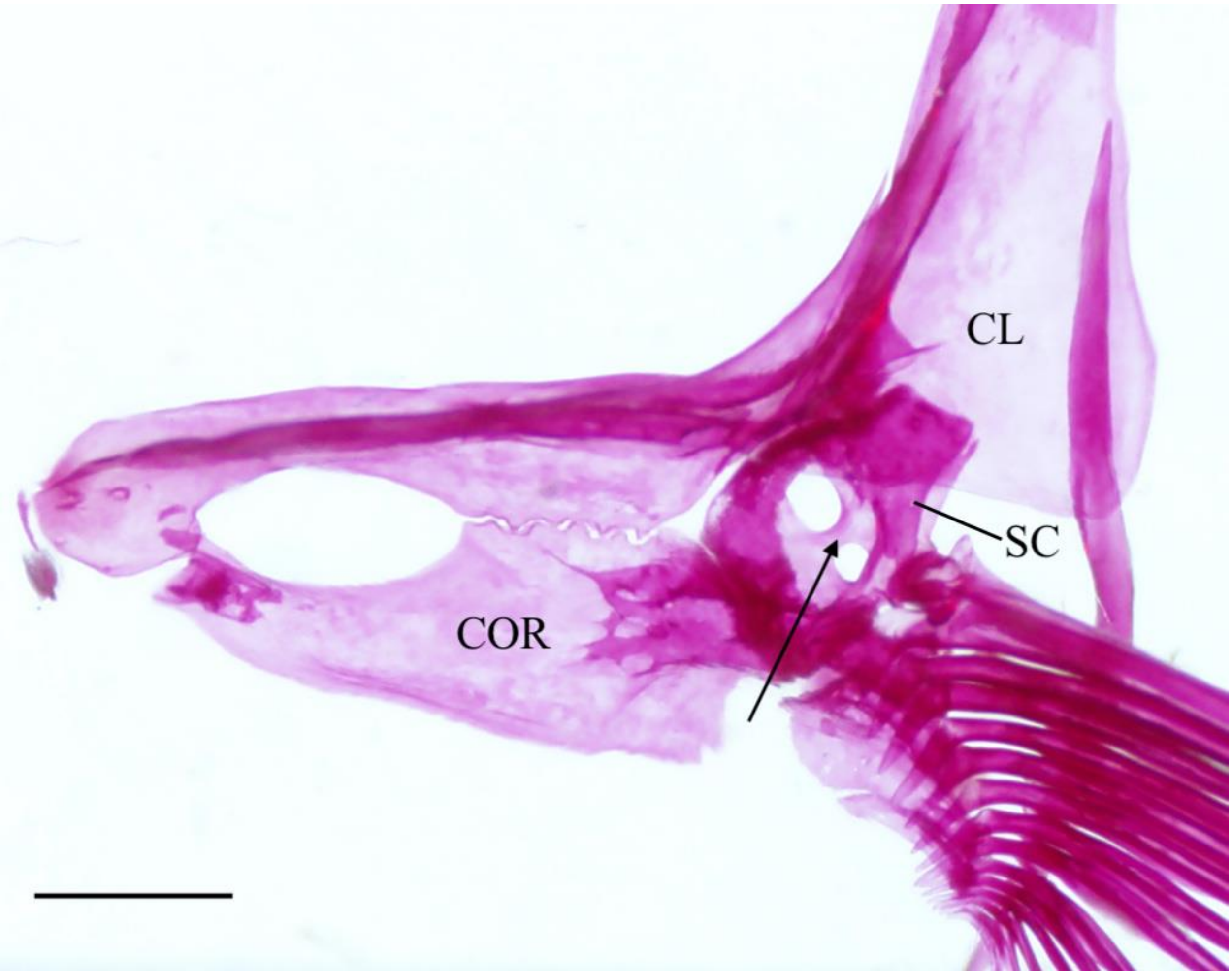

Figure 2.37. The left pectoral girdle of *Notropis hudsonius* UAMZ F1258, specimen 1, in lateral view, anterior to left. Specimen shows a scapular foramen divided by a bony strut (indicated by arrow). Scale bar = 1 mm.

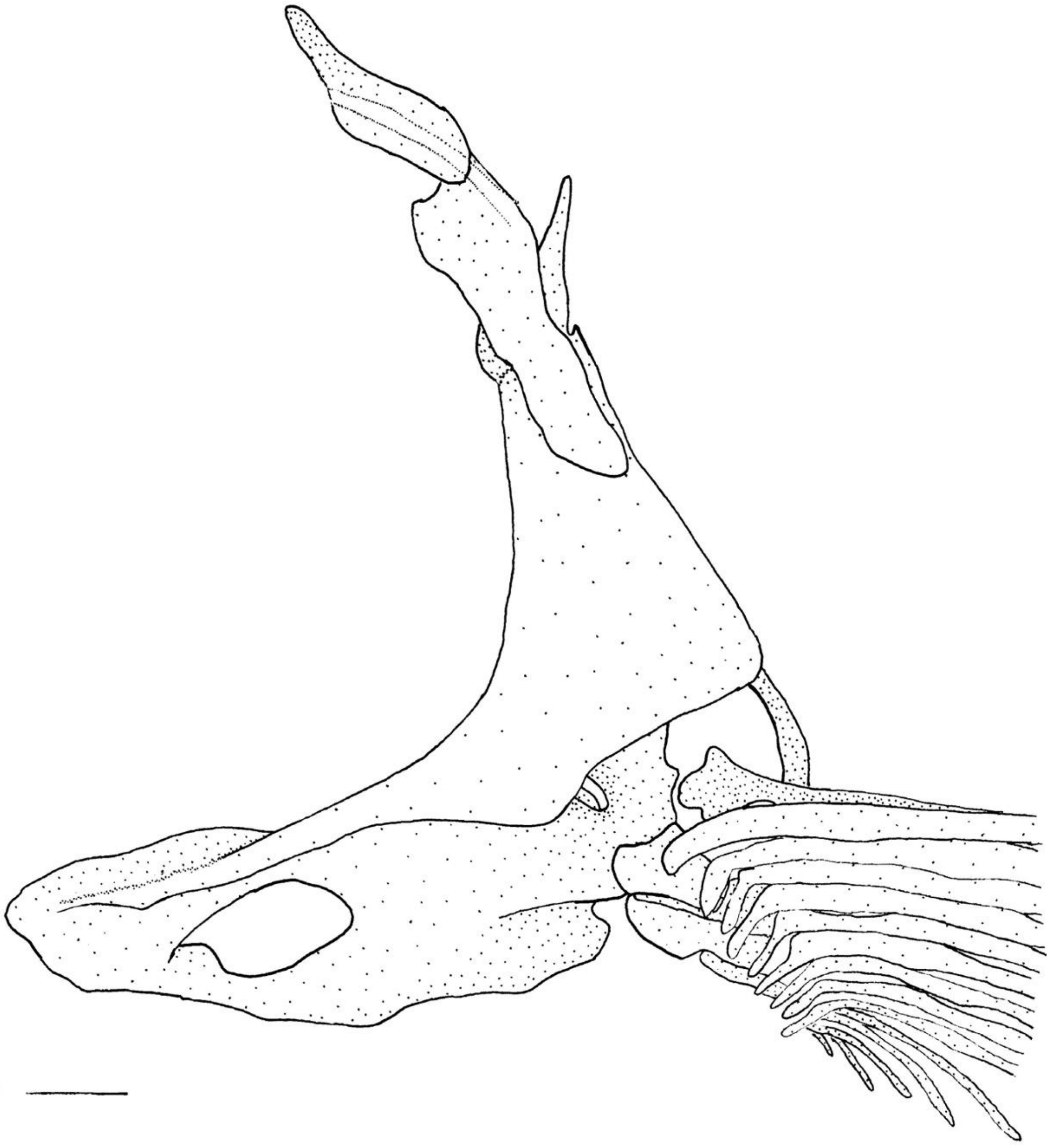

Figure 2.38. Illustration of the pectoral girdle of *Notropis hudsonius* MZF 680, specimen 3, in lateral view, anterior to left. Specimen shows fusion of the cleithrum, coracoid, mesocoracoid and scapula. Scale bar = 1 mm.

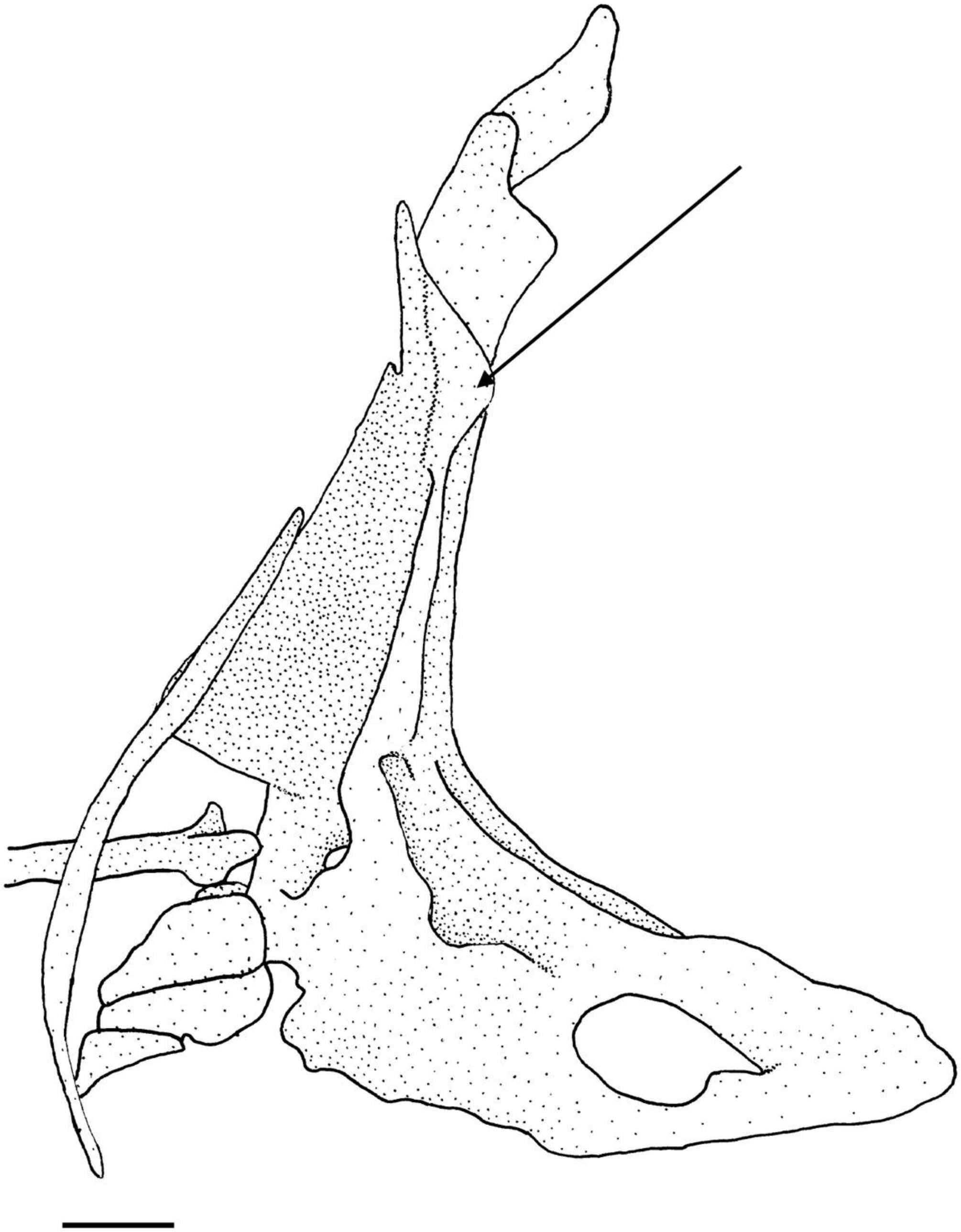

Figure 2. 39. Illustration of the pectoral girdle of *Notropis hudsonius* MZF 680, specimen 3, in medial view, anterior to right. Specimen shows fusion of the cleithrum, coracoid, mesocoracoid and scapula, and an enlarged dorsal flange on the medial ridge of the cleithrum (indicated by arrow). Scale bar = 1 mm.

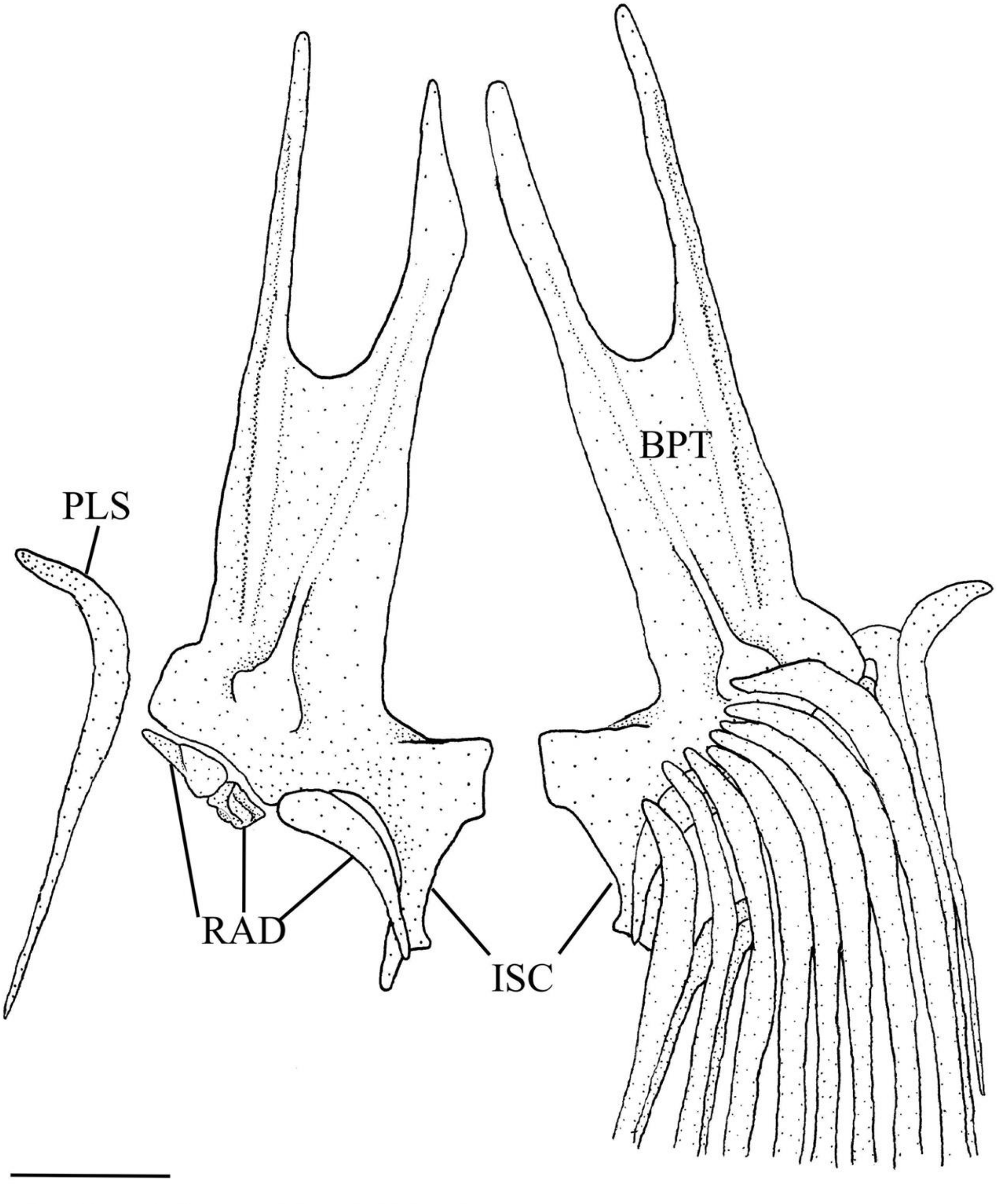

Figure 2.40. Illustration of the pelvic girdle of *Notropis hudsonius* UAMZ F9131, specimen 3, in dorsal view, anterior to top of page. The cartilage joining the basipterygia is not illustrated. Scale bar = 1 mm.

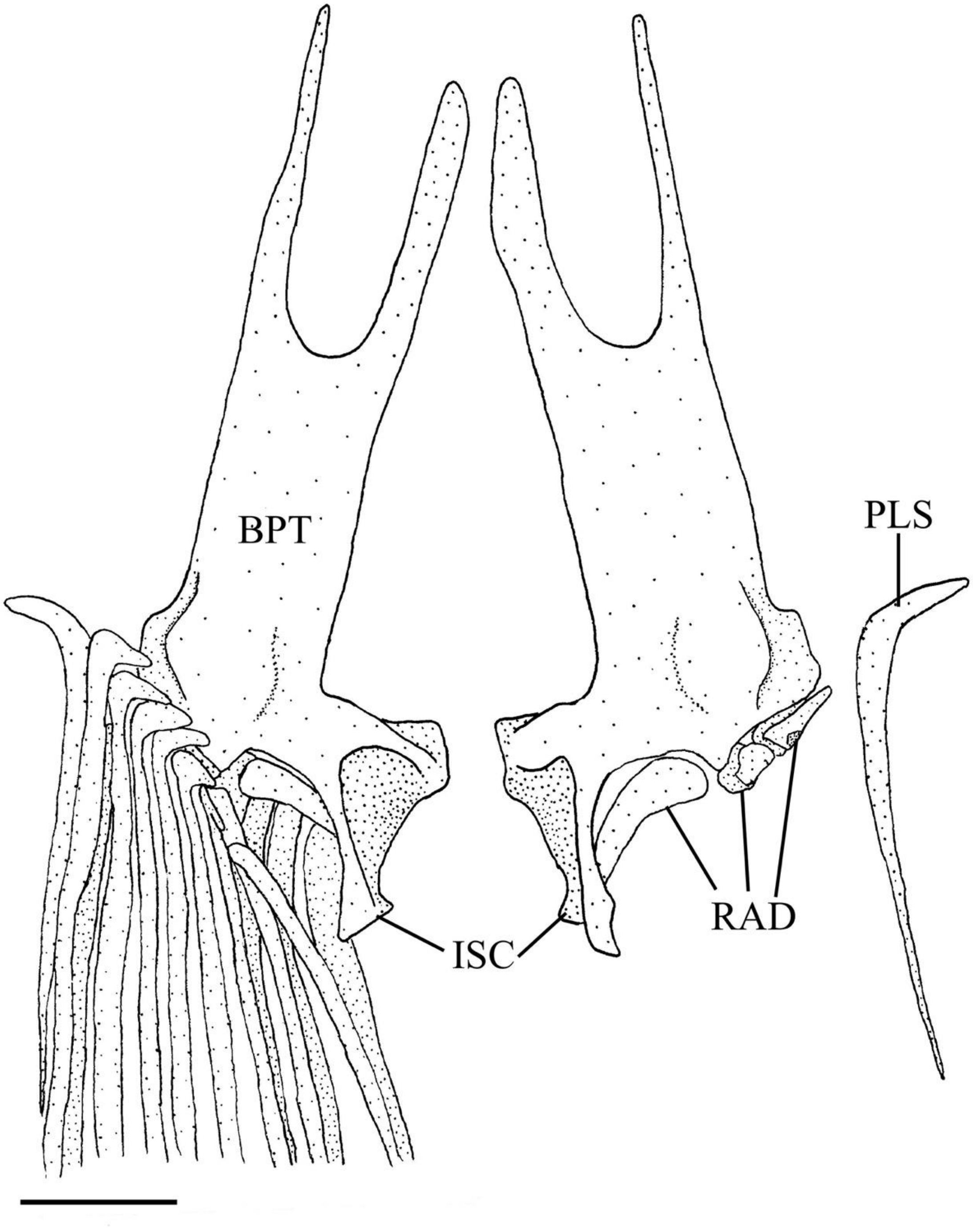

Figure 2.41. Illustration of the pelvic girdle of *Notropis hudsonius* UAMZ F9131, specimen 3, in ventral view, anterior to top of the page. The cartilage joining the basipterygia is not illustrated. Scale bar = 1 mm.

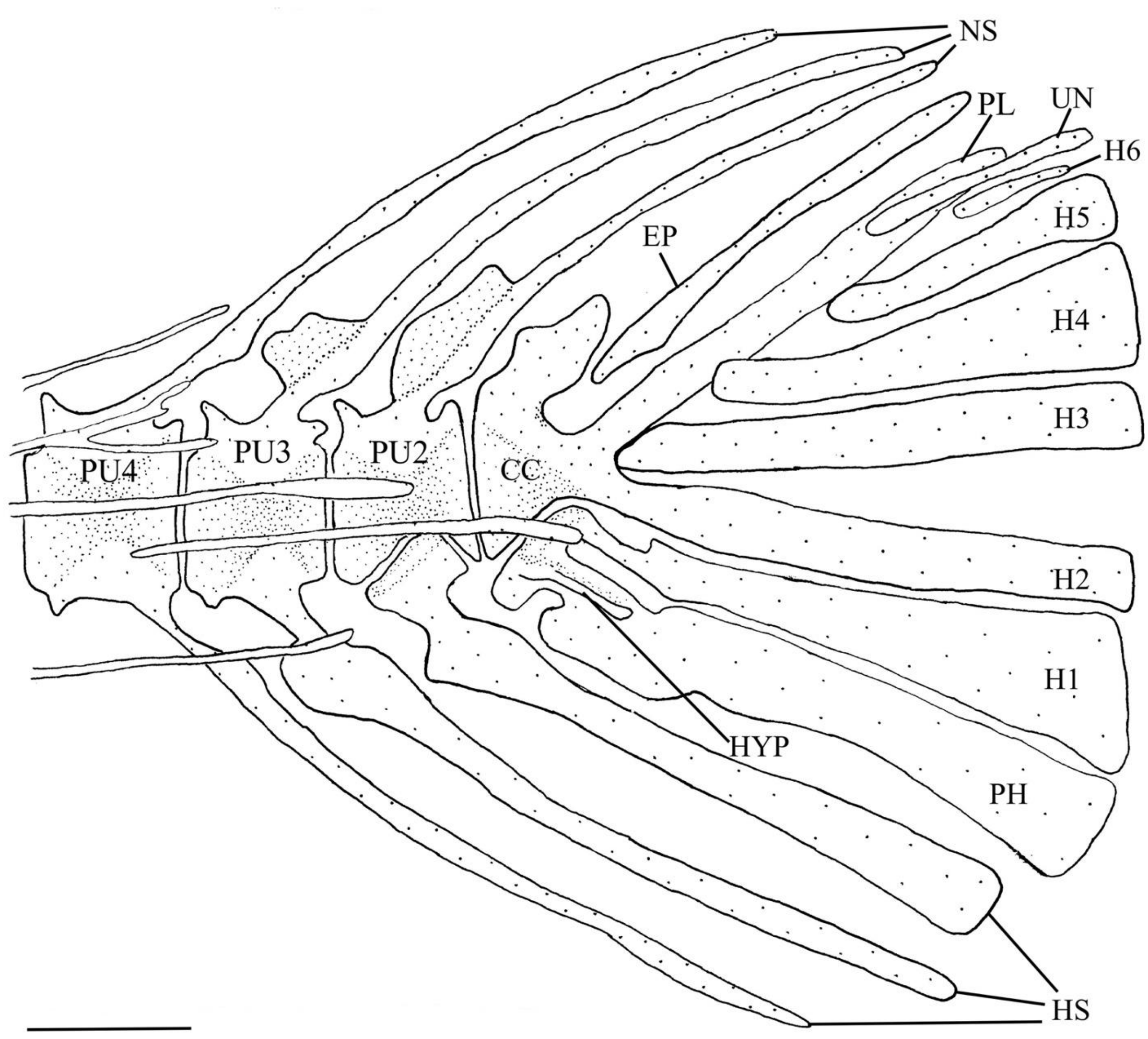

Figure 2.42. Illustration of the caudal skeleton of *Notropis hudsonius* UAMZ F9131, specimen 1, in left lateral view, anterior to left. Scale bar = 1 mm.

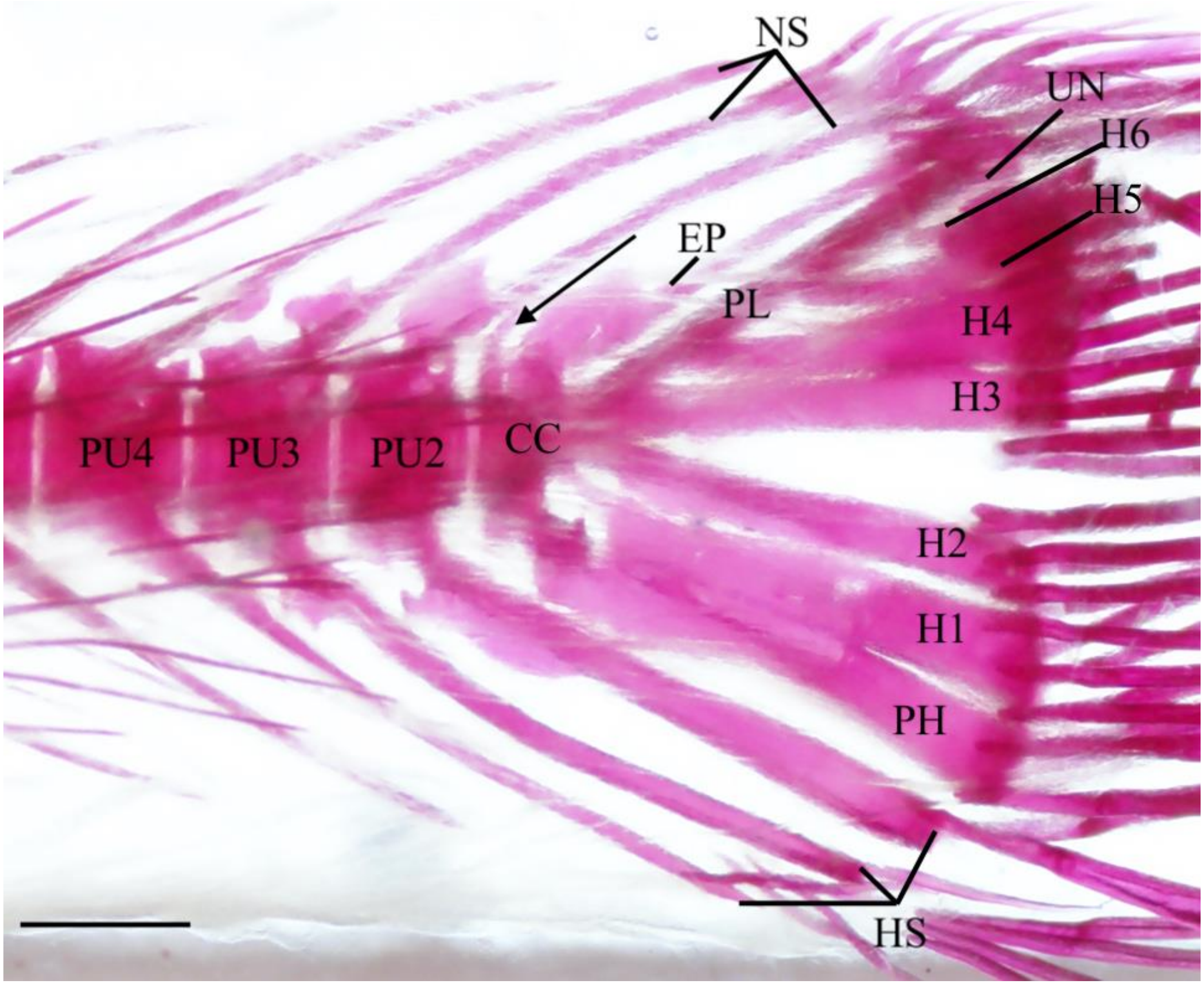

Figure 2.43. The caudal skeleton of *Notropis hudsonius* MZF 2506, specimen 1, in left lateral view, anterior to left. Specimen shows secondary neural spine on compound centrum (indicated by arrow). Scale bar = 1 mm.

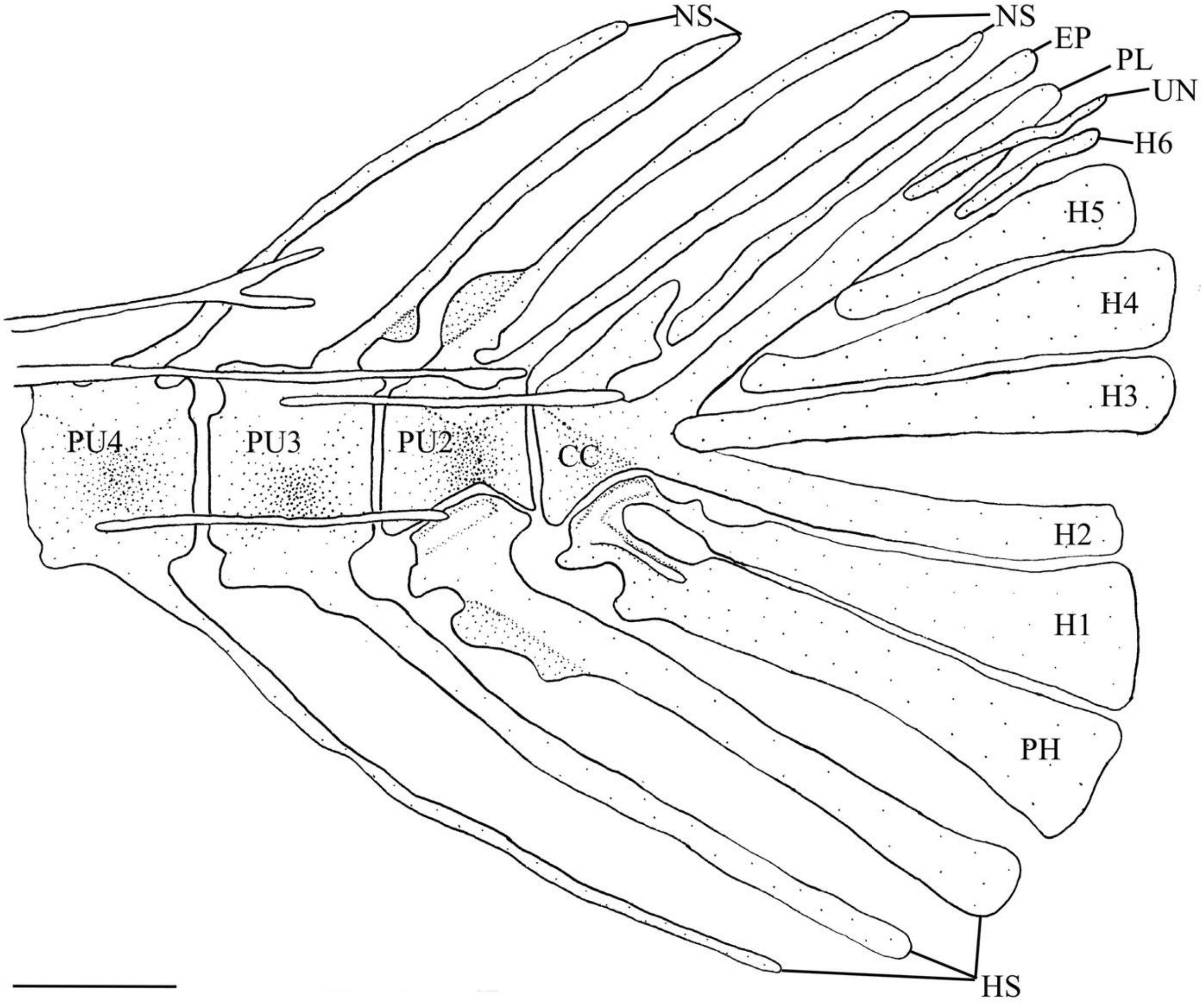

Figure 2.44. Illustration of the caudal skeleton of *Notropis hudsonius* UAMZ 3060, specimen 2, in left lateral view, anterior to left. Specimen shows two neural spines on the second preural centrum. Scale bar = 1 mm.

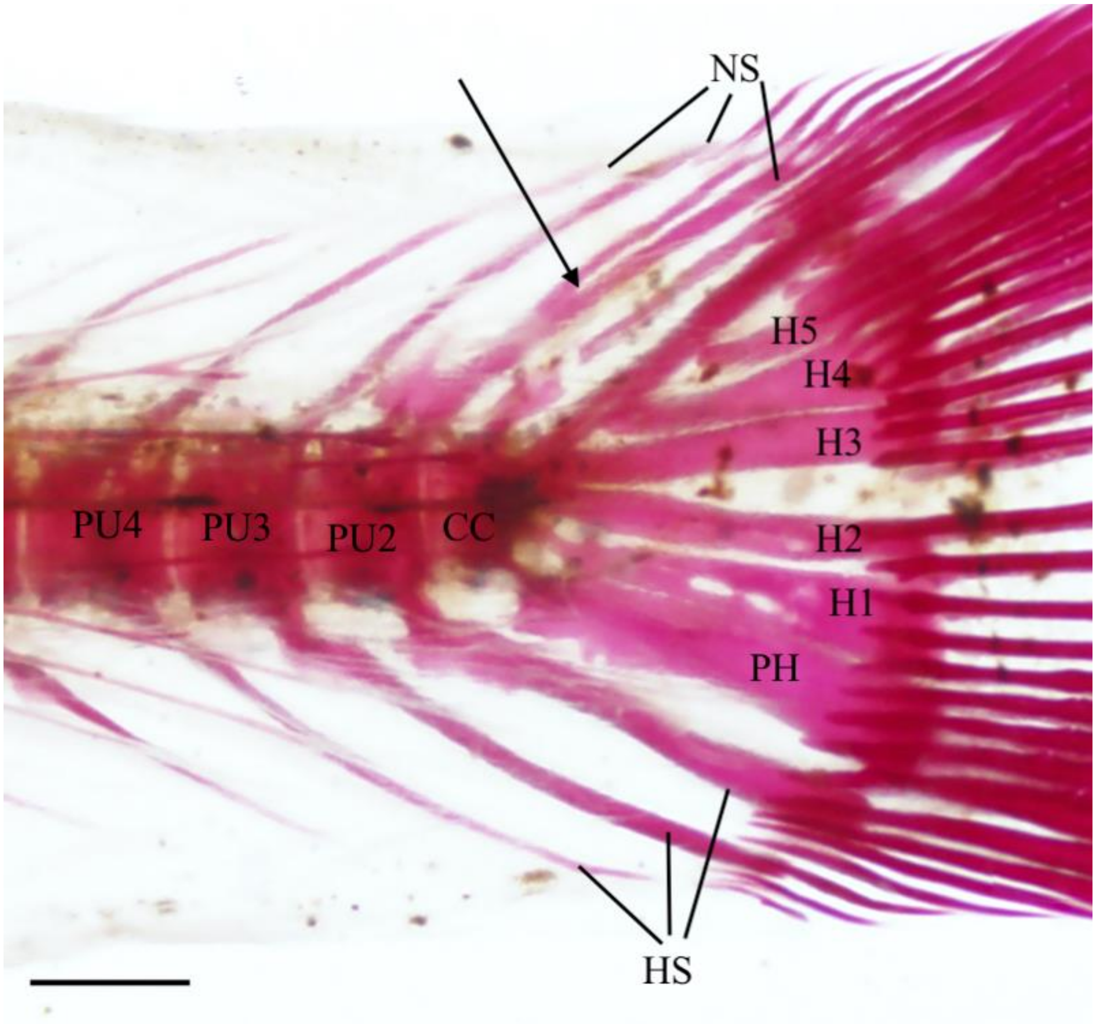

Figure 2.45. The caudal skeleton of *Notropis hudsonius* UAMZ F9126, specimen 2, in left lateral view, anterior to left. Specimen shows division of the neural spine of first preural centrum (indicated by arrow). Scale bar = 1 mm.

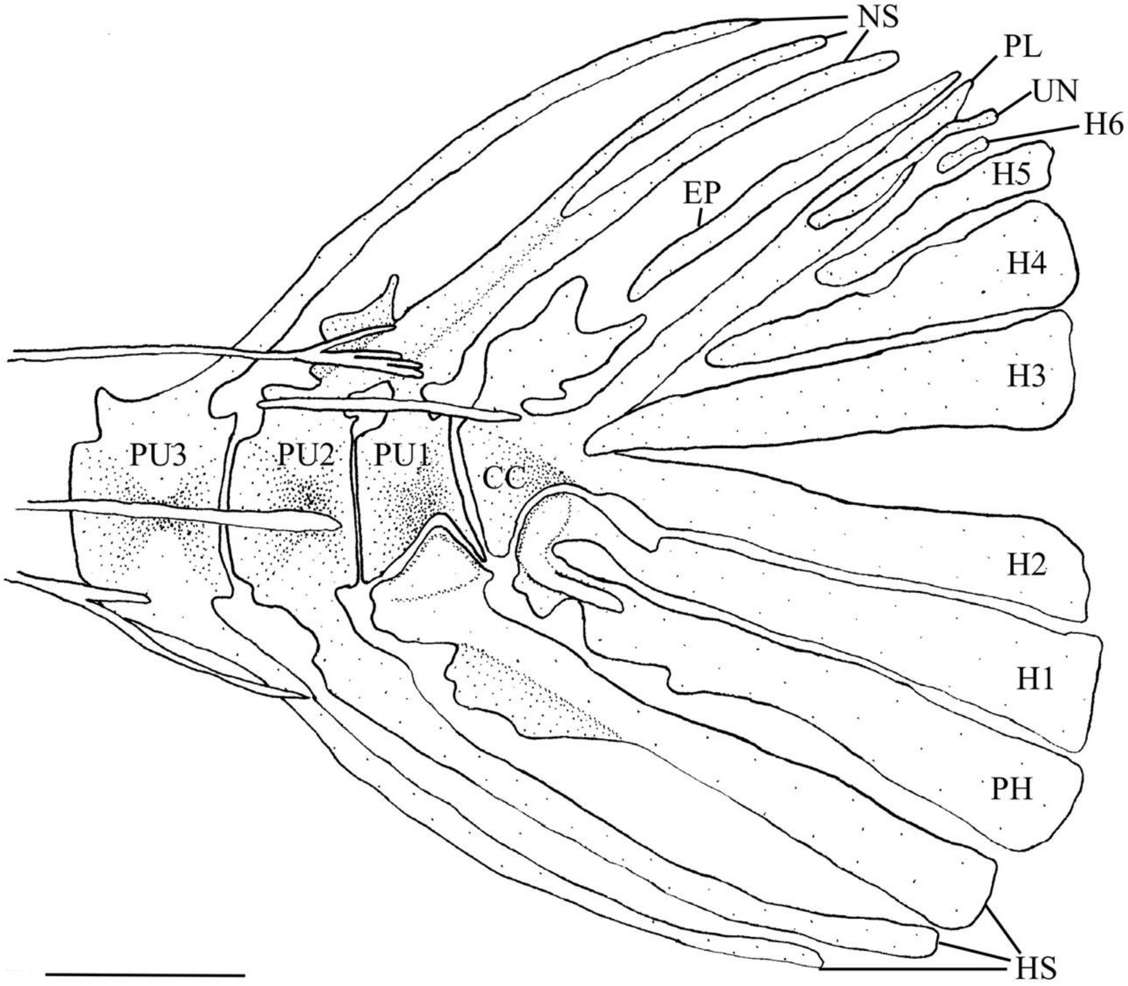

Figure 2.46. Illustration of the caudal skeleton *of Notropis hudsonius* UAMZ 209, specimen 1, in left lateral view, anterior to left. Specimen shows fusion of the neural spines of the second and third preural centra. Scale bar = 1 mm.

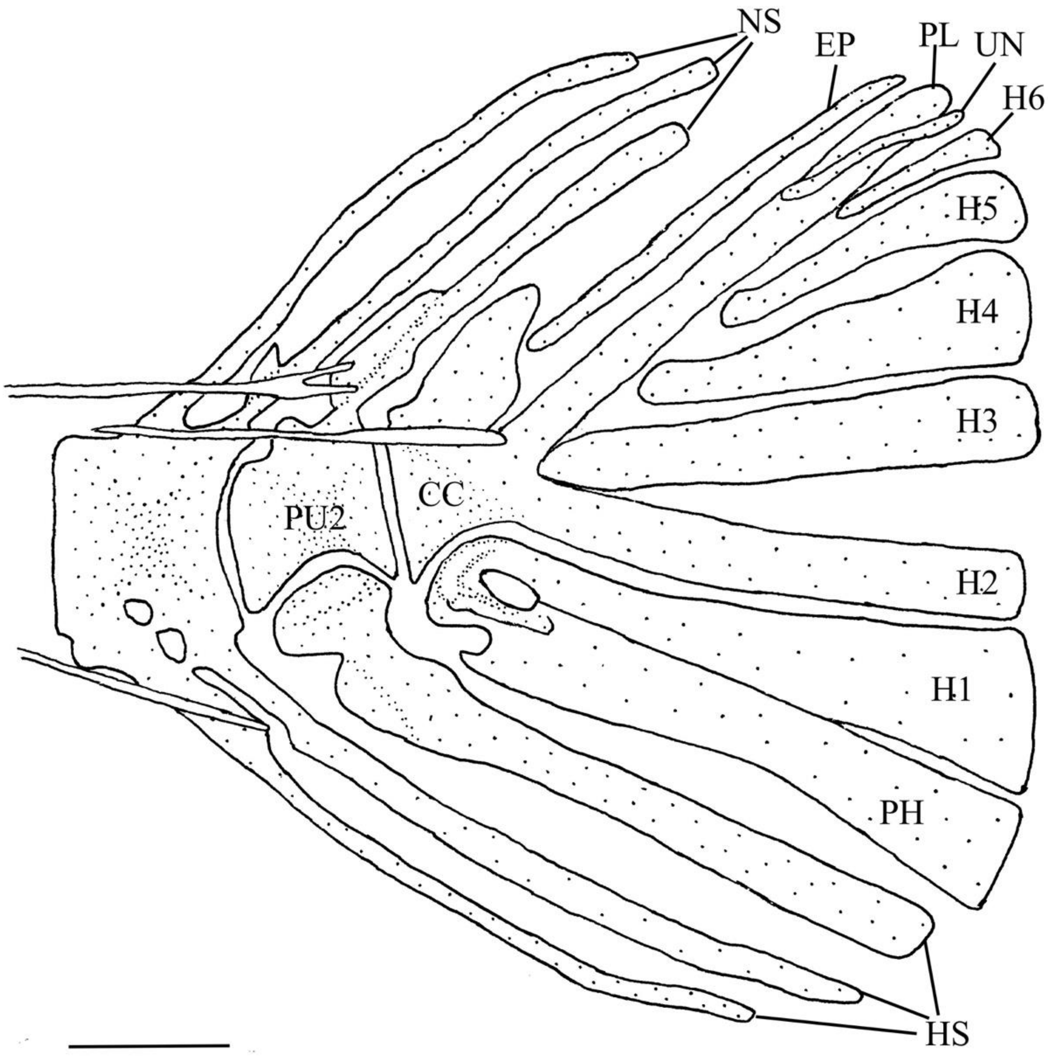

Figure 2.47. Illustration of the caudal skeleton of *Notropis hudsonius* UAMZ F9131, specimen 3, in left lateral view, anterior to left. Specimen shows abutting of the parhypural and first hypural and fusion of the third and fourth preural centra. Scale bar = 1 mm.

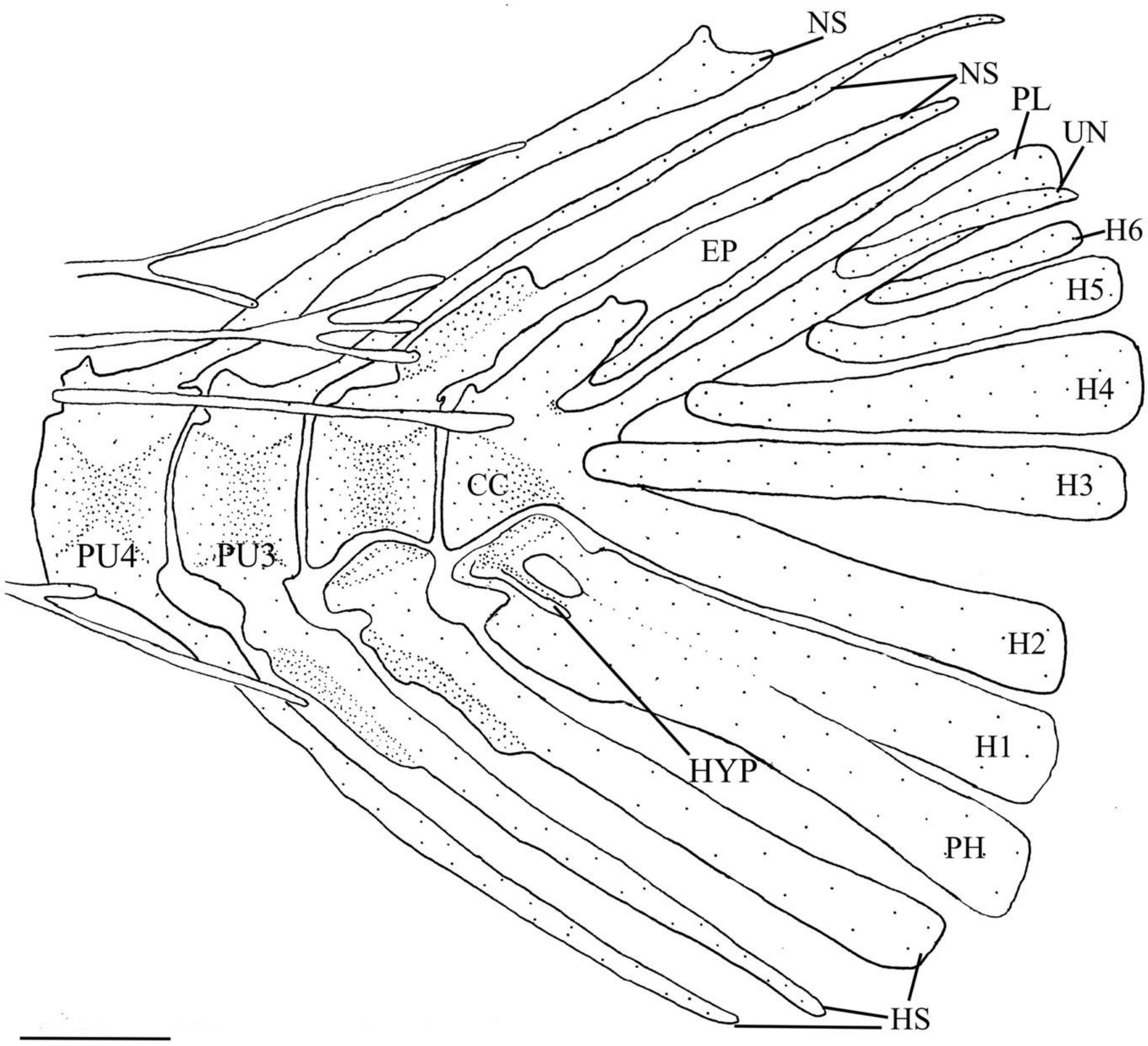

Figure 2.48. Illustration of the caudal skeleton of *Notropis hudsonius* UAMZ F9131, specimen 2 in left lateral view, anterior to left. Specimen shows patrial fusion of the parhypural and first hypural distally. Scale bar = 1 mm.

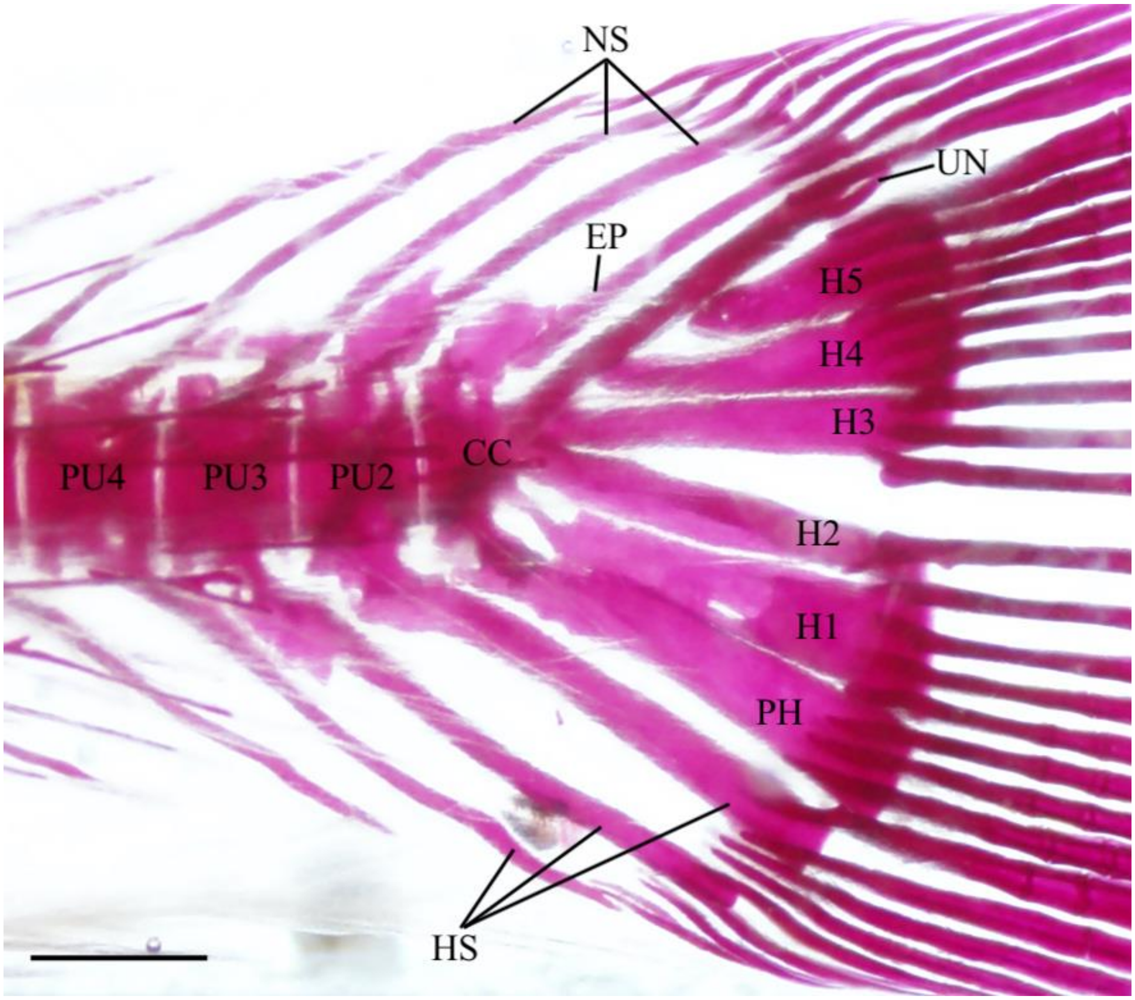

Figure 2.49. The caudal skeleton of *Notropis hudsonius* MZF 680, specimen 1, in left lateral view, anterior to left. Specimen shows fusion of the epural to the compound centrum, lack of the sixth hypural and an enlarged fifth hypural. Scale bar = 1 mm.

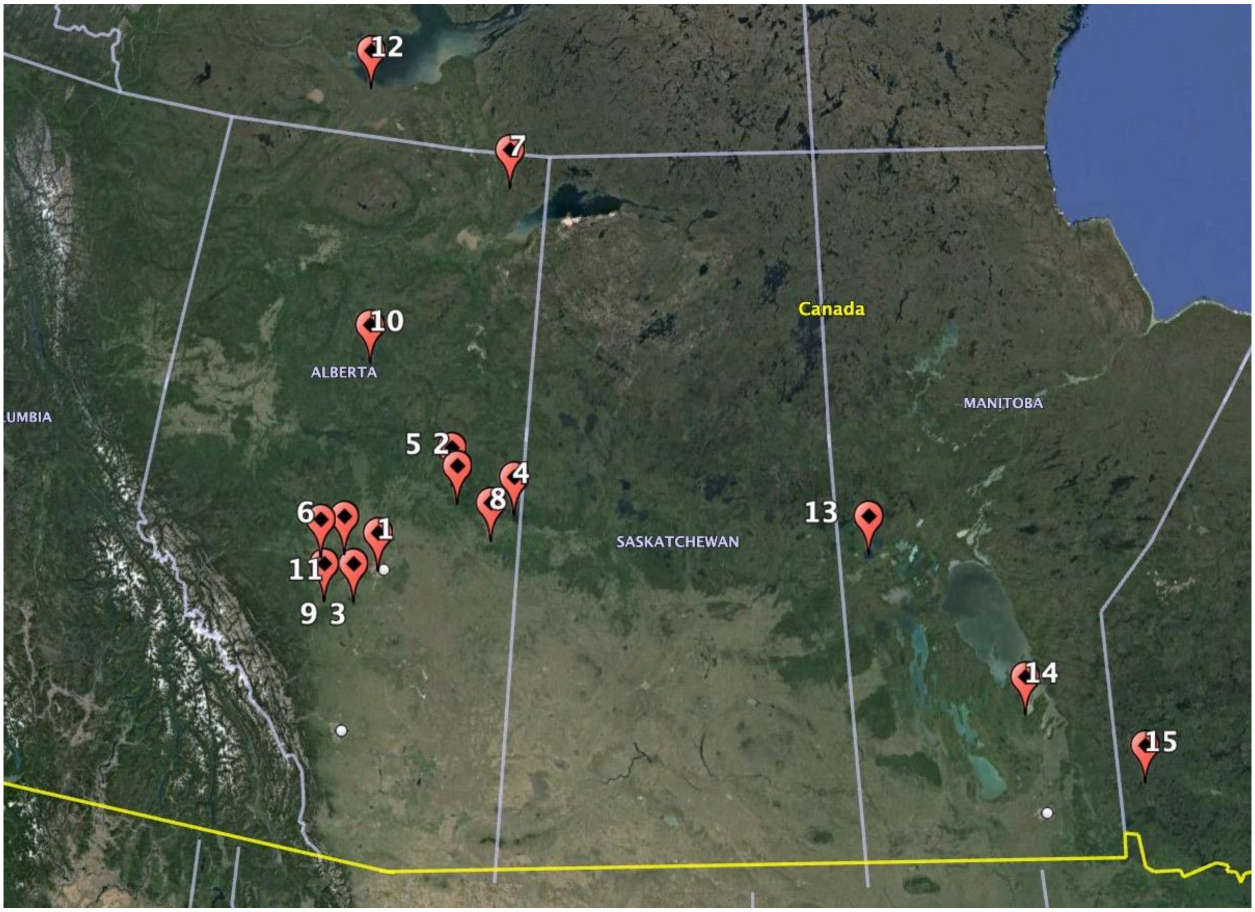

Figure 2.50. Distribution of *Notropis hudsonius* specimens examined. Samples are as follows: (1) UAMZ 209, UAMZ 214 (2), UAMZ 214 (3), UAMZ 220 (4), UAMZ 221 (5), UAMZ 1525 and UAMZ 1528 (6), UMAZ 3215 (7), UAMZ 4950 (8),UAMZ F5644.1 (9), UAMZ F9126 (10), UAMZ F9131(11), UAMZ 3060 (12), MZF 680 (13), MZF 2507 (14) and MZF 2506 (15).

2.7 Literature Cited

Agassiz, L. 1855. Art. XXII.--Synopsis of the ichthyological fauna of the Pacific slope of North America, chiefly from the collections made by the U. S. Expl. Exped. under the command of Capt. C. Wilkes, with recent additions and comparisons with eastern types. American Journal of Science and Arts 19:215–231.

Bird, N. C., and L. P. Hernandez. 2007. Morphological variation in the Weberian apparatus of Cypriniformes. Journal of Morphology 268:739–757.

Bird, N. C., J. R. Abels, and S. S. Richardson. 2020. Histology and structural integration of the major morphologies of the Cypriniform Weberian apparatus. Journal of Morphology 281:273–293.

Buhan, P. J. 1970. The comparative osteology and taxonomy of the North American cyprinid genera, *Richardsonius Ctinostomus* and *Semotilus*, with notes on other minnows. PhD dissertation, Virginia Polytechnic Institute, 332 pp.

Buhan, P. J. 1972. The comparative osteology of the caudal skeleton of some North American minnows (Cyprinidae). American Midland Naturalist 88:484–490.

Clinton, D. 1824. Description of a new species of fish, from the Hudson River. Annals of the Lyceum of Natural History of New York 1:49–50.

Coburn, M. M. 1982. Anatomy and relationships of *Notropis atherinoides*. PhD dissertation, Ohio State University, 384 pp.

Coburn, M. M., and T. M. Cavender. 1992. Phylogenetic relationships of North American Cyprinidae; pp. 328–373 in Systematics, historical ecology, and North American freshwater fishes. Stanford University Press, Stanford, California.

Cope, E. D. 1867. Synopsis of the Cyprinidae of Pennsylvania. Transactions of the American Philosophical Society 13:351–410.

Cope, E. D. 1870. A partial synopsis of the fishes of the fresh waters of North Carolina. Proceedings of the American Philosophical Society 84:448–495.

Cubbage, C. C., and P. M. Mabee. 1996. Development of the cranium and paired fins in the zebrafish *Danio rerio* (Ostariophysi, Cyprinidae). Journal of Morphology 229:121–160.

Eastman, J. T., and J. C. Underhill. 1973. Intraspecific variation in the pharyngeal tooth formulae of some cyprinid fishes. Copeia 1973:45–53.

Evans, H. E., and E. E. Deubler. 1955. Pharyngeal tooth replacement in *Semotilus atromaculatus,* and *Clinostomus elongatus*, two species of cyprinid fishes. Copeia 1955:31.

Fink, S. V., and W. L. Fink. 1981. Interrelationships of the ostariophysan fishes (Teleostei). Zoological Journal of the Linnean Society 72:297–353.

Fowler, H. W. 1935. Notes on South Carolina fresh-water fishes. Contributions from the Charleston Museum 7:1–28.

Froese, R., and D. Pauly. 2023. FishBase.World Wide Web electronic publication. Available at www.fishbase.org. Accessed April 21, 2024.

Gidmark, N. J., and A. M. Simons. 2014. Cyprinidae: carps and minnows; pp. 334–450 in Freshwater Fishes of North America. Johns Hopkins University Press, Baltimore, Maryland.

Girard, C. F. 1856. Research upon the cyprinoid fishes inhabiting the fresh waters of the United States, west of the Mississippi Valley, from specimens in the museum of the Smithsonian Institution. Proceedings of the Academy of Natural Sciences of Philadelphia 2:165–213.

Günther, A. 1868. Catalogue of the Physostomi, containing the families Heteropygii, Cyprinidæ, Gonorhynchiidæ, Hypodontidæ, Osteoglossidæ, Clupeidæ, Chirocentridæ, Alepochephalidæ, Notopteridæ, Halosauridæ, in the collection of the British Museum. Catalogue of the Fishes in the British Museum 7:1–512.

Harrington, R. W. 1955. The Osteocranium of the American Cyprinid Fish, *Notropis bifrenatus*, with an Annotated Synonymy of Teleost Skull Bones. Copeia 1955:267–290.

Hubbs, C. L., and K. F. Lagler. 2004. Fishes of the Great Lakes Region, Revised Edition (G. R. Smith (ed.)). Ann Arbor: University of Michigan Press, 276 pp.

Illick, H. J. 1956. A Comparative Study of the Cephalic Lateral-Line System of North American Cyprinidae. American Midland Naturalist 56:204.

Lundberg, J. G., and J. N. Baskin. 1969. The caudal skeleton of the catfishes, order Siluriformes. American Museum Novitates 2398:1–49.

Mayden, R. L. 1989. Phylogenetic studies of North American minnows, with emphasis on genus *Cyprinella*. Miscellaneous Publication University of Kansas Publications, Museum of Natural History 80:1–189.

Mayden, R. L., A. M. Simons, R. M. Wood, P. M. Harris, and B. R. Kuhajda. 2006. Molecular systematics and classification of North American notropin shiners and minnows (Cypriniformes: Cyprinidae); pp. 72–101 in Studies of North American Desert Fishes in Honor of EP (Phil) Pister, Conservationist. Universidad Autonoma de Nuevo Leon, Mexico.

Myers, G. S. 1925. *Notropis cummingsae*, a new minnow from Wilmington, North Carolina. American Museum Novitates 164.

Nelson, J. S., and M. J. Paetz. 1992. The Fishes of Alberta. The University of Alberta Press, Edmonton, Alberta, 437 pp.

Page, L. M., and B. M. Burr. 2011. A Field Guide to Freshwater Fishes: North America North of Mexico, 2nd ed. Houghton Mifflin Harcourt Publishing Company, New York, New York, 663 pp.

Peer, D. L. 1961. Aspects of the LIife History and Ecology of the SpottailL Shiner *Notropis Hudsonius* (Clinton). Master's Thesis, University of Saskatchewan, 69 pp.

Rafinesque, C. S. 1818. Descriptions of two new genera of North American fishes, Opsanus and Notropis. American Monthly Magazine and Critical Review 2:203–204.

Schönhuth, S., J. Vukić, R. Šanda, L. Yang, and R. L. Mayden. 2018. Phylogenetic relationships and classification of the Holarctic family Leuciscidae (Cypriniformes: Cyprinoidei). Molecular Phylogenetics and Evolution 127:781–799.

Scott, W. B., and E. J. Crossman. 1973. Freshwater Fishes of Canada. Fisheries Research Board of Canada, 966 pp.

Seghers, B. H. 1981. Facultative schooling behavior in the spottail shiner (*Notropis hudsonius*): possible costs and benefits. Environmental Biology of Fishes 6:21–24.

Stout, C., S. Schonhuth, R. Mayden, N. L. Garrison, and J. W. Armbruster. 2022. Phylogenomics and classification of *Notropis* and related shiners (Cypriniformes: Leuciscidae) and the utility of exon capture on lower taxonomic groups. PeerJ 10:e14072.

Taylor, W. R., and G. C. Van Dyke. 1985. Revised procedures for staining and clearing small fishes and other vertebrates for bone and cartilage study. Cybium 9:107–119.

Uyeno, T. 1961. Osteology and phylogeny of the American cyprinid fishes allied to the genus *Gila*. PhD dissertation, University of Michigan, 174 pp.

Chapter 3: Interspecific osteological variation among eleven species of *Notropis* (Cypriniformes: Leuciscidae)

3.1 Introduction

The genus *Notropis* Rafinesque, 1818, represents one of North America's largest genera of freshwater fishes, comprising 91 species (Page and Burr, 2011; Froese and Pauly, 2023). Over the past several decades, a concerted effort has been made to try to decipher the evolutionary relationships within *Notropis* (both s.s. and s.l). Early authors examined the osteology of *Notropis* to delineate phylogenetic relationships*,* both within the genus and between *Notropis* and other cyprinoid groups (Coburn, 1982; Mayden, 1989; Cavender and Coburn, 1992; Coburn and Cavender, 1992). In the last thirty years, molecular data has been adopted as a new way to discern phylogenetic relationships and determine closely related genera (Simons and Mayden, 1998, 1999; Bielawski and Gold, 2001; Schönhuth and Doadrio, 2003; Simons et al., 2003; Mayden et al., 2006; Schönhuth and Mayden, 2009; Hollingsworth et al., 2013; Schönhuth et al., 2018; Stout et al., 2022). These studies have consistently shown that *Notropis*, as it is currently understood, is polyphyletic (Simons et al., 2003; Mayden et al., 2006; Hollingsworth et al., 2013; Schönhuth et al., 2018; Stout et al., 2022). This problem has persisted, even when reclassifications have been proposed (Mayden et al., 2006; Stout et al., 2022).

For the third chapter of this thesis, I aim to reassess and compare the osteology of eleven species of *Notropis*: *Notropis atherinoides* Rafinesque, 1818, *N. blennius* Girard, 1856, *N. buchanani* Meek, 1896, *N. dorsalis* Agassiz, 1854, *N. heterodon* Cope, 1865, *N. heterolepis* Eigenmann & Eigenmann, 1893, *N. hudsonius* Clinton, 1824, *N. percobromus* Cope, 1871, *N. stramineus* Cope, 1865, *N. texanus* Girard, 1856, and *N. volucellus* Cope, 1865. All of these species are endemic to Western Canada (Page and Burr, 2011), with the exception of *N. buchanani*, which has a limited range in southwestern Ontario (Holm and Houston, 1993).

Sensu Mayden et al. (2006), nine of these species are classified into four subgenera, while two are of uncertain placement (Fig. 1.1). *Notropis hudsonius* is placed in subgenus *Notropis (Hudsonius)* Clinton, 1824 and is the most basal of these species according to the analysis of Mayden et al. (2006). *Notropis blennius* and *N. texanus* are placed within subgenus *Notropis (Alburnops)* Girard, 1856, although they are more distantly related compared to other species in the subgenus. *Notropis stramineus* and *N. heterodon* are placed in subgenus *Notropis (Miniellus)* Jordan, 1882. While Mayden et al. (2006) resolved *N. heterodon* and *N. stramineus* as sister species, Schönhuth et al. (2018) found *N. heterodon* to be sister to a clade containing *N. stramineus* and *N. topeka* Gilbert, 1884. However, both authors agree that these two species are closely related.

Notropis atherinoides, *N. percobromus*, *N. buchanani* and *N. volucellus* were placed in subgenus *Notropis (Notropis)* Rafinesque, 1818 by Mayden et al. (2006). *Notropis atherinoides* and *N. percobromus* were resolved in a clade separate from *N. buchanani* and *N. volucellus*. *Notropis buchanani* and *N. volucellus* were further resolved as sister species. Schönhuth et al. (2018) came to a different conclusion, finding *N. buchanani* and *N. volucellus* to be in its own, distantly related clade distantly related to *N. atherinoides* and *N. percobromus*. Stout et al. (2022) later reassigned *N. buchanani* and *N. volucellus* to subgenus *Notropis (Paranotropis)* Fowler, 1904. However, both Mayden et al. (2006) and Stout et al. (2002) agreed that among the eleven species examined in this chapter, *N. atherinoides* is the closest relative of *N. percobromus* while *N. buchanani* is the closest relative of *N. volucellus*

Notropis dorsalis and *Notropis heterolepis* are of unclear placement. Mayden et al. (2006) found *N. dorsalis* to be in a clade with *Notropis nazas* Meek, 1904 and *Notropis scepticus* Jordan and Gilbert, 1883, that formed a polytomy with genus *Cyprinella* Girard, 1856 and subgenus *Notropis (Miniellus).* Schönhuth et al. (2022) and Stout et al. (2022) instead supported *N. dorsalis* as sister to genus *Ericymba* Cope, 1865. *N. heterolepis* was resolved by Mayden et al. (2006) to form a clade with *Notropis rupestris* Page and Beckham, 1987, that was in a polytomy with *Aztecula* Jordan & Everman, 1896, *Graodus* Günther, 1868, *Yuriria* Jordan and Everman, 1896 and *Pteronotropis* Fowler, 1935. However, later work by Schönhuth et al. (2018), and Stout et al. (2022) came to widely different conclusions about the evolutionary relationships of *N. heterolepis*, making its exact placement unclear.

Building on the osteological description of *Notropis hudsonius* provided in Chapter 2, in this chapter I will review and compare the osteological characteristics of the eleven species listed above, keeping the phylogenies and subgenera established by Mayden et al. (2006) in mind. As in the previous chapter, I will analyze and compare osteological features of the cranial, branchial, pectoral, pelvic and caudal regions, with the aim of identifying interspecific differences. This osteological analysis will establish a better understanding of the osteology of eleven *Notropis* species, four subgenera, and two species of unclear placement *sensu* Mayden et al. (2006).

3.2 Materials and Methods

3.2.1 Materials

The specimens included in this study (Appendix A) are cataloged in the University of Alberta Museum of Zoology Ichthyology Collection, Edmonton, Alberta, Canada (UAMZ) and the University of Manitoba Ichthyology Collection, Winnipeg, Manitoba, Canada (MZF) . I examined a total of 128 specimens of the species *Notropis atherinoides* (*n* = 8), *Notropis blennius* (*n* = 11), *Notropis buchanani* (*n* = 3), *Notropis dorsalis* (*n* = 3), *Notropis heterodon* (*n* = 3), *Notropis heterolepis* (*n* = 7) *Notropis hudsonius* (*n* = 72), *Notropis percobromus* (*n* = 3), *Notropis stramineus* (*n* = 8), *Notropis texanus* (*n* = 2) and *Notropis volucellus* (*n* = 7). Ten of the *N. hudsonius* and six of the *N. blennius* specimens from the University of Alberta's collections were cleared and stained prior to this study and stored in 100% glycerin. All remaining specimens were initially preserved in alcohol and some were then cleared and stained following the protocols of Taylor and Van Dyke (1985). Specimen numbers correspond to different populations. For more details on the specimens used, please consult Appendix A.

3.2.2 Measurements and Statistical Analysis

Measurements, meristic counts and dental formulas for the *Notropis* specimens used in this study were documented according to Hubbs and Lagler (2004). Scale counts were collected according to Armbruster (2012), while preanal, prepectoral and prepelvic length follow Habib et al. (2019). Definitions for these measurements and meristic counts can be found in Appendix B. Vertebral counts included the four Weberian centra and the compound centrum of the caudal skeleton (Fink and Fink, 1981). Pore counts of the supraorbital, supratemporal, infraorbital, preopercular mandibular and postocular commissure sensory canals of the skull were taken from cleared and stained specimens and counted according to Illick (1956). Measurements and meristic counts (including vertebral counts) were further analyzed using principal component analysis (PCA). These analyses were done to determine if and how osteological related measurements and meristic counts, namely from the fins, gill rakers and vertebral counts, tie into the interspecific differences amongst the 11 *Notropis* species examined. PCA was completed using R Studio version 4.2.2, using "princomp" function of pcaMethods package. To account for size, measurements were analyzed as a proportion of standard length.

A total of 100 cleared and stained *Notropis* specimens were examined. Photographs for osteological drawings were taken with a Nikon 1200 camera mounted on a Zeiss Stereo

Discovery.V8 stereomicroscope with a Carl Zeiss 44403 6-9000 eyepiece (8x) and a variety of lenses (Zeiss Achromat S 0.3x FWD 236 mm, Zeiss Plan Apo S 0.63x FWD 81 mm, and Zeiss Plan Apo S 1.0x FWD 60 mm), using NIS-Elements F software package 2.20, version 5.03. Osteological terminology generally follows Coburn (1982) and Conway (2011) unless otherwise specified. Terminology relating to the sensory canal system follows Reno (1966). My analysis focused on the oral jaws, suspensorium, opercular series, branchial apparatus, hyoid region, circumorbital series, Weberian apparatus, pectoral girdle, pelvic girdle, and caudal skeleton. I also analyzed elements of the skull, organizing my analysis into an ethmoid region, orbital region, otic and occipital region, and basicranial region. I dissected out the branchial apparatus from at least one specimen of each species to facilitate examination of the branchial apparatus, otic, occipital and basicranial regions. My analysis of these regions was limited by the number of specimens I had permission to dissect.

3.3 Results

3.3.1 Measurements and Statistical Analysis

The PCA conducted on the measurements of 11 *Notropis* species examined (Tables 1 to 10) showed that the vast majority of variance was explained by the first four principal components (Fig. 3.1). For PC1, the largest loadings are from preanal length, prepelvic length and body depth, all of which are positively correlated with PC1. For PC2, the largest loadings are from preanal length and predorsal length, which are positively correlated with PC2 and peduncle and dorsal fin length, which are negatively correlated with PC2. For PC3, predorsal length has the highest loadings by far and is negatively correlated with PC3 (Fig. 3.2). For PC4, the anal fin base, pectoral fin length and peduncle length have the highest loadings, with the first two being negatively correlated and the last positively correlated. When PC1 and PC3 is plotted against PC2 and PC4, respectively, there was no distinct separation of the species (Fig. 3.3).

3.3.2 Osteology

3.3.2.1 Ethmoid Region

Interspecific differences in the ethmoid region relate to the ossification of the nasals, the overall size and shape of the ethmoid block (Conway, 2011), the olfactory foramen, lateral ethmoids, and vomer. In most species examined, the nasals are well ossified, except for *Notropis buchanani* and *Notropis heterolepis*. However, the nasal sensory canals are still present. The posterior portion of the olfactory foramen, formed by the lateral ethmoids, is broad and round in most of the species examined. For *Notropis buchanani*, *Notropis hudsonius, Notropis stramineus, Notropis heterodon* and *Notropis texanus*, the posterior margin of the olfactory foramen is narrowed. In one of the *N. blennius* specimens I examined, the olfactory foramen is isolated within the lateral ethmoids. This is most likely an individual variant, similar to that observed in *N. hudsonius* (Chapter 2).

The ethmoid block itself is noticeably elongate in *Notropis blennius*, *Notropis dorsalis* and *Notropis volucellus* and short in *Notropis heterodon*, *Notropis percobromus* and *Notropis texanus*. The ethmoid blocks of the remaining species are of intermediate length (Fig. 3.4). The anterior notch of the ethmoid block is deep in *N. dorsalis* and *Notropis heterolepis*, as observed by both Coburn (1982) and Mayden (1989), while in *Notropis (Miniellus)*, *N. percobromus* and *N. texanus*, the anterior notch of the ethmoid block is shallow (Figs. 3.5 and 3.6). In dorsal view, the supraethmoid portion of the ethmoid block has a constricted waist that is narrower than the anterior and posterior ends. This constriction is absent in *N. blennius*, *Notropis buchanani* and *N. texanus*. The anterior end of the supraethmoid portion is wider than the posterior end for most species examined. The anterior and posterior ends are equal in *N. percobromus* and *N. heterolepis,* while the posterior end broader in *Notropis heterodon* (Figs. 3.5 and 3.6). For *N. buchanani* and *N. volucellus*, the supraethmoid flares dorsolaterally and is much wider anteriorly than it is posteriorly, corroborating the observations of Coburn (1982). In lateral view, the mesethmoid portion of the ethmoid block is distinctly round in *N. atherinoides* (Fig. 3.6), again corroborating the observation of Coburn (1982).

In ventral view, the lateral ethmoid has an anterior notch in most species examined. This anterior notch is present but shallow in *Notropis heterolepis, Notropis percobromus, Notropis texanus* and *Notropis volucellus*. In *Notropis dorsalis*, this anterior notch is absent (Fig. 3.7). In lateral view, the posterior end of the lateral ethmoid is horizontally broadened in *Notropis blennius, N. dorsalis* and *N. volucellus* and horizontally short in *Notropis atherinoides*. An ovular foramen formed between the posterior and anterior margins of the lateral ethmoids and orbitosphenoid is observed in *Notropis hudsonius, Notropis heterolepis, N. percobromus* and *N. texanus.*

The posterior process of the vomer is elongate in most of the species examined. This process is broad in *Notropis heterodon* and short in *Notropis atherinoides*, *Notropis blennius*, *Notropis percobromus* and *Notropis texanus* (Fig. 3.8). In most species examined, the vomer has a pair of posterolateral processes on either side (Fig. 3.8). These processes is absent in *Notropis buchanani, Notropis hudsonius, Notropis heterolepis* and *Notropis volucellus.* The anterior margin of the vomer was shallowly notched for most of the species examined, deeply notched in *N. percobromus*, and straight in Notropis heterodon (Fig. 3.8). In dorsal view, the anterior edge of the vomer extends beyond the anterior end of the ethmoid block in *N. heterodon* and *N. percobromus* (Fig. 3.5 and 3.6).

3.3.2.2 Orbital Region

The orbitosphenoid, frontal and supraorbital of the skull all show interspecific differences related to shape. The medial ridge of the orbitosphenoid is narrow in *Notropis atherinoides, Notropis percobromus* and *Notropis texanus* (Fig. 3.4). In *Notropis heterodon,* the medial ridge is also narrow but constricted in the middle (Fig. 3.4). The medial ridge is broade in *Notropis blennius, Notropis heterolepis, Notropis stramineus* and *Notropis volucellus*. In *Notropis dorsalis,* the medial ridge is also broade but proportionally shorter, and the posterior margin is consistently fused to the parasphenoid, unlike the other species in which there is no fusion with the parasphenoid (Fig. 3.4). The medial ridge of the orbitosphenoid is similarly shorten in *N. heterolepis*.

In ventral view, the lateral shelf of the frontal is narrow in *Notropis buchanani* and *Notropis heterodon* and broad in *Notropis blennius* (Fig. 3.9). The lateral margin of the frontal shelf is moderately concave in most species, deeply concave in *Notropis dorsalis*, and straight in *Notropis atherinoides* and *Notropis percobromus*. For most of the species examined, the supraorbital bone is generally oval with species level differences in the shape of the lateral and posterior margins. In *Notropis atherinoides*, *N. heterodon* and *Notropis volucellus,* the supraorbital is thin and elongate (Fig. 3.9).

3.3.2.3 Otic and Occipital Regions

The sphenotic and pterotic are two elements that show notable interspecific differences. For the sphenotic, these differences are reflected in the shape of the post orbital process and sphenotic spine. The postorbital process is, in comparison to other species, shorten in *Notropis atherinoides, Notropis buchanani* and *Notropis percobromus* and elongate in *Notropis dorsalis* and *Notropis heterodon*. In *Notropis blennius* the lateral edge of the post orbital process is convex instead of straight (Fig. 3.9). With the exception of *N. blennius* and *Notropis stramineus*, the shape of the sphenotic spine diverges from the short, blunt shape observed in *Notropis* *hudsonius*. The exact shape, whether elongate and broad, elongate and sharp, short and blunt or short, varies at the species level. Notably, the sphenotic spine of *Notropis dorsalis* is medially curved, while the sphenotic spine of *Notropis heterolepis* is laterally oriented. The pterotic, specifically its posterolateral spine, is also highly variable among species. This posterolateral spine ranges from broad and blunt (*N. dorsalis*), broad and pointed (*N. heterolepis* and *Notropis volucellus*), short and blunt (*Notropis texanus*), short and pointed (*N. buchanani* and *N. percobromus*), or even elongate and medially curved (*Notropis stramineus*). (Fig. 3.10).

3.3.2.4 Basicranial Region

Interspecific differences in the basicranial region is observed in the basioccipital, parasphenoid, and the open posterior myodome (OPM). For the basioccipital, interspecific differences are reflected in the size, shape and orientation of the pharyngeal process and the shape of the masticatory plate. For most of the species examined, the pharyngeal process was elongate, stopping just short of the os suspensorium. The pharyngeal process of *Notropis atherinoides, Notropis buchanani* and *Notropis heterolepis* is instead reduced and short, falling well short of the os suspensorium (Fig. 3.11). Coburn (1982) made a similar observation for *N. atherinoides*. For most species, the pharyngeal process is broad and round, expanding posteriorly. In *N. buchanani*, *Notropis heterodon*, *N. heterolepis*, and *Notropis volucellus*, the pharyngeal process is round and uniform in width, while in *N. atherinoides* and *Notropis stramineus*, the pharyngeal process is slender (Fig. 3.12). The masticatory plate of most species examined is round with laterally projecting wings at the broadest point of the plate, contrasting the square wings observed in *Notropis hudsonius*. The ventral surface of the masticatory plate is concave in a majority of the species examined but is flat in *Notropis dorsalis*, *Notropis percobromus* and *N. heterolepis.*

The parasphenoid and OPM vary widely among the species examined. The ascending wings of the parasphenoid are straight and horizontally oriented in *Notropis atherinoides*, *Notropis blennius*, *Notropis percobromus* and *Notropis hudsonius*. The first three species are further distinguished by a drawn out anterolateral corner that is slender in *N. atherinoides* and *N. percobromus*, but broaden in *N. blennius.* For the other species I examined, the ascending wings are short and posteriorly directed. For *Notropis dorsalis*, the ascending wings are elongate but still posteriorly directed (Fig. 3.10). In *Notropis buchanani* and *Notropis volucellus*, the ascending wings are broad (Fig. 3.10), corroborating the observations of Coburn (1989).

The OPM itself varies in the size and degree of closure in the species examined. The OPM is large in *Notropis atherinoides*, *Notropis heterolepis*, *Notropis volucellus* and both species of subgenus *Notropis (Miniellus)*. As a result, the posterior end of the parasphenoid is also deeply forked in these species (Fig. 3.10). In *Notropis buchanani*, *N. dorsalis*, *N. percobromus* and both species of subgenus *Notropis (Alburnops)*, the OPM is small, resulting in a shallowly forked parasphenoid. In *N. buchanani* specifically, the OPM is extremely small and almost closed up (Fig. 3.10). The OPM, as discussed in the previous chapter, is completely closed in *Notropis hudsonius*, conflicting with the findings of both Coburn (1982) and Mayden (1982).

3.3.2.5 Branchial Apparatus

Overall, the pharyngobranchials are very conservative in shape and proportion for the species examined. The ceratobranchials are also fairly conservative, with a few species level differences in proportion and shape (Figs. 3.13 and 3.14) The epibranchials are also fairly consistent across species. There are, however, a few notable differences. The third epibranchial of *Notropis hudsonius* is distinct, having a broad dorsal process not observed in any other species. The dorsal process of the fourth epibranchial is variably absent, as discussed in the second chapter. The first epibranchial of *Notropis dorsalis* is long and thin, with no uncinate process or posterior notch (Fig. 3.15). The first and second epibranchials of *Notropis heterolepis* have a reduced uncinate process and posterior notch. In one of the specimens examined, the first and second epibranchials lack an uncinate process and posterior notch altogether (Fig. 3.15). In *Notropis percobromus*, the uncinate process of the third epibranchial is laterally directed and the dorsal process of the fourth epibranchial originates halfway down the element, unlike other species in which it originates towards the proximal end.

The fifth ceratobranchial arches and the corresponding pharyngeal teeth are highly variable (Fig. 3.16). For most species, the anterior limb of the arch has a moderately developed ventral flange. This flange is strongly developed in *Notropis stramineus* and weakly developed in *Notropis heterodon*. A unique state is observed in *Notropis heterolepis*, where the ventral flange of the anterior limb is moderately developed but remains the same width leading up to the ascending limb (Fig. 3.16). The anterior angle of the ascending limb is strongly developed in most species but short and blunt in *Notropis dorsalis*, *Notropis stramineus*, *Notropis texanus* and *Notropis volucellus.* The ascending limb is also weakly arched in most species, with an weak posterior angle. By contrast, the ascending limbs of *Notropis texanus* and both species of subgenus *Notropis (Miniellus)* are strongly arched with a prominent posterior angle that gives the limb a distinct, square shape (Fig. 3.16). *Notropis atherinoides* and *Notropis percobromus* show an intermediate shape in which the ascending limb is moderately arched with a posterior angle visible but not strongly developed (Fig. 3.16).

The ascending limb of *Notropis heterolepis* is the most distinct among the species examined. The limb itself is flat and its medial edge forms a distinct ridge for the posterior most tooth of the major row to sit upon. The anterior and posterior angles of the ascending limb are round, giving the lateral margin a distinct, semicircular shape. The same condition was observed in this species by Coburn (1982).

The dental formulae of the species examined generally conform to those outlined by Eastman and Underhill (1973) and Page and Burr (2011). *Notropis buchanani*, *Notropis stramineus*, *Notropis heterolepis* and *Notropis volucellus* have a dental formula of 0,4-4,0. *Notropis heterodon, Notropis hudsonius and Notropis* dorsalis have a dental formula of 1,4-4,1. *Notropis buchanani*, *Notropis stramineus*, *Notropis heterolepis* and *Notropis volucellus* have a dental formula of 2,4-4,2. Contrary to what has been reported by previous authors (Eastman and Underhill, 1973; Coburn, 1982; Nelson and Paetz, 1992), I found the dental formula of *Notropis atherinoides* to be 1,4-4,1 in all three specimens examined. Some variation was noted in *Notropis heterodon*, *Notropis hudsonius*, and *Notropis texanus.* One *N. heterodon* specimen had a formula of 0,4-4,1, while one *N. texanus* specimen had a formula of 2,4-4, 1. *N. hudsonius*, as discussed in Chapter 2, shows several deviations from the typical formula of 1,4-4,1.

In addition to dental formulae there are two notable differences in tooth form. Generally, the pharyngeal teeth are elongate and conical with hooked ends (Fig. 3.16). The teeth of *Notropis heterodon* and *Notropis texanus* have serrated, medially directed cutting edges, as previously noted by Swift (1970), Coburn (1982) and Mayden (1989). The pharyngeal teeth on *Notropis buchanani* and *Notropis volucellus* have elongate, sharp, medially directed cutting edges (Fig. 3.16).

The hypobranchials are consistently nodular in most species examined, with the exception of *Notropis heterolepis*. In *N. heterolepis*, the first and second pair of hypobranchials are flat with a distinct, folded appearance (Fig. 3.13).

The basibranchials, especially the first basibranchial, show several variations among species. In dorsal view, the first basibranchial typically has a short, triangular shape that narrows anteriorly (Fig. 3.13 and 3.14). In *Notropis atherinoides*, *Notropis dorsalis*, *Notropis heterodon*, *Notropis stramineus*, and *Notropis percobromus,* the first epibranchial is elongate with equal size/length/? anterior and posterior ends. The first epibranchial is also elongate in *Notropis volucellus*, but the anterior end is much wider and the middle is deeply constricted. A pair of deep lateral notches are observed in *N. dorsalis* and both species of subgenus *Notropis (Miniellus).* A ventral process is present in both species of subgenus *Notropis (Miniellus)* and *Notropis volucellus* (Fig. 3.17). A ventral process is also present in *Notropis buchanani* but is weakly developed. The anterior end of the first basibranchial has a constricted neck in *Notropis hudsonius* and *N stramineus*. In dorsal view, the anterior end of the second basibranchial is generally wider than the posterior end for most species. However, the anterior and posterior ends are equal for *N. atherinoides*, *N. dorsalis* and *Notropis hudsonius.*

For most of the species examined, the basihyal has a pair of tubercles positioned on the lateral margin, with the exception of *Notropis hudsonius*, *Notropis heterolepis*, *Notropis stramineus* and *Notropis texanus.* The basihyals of *Notropis atherinoides*, *N. texanus* and *Notropis percobromus* can be distinguished by the presence of a posteroventral projection, or basihyal projection, that extends underneath the anterior end of the first basibranchial, as noted by Coburn (1982). Coburn (1982) and Coburn and Cavender (1992) also reported basihyal projections in *Notropis blennius*, *Notropis heterodon,* and *Notropis volucellus*; however, I did not observe a basihyal projection in any of these species (Fig. 3.17). In dorsal view, the basihyal of *N. texanus* has a much wider anterior end relative to the posterior end when compared to other species (Fig. 3.14).

3.3.2.6 Hyoid Region

In the hyoid region, interspecific differences relate to the proportions of the anterior and posterior ceratohyals, shape of the branchiostegal rays, shape of the hypohyal foramen, and shape of the urohyal. In the vast majority of the species examined, the posterior ceratohyal is roughly two thirds the length of the anterior ceratohyal. In comparison, the posterior ceratohyal of *Notropis dorsalis* is elongate (Fig. 3.18), being roughly four fifths of the length of the anterior ceratohyal.

In most of the species examined, the head of the second branchiostegal ray is larger than the third. The opposite is observed in *Notropis blennius* and *Notropis buchanani*. In *Notropis heterodon*, *Notropis heterolepis* and *Notropis percobromus* the heads of the second and third branchiostegal rays are equal in size. The clupeoid projection of the first branchiostegal ray (McAllister, 1968) is usually broad and round. In *N. heterolepis*, it has a distinct anterior point. The clupeoid projection is reduced in *Notropis atherinoides* and *N. percobromus* and rudimentary in *Notropis dorsalis* (Figs. 3.18 and 3.19). The head of the first branchiostegal is elongate and blunt in most species, broadened in *Notropis stramineus*, short in *N. atherinoides* and rudimentary in *N. dorsalis* and *N. percobromus.* In *N. heterolepis*, the head of the first branchiostegal is thin, cylindrical and highly elongate (Fig 3.19).

The hypohyal foramen is usually formed by the anterior ceratohyal and the dorsal and ventral hypohyals. This foramen penetrates deep enough into the anterior ceratohyal to give it a forked appearance. The degree of penetration into the anterior ceratohyal is notably shallower in *Notropis dorsalis* and *Notropis heterodon* and is noticeably deepened in *Notropis buchanani* and *Notropis volucellus*, penetrating into the first third of the bone (Fig. 3.20). In one specimen of *N. buchanani*, the hypohyal foramen is isolated within the anterior ceratohyal but is otherwise bordered by all three elements. In *Notropis hudsonius*, the hypohyal foramen is variable, and can also be bordered only by the dorsal and ventral hypohyals (see Chapter 2).

Variations of the urohyal (Fig. 3.21) are observed in the overall shape, the depth of the anterior notch, the shape of the neck, the shape of the dorsal and ventral wings, and the length of the wings relative to each other. In dorsal view, the urohyals of *Notropis atherinoides* and *Notropis heterolepis* are narrow. The posterodorsal corner of the dorsal wing is distinctive in *Notropis heterolepis* and western populations of *Notropis hudsonius,* forming a broad, round semicircular edge. In dorsal view, the ventral wings are the same length as the dorsal wings in *Notropis atherinoides*, *N. blennius*, and *N. heterolepis*. In western populations of *N. hudsonius*, the dorsal wing is longer than the ventral wings. Otherwise, the ventral wings are longer relative to the dorsal wing for all other species. In *N. heterodon*, the ventral wings are much longer in proportion to the dorsal wing, being almost twice as long.

The urohyal of *Notropis heterolepis* is the most distinctive among the species examined. The ventral wings are greatly reduced, giving the urohyal a distinct, laterally compressed appearance. In the other species examined, the posterior corners of the ventral wings create a distinct notch in ventral view. In *N. heterolepis*, the posterior corners of the ventral wings are either absent or greatly reduced, giving the urohyal and ovoid appearance. A similar condition is described by Chernoff and Miller (1981) and Coburn (1982) for this species.

The anterior region of the urohyal of *Notropis dorsalis* is distinct from the other species examined. The anterior processes are proportionally much shorter and broader, creating a shallow anterior notch. The anterior neck separating the wings from the anterior notch is short and wide. A short anterior neck is also observed in *Notropis buchanani* (Fig. 3.21).

3.3.2.7 Opercular Series

All four elements of the opercular series (Fig. 3.22) show interspecific variation. Interspecific variation of the opercle is observed in the shape of the anterodorsal, posterodorsal and posteroventral edges, the shape and length of the opercular process, and overall width. The anterodorsal edge is straight in *Notropis atherinoides*, *Notropis percobromus* and *Notropis volucellus*, deeply concave in *Notropis dorsalis*, *Notropis heterolepis* and *Notropis stramineus*, and shallowly concave for the other species examined. The posterodorsal edge is straight in *Notropis dorsalis* and *Notropis heterolepis* and sigmoidal for the remaining species. The posteroventral edge is convex in *Notropis buchanani, Notropis heterodon, Notropis heterolepis* and *Notropis texanus* and straight for all other species. The opercular process forms a short, sharp, indistinct corner in *N. atherinoides* and *N. volucellus* and a distinct, intermediately sized corner in most other species. It is drawn out into a long, broad process in *N. dorsalis* and N. *heterolepis* (Figs. 3.22 and 3.23). The opercular process in *N. heterolepis* is unique among species examined, overlapping the posterior margin of the hyomandibula and the posteroventral margin of the sphenotic. The opercle is overall broadened in *N. dorsalis* and *N. heterolepis* and narrow in *Notropis buchanani*. In all cases, the dorsal margin is proportionally similar in length to the ventral margin.

Variation of the subopercle is observed in the concavity of the dorsal edge, orientation of the anterior margin, shape and length of the anterodorsal process, and general shape. The dorsal edge is straight and posterodorsally directed in *Notropis stramineus* and *Notropis volucellus* (Fig. 3.22) and concave in all other species. The anterior margin is concave in *Notropis dorsalis*, straight and posterodorsally oriented in *Notropis buchanani* and *Notropis heterodon*, and straight and posteroventrally oriented for all other species (Fig. 3.22). The anterodorsal process is long, distinct and sharp in *Notropis dorsalis* and *N. stramineus*, long and broad in *Notropis blennius,* short but still distinct and variably pointed or round in *Notropis hudsonius* (see Chapter 2) and a simple, square corner in all other species. The subopercle is narrowest in *Notropis texanus* and *Notropis heterodon* and widest in *Notropis hudsonius* and N. volucellus.

Interspecific differences in the interopercle relate to the depth and shape of the posterior margin. *Notropis heterolepis* has the deepest interopercle of all species examined. It is moderately deep in *Notropis dorsalis, Notropis hudsonius, Notropis percobromus, Notropis stramineus* and *Notropis volucellus* and shallow in the remaining species (Fig. 3.22). The posterior margin is straight and anteroventrally directed specifically in *Notropis atherinoides* and *Notropis blennius,* and convex in other species.

Variation of the preopercle is observed in the proportions of the horizontal and vertical limbs, and the overall shape. While the horizontal limb is always shorter than the vertical limb across species, the relative widths differ. In *Notropis atherinoides*, *Notropis buchanani, Notropis dorsalis, Notropis heterodon* and *Notropis percobromus*, the horizontal limb is proportionally much thinner than the vertical limb (Fig. 3.22). The preopercle of *Notropis heterolepis* has a distinct, broadened shape, with both vertical and horizontal limbs being of similar width (Fig. 3.22).

3.3.2.8 Suspensorium

All seven elements of the suspensorium (Figs 3.24-3.33) show some sort of interspecific variation, though to different degrees. Variation in the hyomandibula occurs in the placement of the opercular condyle, development of the adductor ridge and the size and shape of the wings. Usually, the opercular condyle is placed about one quarter down the posterior margin of the hyomandibula. In *Notropis heterolepis*, the opercular condyle is placed higher, about one fifth down, while in *Notropis dorsalis*, the opercular condyle is placed lower, about one third down. The adductor ridge is undeveloped in most species, conflicting with earlier descriptions of other cyprinoids (Uyeno, 1961; Buhan, 1970; Coburn, 1982; Mayden, 1989). However, the adductor ridge can be observed in *Notropis atherinoides, Notropis blennius, Notropis buchanani*, *N. dorsalis* and *Notropis percobromus*. The anterior wing of the hyomandibula expands dorsally and, in most species, has a distinct hyomandibular notch at the base. In *Notropis atherinoides* and *Notropis percobromus*, this notch is absent (Figs. 3.24 and 3.30) while in *Notropis buchanani*, the anterior wing of the hyomandibula is constricted at the very base (Fig. 3.26). The posterior wing is enlarged in *Notropis dorsalis* and notched at the base in *N. buchanani* but is otherwise consistent in shape and size across species.

The metapterygoid is one of the most variable elements of the suspensorium. The anterodorsal process is especially variable in shape and width (Figs 3.24-3.33). However, there is no consistency in shape among subgenera or even sister species. In addition, I also observed the anterodorsal process to be variable in shape and in width in *Notropis blennius, Notropis hudsonius* (see Chapter 2) and *Notropis volucellus.* The posterodorsal process is similarly variable in terms of development and shape, with no consistency among subgenera or genera. The metapterygoid of *N. blennius* is the most distinct of the species I examined. The posterodorsal process is very broad, positioned almost level with the anterodorsal process, while the dorsal margin has a narrow notch. The ventral margin forms an anteriorly positioned point (Fig. 3.25).

Interspecific differences in the endopterygoid are observed in overall size, shape of the anterior process dorsal edge, and development of the lateral flange. For *Notropis hudsonius* and *Notropis blennius*, the posterior edge of the endopterygoid is short, aligning with the posterior most edge of the quadrate blade (Fig. 3.34). For most species, the endopterygoid is more enlarged, extending posteriorly beyond the quadrate blade to varying degrees (Fig. 3.34). In *Notropis atherinoides*, the endopterygoid is especially enlarged, extending posteriorly well beyond the quadrate blade (Fig. 3.34). The anterior process of the endopterygoid is short in most species and in *Notropis stramineus* is distinctly pointed. This anterior process is more elongate in *Notropis buchanani*, *Notropis heterodon* and *Notropis texanus*. The dorsal edge of the endopterygoid is roughly straight for most species, concave in *N. heterodon*, *Notropis heterolepis* and *Notropis percobromus*, and convex in *Notropis dorsalis* (Fig. 3.27). In *Notropis blennius*, there is a distinct, concave notch towards the anterior end that is preceded by a small, sharp tubercle at the base of the anterior process (Fig. 3.25). The lateral flange, extending posteroventrally along the lateral side, is poorly developed in most species but well developed in Notropis hudsonius, *Notropis volucellus* and both species of subgenus *Notropis (Miniellus)* (Figs. 3.28, 3.31 and 3.33).

The palatine varies in the shape of the lateral, ventral and dorsal processes, and the medial groove for the preethmoid. In dorsal view, the palatine is roughly triangular, with the lateral process forming a short, flat, laterally directed wing for most species. However, this lateral process is anterolaterally directed in *Notropis buchanani* and *Notropis heterolepis* (Fig. 3.6), as previously noted by Mayden (1989). Mayden (1989) also found the lateral process of *Notropis volucellus* to also be anterolaterally directed. However, in the *N. volucellus* specimens I examined, this was not the case. The ventral process of the palatine is consistently shorter than the dorsal process and, in post species, tapers to a point. However, in *N. buchanani*, *N. heterolepis* and *N. volucellus,* the ventral process is short, broad and blunt. The dorsal process is more variable in shape. In most species, it is elongate and pointed but it is broadened in *N. buchanani* and *Notropis dorsalis*, with the latter being the broadest. In dorsal view, the dorsal process appears narrow and reduced in *Notropis atherinoides* and *Notropis percobromus.* In both species of subgenus *Notropis (Alburnops),* the dorsal process is greatly elongate, especially in *Notropis blennius* (Fig. 3.25). In *N. buchanani*, *N. heterolepis* and *N. volucellus*, the dorsal and ventral processes form a deep, restricted cup for the preethmoid, a feature also noted by Mayden (1989).

Interspecific differences are also observed in the symplectic, quadrate and ectopterygoid, though to a lesser degree. The symplectic is thinner in *Notropis buchanani*, *Notropis percobromus* and *Notropis stramineus.* In *Notropis blennius*, the symplectic is curved ventrally, reflecting the shape of the ventral edge of the metapterygoid (Fig. 3.25). The posterior process of the quadrate is narrow in *Notropis atherinoides*, *Notropis heterodon*, *Notropis heterolepis* and *Notropis volucellus* (Figs. 3.27, 3.31. 3.32 and 3.36). and short in *N. blennius* (Fig. 3.25). The ectopterygoid is broader in *N. heterolepis* compared to the narrow, ovular shape observed in most species (Fig. 3.29).

3.3.2.9 Oral Jaws

The dentary, maxilla, premaxilla, coronomeckelian, retroarticular and kinethmoid are all variable between species. Interspecific differences in the dentary are seen in the development of the dorsolateral shelf and the coronoid process. The coronoid process is typically broad and round but is narrow in *Notropis blennius*, *Notropis stramineus* and *Notropis texanus.* For most species, the coronoid process is oriented posteriorly. For *Notropis percobromus*, the coronoid process is strongly posteriorly oriented, while in *N. buchanani, Notropis heterolepis, N. stramineus*, and *N. texanus*, the coronoid process is dorsally oriented.

The posterior shaft of the premaxilla is weakly decurved in most species, but straight in *Notropis atherinoides* and *Notropis percobromus* (Fig.3.35). Generally, the posterior shaft is also flat and narrows posteriorly. However, in *N. percobromus,* the posterior shaft is thin and cylindrical, ending in a sharp point, while in *Notropis heterolepis,* the posterior shaft is broad and does not taper into a narrow end (Fig. 3.35). The ascending process of the premaxilla is proportionally shorter in both species of both subgenera *Notropis (Alburnops)* and *Notropis (Miniellus)* as well as *N. percobromus*.

Several interspecific differences in the maxilla are also observed, specifically in the neck, premaxillary process, rostral process, ascending process and posterior flange. The neck connecting the anterior and posterior ends of the maxilla is narrow in *Notropis percobromus* and *Notropis texanus*, broad in *Notropis dorsalis*, and even more broad in *Notropis heterolepis* (Fig. 3.35). In all other species, the neck of the maxilla is of intermediate width. The premaxillary process is narrow in *Notropis atherinoides*, *Notropis buchanani*, *Notropis heterolepis* and *Notropis percobromus* and broadest in *Notropis dorsalis*. In medial view the rostral process has an obtuse 'bent' shape of most species (Fig. 3.36), corresponding with an anteromedial orientation in dorsal view (Fig. 3.5-3.6). In *Notropis dorsalis*, the rostral process is almost straight in medial view, and in dorsal view is roughly horizontally oriented (Fig. 3.5). In *Notropis volucellus*, the rostral process has a distinct 'L-shape' in medial view (Fig. 3.35), while in dorsal view, it is short and laterally oriented (Fig. 3.6). The ascending process of the maxilla is highly variable among species. It can vary in width, height and overall shape and can vary widely even among species of the same subgenus. The flange at the posterior end of the maxilla is typically oval in shape. In *N. atherinoides*, *N. percobromus* and *Notropis heterodon*, it is noticeable elongate. In *N. dorsalis*, the posterior flange has a triangular shape, while in *N. heterolepis*, the posterior flange is broad and angular with distinct anterior, ventral and posterior edges (Fig. 3.35).

The coronomeckelian is highly variable in regards to overall shape and size at the species level. However, the main variant of note is the position of the coronomeckelian on the anguloarticular. For most of the species examined, the medial side of the coronomeckelian contacts the anguloarticular completely. In both species of subgenus *Notropis (Miniellus*), the coronomeckelian is positioned so that it extends beyond the dorsal margin of the anguloarticular (Fig. 3.36). A similar condition is found in *Notropis volucellus*, but to a lesser degree. The retroarticular is similarly variable among individual species. However, I did not observe any notable differences beyond shape and size.

The overall length and shape of the kinethmoid varies widely among species. It is elongate in *Notropis buchanani*, *Notropis dorsalis* and *Notropis hudsonius* and short in *Notropis blennius*, *Notropis heterodon*, *Notropis percobromus* and *Notropis texanus* (Fig. 3.37). For *N. heterodon and N. percobromus* specifically, the kinethmoid has a distinct, oval shape in anterior view (Fig. 3.37). In *Notropis heterolepis*, the kinethmoid is constricted dorsally, with an expanded ventral base. Coburn (1982) described the kinethmoid of *N. dorsalis* as elongate and straight. Instead, I found the kinethmoid of *N. dorsalis* to be curved. In *Notropis heterolepis* and *Notropis texanus*, the ventral process is replaced by a ventral notch. In *N. texanus*, this ventral notch is exceptionally deep (Fig. 3.37).

3.3.2.10 Circumorbital Series

Interspecific differences in the infraorbital series are primarily in the lacrimal and the development of the other infraorbital bones. Among species, the lacrimal is distinct in its overall shape (Figs. 3.41). While the dorsal edge of the lacrimal is shallowly concave in most species, it is deeply concave in *Notropis volucellus*, and straight in *Notropis buchanani* (Fig. 3.38). The other infraorbitals typically vary in their overall shape (Fig. 3.38), except for the dermosphenotic. In *Notropis texanus*, the second infraorbital appears to be divided into two tubular elements (Fig. 3.38). In both *N. buchanani* and *Notropis heterolepis*, all infraorbital bones, except the lacrimal, can be small or absent (Fig. 3.39). In the three *N. buchanani* specimens that I examined, the lacrimal and infraorbitals two to four are present. In another, the second infraorbital was absent, while in the third (Fig. 3.39), only the lacrimal and third infraorbital are present. In the two *N. heterolepis* specimens whose infraorbitals I could examine, the first four infraorbitals are all present, with the second and fourth infraorbitals being much smaller in size (Fig. 3.39). The second specimen was similar, except that the fourth infraorbital was absent. In the *N. buchanani*, *N. heterolepis* and *Notropis heterodon* specimens that I examined, the dermosphenotic was absent. The loss and reduction of these infraorbital bones is a reflection of the degree of development of the infraorbital canals and postocular commissure (Swift, 1970). The two *N. texanus* specimens that I examined also lacked dermosphenotics. However, like the sensory canals, this observation is probably a reflection of their small size rather than species differences (Swift, 1970).

3.3.2.11 Sensory Canal System

Most of the species examined show a fully developed sensory canal system, including a full set of supraorbital, supratemporal, infraorbital, preopercular mandibular and postocular commissure canals present. The pore counts of these canals fall within the range reported for *Notropis hudsonius* (Chapter 2). The one exception is the infraorbital canal system of *Notropis volucellus*. While the infraorbital canals had the usual seven pores, three of these pores are on the lacrimal and third infraorbital (Fig.3.37) as opposed to the usual two.

Notropis buchanani, Notropis heterodon and *Notropis heterolepis* show poor development and even total loss of the sensory canals, as previously noted by Reno (1966) and Swift (1970). *N. heterodon* shows the highest degree of canal development of these three species, with only the postorbital commissure being poorly developed. In *N. buchanani*, only the supraorbital and preopercularmandibular canals are fully developed (Fig. 3.39). However, the preopercularmandibular canal is broken in one specimen examined. In two of the three *N. buchanani* specimens I examined, the postocular commissure is also somewhat developed but lacks pores. One specimen also has a somewhat developed supratemporal canal with a single pore instead of the usual three. *Notropis heterolepis* shows the poorest degree of sensory canal development. In one of the two specimens I was able to examine, only the anterior portions of the supraorbital, infraorbital, preopercular mandibular and canals are developed (Fig. 3.39). The infraorbital canal specifically was present only on the anterior end of the lacrimal. In the second, larger specimen, the supraorbital canal is more developed but has six pores as opposed to the typical eight seen in other species. The supratemporal and preopercularmandibular canals are also more developed but has no pores. The infraorbital canal is developed only on the lacrimal and second infraorbital.

In the two *Notropis texanus* specimens examined, the sensory canal system also appears underdeveloped, particularly along the postocular commissure and post temporal canals. However, my observations closely reflect the pattern of sensory canal development illustrated by Swift (1970) for a *Notropis* species of small size. Thus, the underdeveloped canals in these *N. texanus* are probably a reflection of size and age rather than species.

3.3.2.12 Weberian Apparatus

The pars sustentaculum is fairly consistent among the species examined. The only notable differences are in the neural complex, the first predorsal bone, and the neural spine of centrum four. The neck of the neural complex is typically constricted and vertically oriented. However, In *Notropis atherinoides* and *Notropis buchanani*, the neck of the neural complex is broad and unconstricted, while in *Notropis dorsalis* the neck is highly constricted and anteriorly oriented (Fig. 3.11). The double crest of the neural complex is greatly elongate in *Notropis blennius* and *Notropis stramineus*, extending over the entirety of the second neural arch, in contrast to other species examined in which it extends roughly halfway. In *N. dorsalis* and *Notropis heterolepis*, the double crest is short, with the lamellae making up the crest either greatly reduced, as seen in *N. dorsalis*, or absent, as seen in *N. heterolepis* (Fig. 3.12). The first predorsal bone is positioned between the double crest in *N. atherinoides*, *Notropis percobromus*, *Notropis stramineus*, and *Notropis volucellus* (Fig. 3.12).

The neural spine of the fourth vertebra is anteriorly oriented in *Notropis dorsalis*, *Notropis heterodon*, *Notropis heterolepis*, *Notropis hudsonius* and N*otropis stramineus,* vertically oriented in both species of subgenus *Notropis (Alburnops)* and *Notropis volucellus* and posteriorly directed in *Notropis atherinoides*, *Notropis buchanani* and *Notropis percobromus*. The fourth neural spine is also short in both species of *Notropis (Alburnops)* as well as *N. dorsalis, N. stramineus* and *N. percobromus* (Fig.3.40).

The claustrum and scaphium are largely uniform in morphology among amongst the species examined. However, the two posterior-most ossicles, the intercalarium and tripus, show several notable interspecific differences. Interspecific differences in the intercalarium are reflected in the ascending process and, to a lesser extent, the posterior arm. The ascending process is typically thin and elongate in most of the species examined. In *Notropis blennius, Notropis dorsalis, Notropis hudsonius* and *Notropis stramineus*, this process is short. In *N. dorsalis* specifically, the ascending process is broad. In *N. stramineus*, the posterior arm of the intercalarium is much broader in comparison to other species (Fig. 3.41).

The tripus varies based on the length and shape of the anterior arm and the development of a dorsal ridge. For most species, the anterior arm has a short, broad shape with a dorsomedial curve. The anterior arm is short straight, and pointed in *Notropis atherinoides* and *Notropis texanus*, short, thin, and pointed in *Notropis heterodon* and *Notropis heterolepis*, and thin and elongate in *Notropis dorsalis* (Fig. 3.41). The dorsal ridge of the tripus is poorly developed or absent in *Notropis blennius*, *Notropis heterodon*, *Notropis heterolepis*, *Notropis percobromus* and *Notropis volucellus* but well developed in all other species (Fig. 3.42).

3.3.2.12 Pectoral Girdle

Interspecific differences are observed in the posttemporal, supracleithrum, cleithrum, coracoid, mesocoracoid and scapula of the pectoral girdle. For the posttemporal, interspecific differences relate to the shape, and size relative to the supracleithrum. Overall, the supracleithrum is teardrop shaped in all species examined. However, the dorsal end is noticeably constricted in *Notropis dorsalis*, *Notropis heterodon* and *Notropis volucellus* (Fig. 3.43). In terms of size, the posttemporal is roughly three quarters the length of the supracleithrum. For *Notropis hudsonius, Notropis stramineus* and *Notropis percobromus*, the supracleithrum is half the length of the posttemporal, while in *Notropis blennius*, *Notropis buchanani* and *N. dorsalis*, the supracleithrum is two thirds the length (Fig. 3.43). The supracleithrum itself varies in the size and the shape of the dorsal process. Overall, the supracleithrum is proportionally broad in *N. volucellus* and narrow in *N. blennius* and *N. percobromus*. While the dorsal process is hooked in most species, it is consistently straight in *N. heterolepis* and *N. percobromus* (Fig. 3.43).

The cleithrum is highly variable among the species examined. This variation is seen in the proportions of the horizontal and vertical limbs, shape of the lateral plate, shape of the anterior end of the horizontal limb, and the development of the medial ridge of the vertical limb. For most species, the horizontal and vertical limbs are of equal length, while the horizontal limb is longer than the vertical limb in *Notropis buchanani*, *Notropis dorsalis* and *Notropis heterodon* (Fig. 3.44). The dorsal spine of the cleithrum is noticeably short in *N. buchanani, N. heterodon, Notropis heterolepis, Notropis texanus,* both species of subgenus *Notropis (Miniellus)* and occasionally *Notropis hudsonius* (Chapter 2). The lateral plates of *Notropis dorsalis* and *N. heterodon* have a deeply concave ventral margin, giving the entire cleithrum a distinctly curved appearance. This lateral plate also has a convex ventral margin (Fig. 3.44), contrasting with the roughly straight margin seen in other species.

In dorsal view, the horizontal limb of the cleithrum is also variable in shape. For most species, the anterolateral margin is concave (Fig 3.45). For *Notropis buchanani*, *Notropis dorsalis*, and *Notropis volucellus*, the anterolateral margin forms a straight, anterolaterally directed edge. For *N. dorsalis* specifically, this edge is longer and slanted at a shallower angle. In *Notropis blennius* and *Notropis percobromus*, the anterolateral margin is straight, and the anterior edge is horizontal, giving the horizontal limb a distinct, square appearance. The anterolateral margin is similarly straight in *Notropis atherinoides*, but the anterior margin is convex, giving the horizontal limb a distinct, round appearance. The medial ridge of the vertical limb of the cleithrum is also variable and interspecifically distinct. In *N. volucellus*, the medial ridge is especially broad, terminating in a wide dorsal flange. For *N. dorsalis* and *N. heterodon*, the medial ridge is more anteriorly positioned and terminates in an elongate flange (Fig. 3.43) *In Notropis heterolepis*, the medial ridge is strongly developed, with the dorsal flange extending down most of the vertical limb (Fig. 3.44).

Compared to most species, the anterior end of the coracoid is constricted in *Notropis dorsalis, Notropis heterolepis, Notropis stramineus* and *Notropis texanus* (Fig. 3.44). The foramen` formed between the coracoid and cleithrum is notably smaller in *Notropis heterodon* and *N. texanus* and enlarged in *Notropis atherinoides* (Fig. 3.44). The coracoid of *N. heterodon* is distinctive. The posterior margin is angular, forming a distinctive posterior and anterior corner, giving the element a unique, square appearance.

The mesocoracoid is fairly conservative, with distinct differences observed only in *Notropis blennius* and *N. heterolepis*. The mesocoracoid of *N. blennius* has a broadened ventral base, while the mesocoracoid of *N. heterolepis* has a well-developed anterodorsal process (Figure 3.45). Intraspecific differences of the scapula are seen in the size of the scapular foramen and the development of the posterodorsal flange. The scapular foramen is small for most species but large in *N. atherinoides* and *Notropis percobromus.* The posterodorsal flange is weakly developed in *Notropis hudsonius* and *N. percobromus*, moderately developed in most species, and strongly developed in *N. dorsalis*, *N. heterodon* and *Notropis volucellus* (Figs. 3.44 and 3.46). As outlined in Chapter 2, the cleithrum, coracoid, mesocoracoid and scapula of *N. hudsonius* could be fully or partly fused together into one element. For one of the *N. heterodon* and *N. volucellus* specimens I examined, the same elements are also partly fused together.

3.3.2.13 Pelvic Girdle

The pelvic girdle is generally very conservative amongst the eleven species examined. The two variants of note are observed in the anterior processes and the ischiac process. For most of the species examined, the lateral anterior process is longer and narrower than the medial process. In *Notropis dorsalis*, the medial anterior process is longer but still broader than the lateral process (Fig. 3.47). In species of subgenus *Notropis (Miniellus)* plus *Notropis texanus,* the anterior processes are short. For *Notropis heterodon* specifically, the medial anterior process is broad. The ischiac process is broad and blunt, curving laterally in most species examined. In

Notropis atherinoides, *Notropis heterolepis* and *Notropis percobromus,* the ischiac process tapers laterally into a sharp point. The ischiac process of *N. heterodon* is elongate and deeply curved (Fig. 3.47).

3.3.2.14 Caudal Skeleton

Overall, the caudal skeleton (Figs. 3.48 to 3.53) is conservative in the species examined. However, a few differences are observed in the parhypural and first hypural, epural and hypurapophysis. For *Notropis hudsonius* exclusively, the parhypural and first hypural occasionally abut or even fuse together (see Chapter 2). Buhan (1972) also made a similar observation. In *Notropis heterodon*, the epural is noticeably small and, in one specimen, is absent (Fig. 3.50). In both *Notropis dorsalis* and *Notropis percobromus*, the hypurapophysis has a distinct, dorsally directed curve, contrasting with the straight shape observed in all other species (Fig. 3.49 and 3.51). For several species and specimens, I observed traits that could be interpreted as an interspecifically variable. For example, both *Notropis texanus* specimens has two neural spines on the second preural centrum, while in two *Notropis buchanani* specimens, the hemal spine of one centrum is branched (Figs. 3.48 and 3.53). However, I interpret these traits as individual variants based on my findings in the previous chapter.

3.4 Discussion

3.4.1 Measurements and Statistical Analyses

The results of PCA conducted on the measurements and corresponding proportions of the 11 *Notropis* species examined in this study are overall indicative of intraspecific morphometric variation. *Notropis atherinoides*, *Notropis heterolepis*, *Notropis hudsonius*, *Notropis stramineus Notropis volucellus,* all of which include specimens sampled from at least two different populations (3.54), have a wide spread along PC1, reflecting the variability in their body depth as well as the preanal, and peduncle lengths. PC2 also emphasized preanal and peduncle length as a source of intraspecific variation, particularly for *N. heterolepis* and *N. hudsonius,* and to a lesser extent predorsal and dorsal fin lengths. PC3 and PC4 likewise emphasize predorsal and preanal lengths, body depth and peduncle length. Several species, particularly *N. heterolepis* and *N. hudsonius* have a wide spread across both PC3 and PC4, though not to the same extent as PC1. Overall, the results of the PCA reflect intraspecific morphometric variation more than interspecific differences.

3.4.2 Synapomorphies and Convergent Evolution

From my analysis of these 11 *Notropis* species examined, I have observed an array of interspecific differences. Some of these differences are shared among species of the same subgenera *sensu* Mayden et al. (2006), and could indicate possible synapomorphies. However, it should be noted that these potential synapomorphies are typically identified from my analysis of only two species of a single subgenus and will require analysis of other *Notropis* species excluded from this study to confirm their utility. I also noted several convergent osteological traits and character traits that are shared among distantly related species that provide insight into the adaptive traits and evolution of notropin fishes.

Both species of subgenus *Notropis(Alburnops)*, *Notropis blennius* and *Notropis texanus*, show osteological similarities observed in elements of the ethmoid region, suspensorium, basicranial region, Weberian apparatus (specifically the pars sustentaculum), oral jaws, and branchial apparatus. Within these regions, only the palatine, specifically presence of an elongate dorsal process, appears to be unique to the subgenus *Notropis(Alburnops). Notropis heterodon* and *Notropis stramineus* of subgenus *Notropis(Miniellus)* show osteological similarities in the ethmoid region, basicranial region, pelvic girdle, Weberian apparatus, oral jaws and branchial apparatus. However, the supposed synapomorphies shared among these species are also shared with *Notropis* species in other subgenera.

Collectively, *Notropis atherinoides*, *Notropis buchanani*, *Notropis percobromus* and *Notropis volucellus* of subgenus *Notropis (Notropis)* show no common osteological traits to unite them. The findings of Coburn (1982) and Coburn and Cavender (1992) would suggest that the only synapomorphy these four species share is a basihyal projection. This trait has traditionally been regarded as systematically important (Coburn, 1982; Mayden, 1989; Coburn and Cavender, 1992). However, while I observed this trait in *N. atherinoides*, *N. buchanani*, and *N. percobromus*, I did not observe it in *N. volucellus*. However, I examined only two specimens. The possibility remains that these specimens simply show a variant of *N. volucellus* and that overall, a basihyal projection is typically present in the species. It should be noted that the basihyal projection was also absent in examined material of *Notropis blennius* and *Notropis heterodon*, conflicting with the findings of past authors (Coburn, 1982; Coburn and Cavender, 1992). It may also be the case that the specimens I examined also reflect a variant of both of these species. However, these inconsistencies among these authors and my own findings brings the validity and systematic value of the basihyal projection into question.

The OPM, which has also been considered to be of systematic value (Mayden, 1989) is also variable. My findings indicate that the size of the OPM is variable in size. In *Notropis hudsonius* specifically, the OPM is closed off creating a closed posterior myodome. This closed posterior myodome (CPM) has been observed in other notropin species, (Harrington, 1955; Mayden, 1989). However, the CPM has not been previously reported in *N. hudsonius* specifically, even in studies that have included *N. hudsonius* specimens (Coburn, 1982; Mayden, 1989). Thus, these inconsistencies among these authors and my findings also raises questions about the validity and systematic value of the OPM.

When these four species are broken down into two separate clades, one with *Notropis atherinoides* and *Notropis percobromus*, and the other with *Notropis buchanani* and *Notropis volucellus sensu* Mayden et al. (2006), shared osteological traits become apparent. *N. atherinoides* and *N. percobromus* share several similarities in the ethmoid region, orbital region, basicranial region, Weberian apparatus, pectoral and pelvic girdle, suspensorium, oral jaws, hyoid bar and branchial apparatus. Of these, I noted several traits that are specific to only *N. atherinoides* and *N. percobromus*. These traits include a moderately developed posterior angle of the ascending limb of the fifth ceratobranchial, a reduced clupeoid projection and head of the first branchiostegal ray, a reduced dorsal process of the palatine, a straight posterior shaft of the premaxilla, and a large scapular foramen.

Osteological similarities for *Notropis buchanani* and *Notropis volucellus* are seen in the ethmoid region, basicranial region, suspensorium, hyoid bar and branchial apparatus. Of these regions, the traits specific only to *N. buchanani* and *N. volucellus* include pharyngeal teeth with elongate, sharp edges, a deep hypohyal foramen, an ethmoid block with a supraethmoid portion that is much wider at the anterior end and flares laterally, and broad parasphenoid wings. Mayden (1989) used the morphology of the palatine as a justification to put *N. buchanani*, *N. volucellus* and *Notropis heterolepis* into a *Notropis volucellus* species group. More specifically, he observed that these three species all had an anterolaterally directed lateral process and a deep, restricted preethmoid cup that was formed by the dorsal and ventral processes. Mayden (1989) concluded that these features were synapomorphies. I also observed the deep preethmoid cup for all three species but not the anterolaterally directed lateral process in *N. volucellus.* Further, while recent molecular studies agree that *N. volucellus* and *N. buchanani* are at the very least closely related, they also agree that *N. heterolepis* is not closely related to either species at all (Mayden et al., 2006; Schönhuth et al., 2018; Stout et al., 2022). With these findings in mind, it would be more accurate to conclude that this deep preethmoid socket is a possible synapomorphy for *N. buchanani* and *N. volucellus* that has evolved independently in *N. heterolepis*.

In the same study, Mayden (1989) also placed *Notropis heterodon* and *Notropis texanus* into a *Notropis texanus* species group based on the observation that both species have serrated pharyngeal teeth. I made the same observation. However, recent molecular studies have since placed these species into two separate subgenera (Mayden et al., 2006; Schönhuth et al., 2018; Stout et al., 2022). Thus, the serrated teeth of *N. heterodon* and *N. texanus* can be interpreted as a trait that evolved independently, presumably as a means to process similar food items. A similar conclusion of convergent evolution can be drawn about the sensory canal system. In *Notropis buchanani*, *Notropis heterodon* and *Notropis heterolepis*, the sensory canal system is seen to be poorly developed to varying degrees, corroborating the finding of Reno (1966) and Swift (1970). The underdevelopment of the sensory canal system is found in notropin species that are adapted to swamps, lakes and other slow-moving bodies of water. It should be noted that Reno (1966) also found that the sensory canal system of *Notropis volucellus* could be underdeveloped in adults, specifically the postocular commissure and the preopercularmandibular canals. However, the specimens that I examined have a fully developed sensory canal system and were also sampled from a river (Appendix A). The specimens examined here, therefore, probably reflect the turbid environment they came from. If I were to examine *N. volucellus* specimens from a low turbidity environment such as a lake, I would expect to observe an underdeveloped sensory canal system similar to that described by Reno (1966).

3.4.2 Conclusions

Our understanding of the evolution of the osteology of *Notropis* is complicated by homoplasy. Early authors relied on osteological characteristics to determine the evolutionary relationships of *Notropis* (both s.s. and s.l.) and its relatives (Coburn, 1982; Mayden, 1989; Cavender and Coburn, 1992; Coburn and Cavender, 1992). However, the advent of molecular systematics has radically changed our current understanding of these evolutionary relationships (Mayden et al., 2006; Schönhuth et al., 2018; Stout et al., 2022). In the context of phylogenies produced by molecular systematic studies, I still observed some osteological characteristics that could be interpreted as synapomorphies for closely related species. However, I still found many osteological similarities among the 11 species examined, even species from different subgenera. Furthermore, molecular systematics gives us cause to reassess and reinterpret which osteological characteristics might be synapomorphies and which may be the result of convergence. From my analysis, it is clear that convergent evolution and adaptation to similar habitats and niches play a role in shaping osteology. Going forward, an alternative approach may be to instead re-examine and reassess notropin osteology in the context of niche and habitat rather than their evolutionary relationships.

My results also show some inconsistencies in the osteological characteristics given by earlier authors and what I observed myself. For example, I found the kinethmoid of *Notropis dorsalis* to be curved, while Coburn (1982) described it as straight. Furthermore, Mayden (1989) found the lateral process of the palatine to be anterolaterally oriented in *Notropis volucellus,* but I made a different observation. Although I examined many more *Notropis hudsonius* specimens when compared to the other species, I also observed some osteological variability in other species similar to those I found in *N.* hudsonius (Chapter 2). The width of the anterodorsal process of the metapterygoid is, for example, especially variable in the *Notropis blennius* specimens that I examined. The results of the PCA conducted on both the measurements and meristic counts of the *Notropis* specimens used in this study also indicate potential morphological variability beyond osteology. Another area for future research should, therefore, not only focus on the intraspecific osteological variation of more *Notropis* species, similar to my study of *N. hudsonius* (Chapter 2), but also look at intraspecific morphological variation as a whole.

3.5 Tables

Table 3.1. Measurements for *Notropis atherinoides* ($n = 8$). Measurements are in millimeters.

Measurement	**Minimum**	**Maximum**	**Mean**	**SD**
Standard length (SL)	50.63	61.2	56.09	3.55
Preanal length SL^{-1}	0.66	0.75	0.71	0.03
Predorsal length SL^{-1}	0.51	0.60	0.55	0.02
Prepelvic length SL^{-1}	0.47	0.54	0.50	0.03
Prepectoral length SL^{-1}	0.23	0.29	0.25	0.02
Head length (HL) SL^{-1}	0.23	0.27	0.25	0.01
Snout length SL^{-1}	0.06	0.08	0.07	0.01
Snout length HL^{-1}	0.24	0.31	0.27	0.02
Postorbital length SL^{-1}	0.08	0.12	0.10	0.01
Postorbital length HL^{-1}	0.33	0.46	0.42	0.04
Dorsal fin base SL^{-1}	0.11	0.14	0.12	0.01
Anal fin base SL^{-1}	0.13	0.16	0.14	0.01
Peduncle length SL^{-1}	0.18	0.25	0.21	0.02
Interorbital width SL^{-1}	0.06	0.09	0.07	0.01
Interorbital width HL^{-1}	0.34	0.24	0.28	0.03
Eye diameter SL^{-1}	0.07	0.08	0.08	0.005
Eye diameter HL^{-1}	0.30	0.33	0.31	0.01
Body depth SL^{-1}	0.17	0.24	0.21	0.02
Caudal peduncle depth SL^{-1}	0.08	0.11	0.10	0.01
Dorsal fin length SL^{-1}	0.19	0.21	0.20	0.01
Anal fin length SL^{-1}	0.15	0.17	0.16	0.01
Pectoral fin length SL^{-1}	0.18	0.20	0.19	0.01
Pelvic fin length SL^{-1}	0.12	0.16	0.15	0.01

Table 3.2. Measurements for *Notropis blennius* (*n* = 5). Measurements are in millimeters.

Measurement	**Minimum**	**Maximum**	**Mean**	**SD**
Standard length (SL)	39.13	41.0	40.25	0.84
Preanal length SL^{-1}	0.71	0.77	0.7	0.02
Predorsal length SL^{-1}	0.53	0.57	0.55	0.02
Prepelvic length SL^{-1}	0.51	0.56	0.53	0.02
Prepectoral length SL^{-1}	0.29	0.31	0.30	0.01
Head length (HL) SL^{-1}	0.26	0.28	0.27	0.01
Snout length SL^{-1}	0.07	0.09	0.08	0.01
Snout length HL^{-1}	0.26	0.34	0.29	0.03
Postorbital length SL^{-1}	0.13	0.15	0.14	0.01
Postorbital length HL^{-1}	0.48	0.52	0.51	0.01
Dorsal fin base SL^{-1}	0.12	0.16	0.14	0.02
Anal fin base SL^{-1}	0.08	0.15	0.11	0.03
Peduncle length SL^{-1}	0.25	0.20	0.23	0.02
Interorbital width SL^{-1}	0.09	0.11	0.10	0.01
Interorbital width HL^{-1}	0.32	0.39	0.36	0.03
Eye diameter SL^{-1}	0.07	0.09	0.08	0.01
Eye diameter HL^{-1}	0.27	0.32	0.30	0.02
Body depth SL^{-1}	0.22	0.25	0.23	0.01
Caudal peduncle depth SL^{-1}	0.11	0.13	0.12	0.01
Dorsal fin length SL^{-1}	0.19	0.23	0.21	0.02
Anal fin length SL^{-1}	0.16	0.19	0.18	0.01
Pectoral fin length SL^{-1}	0.17	0.21	0.19	0.02
Pelvic fin length SL^{-1}	0.14	0.17	0.15	0.01

Table 3.3. Measurements for *Notropis buchanani* (n = 3). Measurements are in millimeters.

Measurement	**Minimum**	**Maximum**	**Mean**	**SD**
Standard length (SL)	31.04	32.4	31.51	0.76
Preanal length SL^{-1}	0.66	0.68	0.7	0.01
Predorsal length SL^{-1}	0.49	0.53	0.51	0.02
Prepelvic length SL^{-1}	0.48	0.50	0.50	0.01
Prepectoral length SL^{-1}	0.28	0.30	0.29	0.01
Head length (HL) SL^{-1}	0.25	0.27	0.26	0.01
Snout length SL^{-1}	0.05	0.05	0.05	0.00
Snout length HL^{-1}	0.19	0.20	0.20	0.01
Postorbital length SL^{-1}	0.12	0.13	0.12	0.01
Postorbital length HL^{-1}	0.46	0.48	0.47	0.01
Dorsal fin base SL^{-1}	0.14	0.17	0.15	0.01
Anal fin base SL^{-1}	0.12	0.14	0.13	0.01
Peduncle length SL^{-1}	0.24	0.26	0.24	0.01
Interorbital width SL^{-1}	0.07	0.08	0.07	0.01
Interorbital width HL^{-1}	0.26	0.30	0.27	0.02
Eye diameter SL^{-1}	0.08	0.09	0.08	0.00
Eye diameter HL^{-1}	0.31	0.34	0.32	0.01
Body depth SL^{-1}	0.26	0.27	0.27	0.01
Caudal peduncle depth SL^{-1}	0.08	0.11	0.10	0.02
Dorsal fin length SL^{-1}	0.20	0.25	0.23	0.03
Anal fin length SL^{-1}	0.17	0.21	0.19	0.02
Pectoral fin length SL^{-1}	0.18	0.19	0.19	0.005
Pelvic fin length SL^{-1}	0.14	0.17	0.16	0.01

Table 3.4. Measurements for *Notropis dorsalis* (*n* = 3). Measurements are in millimeters.

Measurement	**Minimum**	**Maximum**	**Mean**	**SD**
Standard length (SL)	47.70	49.8	48.85	1.07
Preanal length SL^{-1}	0.63	0.66	0.65	0.02
Predorsal length SL^{-1}	0.50	0.54	0.52	0.02
Prepelvic length SL^{-1}	0.48	0.51	0.50	0.01
Prepectoral length SL^{-1}	0.28	0.30	0.29	0.01
Head length (HL) SL^{-1}	0.26	0.28	0.27	0.01
Snout length SL^{-1}	0.08	0.09	0.08	0.01
Snout length HL^{-1}	0.26	0.29	0.28	0.02
Postorbital length SL^{-1}	0.12	0.13	0.13	0.006
Postorbital length HL^{-1}	0.46	0.47	0.46	0.003
Dorsal fin base SL^{-1}	0.11	0.13	0.12	0.01
Anal fin base SL^{-1}	0.11	0.13	0.12	0.01
Peduncle length SL^{-1}	0.23	0.24	0.24	0.01
Interorbital width SL^{-1}	0.08	0.08	0.08	0.002
Interorbital width HL^{-1}	0.27	0.30	0.29	0.02
Eye diameter SL^{-1}	0.07	0.08	0.08	0.002
Eye diameter HL^{-1}	0.26	0.30	0.28	0.02
Body depth SL^{-1}	0.18	0.19	0.18	0.01
Caudal peduncle depth SL^{-1}	0.10	0.10	0.10	0.004
Dorsal fin length SL^{-1}	0.22	0.23	0.23	0.001
Anal fin length SL^{-1}	0.16	0.18	0.17	0.01
Pectoral fin length SL^{-1}	0.16	0.18	0.17	0.02
Pelvic fin length SL^{-1}	0.12	0.15	0.14	0.01

Table 3.5. Measurements for *Notropis heterodon* (*n* = 3). Measurements are in millimeters.

Measurement	**Minimum**	**Maximum**	**Mean**	**SD**
Standard length (SL)	42.9	39.65	41.48	1.66
Preanal length SL^{-1}	0.67	0.64	0.66	0.01
Predorsal length SL^{-1}	0.48	0.50	0.49	0.01
Prepelvic length SL^{-1}	0.49	0.51	0.50	0.01
Prepectoral length SL^{-1}	0.28	0.29	0.29	0.004
Head length (HL) SL^{-1}	0.25	0.26	0.26	0.003
Snout length SL^{-1}	0.06	0.07	0.07	0.01
Snout length HL^{-1}	0.24	0.27	0.26	0.02
Postorbital length SL^{-1}	0.12	0.13	0.12	0.01
Postorbital length HL^{-1}	0.47	0.50	0.48	0.02
Dorsal fin base SL^{-1}	0.11	0.15	0.13	0.02
Anal fin base SL^{-1}	0.11	0.13	0.12	0.01
Peduncle length SL^{-1}	0.20	0.24	0.23	0.02
Interorbital width SL^{-1}	0.07	0.08	0.08	0.003
Interorbital width HL^{-1}	0.29	0.30	0.29	0.01
Eye diameter SL^{-1}	0.09	0.10	0.09	0.003
Eye diameter HL^{-1}	0.36	0.37	0.37	0.01
Body depth SL^{-1}	0.22	0.22	0.22	0.002
Caudal peduncle depth SL^{-1}	0.08	0.09	0.08	0.004
Dorsal fin length SL^{-1}	0.23	0.24	0.23	0.01
Anal fin length SL^{-1}	0.18	0.19	0.18	0.002
Pectoral fin length SL^{-1}	0.17	0.19	0.18	0.01
Pelvic fin length SL^{-1}	0.15	0.17	0.16	0.01

Table 3.6. Measurements for *Notropis heterolepis* (n = 7). Measurements are in millimeters.

Measurement	**Minimum**	**Maximum**	**Mean**	**SD**
Standard length (SL)	32.43	43.83	36.06	3.74
Preanal length SL^{-1}	0.63	0.72	0.67	0.04
Predorsal length SL^{-1}	0.60	0.51	0.54	0.03
Prepelvic length SL^{-1}	0.48	0.56	0.51	0.04
Prepectoral length SL^{-1}	0.27	0.33	0.29	0.02
Head length (HL) SL^{-1}	0.25	0.30	0.27	0.02
Snout length SL^{-1}	0.06	0.07	0.07	0.01
Snout length HL^{-1}	0.22	0.29	0.24	0.03
Postorbital length SL^{-1}	0.12	0.15	0.13	0.01
Postorbital length HL^{-1}	0.45	0.51	0.49	0.02
Dorsal fin base SL^{-1}	0.09	0.16	0.13	0.02
Anal fin base SL^{-1}	0.08	0.13	0.11	0.02
Peduncle length SL^{-1}	0.14	0.31	0.24	0.05
Interorbital width SL^{-1}	0.06	0.09	0.08	0.01
Interorbital width HL^{-1}	0.24	0.32	0.28	0.03
Eye diameter SL^{-1}	0.07	0.11	0.09	0.01
Eye diameter HL^{-1}	0.29	0.39	0.34	0.03
Body depth SL^{-1}	0.16	0.27	0.20	0.04
Caudal peduncle depth SL^{-1}	0.08	0.11	0.09	0.01
Dorsal fin length SL^{-1}	0.14	0.24	0.21	0.04
Anal fin length SL^{-1}	0.17	0.23	0.19	0.02
Pectoral fin length SL^{-1}	0.17	0.20	0.18	0.01
Pelvic fin length SL^{-1}	0.17	0.20	0.18	0.01

Table 3.7. Measurements for *Notropis percobromus* (n = 3). Measurements are in millimeters.

Measurement	**Minimum**	**Maximum**	**Mean**	**SD**
Standard length (SL)	35.65	33.63	34.50	1.04
Preanal length SL^{-1}	0.66	0.66	0.66	0.003
Predorsal length SL^{-1}	0.55	0.57	0.56	0.01
Prepelvic length SL^{-1}	0.48	0.51	0.50	0.02
Prepectoral length SL^{-1}	0.28	0.29	0.28	0.01
Head length (HL) SL^{-1}	0.27	0.28	0.28	0.01
Snout length SL^{-1}	0.06	0.07	0.06	0.003
Snout length HL^{-1}	0.22	0.25	0.24	0.02
Postorbital length SL^{-1}	0.12	0.13	0.12	0.01
Postorbital length HL^{-1}	0.43	0.45	0.44	0.01
Dorsal fin base SL^{-1}	0.10	0.12	0.12	0.01
Anal fin base SL^{-1}	0.15	0.15	0.15	0.00
Peduncle length SL^{-1}	0.20	0.22	0.21	0.01
Interorbital width SL^{-1}	0.08	0.08	0.08	0.004
Interorbital width HL^{-1}	0.30	0.28	0.29	0.01
Eye diameter SL^{-1}	0.08	0.09	0.09	0.004
Eye diameter HL^{-1}	0.32	0.33	0.32	0.01
Body depth SL^{-1}	0.17	0.20	0.18	0.02
Caudal peduncle depth SL^{-1}	0.17	0.20	0.18	0.02
Dorsal fin length SL^{-1}	0.20	0.20	0.20	0.003
Anal fin length SL^{-1}	0.18	0.19	0.18	0.01
Pectoral fin length SL^{-1}	0.19	0.21	0.19	0.01
Pelvic fin length SL^{-1}	0.113	0.14	0.13	0.01

Table 3.8. Measurements for *Notropis stramineus* (n = 8). Measurements are in millimeters.

Measurement	**Minimum**	**Maximum**	**Mean**	**SD**
Standard length (SL)	36.35	43.83	41.09	2.28
Preanal length SL^{-1}	0.67	0.75	0.72	0.03
Predorsal length SL^{-1}	0.49	0.55	0.53	0.03
Prepelvic length SL^{-1}	0.49	0.57	0.53	0.02
Prepectoral length SL^{-1}	0.27	0.32	0.30	0.02
Head length (HL) SL^{-1}	0.25	0.32	0.28	0.02
Snout length SL^{-1}	0.06	0.09	0.07	0.01
Snout length HL^{-1}	0.21	0.27	0.24	0.02
Postorbital length SL^{-1}	0.12	0.15	0.13	0.01
Postorbital length HL^{-1}	0.43	0.49	0.46	0.03
Dorsal fin base SL^{-1}	0.13	0.17	0.15	0.02
Anal fin base SL^{-1}	0.10	0.13	0.12	0.01
Peduncle length SL^{-1}	0.18	0.28	0.24	0.04
Interorbital width SL^{-1}	0.08	0.11	0.09	0.01
Interorbital width HL^{-1}	0.27	0.37	0.32	0.03
Eye diameter SL^{-1}	0.07	0.10	0.09	0.01
Eye diameter HL^{-1}	0.28	0.35	0.32	0.03
Body depth SL^{-1}	0.19	0.29	0.24	0.03
Caudal peduncle depth SL^{-1}	0.19	0.25	0.23	0.02
Dorsal fin length SL^{-1}	0.19	0.25	0.23	0.02
Anal fin length SL^{-1}	0.16	0.21	0.18	0.02
Pectoral fin length SL^{-1}	0.15	0.22	0.19	0.03
Pelvic fin length SL^{-1}	0.13	0.17	0.15	0.02

Table 3.9. Measurements for *Notropis texanus* (*n* = 2). Measurements are in millimeters.

Measurement	**Minimum**	**Maximum**	**Mean**	**SD**
Standard length (SL)	28.87	30.07	29.47	0.85
Preanal length SL^{-1}	0.66	0.67	0.67	0.01
Predorsal length SL^{-1}	0.48	0.51	0.49	0.02
Prepelvic length SL^{-1}	0.50	0.50	0.50	0.002
Prepectoral length SL^{-1}	0.27	0.29	0.28	0.01
Head length (HL) SL^{-1}	0.25	0.26	0.25	0.01
Snout length SL^{-1}	0.05	0.07	0.06	0.01
Snout length HL^{-1}	0.27	0.17	0.22	0.07
Postorbital length SL^{-1}	0.11	0.12	0.11	0.004
Postorbital length HL^{-1}	0.45	0.44	0.45	0.004
Dorsal fin base SL^{-1}	0.12	0.14	0.13	0.01
Anal fin base SL^{-1}	0.11	0.12	0.11	0.005
Peduncle length SL^{-1}	0.22	0.22	0.22	0.003
Interorbital width SL^{-1}	0.07	0.07	0.07	0.004
Interorbital width HL^{-1}	0.28	0.27	0.28	0.003
Eye diameter SL^{-1}	0.08	0.09	0.09	0.01
Eye diameter HL^{-1}	0.35	0.33	0.34	0.01
Body depth SL^{-1}	0.20	0.23	0.21	0.02
Caudal peduncle depth SL^{-1}	0.09	0.09	0.09	0.002
Dorsal fin length SL^{-1}	0.22	0.24	0.23	0.01
Anal fin length SL^{-1}	0.17	0.19	0.18	0.01
Pectoral fin length SL^{-1}	0.18	0.18	0.18	0.002
Pelvic fin length SL^{-1}	0.15	0.15	0.15	0.001

Table 3.10. Measurements for *Notropis volucellus* ($n = 8$). Measurements are in millimeters.

Measurement	Minimum	Maximum	Mean	SD
Standard length (SL)	22.83	43.26	31.78	7.86
Preanal length SL^{-1}	0.65	0.71	0.68	0.02
Predorsal length SL^{-1}	0.52	0.57	0.55	0.02
Prepelvic length SL^{-1}	0.50	0.53	0.51	0.01
Prepectoral length SL^{-1}	0.31	0.28	0.29	0.01
Head length (HL) SL^{-1}	0.26	0.28	0.27	0.01
Snout length SL^{-1}	0.06	0.08	0.08	0.01
Snout length HL^{-1}	0.23	0.31	0.28	0.03
Postorbital length SL^{-1}	0.11	0.14	0.12	0.01
Postorbital length HL^{-1}	0.42	0.50	0.45	0.03
Dorsal fin base SL^{-1}	0.10	0.15	0.13	0.02
Anal fin base SL^{-1}	0.10	0.15	0.13	0.02
Peduncle length SL^{-1}	0.20	0.26	0.24	0.02
Interorbital width SL^{-1}	0.07	0.10	0.08	0.01
Interorbital width HL^{-1}	0.26	0.37	0.31	0.04
Eye diameter SL^{-1}	0.08	0.11	0.09	0.01
Eye diameter HL^{-1}	0.30	0.39	0.34	0.04
Body depth SL^{-1}	0.22	0.25	0.24	0.01
Caudal peduncle depth SL^{-1}	0.09	0.12	0.10	0.01
Dorsal fin length SL^{-1}	0.19	0.24	0.21	0.02
Anal fin length SL^{-1}	0.16	0.20	0.18	0.02
Pectoral fin length SL^{-1}	0.16	0.23	0.20	0.03
Pelvic fin length SL^{-1}	0.13	0.18	0.15	0.02

Table 3.11. Meristics for *Notropis atherinoides* (*n* = 8) unless otherwise stated). The number of specimens for each count is in brackets.

Number of						
Dorsal fin rays	8(3)	9(5)				
Anal fin rays	10(3)	11(3)	12(2)			
Pelvic fin rays	8(7)	9(9)				
Pectoral fin rays	12(1)	14(3)	15(4)			
Lateral line scales	38(2)	39(3)	40(1)	41(2)		
Predorsal scales	16(1)	17(1)	18(3)	19(1)	20(1)	22(1)
Postdorsal scales	16(4)	17(1)	18(2)	19(1)		
Scales above lateral line	7(8)					
Scales below lateral line	3(5)	4(3)				
Circumferential scales	22(6)	23(2)				
Peduncle scales	10(1)	11(5)	12(2)			
Gill rakers	7(2)	8(2)	9(1)	10(1)	11(1)	12(1)
Predorsal vertebrae (*n*=3)	15 (3)					
Total number of vertebrae (*n*=3)	40(2)	41(1)				

Table 3.12. Meristics for *Notropis blennius* (n = 5). The number of specimens for each count is in brackets.

Number of				
Dorsal fin rays	8(4)	10(1)		
Anal fin rays	6(1)	7(4)		
Pelvic fin rays	8(4)	9(1)		
Pectoral fin rays	15(3)	16(1)	17(1)	
Lateral line scales	35(1)	36(1)	37(1)	38(1)
Predorsal scales	11(2)	12(1)	13(1)	14(1)
Postdorsal scales	12(2)	14(1)	15(1)	17(1)
Scales above lateral line	6(5)			
Scales below lateral line	4(4)	5(1)		
Circumferential scales	23(4)	24(1)		
Peduncle scales	11(2)	12(3)		
Gill rakers	5(2)	6(2)	8(1)	
Predorsal vertebrae	11(2)	12(3)		
Total number of vertebrae	37(1)	38(3)	39(1)	

Table 3.13. Meristics for *Notropis buchanani* (*n* = 3). The number of specimens for each count is in brackets.

Number of			
Dorsal fin rays	8(3)		
Anal fin rays	8(3)		
Pelvic fin rays	8(3)	9(3)	
Pectoral fin rays	13(3)		
Lateral line scales	36(1)	37(1)	38(1)
Predorsal scales	13(1)	14(1)	15(1)
Postdorsal scales	15(1)	16(1)	17(1)
Scales above lateral line	6(1)	7(2)	
Scales below lateral line	4(3)		
Circumferential scales	24(3)	25(1)	
Peduncle scales	10(1)	11(1)	12(1)
Gill rakers	7(3)		
Predorsal vertebrae	10(1)	11(2)	
Total number of vertebrae	36(2)	38(1)	

Table 3.14. Meristics for *Notropis dorsalis* (*n* = 3). The number of specimens for each count is in brackets.

Number of			
Dorsal fin rays	8(3)		
Anal fin rays	8(1)	9(2)	
Pelvic fin rays	7(1)	8(2)	
Pectoral fin rays	12(1)	13(1)	
Lateral line scales	40(1)	43(1)	
Predorsal scales	14(1)	16(1)	17(1)
Postdorsal scales	19(3)		
Scales above lateral line	5(3)		
Scales below lateral line	4(1)	5(2)	
Circumferential scales	27(3)		
Peduncle scales	12(2)	13(1)	
Gill rakers	3(1)	4(1)	5(1)
Predorsal vertebrae	11(1)	12(2)	
Total number of vertebrae	36(1)	37(1)	

Table 3.15. Meristics for *Notropis heterodon* (*n* = 3) unless otherwise stated). The number of specimens for each count is in brackets.

Number of			
Dorsal fin rays	7(1)	8(2)	
Anal fin rays	8(3)		
Pelvic fin rays	7(1)	8(2)	
Pectoral fin rays	13(1)		
Lateral line scales	38(1)	39(1)	40(1)
Predorsal scales	13(2)	14(1)	
Postdorsal scales	17(1)	18(1)	19(1)
Scales above lateral line	6(3)		
Scales below lateral line	4(3)		
Circumferential scales	23(3)		
Peduncle scales	11(1)	12(2)	
Gill rakers	6(2)	7(1)	
Predorsal vertebrae	9(1)	10(1)	11(1)
Total number of vertebrae	38(3)		

Table 3.16. Meristics for *Notropis heterolepis* (*n* = 7) unless otherwise stated). The number of specimens for each count is in brackets.

Number of					
Dorsal fin rays	8(6)	9(1)			
Anal fin rays	7(1)	8(6)			
Pelvic fin rays	7(1)	8(6)			
Pectoral fin rays	11(2)	12(3)	13(1)	14(1)	
Lateral line scales	34(1)	35(2)	36(2)	37(2)	
Predorsal scales	13(2)	14(2)	16(1)	17(1)	18(1)
Postdorsal scales	14(1)	16(1)	17(2)	18(2)	19(1)
Scales above lateral line	4(1)	5(4)	6(1)		
Scales below lateral line	4(3)	5(4)			
Circumferential scales	22(1)	24(2)	25(3)	26(1)	
Peduncle scales	10(1)	11(2)	12(3)	13(1)	
Gill rakers	4(1)	5(4)	6(2)		
Predorsal vertebrae (*n* = 5)	11 (5)				
Total number of vertebrae (*n* = 5)	35(1)	36(2)	37(2)		

Table 3.17. Meristics for *Notropis percobromus* (n = 3). The number of specimens for each count is in brackets.

Number of			
Dorsal fin rays	8(3)		
Anal fin rays	10(2)	11(1)	
Pelvic fin rays	8(3)		
Pectoral fin rays	10(2)	11(2)	
Lateral line scales	36(1)	38(1)	39(1)
Predorsal scales	16(1)	17(1)	
Postdorsal scales	15(1)	16(1)	
Scales above lateral line	6(1)	7(2)	
Scales below lateral line	4(2)	5(1)	
Circumferential scales	23(1)	24(1)	
Peduncle scales	10(1)	11(1)	12(1)
Gill rakers	6(1)	7(2)	
Predorsal vertebrae (n = 2)	13(2)	14(1)	
Total number of vertebrae (n = 2)	38(1)	39(2)	

Table 3.18. Meristics for *Notropis stramineus* (*n* = 8) unless otherwise stated). The number of specimens for each count is in brackets.

Number of				
Dorsal fin rays	8(6)	8(2)		
Anal fin rays	7(7)	8(1)		
Pelvic fin rays	8(4)	(4)		
Pectoral fin rays	13(4)	14(3)	15(1)	
Lateral line scales	34(2)	35(3)	36(1)	38(2)
Predorsal scales	13(3)	14(2)	15(2)	16(1)
Postdorsal scales	15(2)	16(3)	17(2)	18(1)
Scales above lateral line	5(1)	6(5)	7(2)	
Scales below lateral line	4(8)			
Circumferential scales	22(1)	23(6)	14(1)	
Peduncle scales	11(1)	12(7)		
Gill rakers	4(2)	5(1)	6(2)	7(3)
Predorsal vertebrae (*n* = 4)	10(4)	11(4)		
Total number of vertebrae (*n* = 4)	35(1)	36(3)		

Table 3.19. Meristics for *Notropis texanus* ($n = 2$). The number of specimens for each count is in brackets.

Number of		
Dorsal fin rays	8(1)	9(1)
Anal fin rays	7(1)	8(1)
Pelvic fin rays	8(2)	
Pectoral fin rays	10(2)	11(2)
Lateral line scales	41(1)	42(1)
Predorsal scales	17(1)	18(1)
Postdorsal scales	18(2)	
Scales above lateral line	4(1)	5(1)
Scales below lateral line	5(2)	
Circumferential scales	25(1)	26(1)
Peduncle scales	11(1)	12(1)
Gill rakers	7(2)	
Predorsal vertebrae	11(1)	
Total number of vertebrae	37(1)	

Table 3.20. Meristics for *Notropis volucellus* (*n* = 8) unless otherwise stated). The number of specimens for each count is in brackets.

Number of						
Dorsal fin rays	7(1)	8(4)	9(3)			
Anal fin rays	8(7)	9(1)				
Pelvic fin rays	8(8)					
Pectoral fin rays	12(5)	13(1)	14(2)			
Lateral line scales	35(2)	36(2)	37(1)	38(1)	39(1)	40(1)
Predorsal scales	12(1)	13(4)	16(2)	18(1)		
Postdorsal scales	14(1)	16(4)	17(1)	18(2)		
Scales above lateral line	5(2)	6(6)				
Scales below lateral line	3(1)	4(6)	5(1)			
Circumferential scales	21(2)	23(1)	24(3)	25(1)	26(1)	
Peduncle scales	10(1)	11(1)	12(5)	13(1)		
Gill rakers	4(1)	5(6)	7(1)			
Predorsal vertebrae (*n* = 2)	10(2)					
Total number of vertebrae (*n* = 2)	35(2)					

3.6 Figures

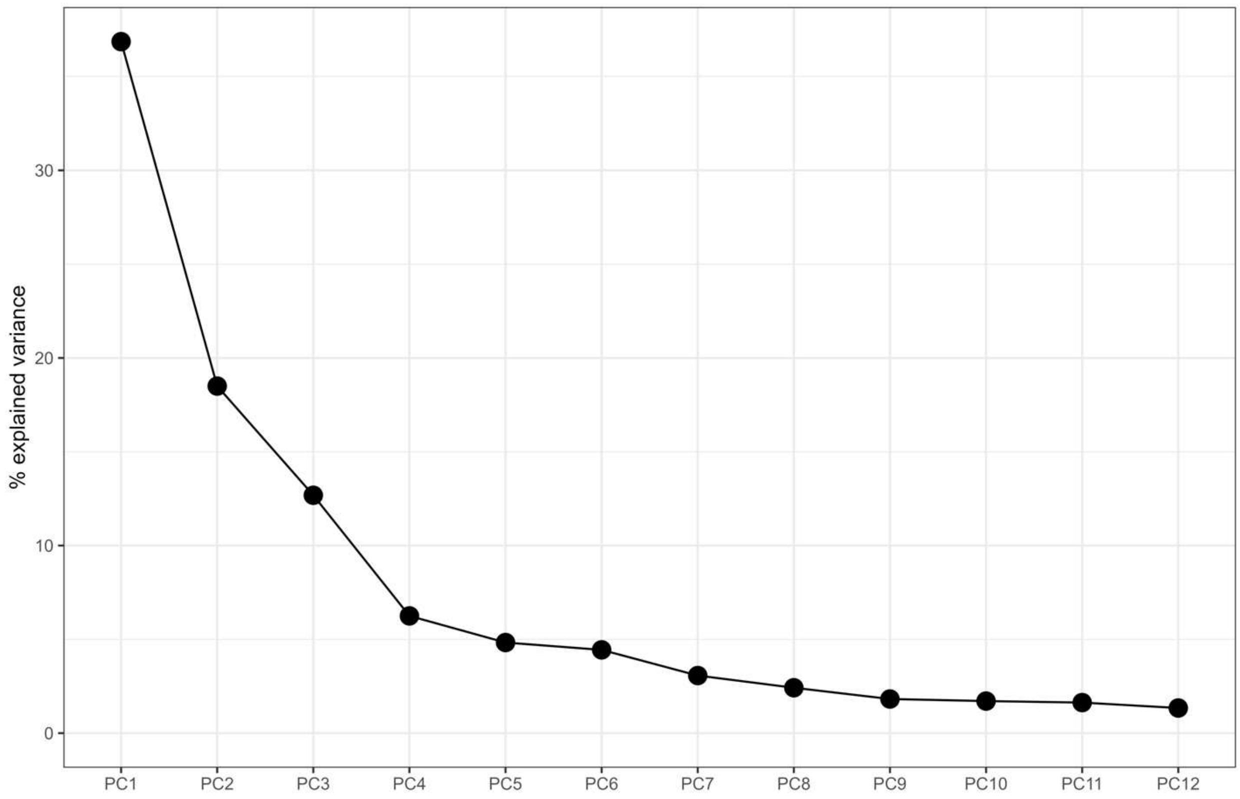

Figure 3.1. Scree plot for first ten principal components for PCA conducted on measurements of 11 *Notropis* species. Measurements were analyzed as ratios of standard length.

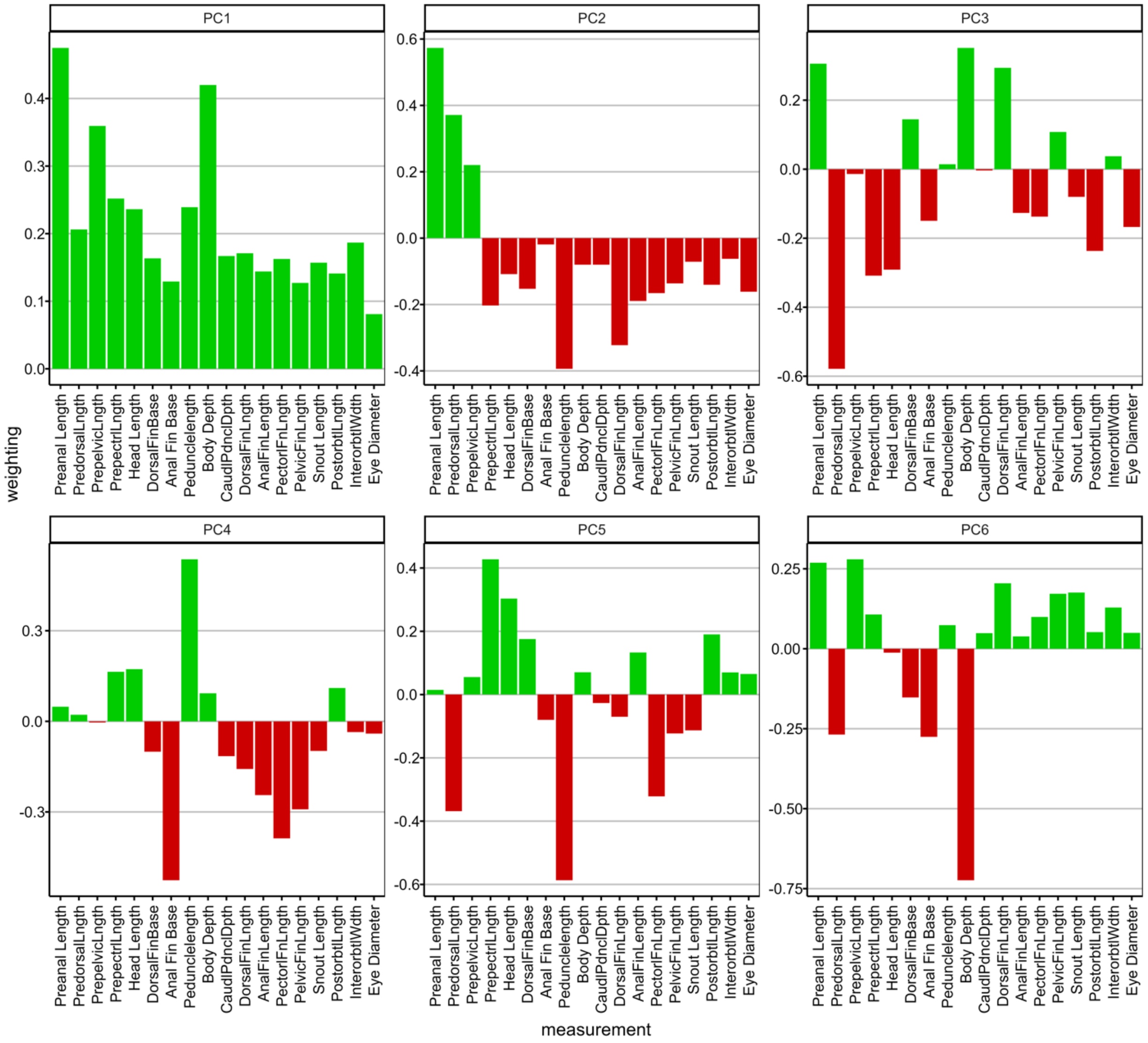

Figure 3.2. Loading plot for first ten principal components for PCA conducted on measurements of 11 *Notropis* species. Measurements were analyzed as ratios of standard length.

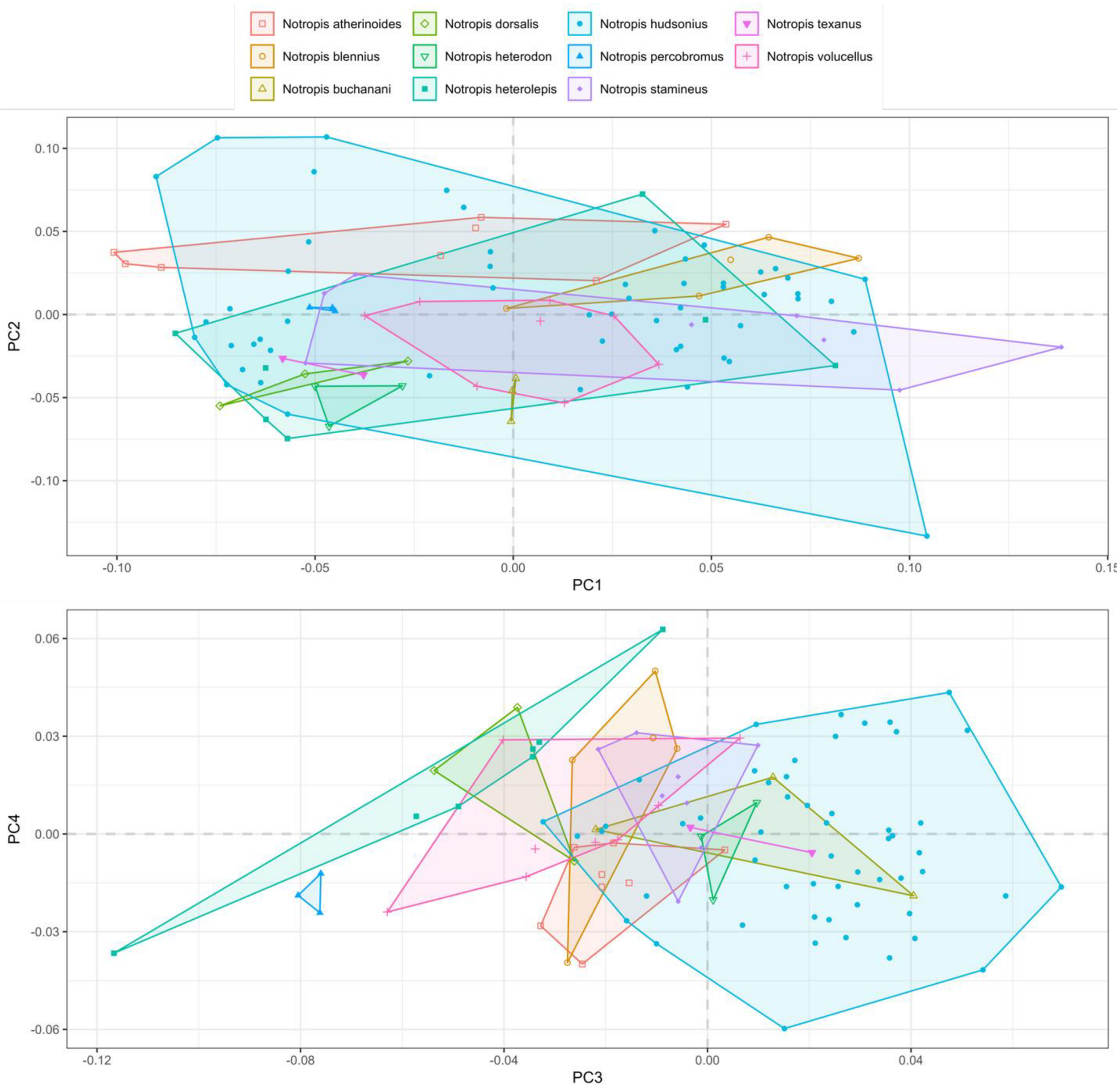

Figure 3.3. PCA scatter plot of measurements for 11 *Notropis* species. PC2 is plotted against PC1 on the top, and PC3 is plotted against PC4 on the bottom. Measurements were analyzed as ratios of standard length.

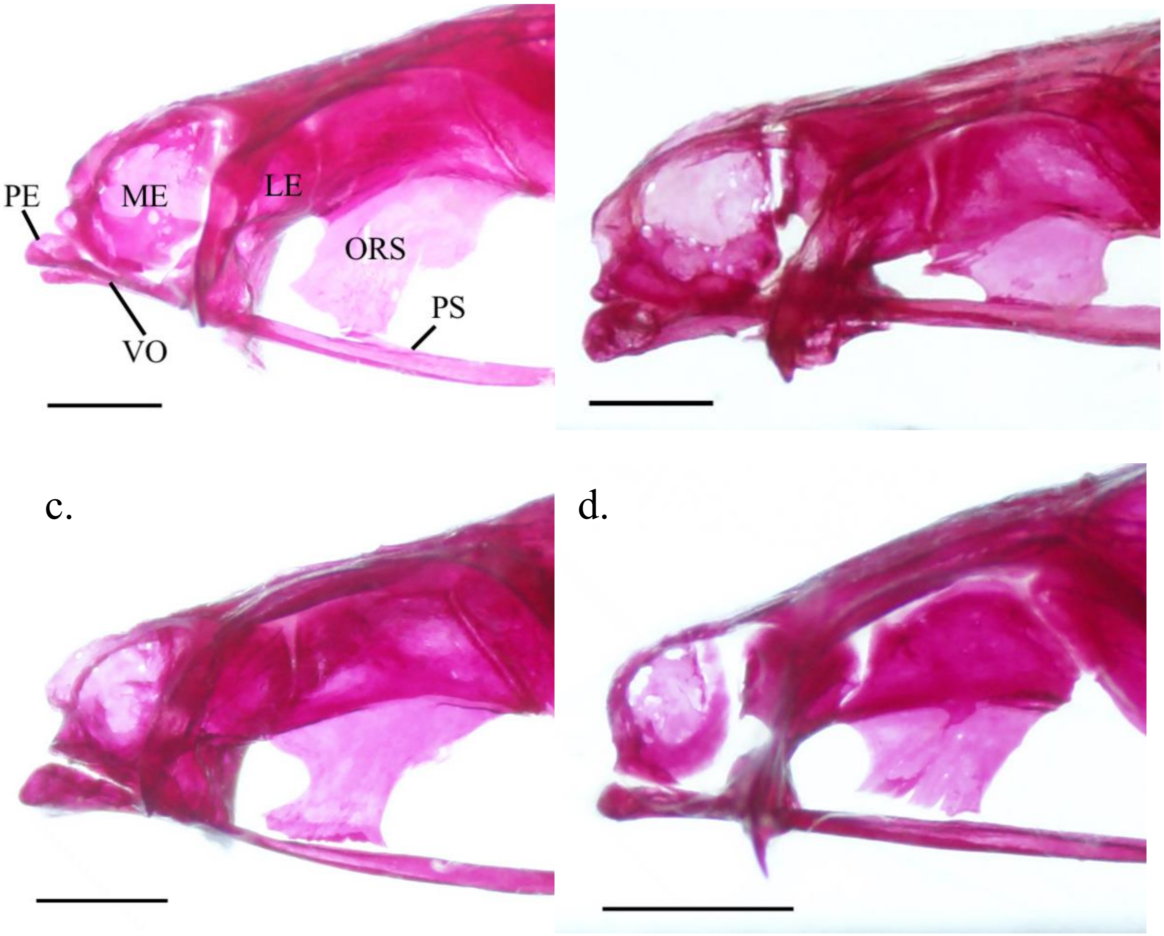

Figure 3.4 The ethmoid an orbital region of (a) *Notropis atherinoides* MZF 766, specimen 1, (b) *Notropis dorsalis* MZF 649, specimen 2, (c) *Notropis heterodon* MZF 2707, specimen 3, and (d) *Notropis texanus* MZF 1445, specimen 1, in lateral view, anterior to left. Scale bars = 1 mm.

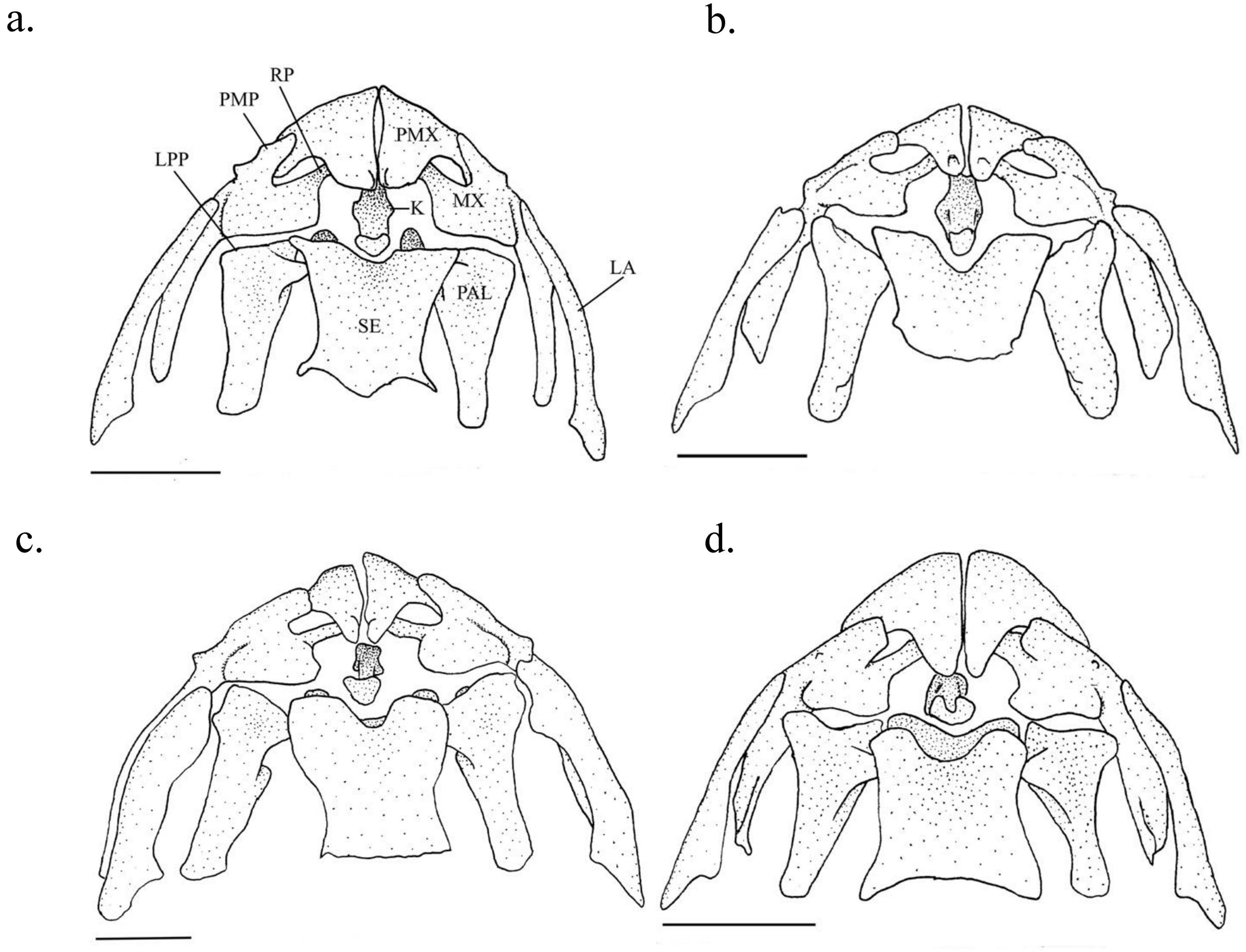

Figure 3. 5. Illustration of the supraethmoid, maxillae, premaxillae and kinethmoid of (a) *Notropis atherinoides* MZF 766, specimen 3, (b) *Notropis buchanani* 1606, specimen 2, (c) *Notropis dorsalis* MZF 649, specimen 3 and (d) *Notropis heterodon* MZF 2027, specimen 2, in dorsal view, anterior to top of page. The nasal bones are not illustrated. Scale bars = 1 mm.

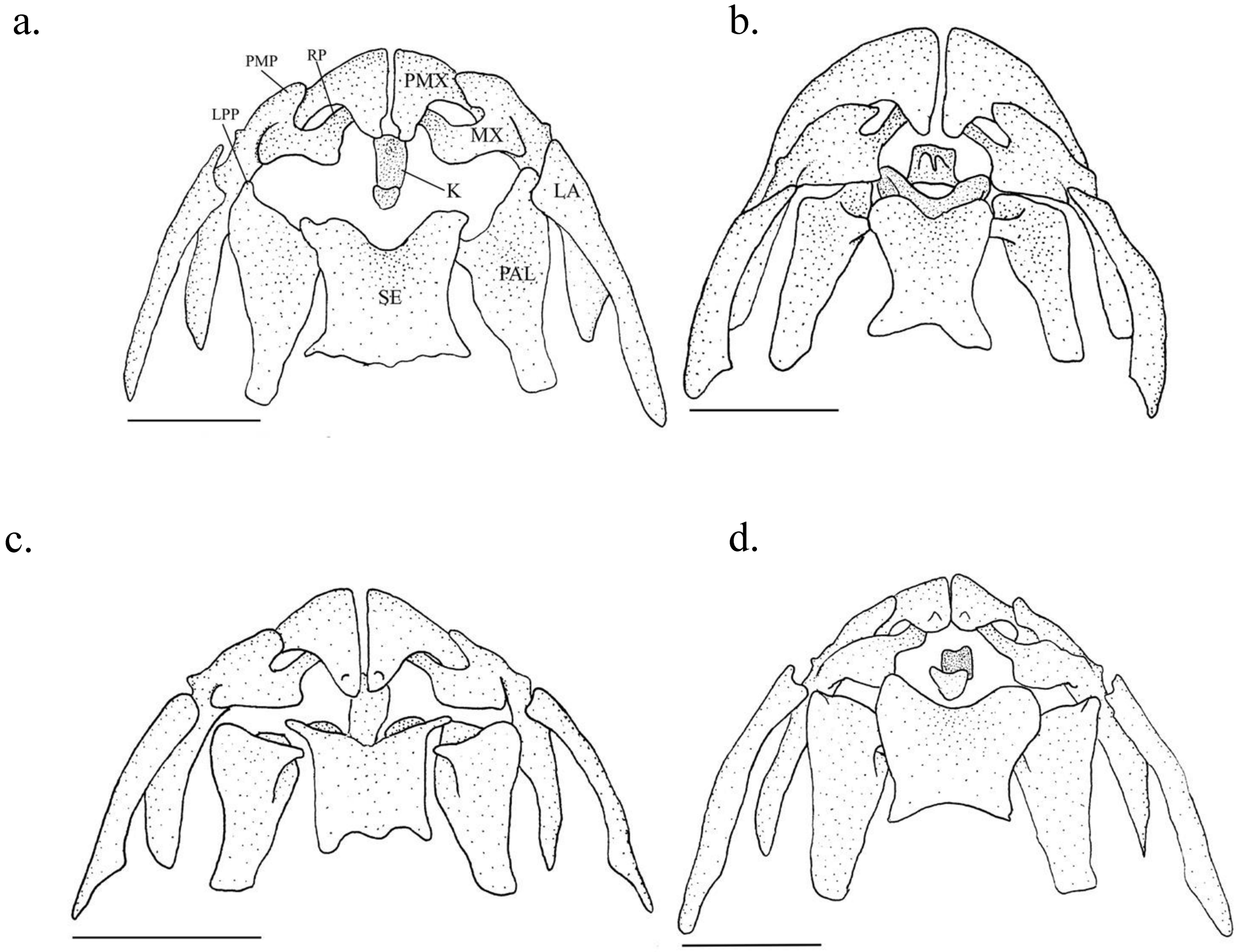

Figure 3.6. Illustration of the supraethmoid, maxillae, premaxillae and kinethmoid of (a) *Notropis heterolepis* MZF 689, specimen 1, (b) *Notropis percobromus* MZF 719, specimen 1, (c) *Notropis texanus* MZF 1445, specimen 2, and (d) *Notropis volucellus* MZF 2036, specimen 3, in dorsal view, anterior to top of page. The nasal bones are not illustrated. Scale bars = 1 mm.

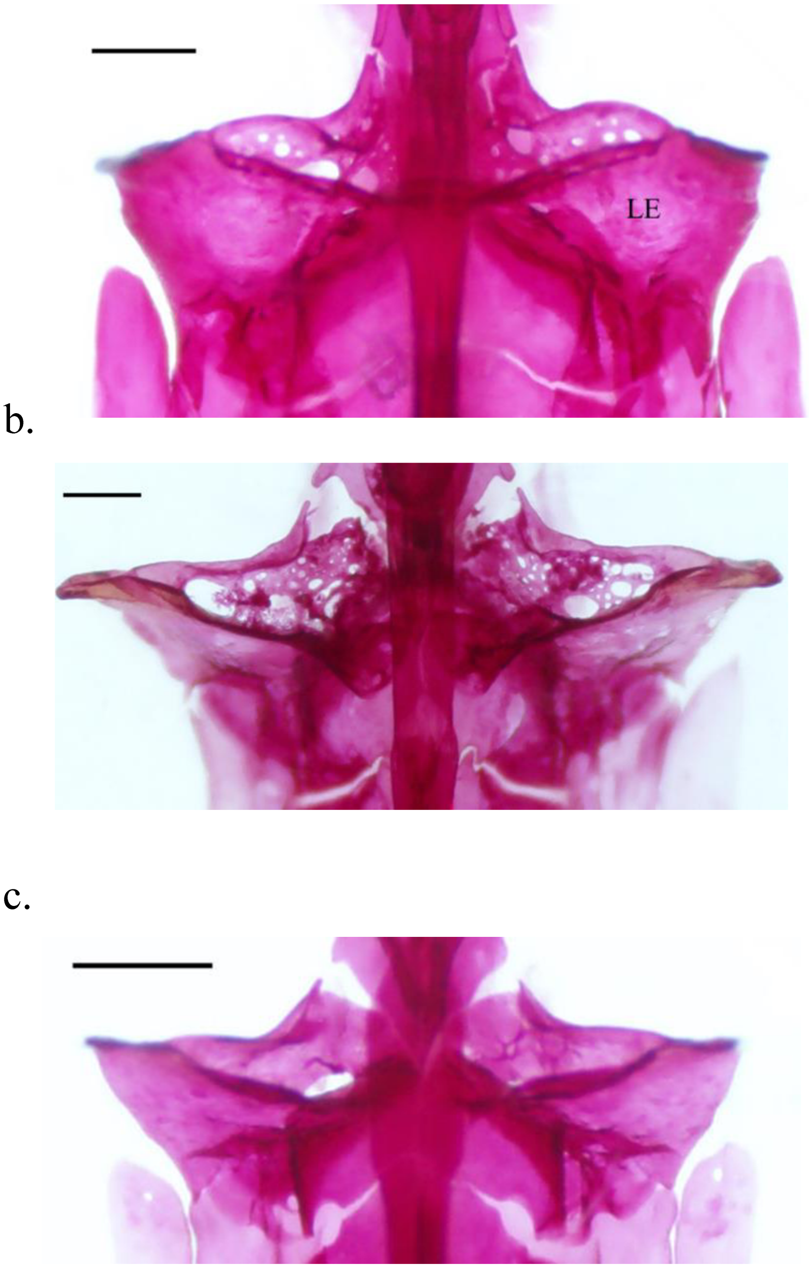

Figure 3.7. The lateral ethmoids of (a) *Notropis atherinoides* MZF 766, specimen 1, (b) *Notropis dorsalis* MZF 649, specimen 2, and (c) *Notropis texanus* MZF 1455, specimen 1, in ventral view, anterior to top of the page. Scale bars = 1 mm.

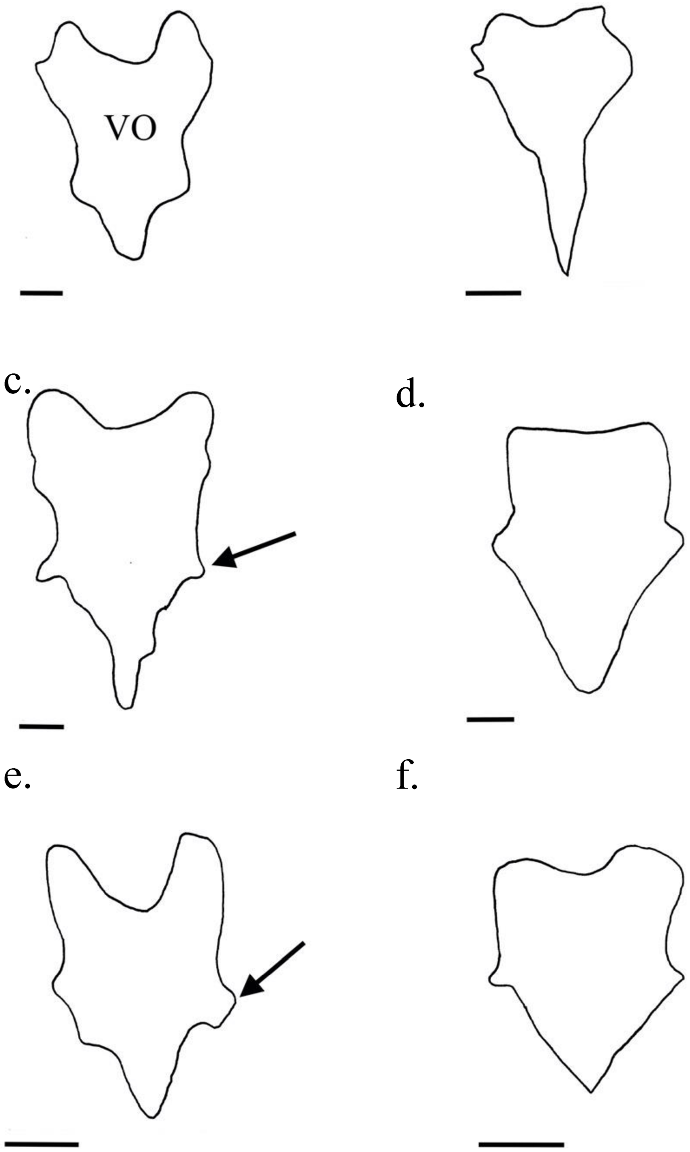

Figure 3.8. Outlines of the vomer of (a) *Notropis atherinoides* MZF 766, specimen 1, (b) *Notropis buchanani* 1606, specimen 3, (c) *Notropis dorsalis* MZF 649, specimen 2, (d) *Notropis heterodon* MZF 2027, specimen 3, (e) *Notropis percobromus* MZF 719, specimen 3 and (f) *Notropis texanus* MZF 1445, specimen 1. Outlines of the vomer are in ventral view, anterior to top of the page. Arrows point to the posterolateral process. Scale bars = 0.25 mm.

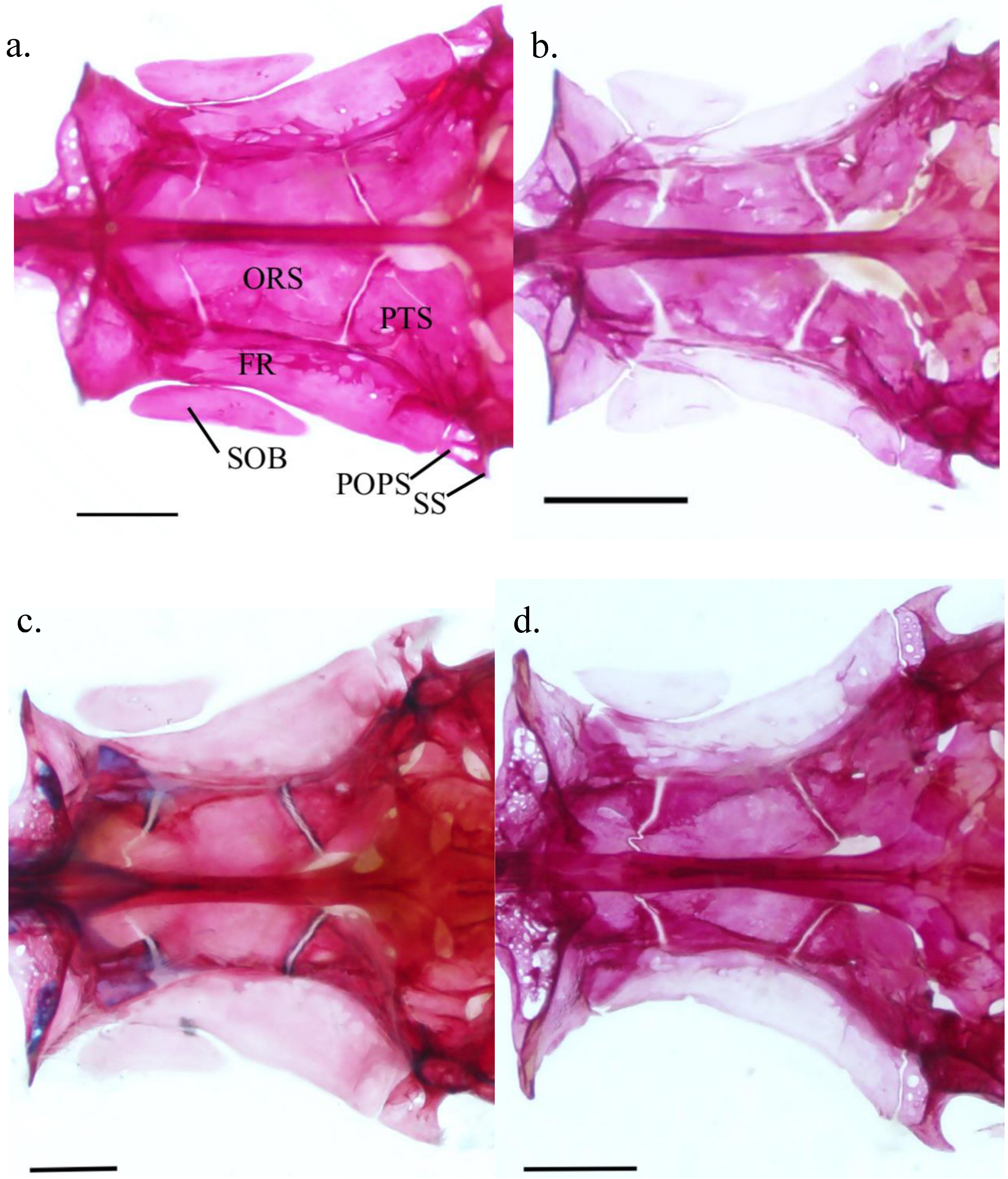

Figure 3.9. The orbital and otic regions of (a) *Notropis atherinoides* MZF 766, specimen 1, (b) *Notropis buchanani* MZF 1606, specimen 3, (c) *Notropis blennius* UAMZ F.55621, specimen 1, and (d) *Notropis dorsalis* MZF 649, specimen 2, in ventral view, anterior to left. Scale bar = 1 mm. The right supraorbital is missing in (d).

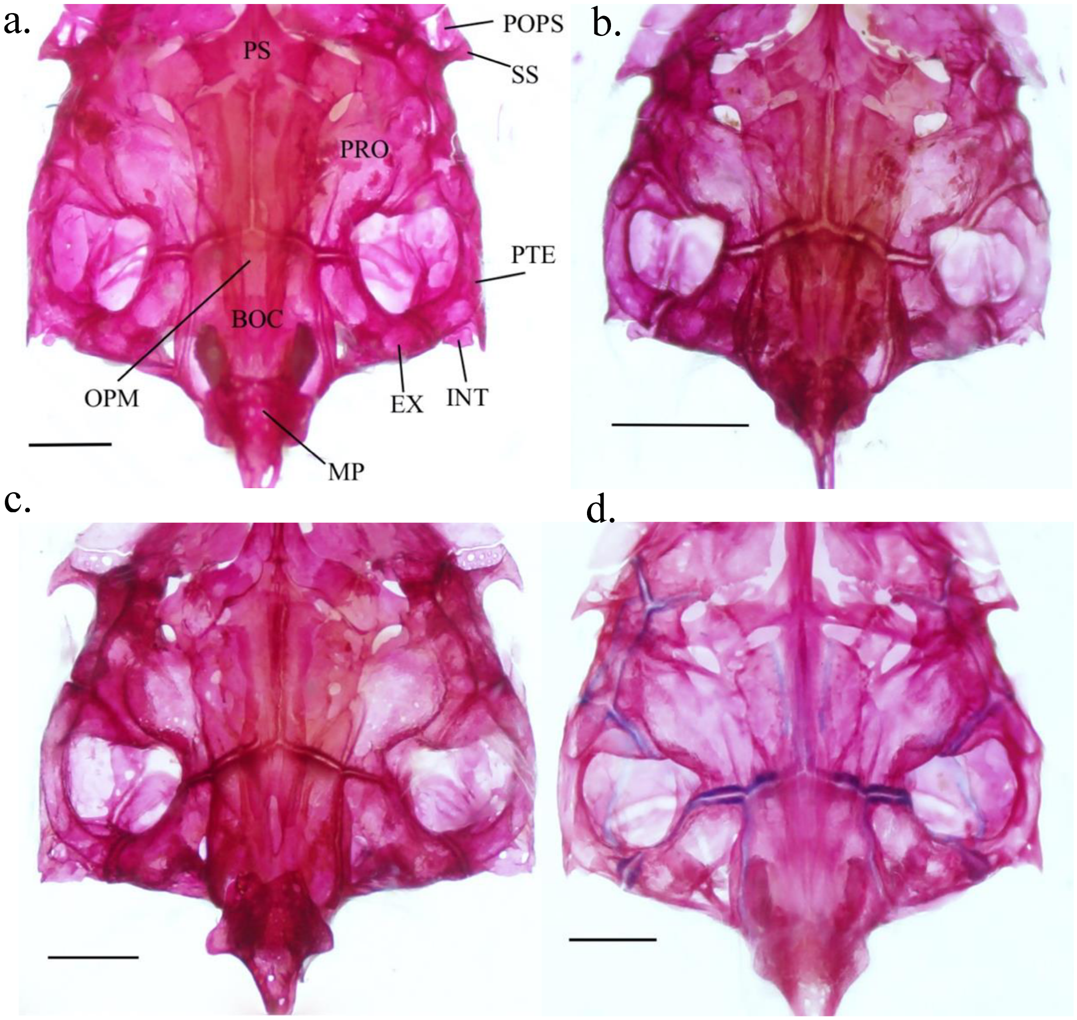

Figure 3.10. The basicranial region of (a) *Notropis atherinoides* MZF 766, specimen 1, (b) *Notropis buchanani* MZF 1606, specimen 3, (c) *Notropis dorsalis* MZF 649, specimen 2, and (d) *Notropis hudsonius* UAMZ 209, specimen 3, in ventral view, anterior top of the page. Scale bars = 1 mm.

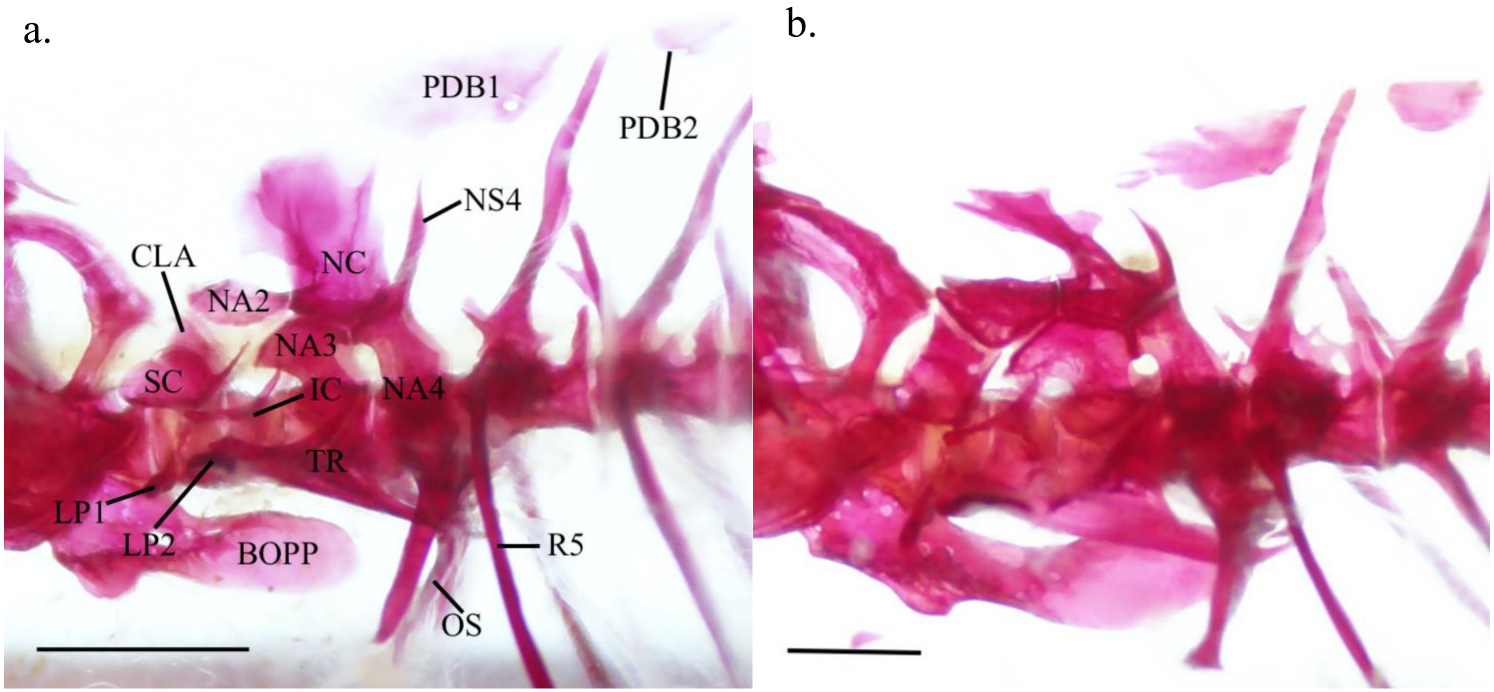

Figure 3.11. The Weberian apparatus of (a) *Notropis buchanani* MZF 1606, specimen 3, and (b) *Notropis dorsalis* MZF 649, specimen 2, in lateral view, anterior to left. Scale bar = 1 mm.

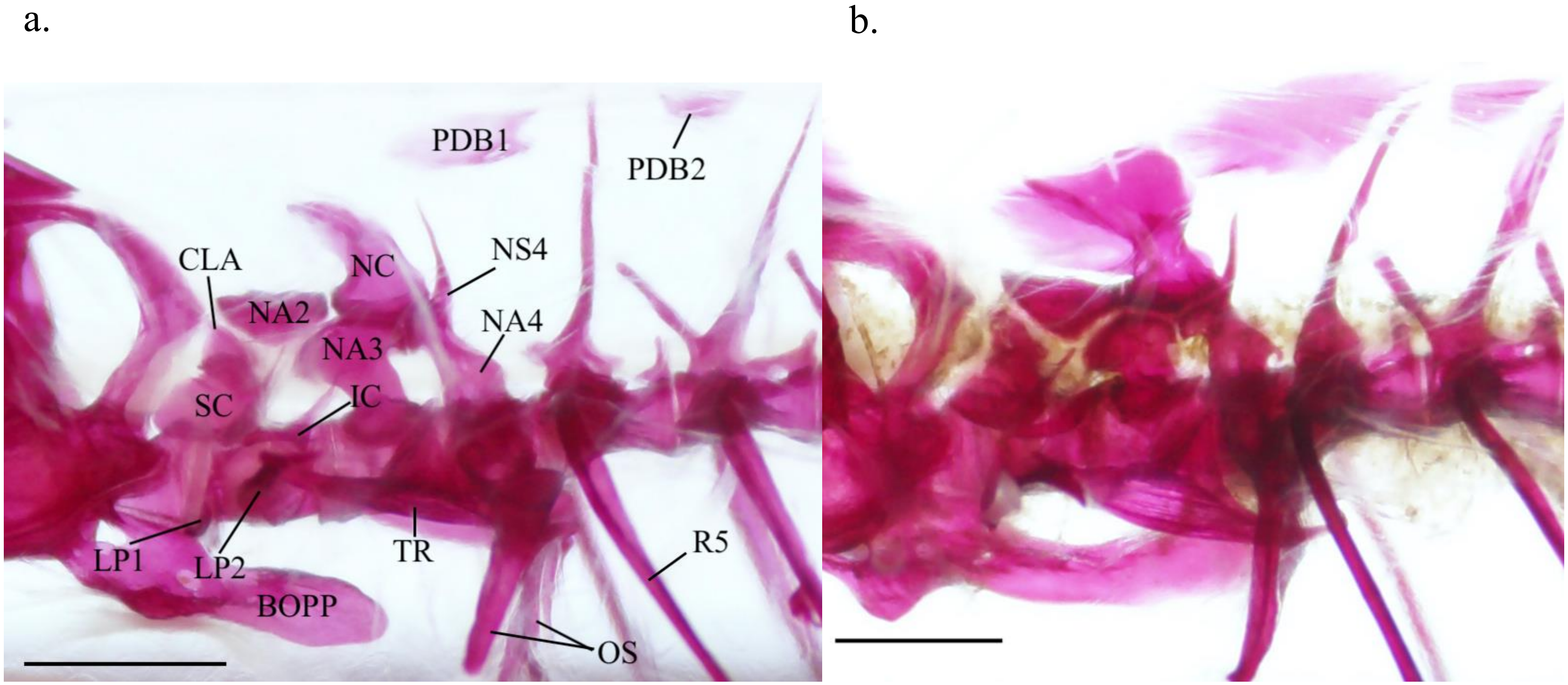

Figure 3.12. The Weberian apparatus of (a) *Notropis heterolepis* MZF 685, specimen 1, and (b) *Notropis stramineus* MZF 1540, specimen 3, in lateral view, anterior to left. Scale bar = 1 mm.

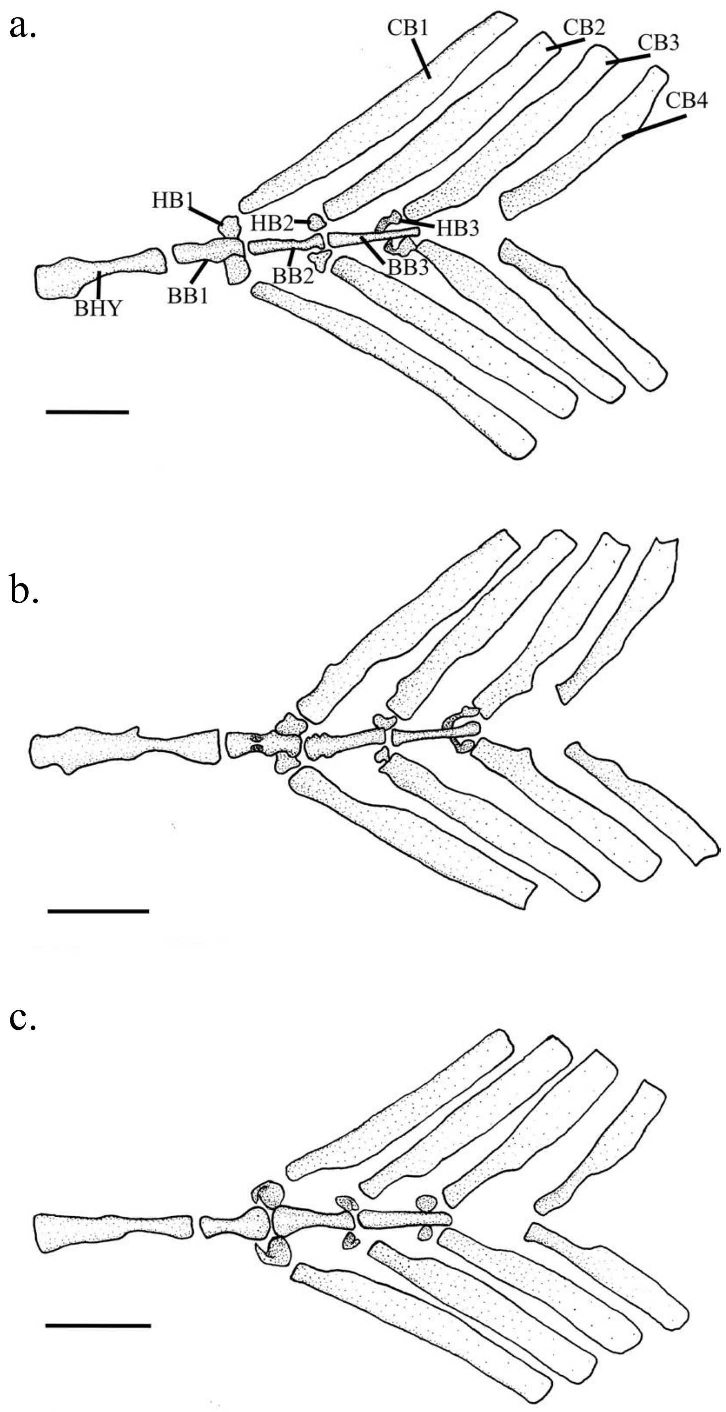

Figure 3.13. Illustration of the ventral portion of the branchial apparatus of (a) *Notropis dorsalis* MZF 649, specimen 2, (b) *Notropis heterodon* MZF 2707, specimen 3, and (c) *Notropis heterolepis* MZF 685, specimen 1, in dorsal view, anterior to left. Scale bars = 0.5 mm.

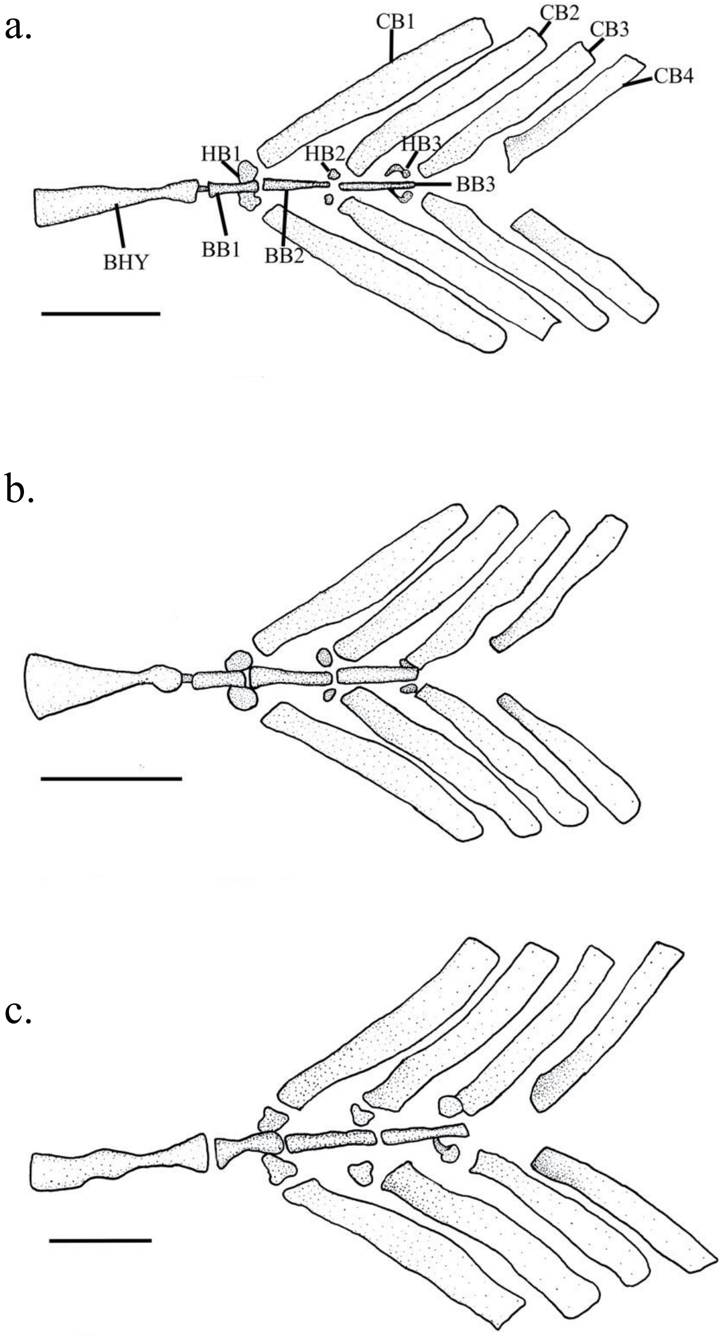

Figure 3.14. Illustration of the ventral portion of the branchial apparatus of (a) *Notropis percobromus* MZF 719, specimen 3, (b) *Notropis texanus* MZF 1445, specimen 1, and (c) *Notropis volucellus* MZF 2036, specimen 1, in dorsal view, anterior to left. Scale bars = 0.5 mm.

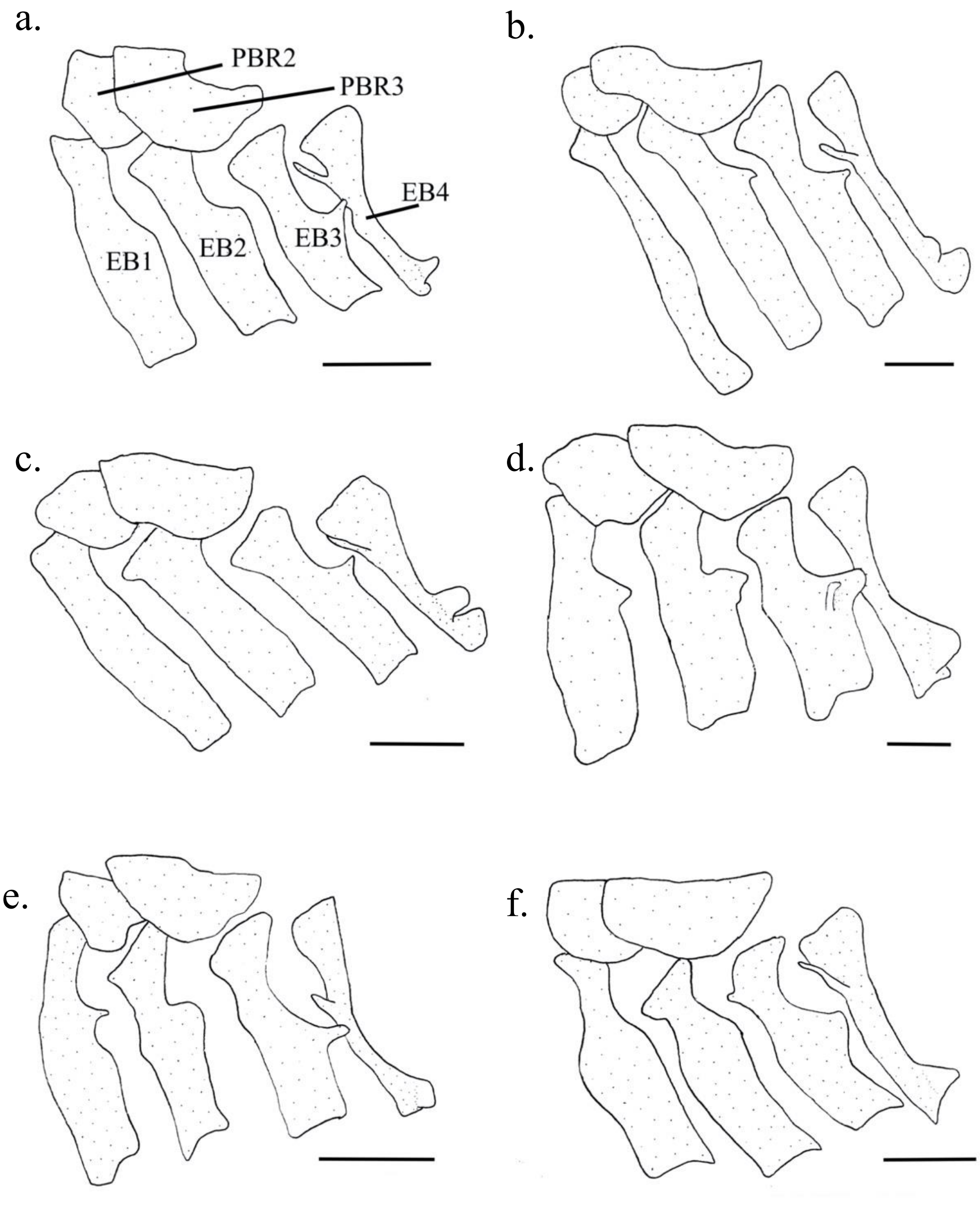

Figure 3.15. Illustration of the epibranchials and pharyngobranchials of (a) *Notropis buchanani* MZF 1606, specimen 3, (b) *Notropis dorsalis* MZF 649, specimen 2, (c) *Notropis heterolepis* MZF 685, specimen 1, (d) *Notropis hudsonius* UAMZ 4950, specimen 1, (e) *Notropis percobromus* MZF 719, specimen 3, and (f) *Notropis volucellus* MZF 2036, specimen 1, in dorsal view, anterior to left. Scale bars = 0.5 mm.

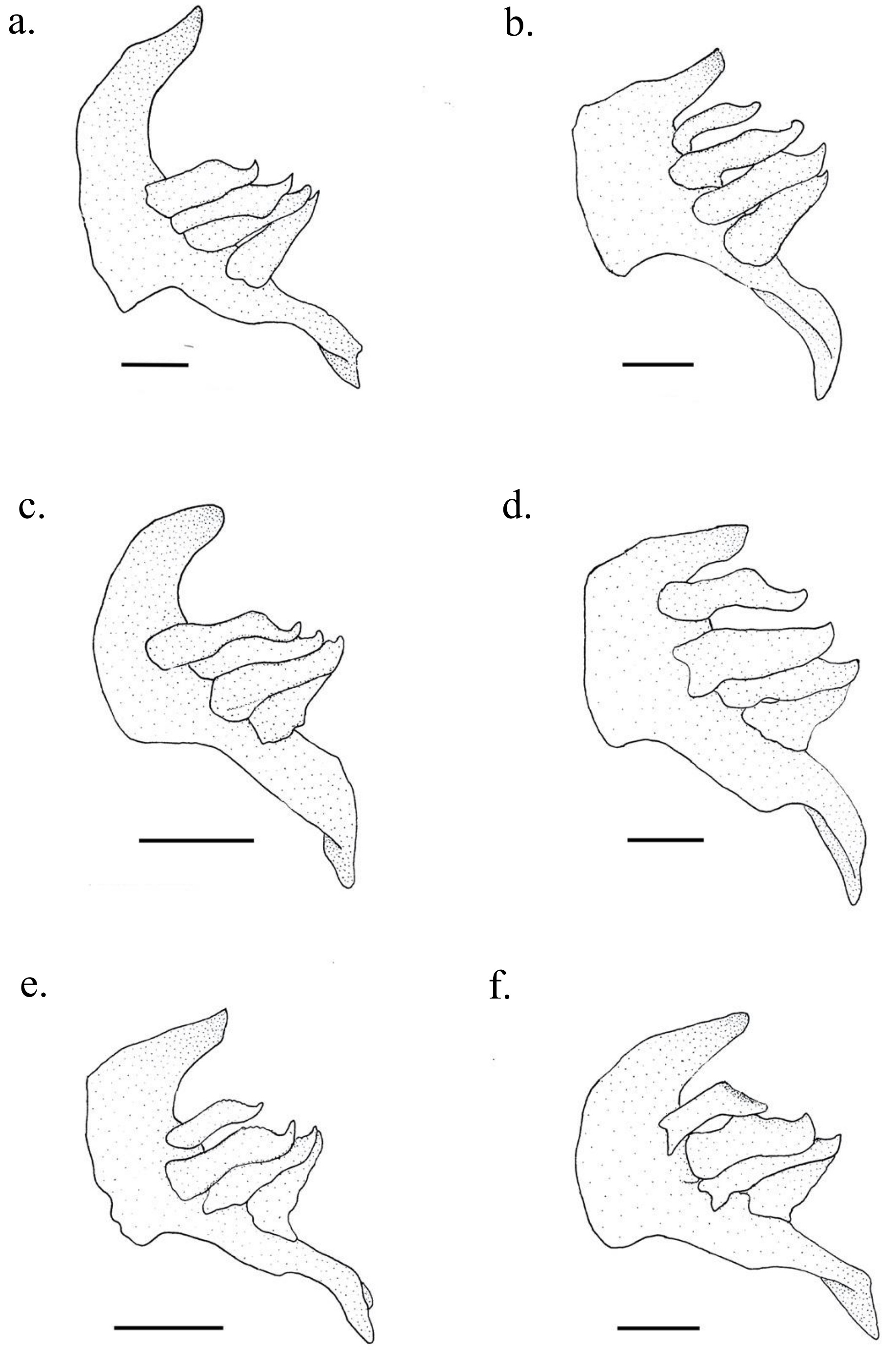

Figure 3.16. Illustration of the left pharyngeal arch of (a) *Notropis atherinoides* MZF 766, specimen 1, (b) *Notropis heterodon* MZF 2027, specimen 3, (c) *Notropis heterolepis* MZF 685, specimen 1, (d) *Notropis stramineus* MZF 1540, specimen 3, (e) *Notropis texanus* MZF 1445, specimen 1, and (f) *Notropis volucellus* MZF 2036, specimen 1, in posteroventral view. Scale bars = 0.5 mm.

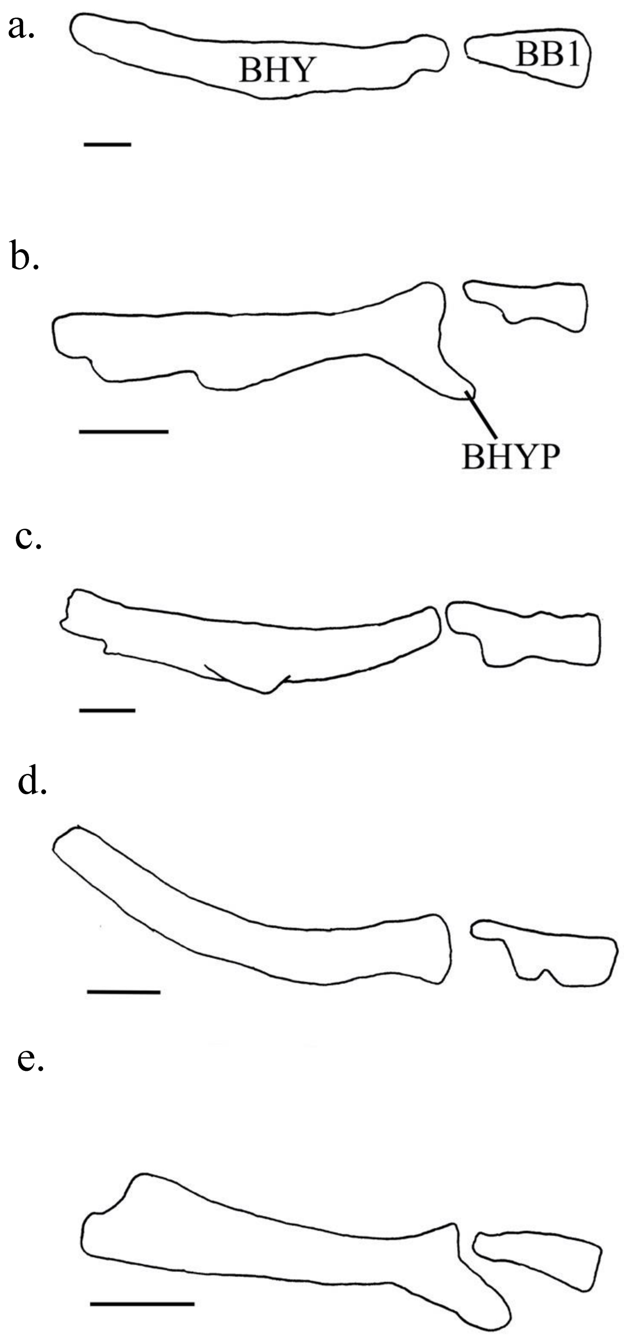

Figure 3.17. Outline of the basihyal and first epibranchial of (a) *Notropis blennius* UAMZ F.55621, specimen 1, (b) *Notropis buchanani* MZF 1606, specimen 3, (c) *Notropis heterodon* MZF 2027, specimen 3, (d) *Notropis stramineus* MZF 1540, specimen 3 and (e) *Notropis texanus* MZF 1445, specimen 1, in lateral view, anterior to left. Scale bars = 0.5 mm.

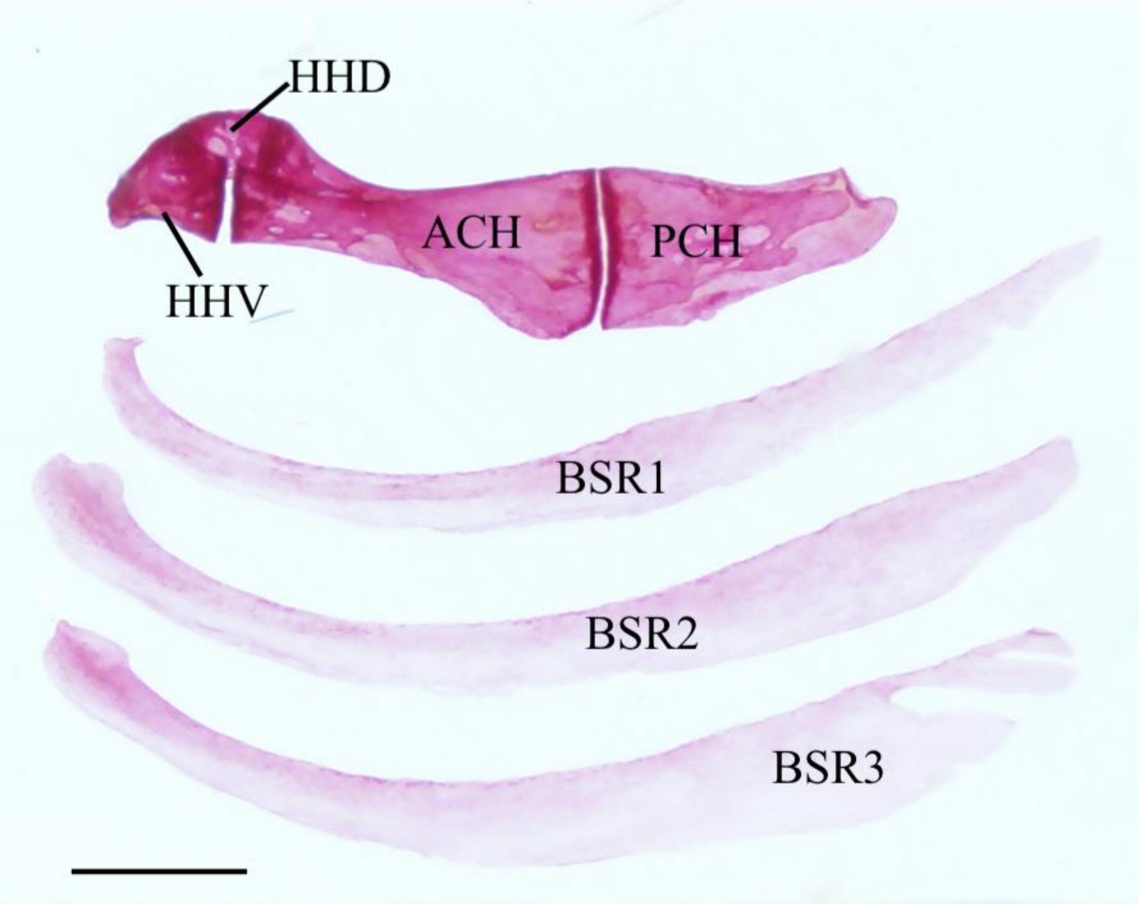

Figure 3.18. The left hyoid arch and disarticulated branchiostegal rays of *Notropis dorsalis* MZF 649, specimen 2, in lateral view, anterior to left. Scale bar = 1 mm.

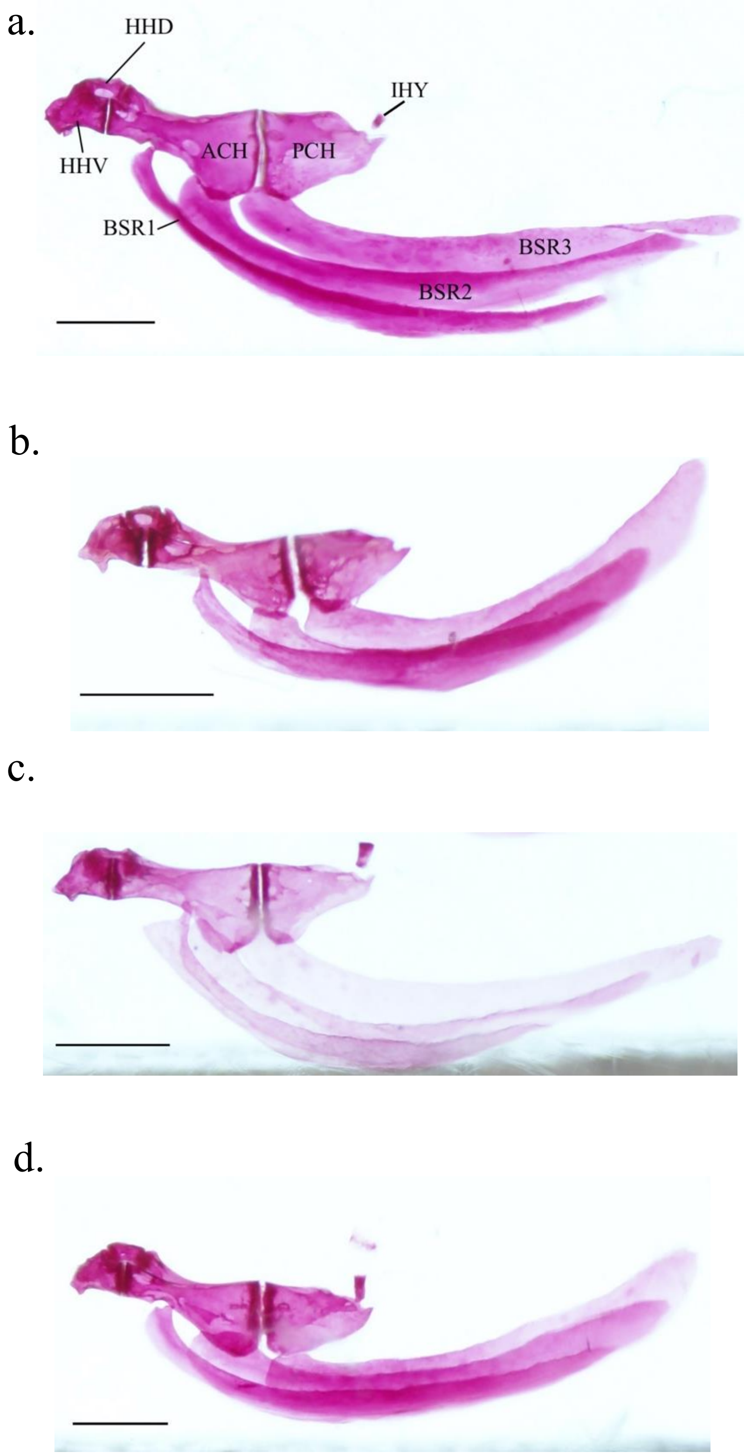

Figure 3.19. The left hyoid bar of (a) *Notropis atherinoides* MZF 766, specimen 1, (b) *Notropis buchanani* MZF 1606, specimen 3, (c) *Notropis heterolepis* MZF 685, specimen 1, and (d) *Notropis stramineus* MZF 1540, specimen 3, in lateral view, anterior to left. Scale bars = 1 mm.

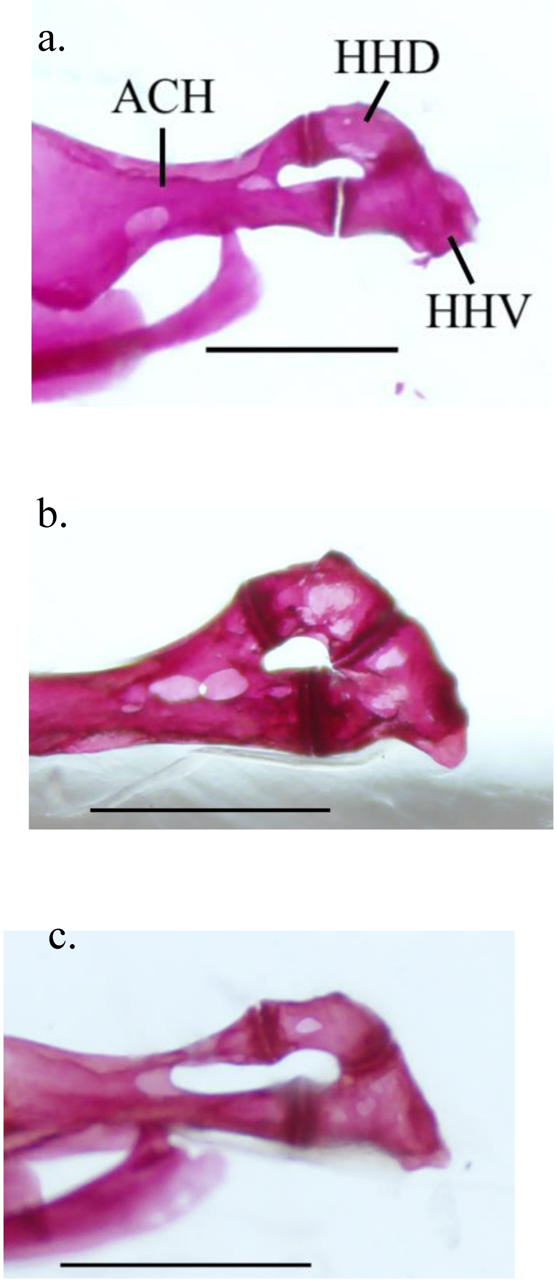

Figure 3.20. Medial view of the left hypohyal foramen of (a) *Notropis atherinoides* MZF 766, specimen 1, (b) *Notropis dorsalis* MZF 649, specimen 2, and (c) *Notropis volucellus* MZF 2036, specimen 1, anterior to right. Scale bars = 1 mm.

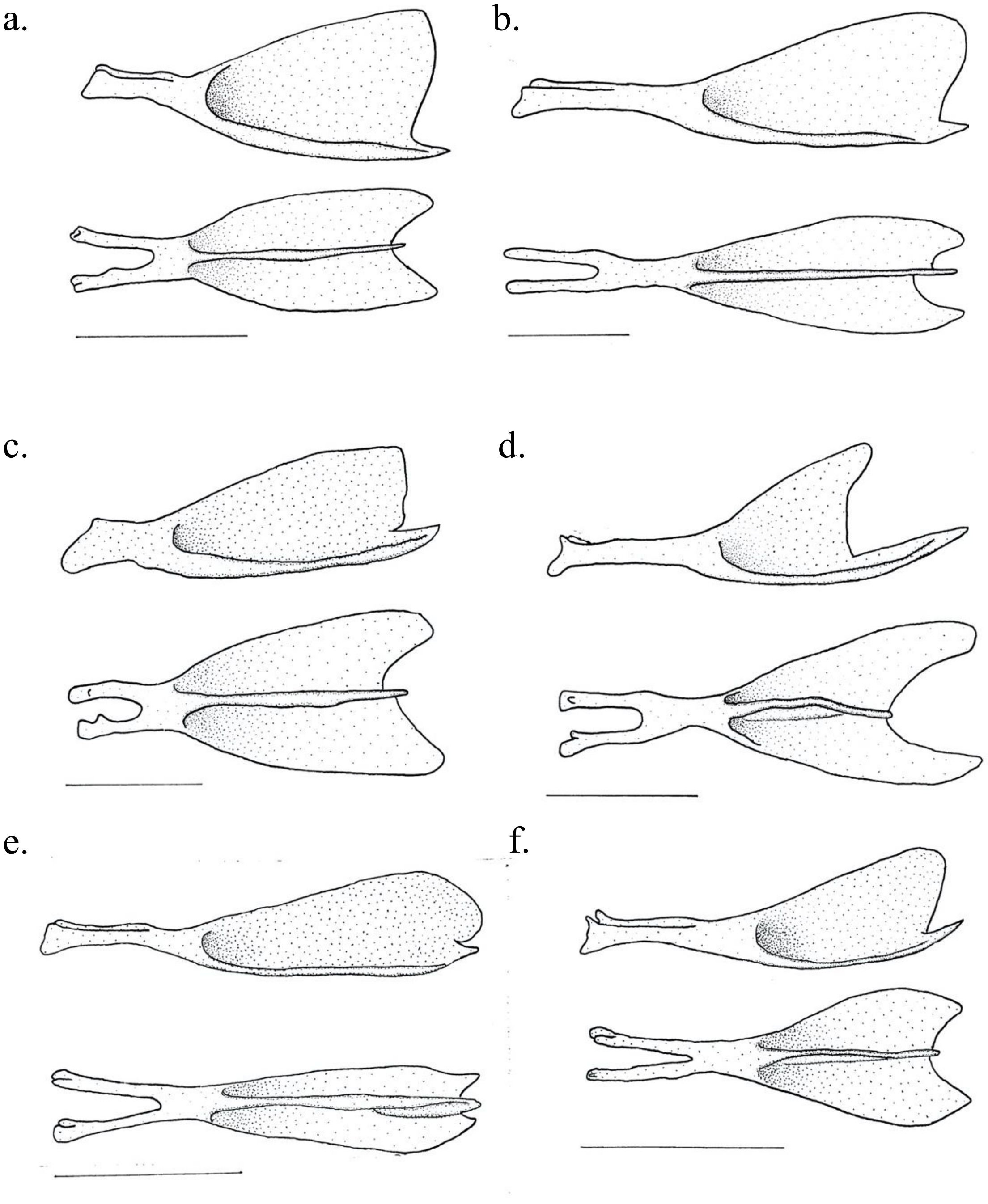

Figure 3.21. Illustration of the urohyal of (a) *Notropis buchanani* MZF 1606, specimen 3, (b) *Notropis blennius* UAMZ F.55621, specimen 1, (c) *Notropis dorsalis* MZF 649, specimen 2, (d) *Notropis heterodon* MZF 2027, specimen 3, (e) *Notropis heterolepis* MZF 685, specimen 1, (f) *Notropis texanus* MZF 1445, specimen 1, in lateral (top) and dorsal (bottom) view, anterior to left. Scale bars = 1 mm.

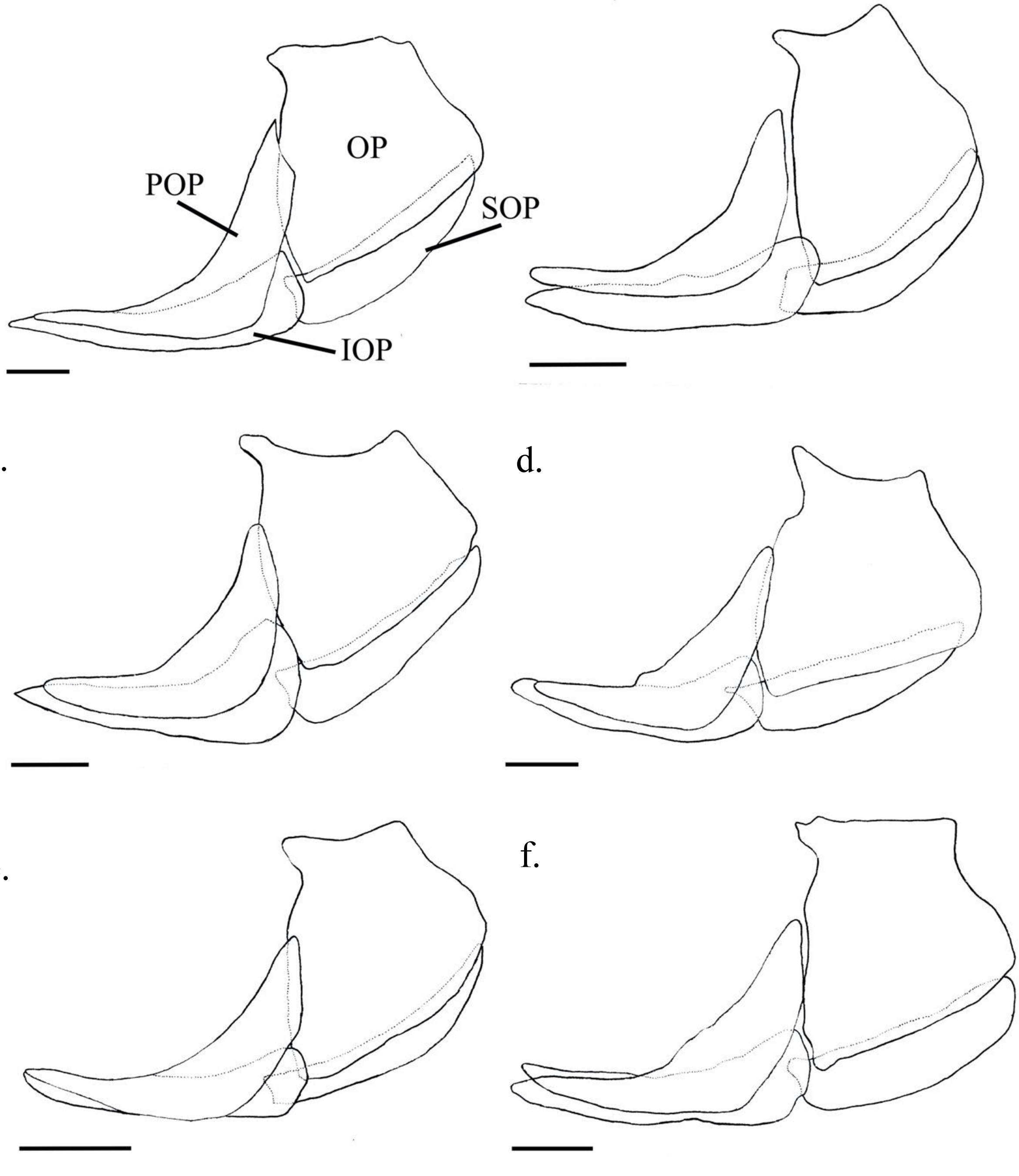

Figure 3.22. Outline of the opercular series of (a) *Notropis atherinoides* MZF 766, specimen 1, (b) *Notropis buchanani* MZF 1606, specimen 3, (c) *Notropis heterolepis* MZF 685, specimen 1 (d) *Notropis stramineus* MZF 1540, specimen 3 (e) *Notropis texanus* MZF 1445, specimen 1, and (f) *Notropis volucellus* MZF 2036, specimen 1, in lateral view, anterior to left. Scale bar = 1 mm.

Figure 3.23. The disarticulated opercular series of *Notropis dorsalis* MZF 649, specimen 2, in lateral view, anterior to left. Scale bar = 1 mm.

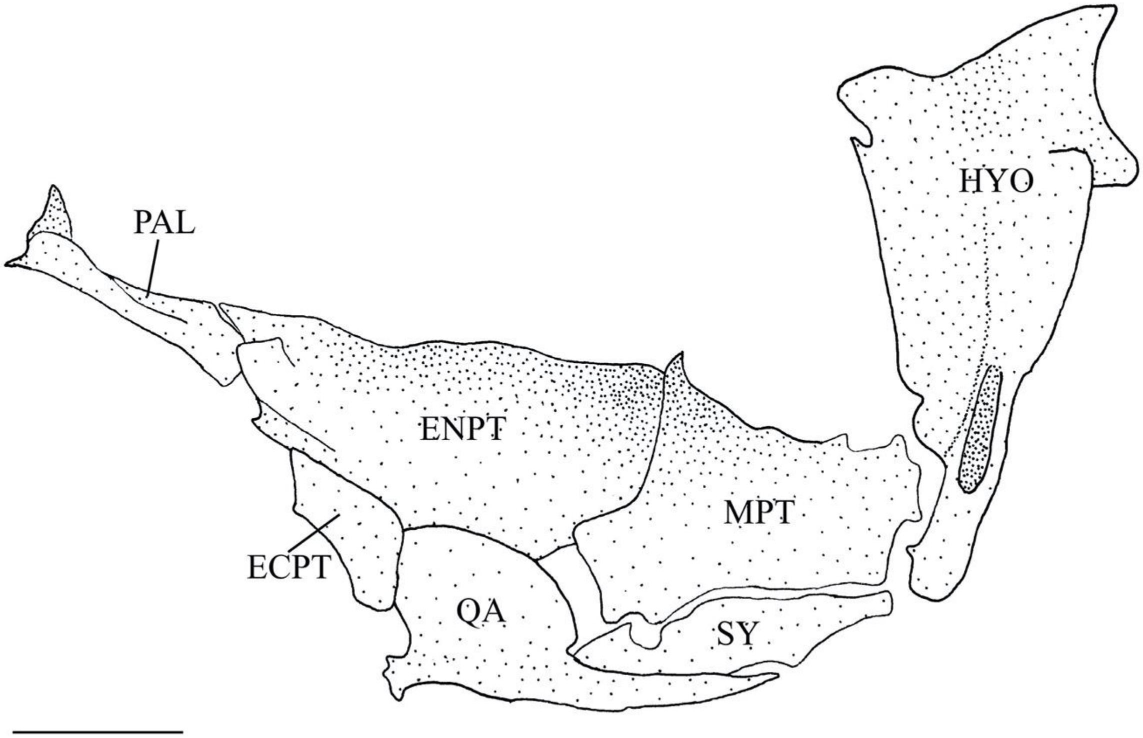

Figure 3.24. Illustration of the suspensorium of *Notropis atherinoides* MZF 766, specimen 1, in lateral view, anterior to left. Scale bar = 1 mm.

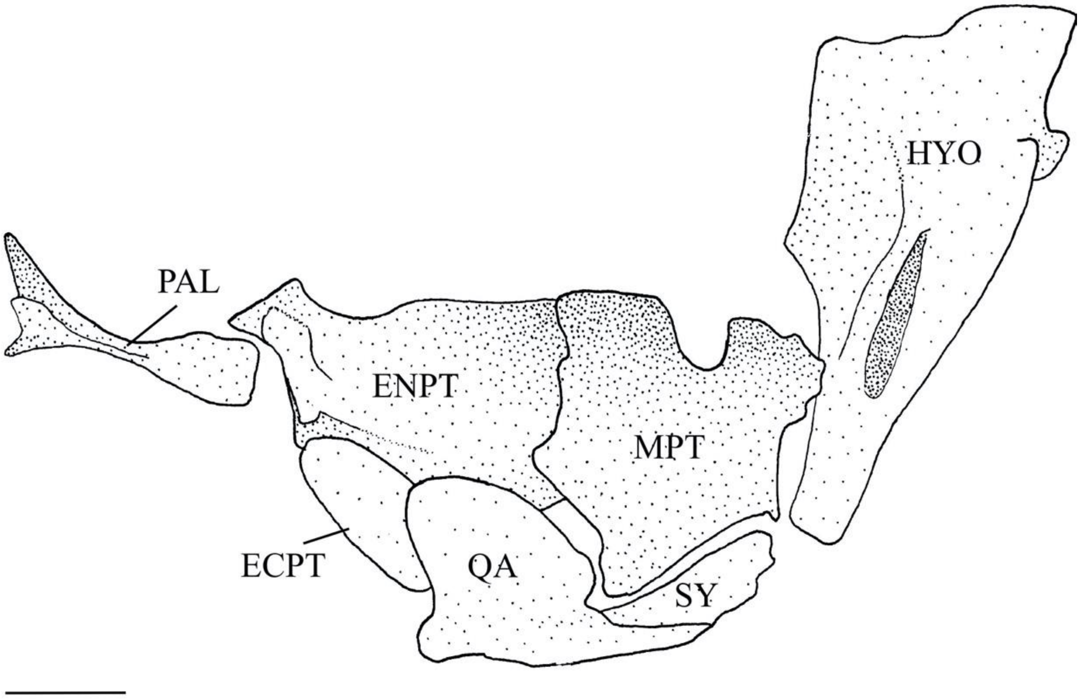

Figure 3.25. Illustration of the suspensorium of *Notropis blennius* UAMZ F.55621, specimen 1, in lateral view. Scale bar = 1 mm.

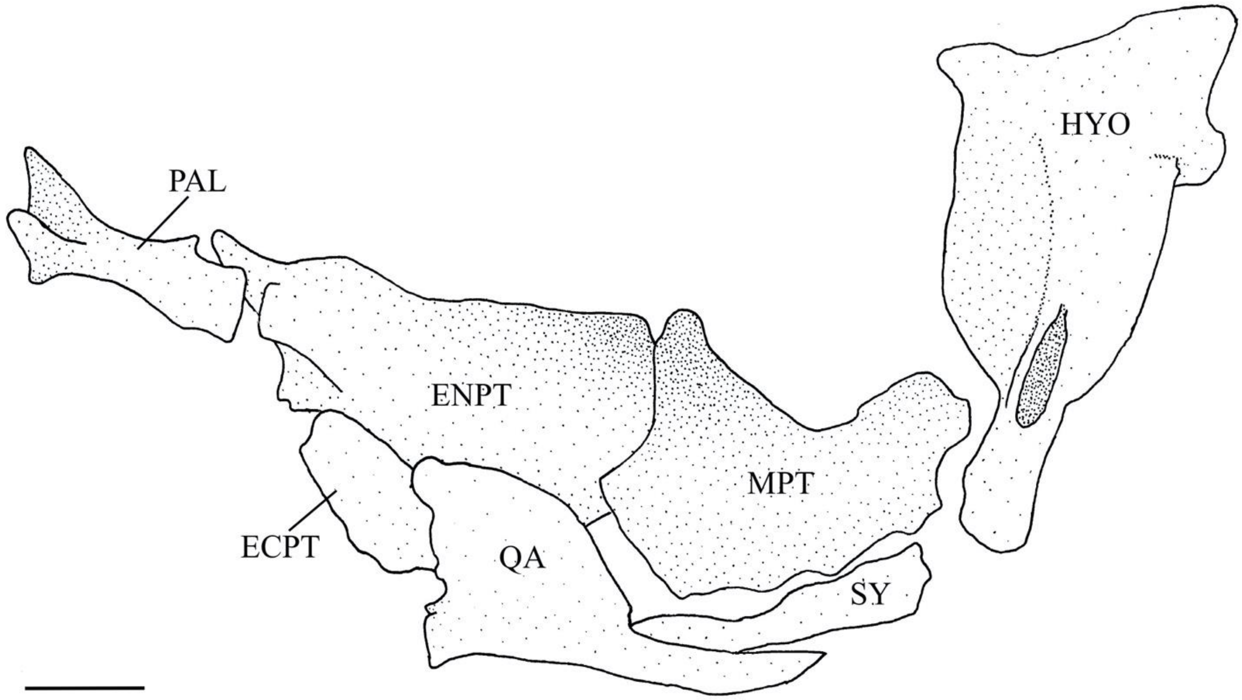

Figure 3.26. Illustration of the suspensorium of *Notropis buchanani* MZF 1606, specimen 3, in lateral view. Scale bar = 0.5 mm.

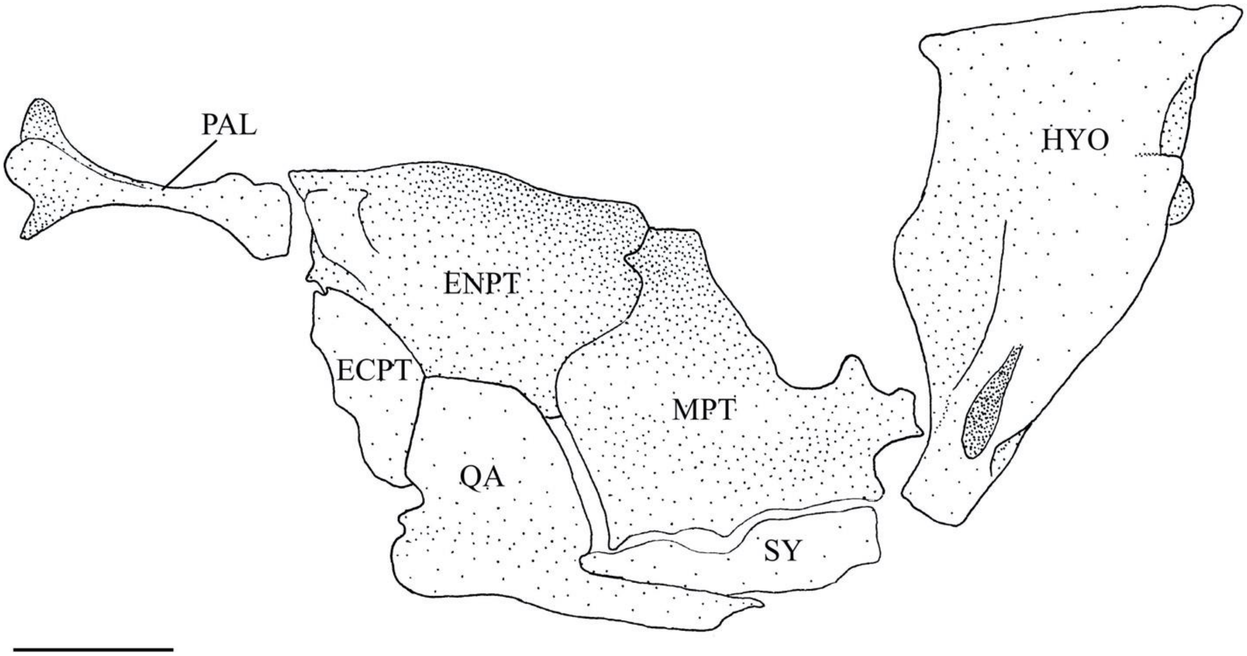

Figure 3.27. Illustration of the suspensorium of *Notropis dorsalis* MZF 649, specimen 2, in lateral view. Scale bar = 1 mm.

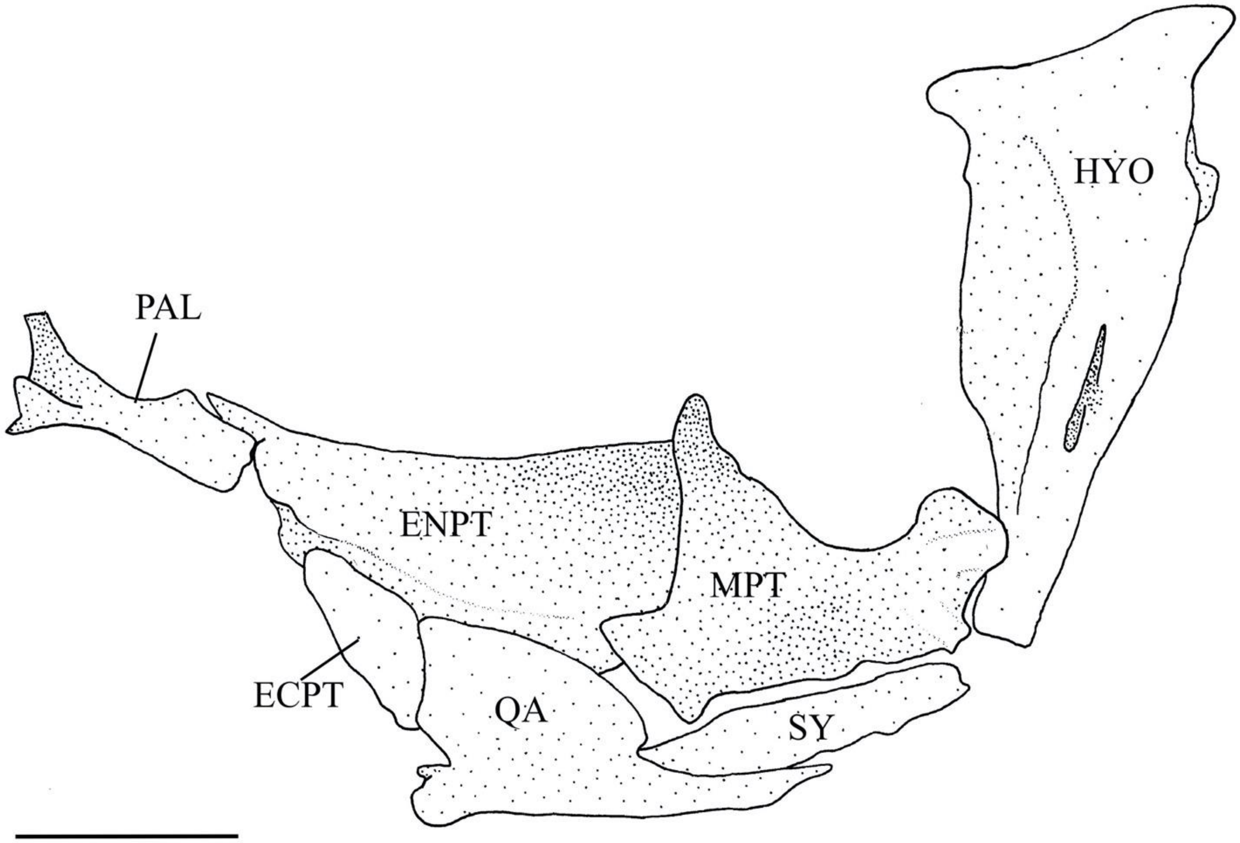

Figure 3.28. Illustration of the suspensorium of *Notropis heterodon* MZF 2027, specimen 3, in lateral view. Scale bar = 1 mm.

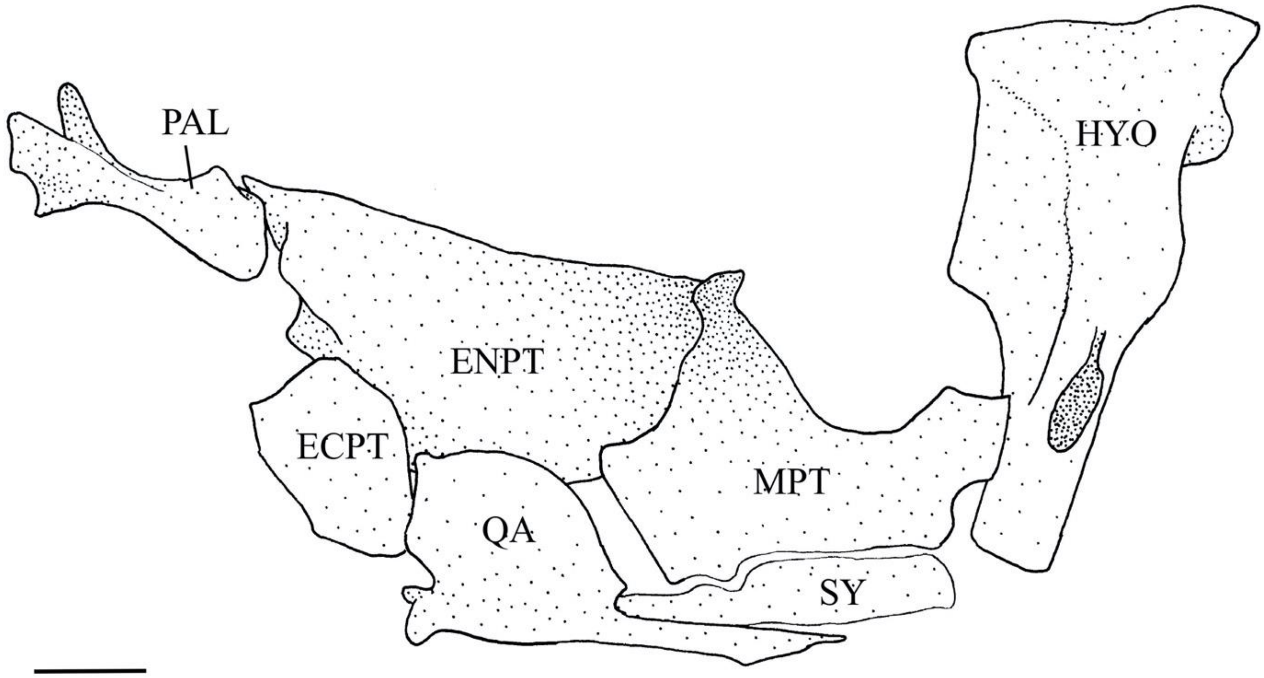

Figure 3.29. Illustration of the suspensorium of *Notropis heterolepis* MZF 685, specimen 1, in lateral view. Scale bar = 0.5 mm.

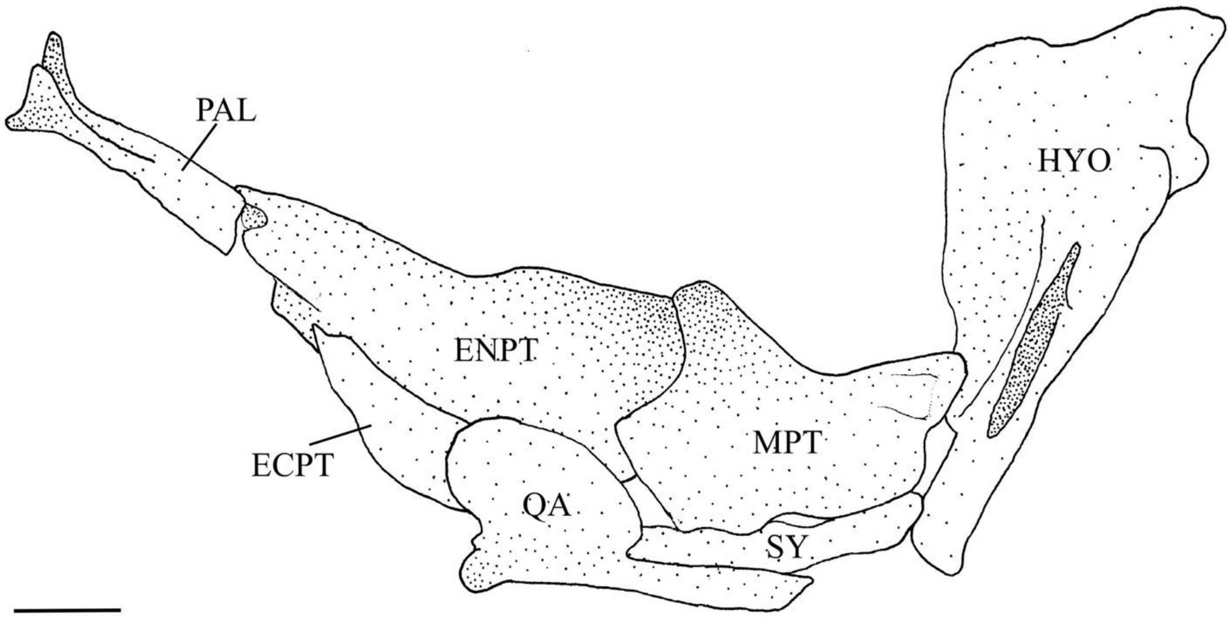

Figure 3.30. Illustration of the suspensorium of *Notropis percobromus* MZF 719, specimen 3, in lateral view. Scale bar = 0.5 mm.

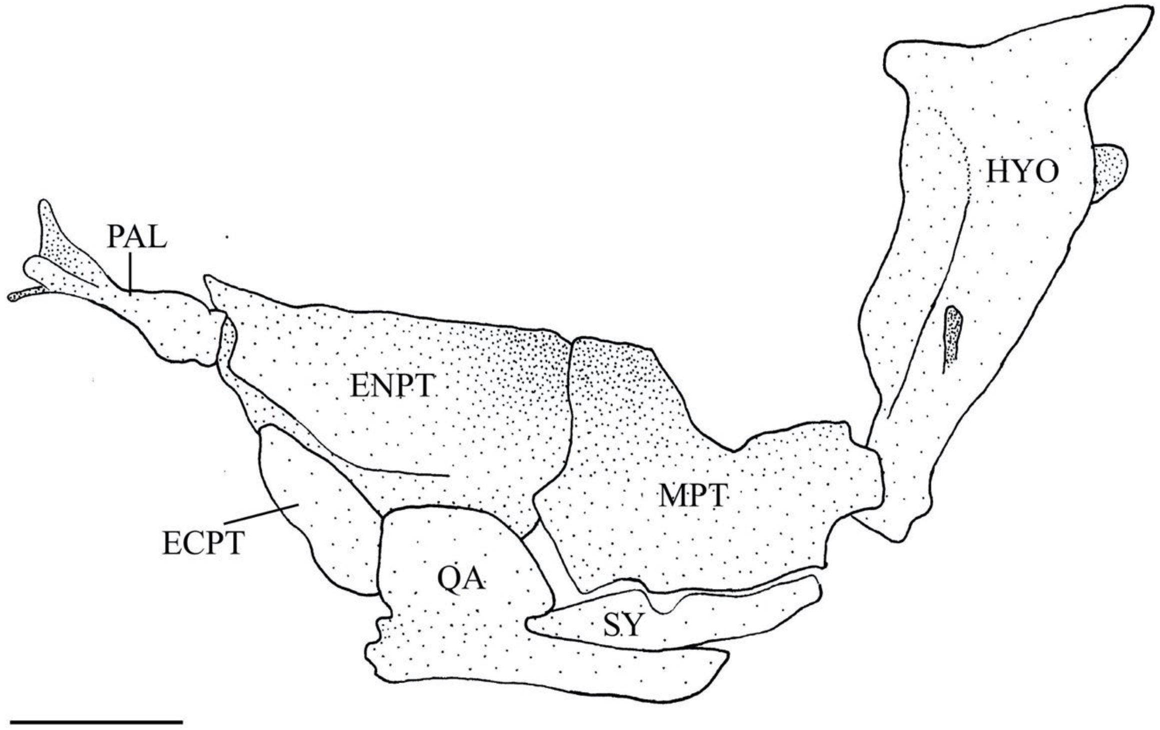

Figure 3.31. Illustration of the suspensorium of *Notropis stramineus* MZF 1540, specimen 3, in lateral view. Scale bar = 1 mm.

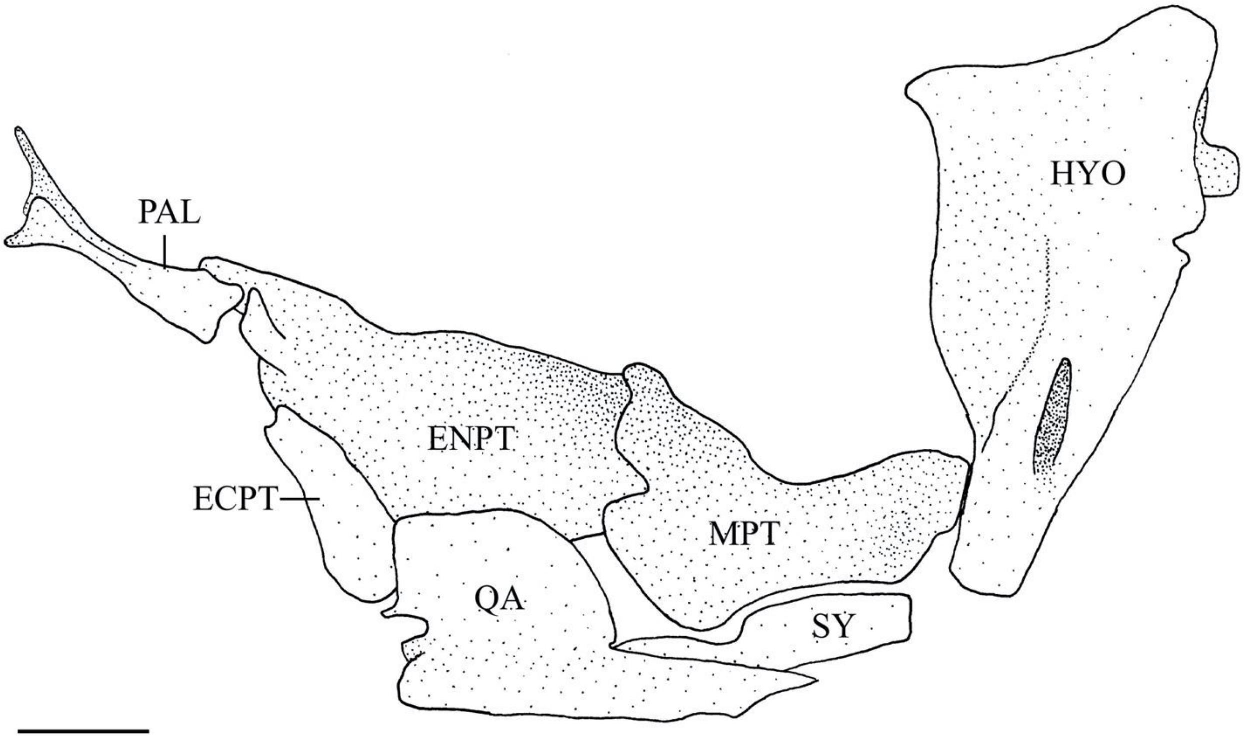

Figure 3.32. Illustration of the suspensorium of *Notropis texanus* MZF 1445, specimen 1, in lateral view. Scale bar = 0.5 mm.

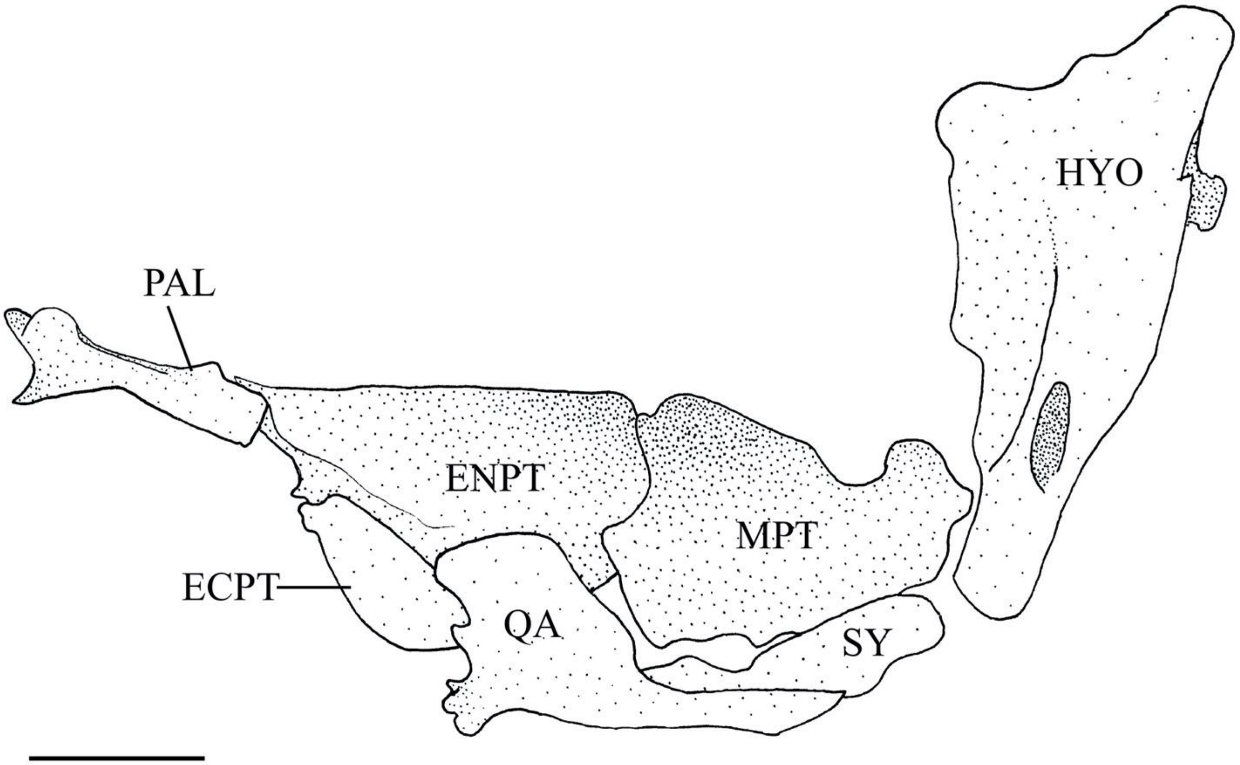

Figure 3.33. Illustration of the suspensorium of *Notropis volucellus* MZF 2036, specimen 1, in lateral view. Scale bar = 1 mm.

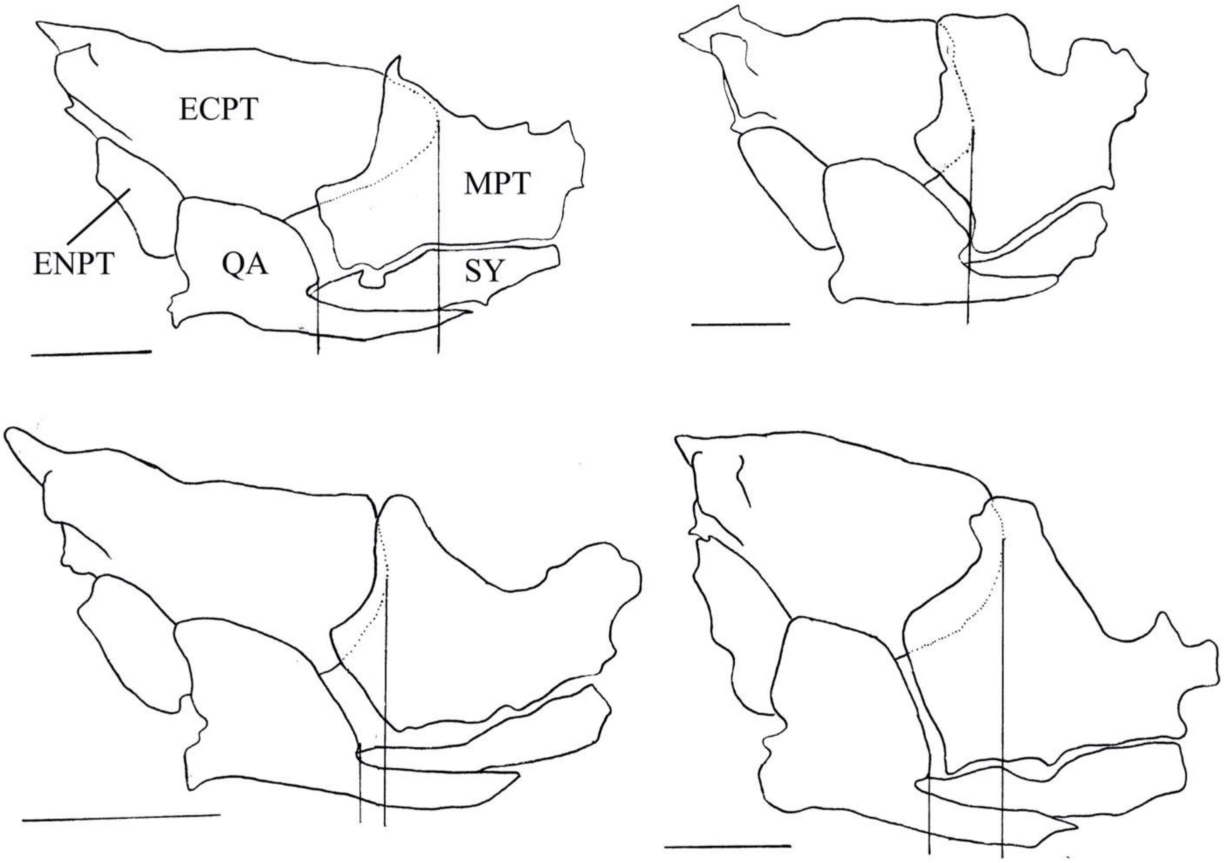

Figure 3.34. Illustration of the suspensorium of (a) *Notropis atherinoides* MZF 766, specimen 1, (b) *Notropis blennius* UAMZ F.55621, specimen 1, (c) *Notropis buchanani* MZF 1606, specimen 3, and (d) *Notropis dorsalis* MZF 649, specimen 2, in lateral view. Vertical lines show relative positions of the posterior end of the endopterygoid and posterior corner of the quadrate blade. Scale bars = 1 mm.

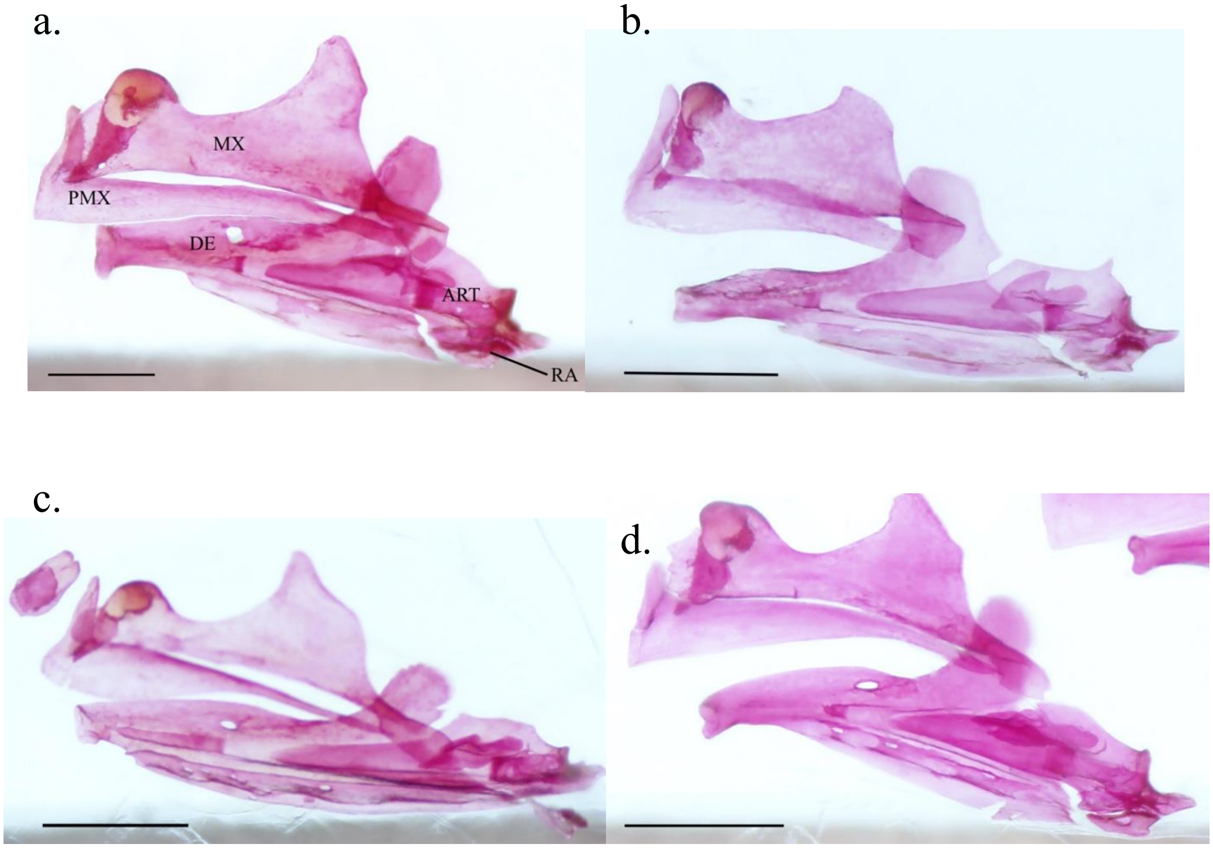

Figure 3.35. The Oral jaws of (a) *Notropis dorsalis* MZF 649, specimen 2, (b) *Notropis heterolepis* MZF 685, specimen 1, (c) *Notropis percobromus* MZF 719, specimen 3, and (d) *Notropis stramineus* MZF 1540, specimen 3, in lateral view, anterior to left. Scale bars = 1

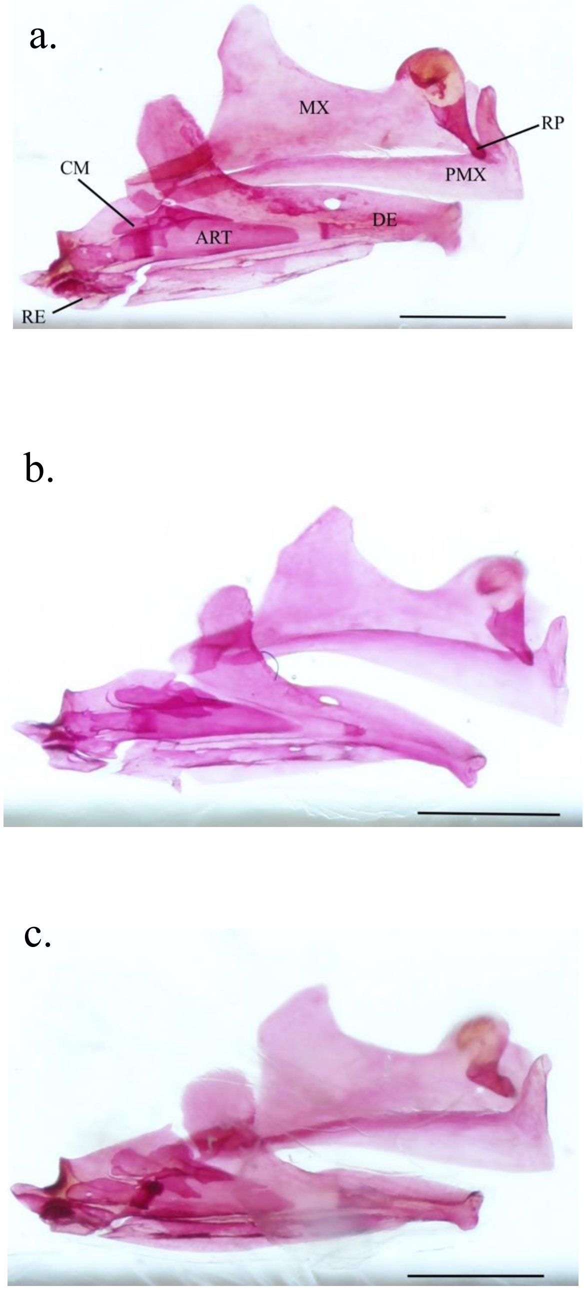

Figure 3.36. The oral jaws of (a) *Notropis dorsalis* MZF 649, specimen 2, (b) *Notropis stramineus* MZF 1540, specimen 3, and (c) *Notropis volucellus* MZF 2036, specimen 1, in medial view, anterior to right. Scale bar = 1 mm.

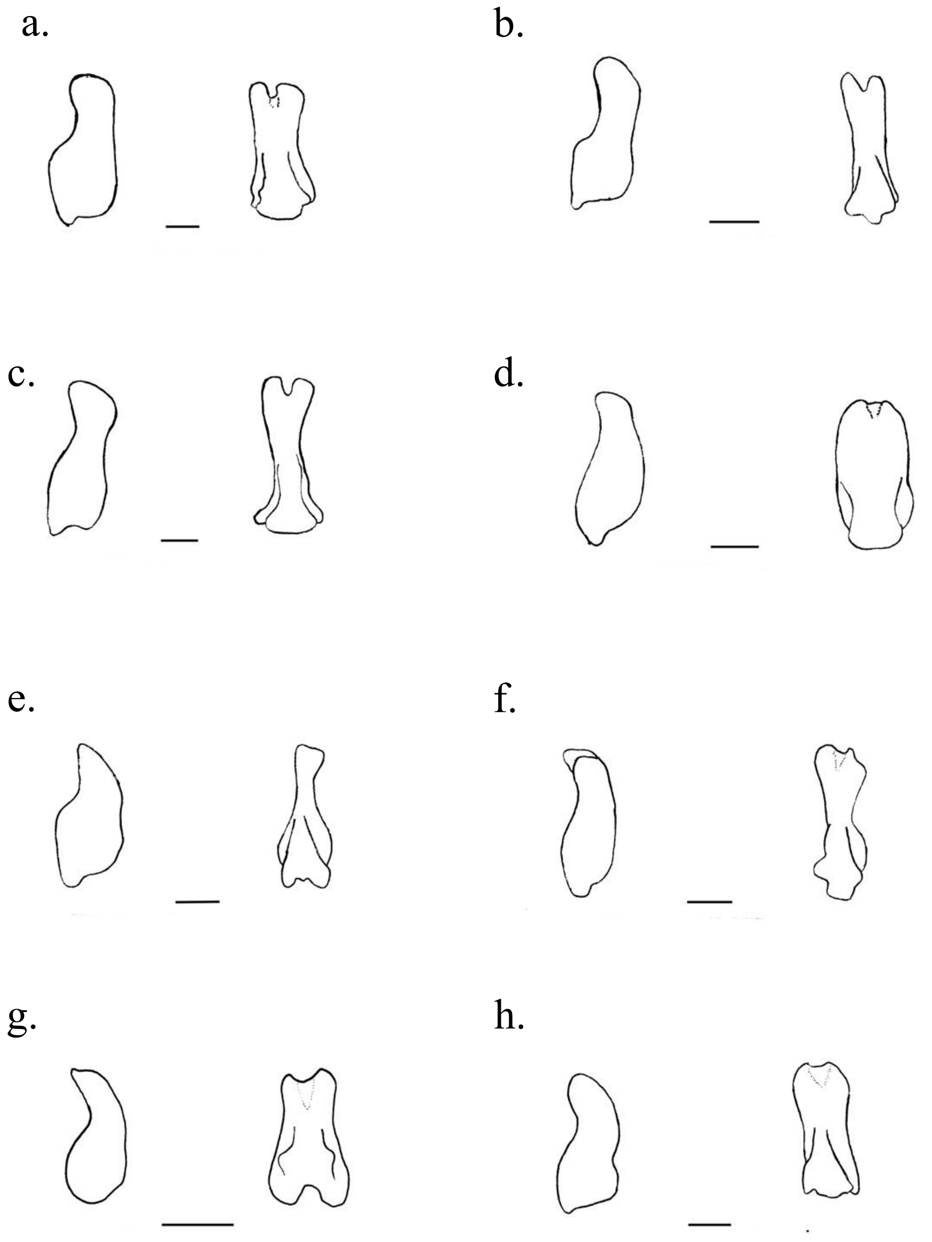

Figure 3.37. Illustration of the kinethmoid of (a) *Notropis blennius* UAMZ F.55621, specimen 1, (b) *Notropis buchanani* MZF 1606, specimen 3, (c) *Notropis dorsalis* MZF 649, specimen 2, (d) *Notropis heterodon* MZF 2027, specimen 3, (e) *Notropis heterolepis* MZF 685, specimen 1, (f) *Notropis stramineus* MZF 1540, specimen 3, (g) *Notropis texanus* MZF 1445, specimen 1, and (h) *Notropis volucellus* MZF 2036, specimen 1, in lateral (left) and anterior (right) view (dorsal region to top of the page) when the mouth is closed. Scale bar = 0.2 mm.

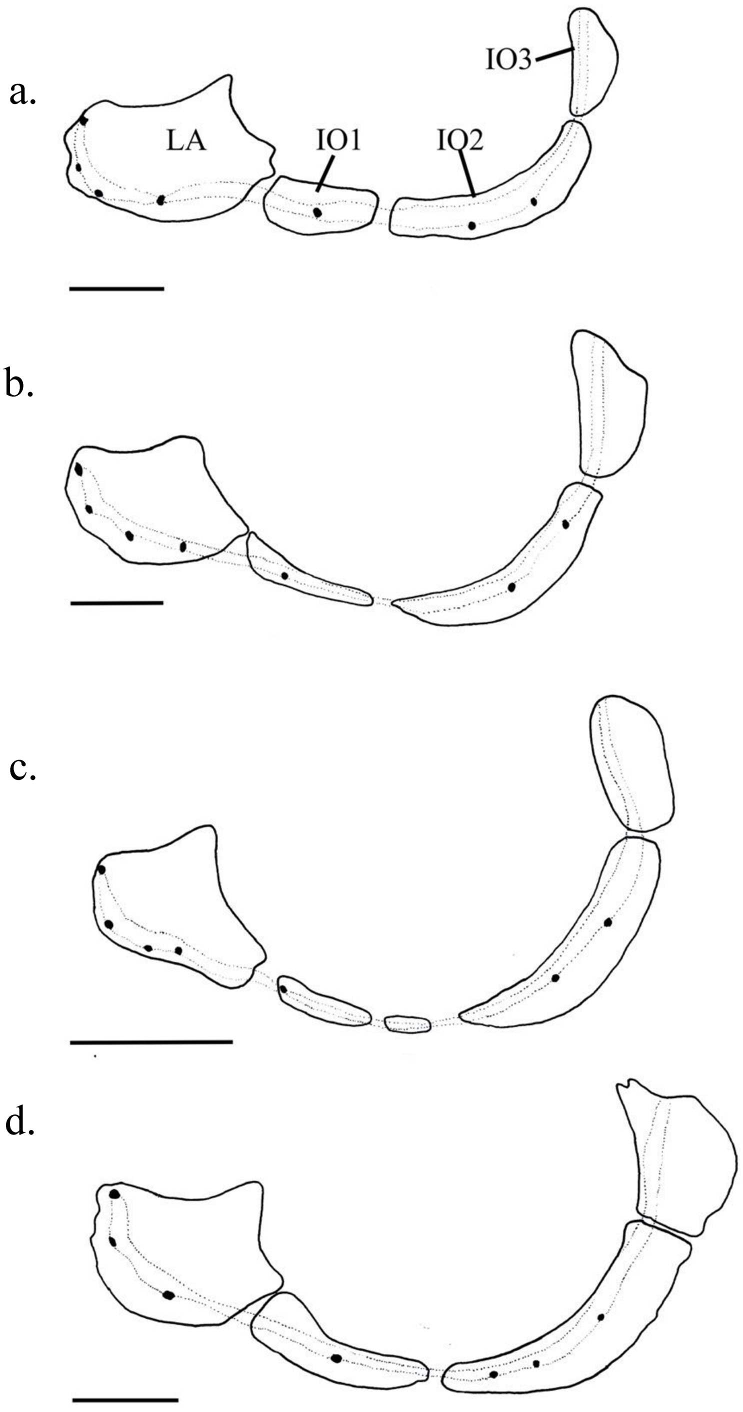

Figure 3.38. Outline of the infraorbital series of (a) *Notropis dorsalis* MZF 649, specimen 2, (b) *Notropis stramineus* MZF 1540, specimen 3, (c) *Notropis texanus* MZF 1445, specimen 2, and (d) *Notropis volucellus* MZF 2036, specimen 1, in lateral view, anterior to left. The dermosphenotic is not illustrated. Scale bar = 1 mm.

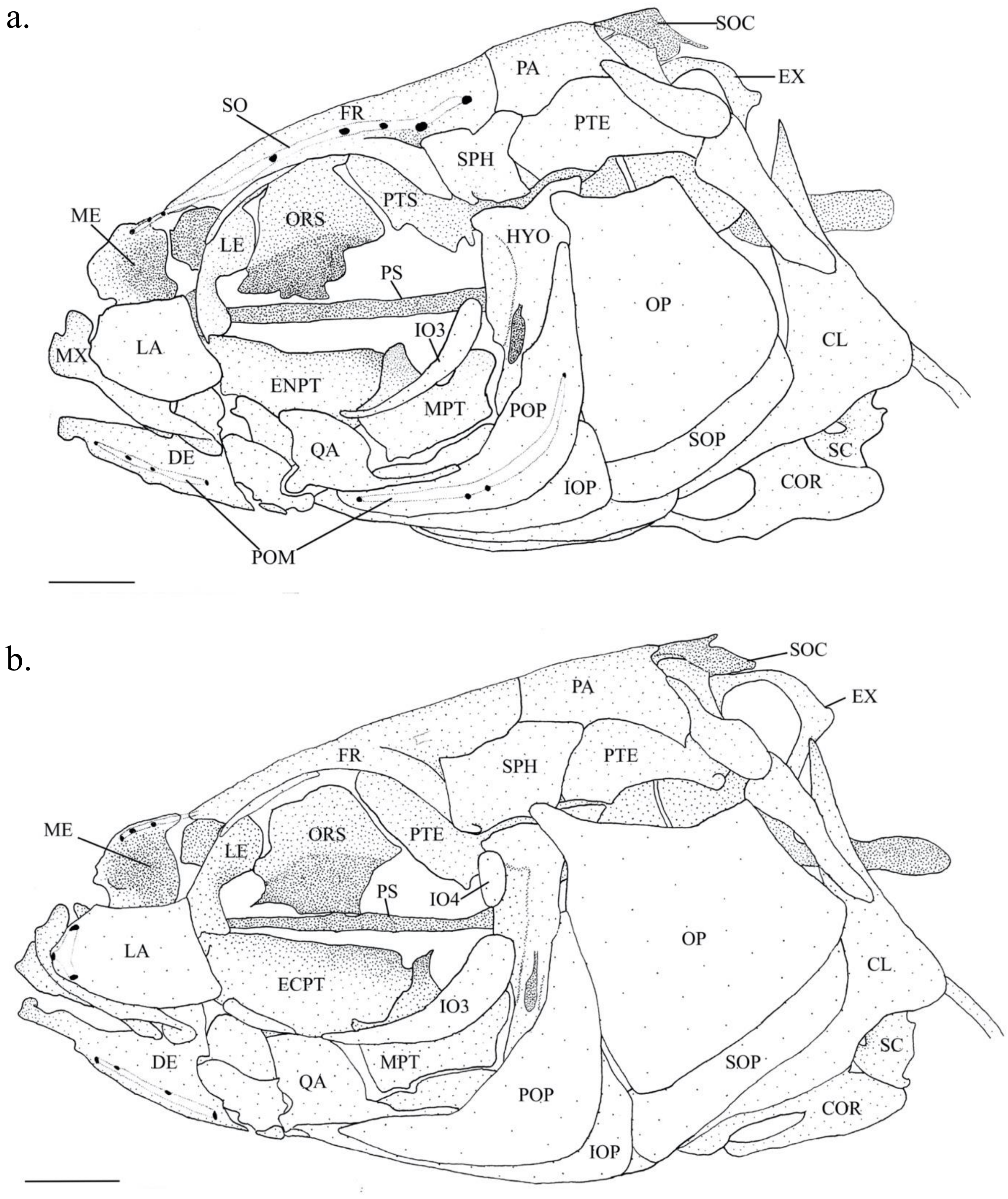

Figure 3.39. Illustrations of the skull and sensory canal system of (a) *Notropis buchanani* MZF 1606, specimen 3, and (b) *Notropis heterolepis* MZF 685, specimen 1, in lateral view, anterior to left. Scale bars = 1 mm.

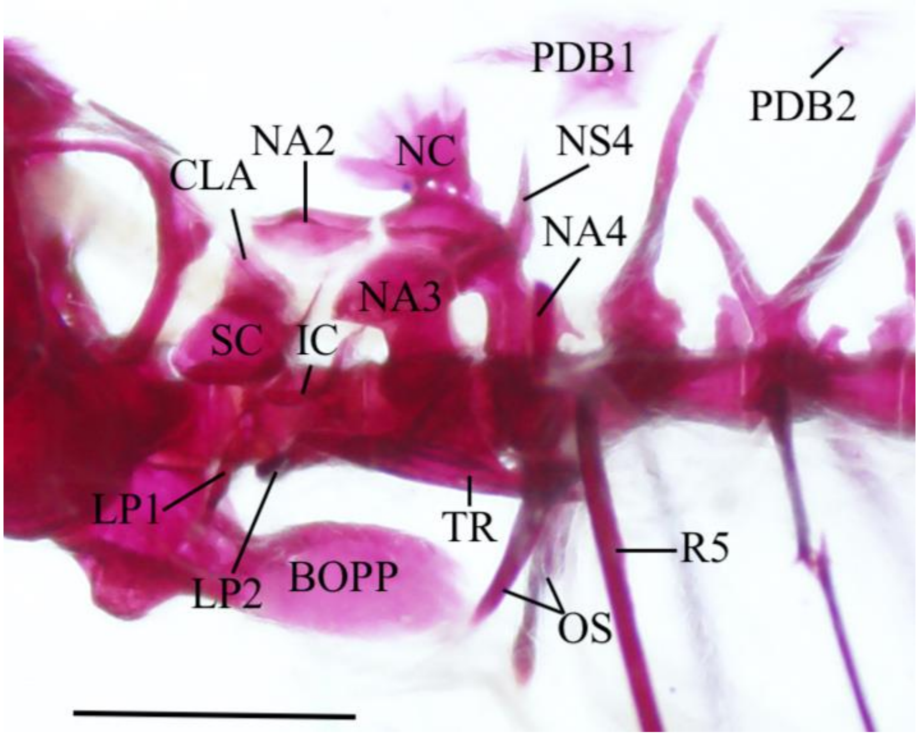

Figure 3.40. The Weberian apparatus of *Notropis texanus* MZF 1445, specimen 1, in lateral view, anterior to left. Scale bar = 1 mm.

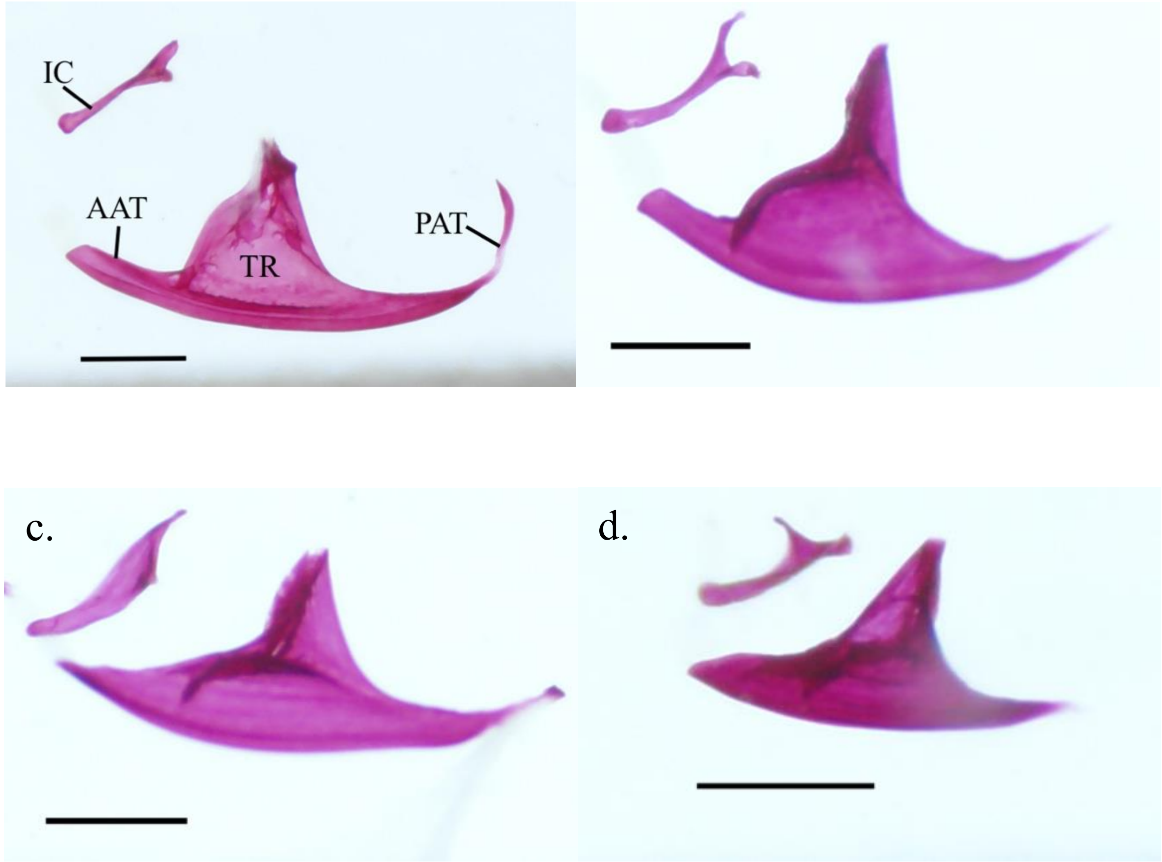

Figure 3.41. The tripus and intercalarium of (a) *Notropis dorsalis* MZF 649, specimen 2, (b) *Notropis heterodon* MZF 2027, specimen 3, (c) *Notropis stramineus* MZF 1540, specimen 3, and (d) *Notropis texanus* MZF 1445, specimen 1, in dorsal view, anterior to left. The posterior arm of (b) and (d) is broken off. Scale bars = 0.5.

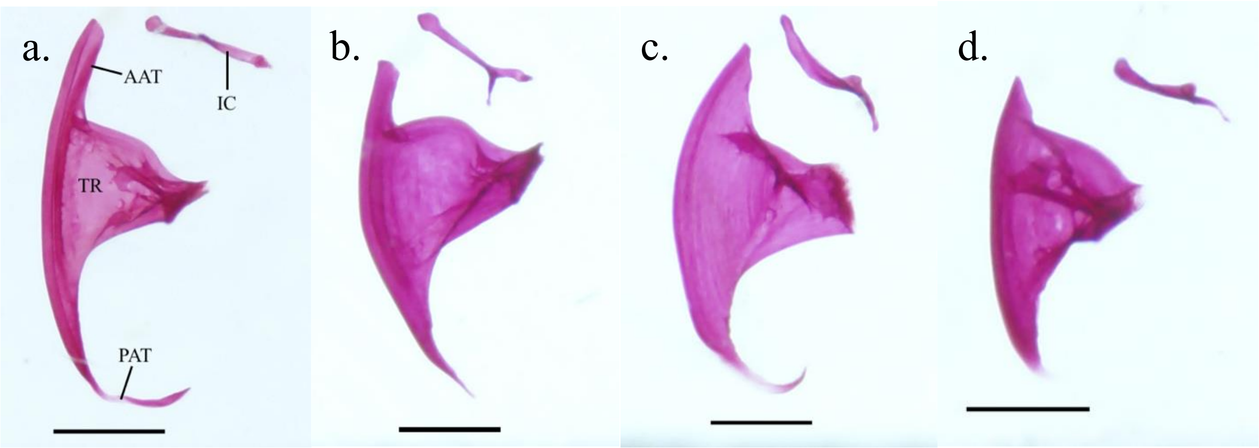

Figure 3.42. The tripus and intercalarium of (a) *Notropis dorsalis* MZF 649, specimen 2, (b) *Notropis heterodon* MZF 2027, specimen 3, (c) *Notropis stramineus* MZF 1540, specimen 3, and (d) *Notropis texanus* MZF 1445, specimen 1, in dorsal view, anterior to top of the posterior arm of (b) and (d) is broken off. Scale bars = 0.5 mm.

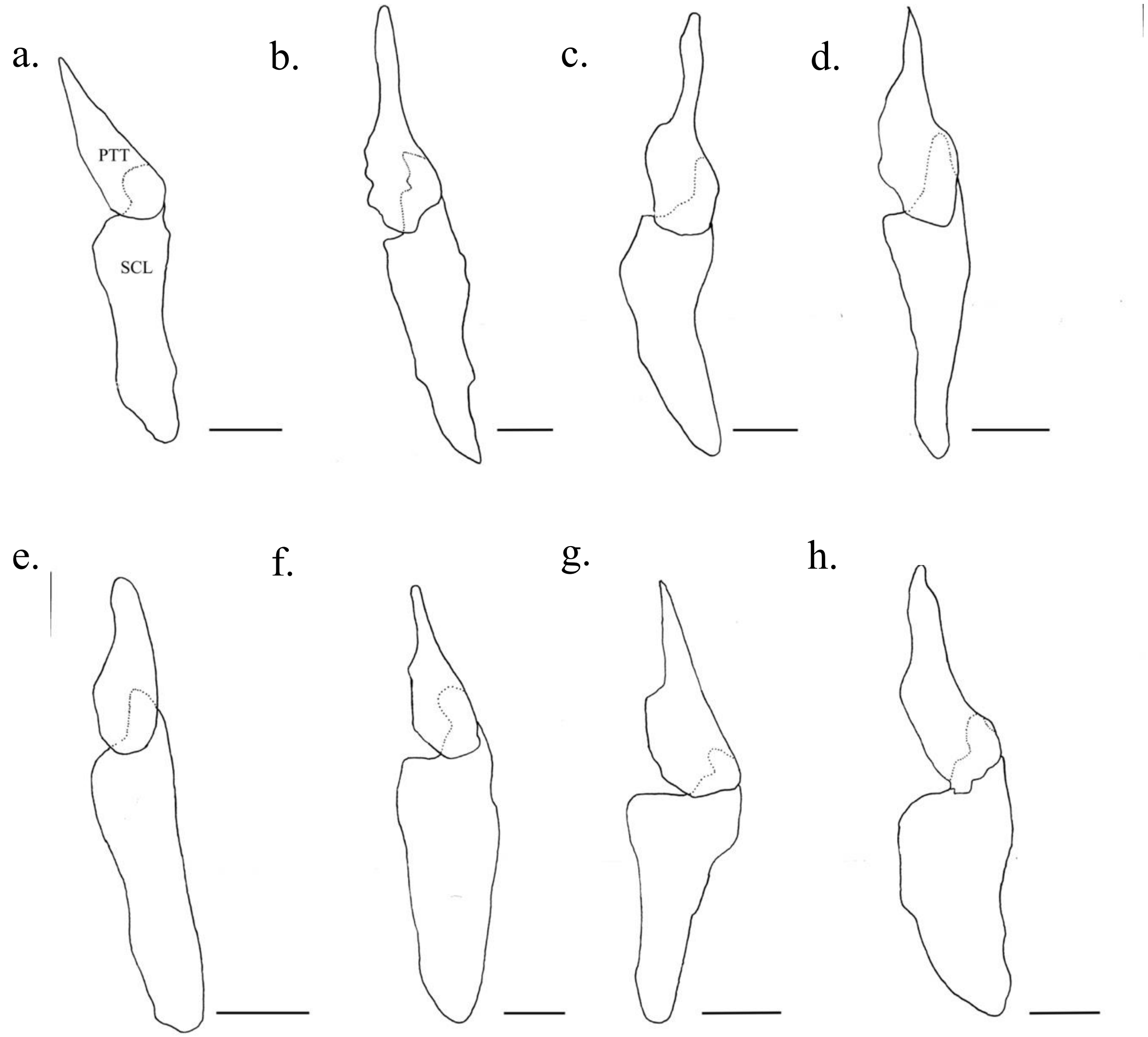

Figure 3.43. Illustration the of the posttemporal and supracleithrum of (a) *Notropis buchanani* MZF 1606, specimen 3, (b) *Notropis dorsalis* MZF 649, specimen 2, (c) *Notropis heterodon* MZF 2027, specimen 3, (d) *Notropis heterolepis* MZF 685, specimen 1, (e) *Notropis percobromus* MZF 719, specimen 3, (f) *Notropis stramineus* MZF 1540, specimen 3 (g) *Notropis texanus* MZF 1445, specimen 1, and (h) *Notropis volucellus* MZF 2036, specimen 1, in lateral view, dorsal to top. Scale bars = 1 mm.

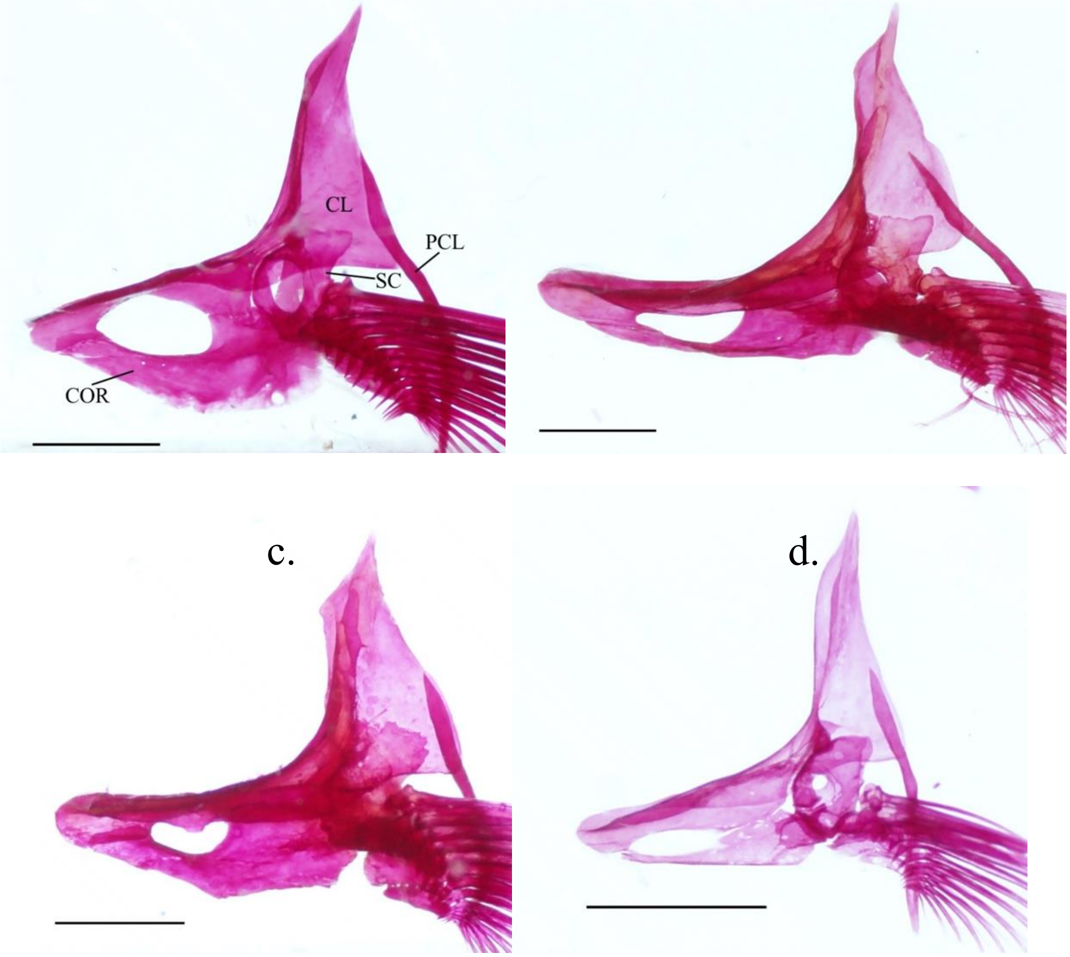

Figure 3.44. The pectoral girdle of (a) *Notropis atherinoides* MZF 766, specimen 1, (b) *Notropis dorsalis* MZF 649, specimen 2, (c) *Notropis heterodon* MZF 2027, specimen 3, and (d) *Notropis heterolepis* MZF 685, specimen 1, in lateral view. The posttemporal and supracleithrum have been removed. Scale bar = 1 mm.

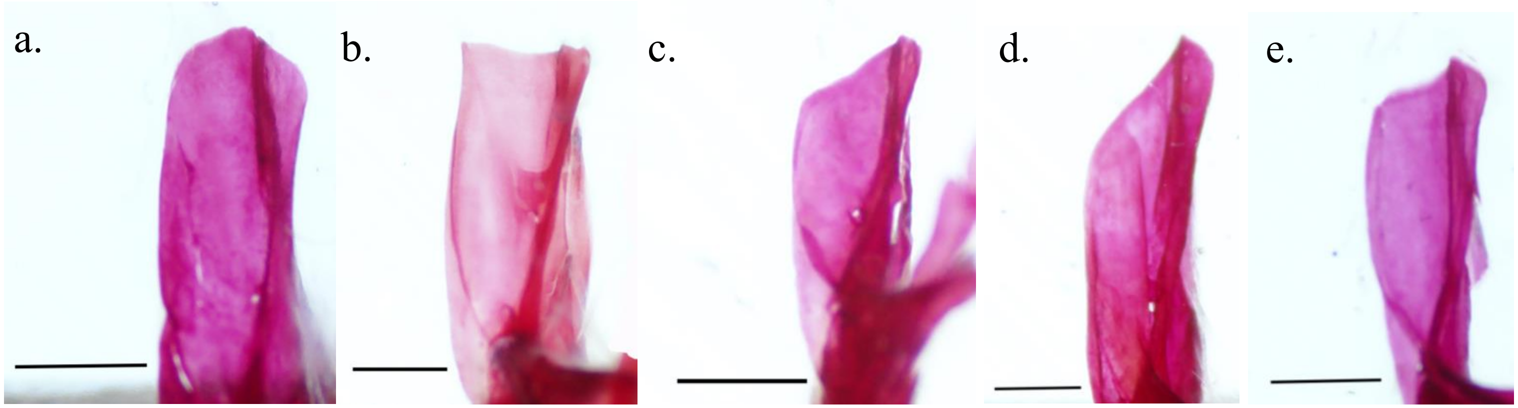

Figure 3.45. Dorsal view of the horizontal limb of the cleithrum of (a) *Notropis atherinoides* MZF 766, specimen 1, (b) *Notropis blennius* UAMZ F.55621, specimen 1, (c) *Notropis buchanani* MZF 1606, specimen 3, (d) *Notropis dorsalis* MZF 649, specimen 2, and (e) *Notropis stramineus* MZF 1540, specimen 3, anterior to top of the page. Scale bars = 1 mm.

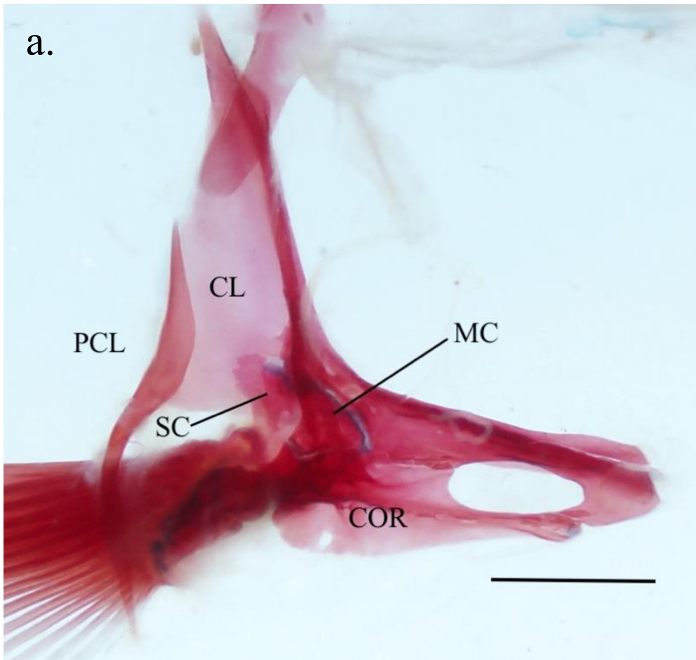

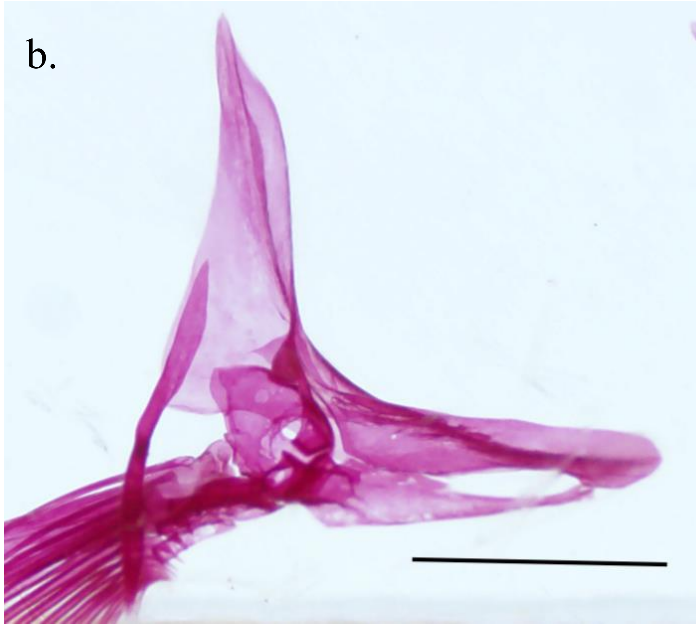

Figure 3.46. The pectoral girdle of (a) *Notropis blennius* UAMZ F.55621, specimen 1, and (b) *Notropis heterolepis* MZF 685, specimen 1, in lateral view. Scale bar = 1 mm.

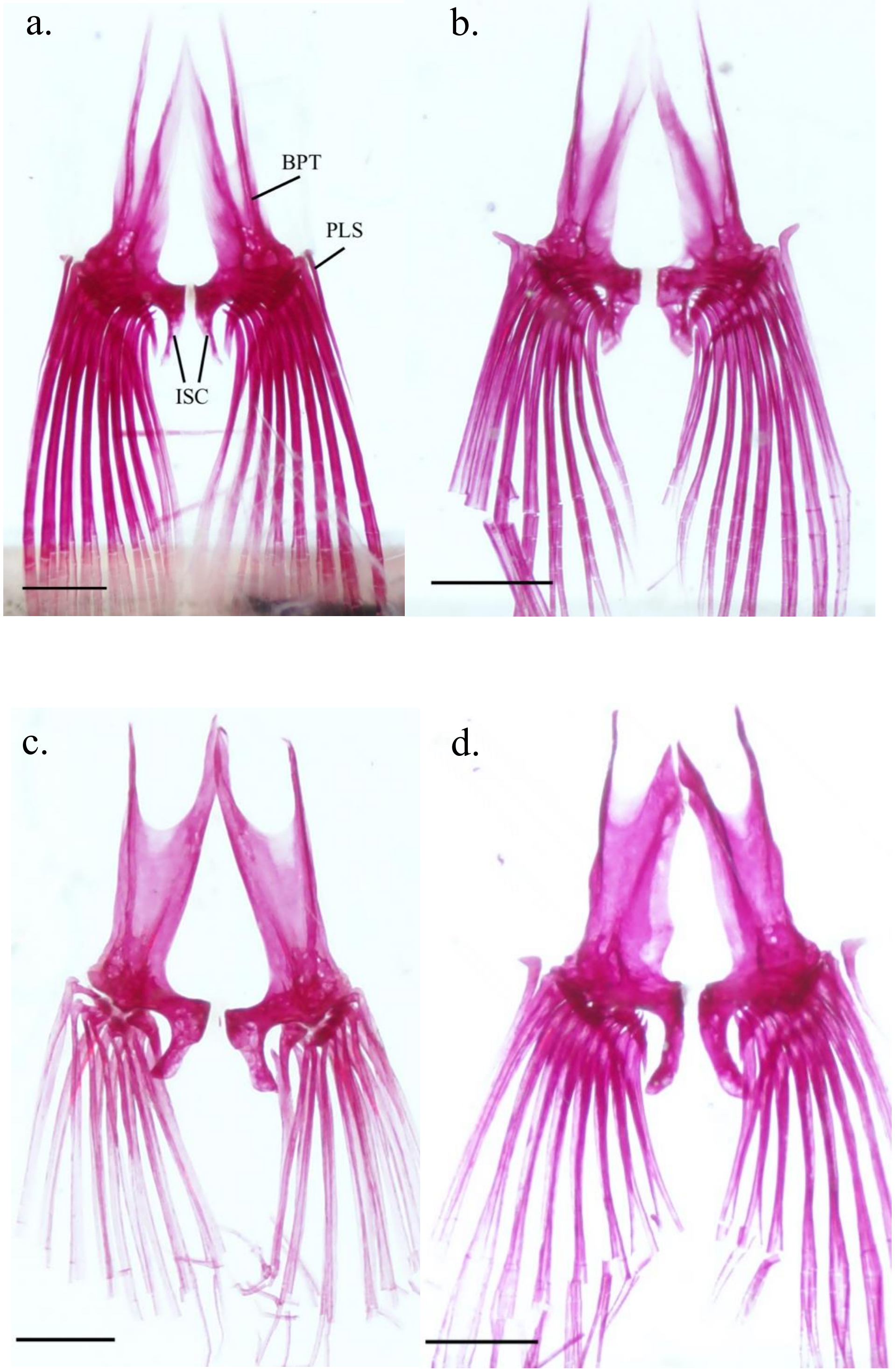

Figure 3.47. The pelvic girdle of (a) *Notropis atherinoides* MZF 766, specimen 1, (b) *Notropis buchanani* MZF 1606, specimen 3, (c) *Notropis dorsalis* MZF 649, specimen 2, and (d) *Notropis heterodon* MZF 2027, specimen 3, in dorsal view, anterior to top of the page. Scale bars = 1 mm.

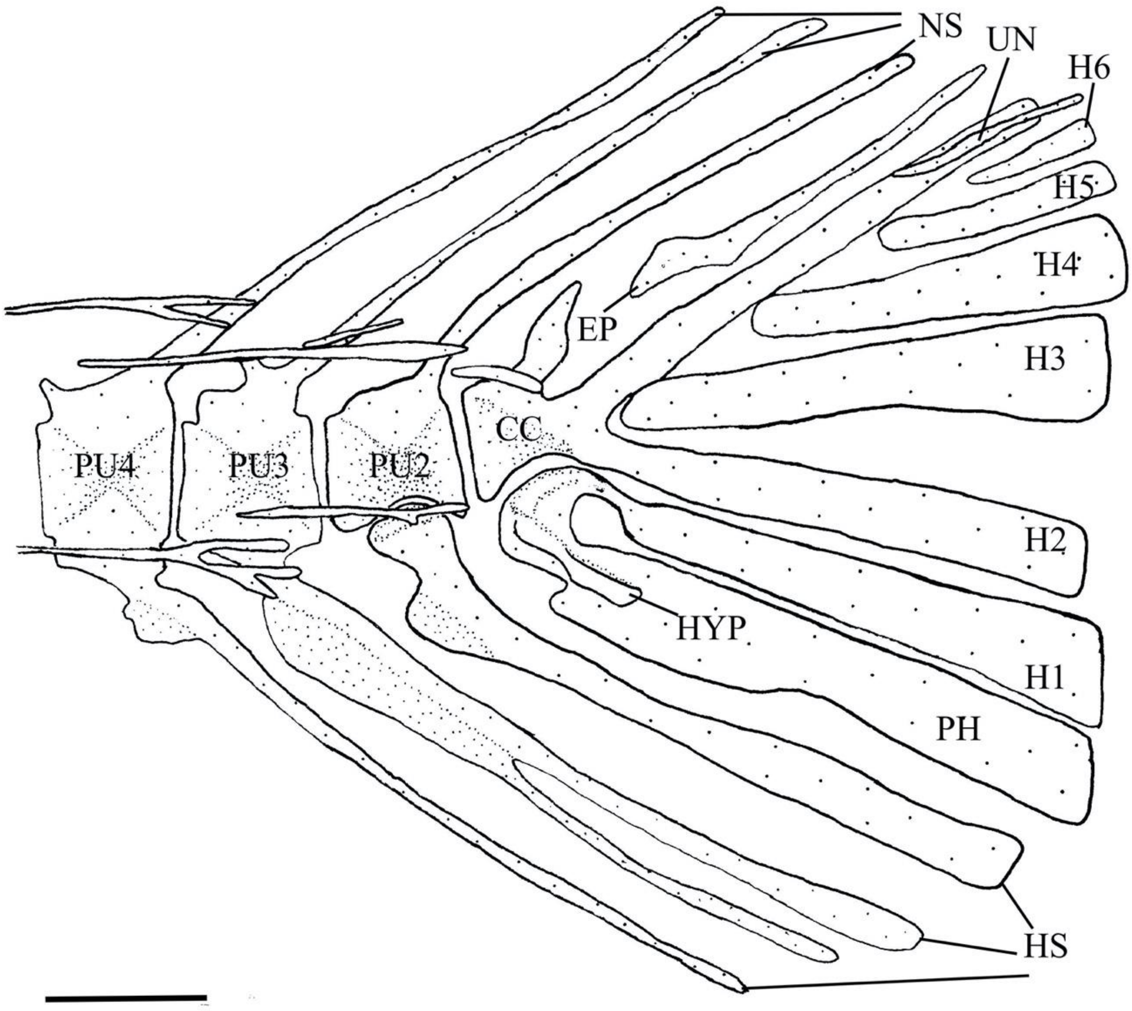

Figure 3.48. Illustration of the caudal skeleton of *Notropis buchanani* MZF 1606, specimen 3, in left lateral view, anterior to left. Scale bar = 0.5 mm.

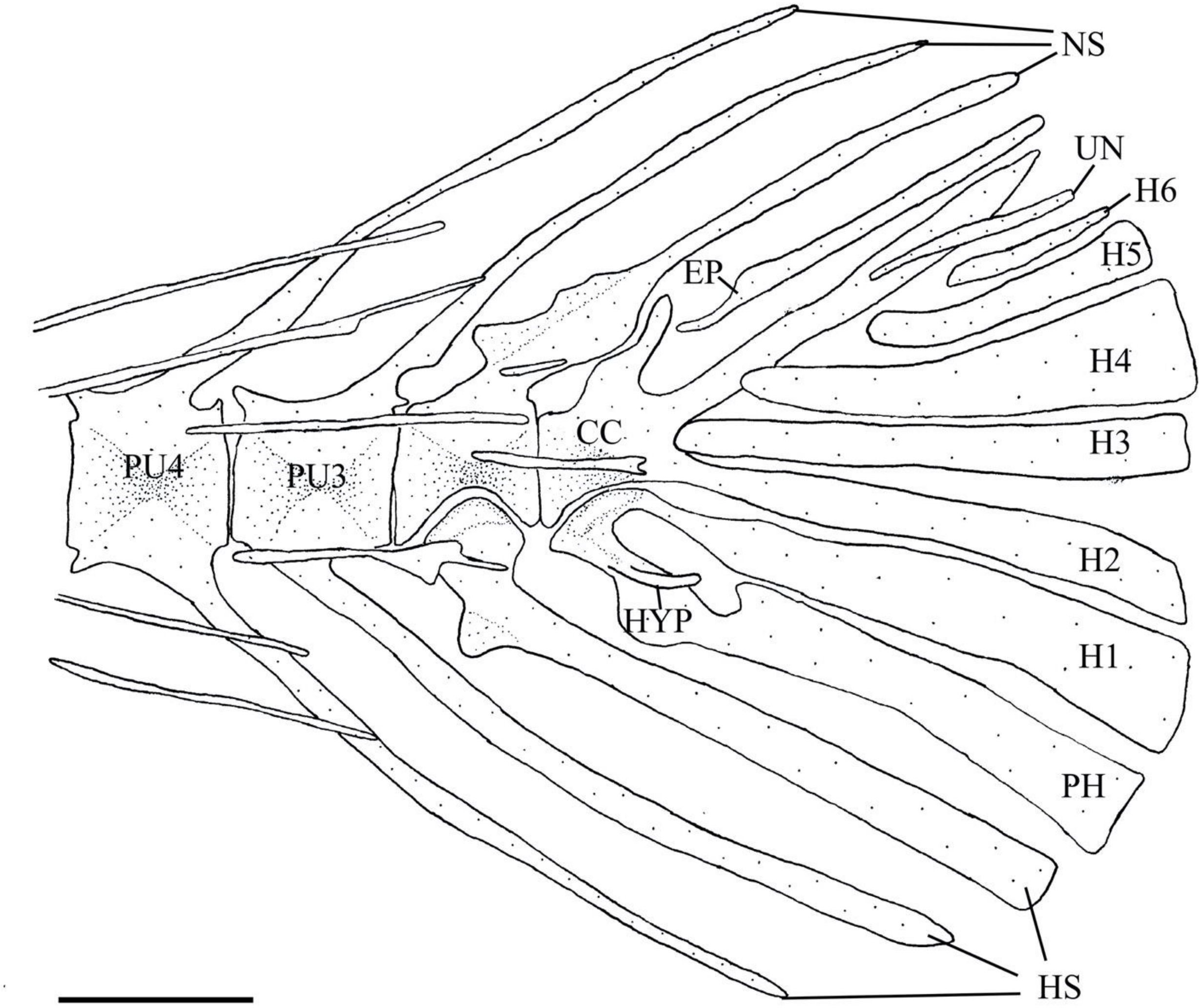

Figure 3.49. Illustration of the caudal skeleton *of Notropis dorsalis* MZF 649, specimen 2, in left lateral view, anterior to left. Scale bar = 1 mm.

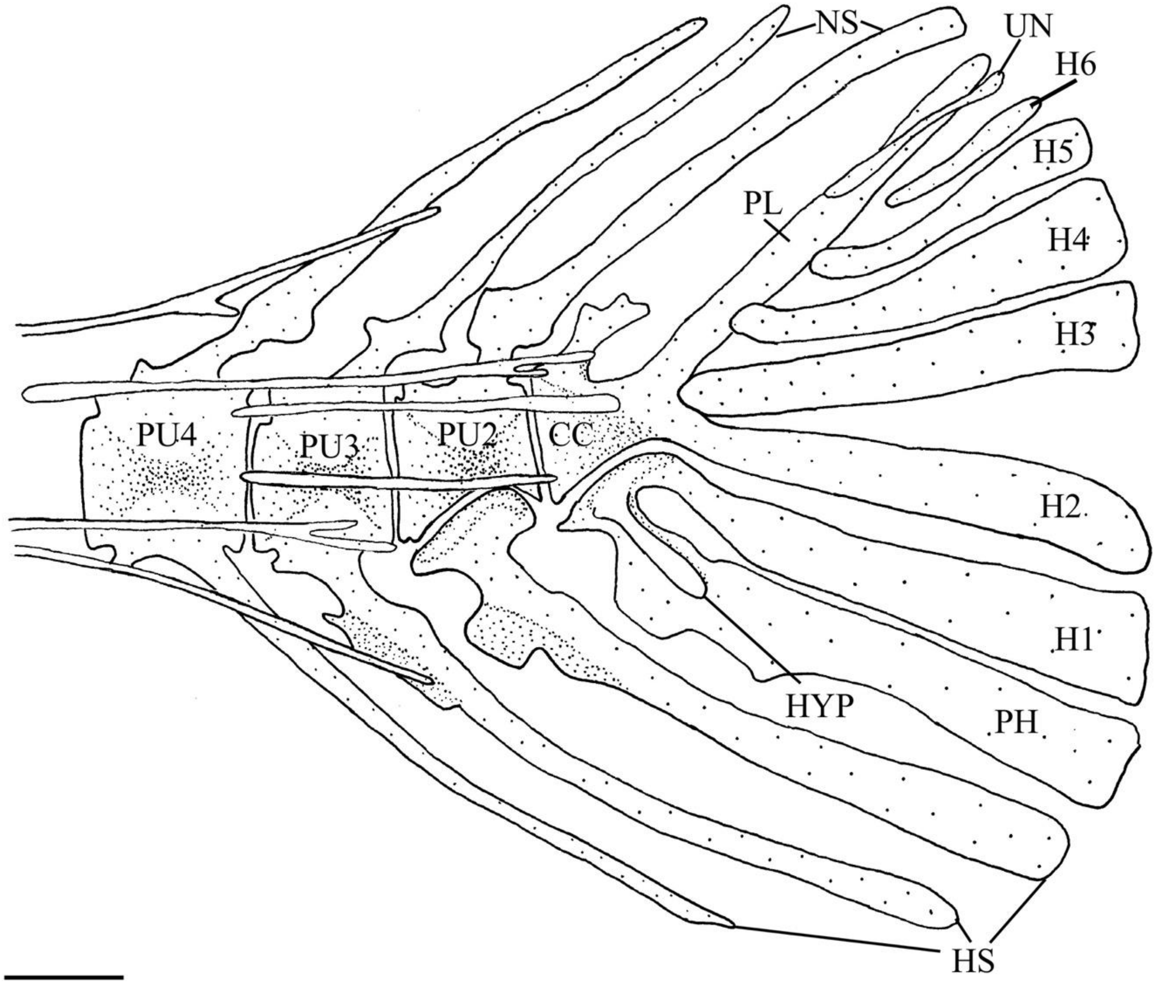

Figure 3.50. Illustration of the caudal skeleton of *Notropis heterodon* MZF 2027, specimen 3, in left lateral view, anterior to left. Scale bar = 0.5 mm.

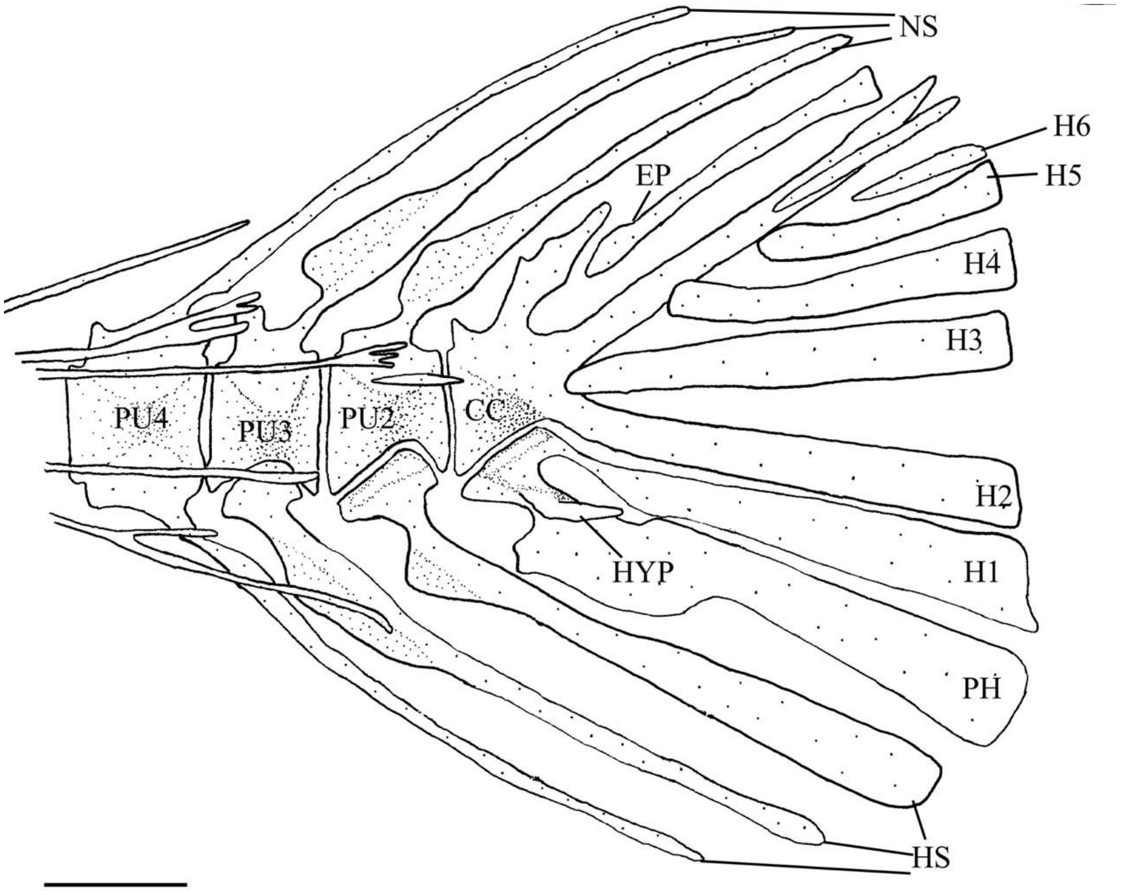

Figure 3.51.Illustration of the caudal skeleton of *Notropis percobromus* MZF 719, specimen 3, in left lateral view, anterior to left. Scale bar = 0.5 mm.

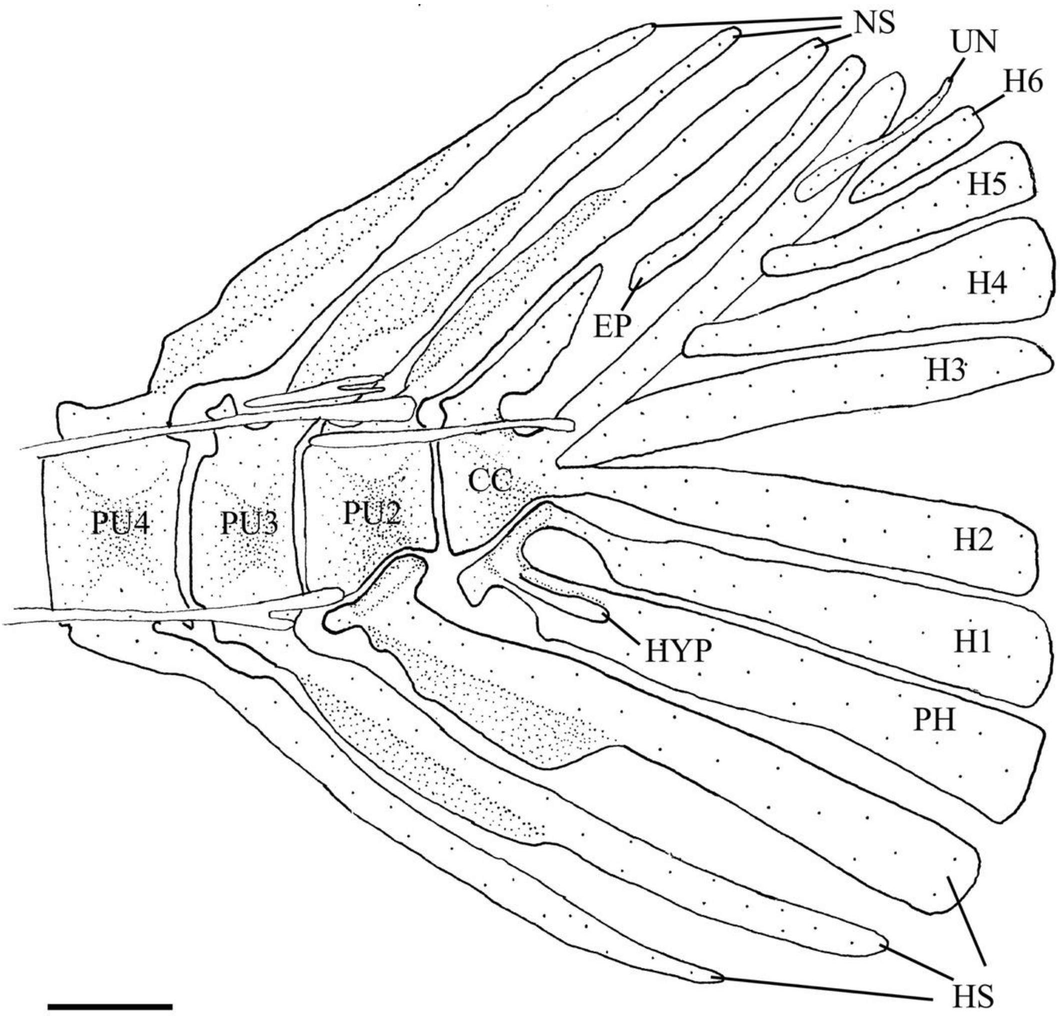

Figure 3.52. Illustration of the caudal skeleton of *Notropis stramineus* MZF 1540, specimen 3, in left lateral view, anterior to left. Scale bar = 0.5 mm.

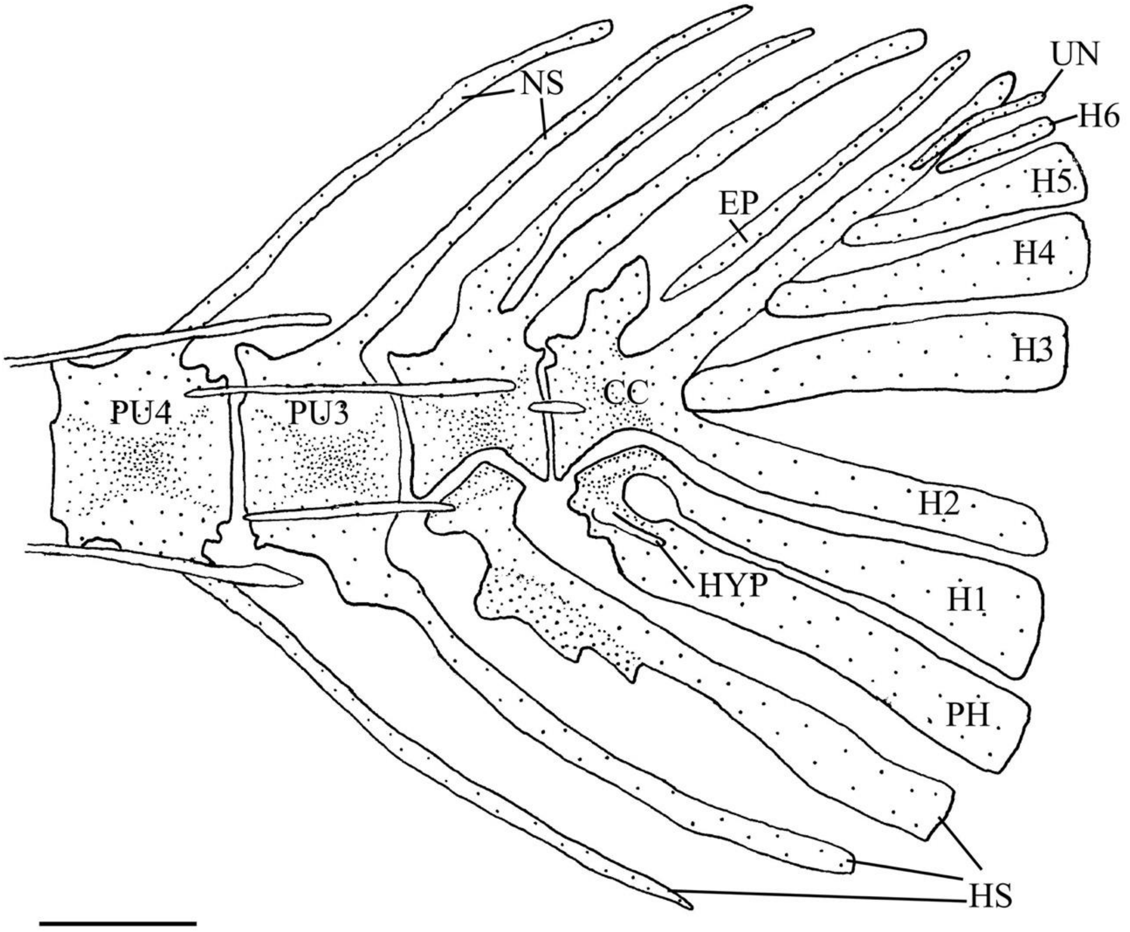

Figure 3.53. Illustration of the caudal skeleton of *Notropis texanus* MZF 1445, specimen 1, in left lateral view, anterior to left. Scale bar = 0.5 mm.

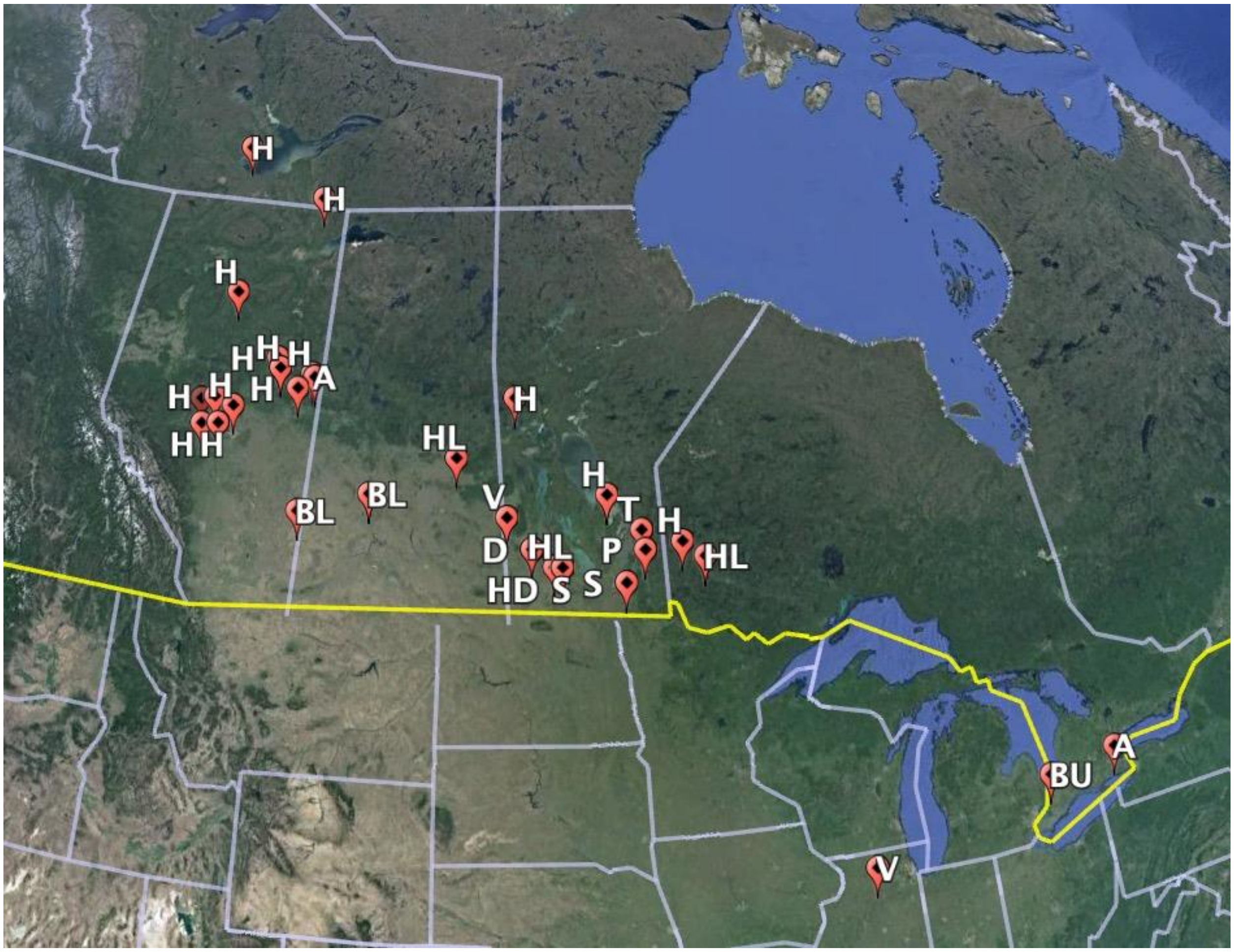

Figure 3.54. Distribution of (A) *Notropis atherinoides,* (BL) *Notropis blennius*, (BU) *Notropis buchanani*, (D) *Notropis dorsalis*, (HD) *Notropis heterodon*, (HL) *Notropis heterolepis*, (H) *Hotropis hudsonius*, (P) *Notropis percobromus*, (S) *Notropis stramineus*, (T) *Notropis texanus* and (V) *Notropis volucellus* specimens examined.

3.7 Literature cited

Agassiz, L. 1854. Notice of a collection of fishes from the southern bend of the Tennessee River, in the State of Alabama. American Journal of Science and Arts 17:297–308, 353–365.

Armbruster, J. W. 2012. Standardized measurements, landmarks, and meristic counts for cypriniform fishes. Zootaxa 3586.

Bielawski, J. P., and J. R. Gold. 2001. Phylogenetic relationships of cyprinid fishes in subgenus *Notropis* inferred from nucleotide sequences of the mitochondrially encoded cytochrome b gene. Copeia 2001:656–667.

Buhan, P. J. 1970. The comparative osteology and taxonomy of the North American cyprinid genera, *Richardsonius Ctinostomus* and *Semotilus*, with notes on other minnows. PhD dissertation, Virginia Polytechnic Institute, 332 pp.

Buhan, P. J. 1972. The comparative osteology of the caudal skeleton of some North American minnows (Cyprinidae). American Midland Naturalist 88:484–490.

Cavender, T. M., and M. M. Coburn. 1992. Interrelationships of North American Cyprinid Fishes; pp. 328–373 in Systematics, historical ecology, and North American freshwater fishes. Stanford University Press, Stanford, California.

Chernoff, B., and R. R. Miller. 1981. Systematics and variation of the aztec shiner, *Notropis sallei*, a cyprinid fish from central Mexico. Proceedings of the Biological Society of Washington 94:18–36.

Clinton, D. 1824. Description of a new species of fish, from the Hudson River. Annals of the Lyceum of Natural History of New York 1:49–50.

Coburn, M. M. 1982. Anatomy and relationships of *Notropis atherinoides*. PhD dissertation, Ohio State University, 384 pp.

Coburn, M. M., and T. M. Cavender. 1992. Phylogenetic relationships of North American Cyprinidae; pp. 328–373 in Systematics, historical ecology, and North American freshwater fishes. Stanford University Press, Stanford, California.

Conway, K. W. 2011. Osteology of the South Asian Genus Psilorhynchus McClelland, 1839 (Teleostei: Ostariophysi: Psilorhynchidae), with investigation of its phylogenetic relationships within the order Cypriniformes: Zoological Journal of the Linnean Society 163:50–154.

Cope, E. D. 1865. Partial catalogue of the cold-blooded Vertebrata of Michigan. Pt. I. Proceedings of the Academy of Natural Sciences of Philadelphia 16:276–285.

Cope, E. D. 1871. Recent reptiles and fishes. Report on the reptiles and fishes obtained by the naturalists of the expedition; pp. 432–442 in Preliminary report of the United States Geological Survey of Wyoming and portions of contiguous territories. vol. 4. Government Printing Office, Washington D.C.

Eastman, J. T., and J. C. Underhill. 1973. Intraspecific variation in the pharyngeal tooth formulae of some cyprinid fishes. Copeia 1973:45–53.

Eigenmann, C. H., and R. S. Eigenmann. 1893. Preliminary descriptions of new fishes from the northwest. American Naturalist 27:151–154.

Fink, S. V., and W. L. Fink. 1981. Interrelationships of the ostariophysan fishes (Teleostei). Zoological Journal of the Linnean Society 72:297–353.

Fowler, H. W. 1904. Notes on fishes from Arkansas, Indian Territory and Texas. Proceedings of the Academy of Natural Sciences of Philadelphia 56:242–249.

Fowler, H. W. 1935. Notes on South Carolina fresh-water fishes. Contributions from the Charleston Museum 7:1–28.

Froese, R., and D. Pauly. 2023. FishBase.World Wide Web electronic publication. Available at www.fishbase.org. Accessed April 21, 2024.

Gilbert, C. H. 1884. Notes on the fishes from Kansas. Bulletin of the Washburn Laboratory of Natural History 1:10–16.

Girard, C. F. 1856. Research upon the cyprinoid fishes inhabiting the fresh waters of the United States, west of the Mississippi Valley, from specimens in the museum of the Smithsonian Institution. Proceedings of the Academy of Natural Sciences of Philadelphia 2:165–213.

Günther, A. 1868. Catalogue of the Physostomi, containing the families Heteropygii, Cyprinidæ, Gonorhynchiidæ, Hypodontidæ, Osteoglossidæ, Clupeidæ, Chirocentridæ, Alepochephalidæ, Notopteridæ, Halosauridæ, in the collection of the British Museum. Catalogue of the Fishes in the British Museum 7:1–512.

Habib, S. S., S. Naz, and R. Mehmood. 2019. Morphometric relationships of some specified species of family cyprinidae in Jinnah barrage Punjab, Pakistan. Journal of Entomology and Zoology Studies 7:155–159.

Hollingsworth, P. R., A. M. Simons, J. A. Fordyce, and C. D. Hulsey. 2013. Explosive diversification following a benthic to pelagic shift in freshwater fishes. BMC Evolutionary Biology 13:272.

Holm, E., and J. Houston. 1993. Status of the ghost shiner, *Notropis buchanani*, in Canada. Canadian Field-Naturalist 107:440–445.

Jordan, D. S. 1882. Report on the fishes of Ohio; pp. 735–1002 in Report of the Geological Survey of Ohio. vol. 4. Columbus, Nevins & Myers, state printers, Columbus,Ohio.

Jordan, D. S., and C. H. Gilbert. 1883. Synopsis of the Fishes of North America. Bulletin of the United States National Museum, 1018 pp.

Jordan, D. S., and B. W. Evermann. 1896. The Fishes of North and Middle America : A Descriptive Catalogue of the Species of Fish-like Vertebrates Found in the Waters of North America, North of the Isthmus of Panama. United States National Museum, Washington, Smithsonian Institution, 1240 pp.

Mayden, R. L. 1989. Phylogenetic studies of North American minnows, with emphasis on genus *Cyprinella*. Miscellaneous Publication University of Kansas Publications, Museum of Natural History 80:1–189.

Mayden, R. L., A. M. Simons, R. M. Wood, P. M. Harris, and B. R. Kuhajda. 2006. Molecular systematics and classification of North American notropin shiners and minnows (Cypriniformes: Cyprinidae); pp. 72–101 in Studies of North American Desert Fishes in Honor of EP (Phil) Pister, Conservationist. Universidad Autonoma de Nuevo Leon, Mexico.

Meek, S. E. 1896. A list of fishes and mollusks collected in Arkansas and Indian Territory in 1894. Bulletin of the U. S. Fish Commission 15:341–349.

Meek, S. E. 1904. The Fresh-Water Fishes of Mexico North of the Isthmus of Tehuantepec. Field Columbian Museum, pp.

Nelson, J. S., and M. J. Paetz. 1992. The Fishes of Alberta. The University of Alberta Press, Edmonton, Alberta, 437 pp.

Page, L. M., and E. C. Beckham. 1987. *Notropis rupestris*, A New Cyprinid from the Middle Cumberland River System, Tennessee, with Comments on Variation in *Notropis heterolepis*. Copeia 1987:659.

Page, L. M., and B. M. Burr. 2011. A Field Guide to Freshwater Fishes: North America North of Mexico, 2nd ed. Houghton Mifflin Harcourt Publishing Company, New York, New York, 663 pp.

Peer, D. L. 1961. Aspects of the LIife History and Ecology of the SpottailL Shiner *Notropis Hudsonius* (Clinton). Master's Thesis, University of Saskatchewan, 69 pp.

Rafinesque, C. S. 1818. Descriptions of two new genera of North American fishes, Opsanus and Notropis. American Monthly Magazine and Critical Review 2:203–204.

Reno, H. W. 1966. The infraorbital canal, its lateral-line ossicles and neuromasts, in the minnows *Notropis volucellus* and *N. buchanani*. Copeia 1966:403–413.

Schönhuth, S., and I. Doadrio. 2003. Phylogenetic relationships of Mexican minnows of the genus *Notropis* (Actinopterygii, Cyprinidae). Biological Journal of the Linnean Society 80:323–337.

Schönhuth, S., and R. L. Mayden. 2009. Phylogenetic relationships in the genus *Cyprinella* (Actinopterygii: Cyprinidae) based on mitochondrial and nuclear gene sequences. Molecular Phylogenetics and Evolution 55:77–98.

Schönhuth, S., J. Vukić, R. Šanda, L. Yang, and R. L. Mayden. 2018. Phylogenetic relationships and classification of the Holarctic family Leuciscidae (Cypriniformes: Cyprinoidei). Molecular Phylogenetics and Evolution 127:781–799.

Simons, A. M., and R. L. Mayden. 1998. Phylogenetic Relationships of the Western North American Phoxinins (Actinopterygii: Cyprinidae) as Inferred from Mitochondrial 12S and 16S Ribosomal RNA Sequences. Molecular Phylogenetics and Evolution 9:308–329.

Simons, A. M., and R. L. Mayden. 1999. Phylogenetic Relationships of North American Cyprinids and Assessment of Homology of the Open Posterior Myodome. Copeia 1999:13–21.

Simons, A. M., P. B. Berendzen, and R. L. Mayden. 2003. Molecular systematics of North American phoxinin genera (Actinopterygii: Cyprinidae) inferred from mitochondrial 12S and 16S ribosomal RNA sequences. Zoological Journal of the Linnean Society 139:63–80.

Stout, C., S. Schonhuth, R. Mayden, N. L. Garrison, and J. W. Armbruster. 2022. Phylogenomics and classification of *Notropis* and related shiners (Cypriniformes: Leuciscidae) and the utility of exon capture on lower taxonomic groups. PeerJ 10:e14072.

Swift, C. C. 1970. A review of the eastern North American cyprinid fishes of the *Notropis texanus* species group (subgenus *Alburnops*), with a definition of the subgenus *Hydrophlox*, and materials for a revision of the subgenus *Alburnops*. PhD dissertation, Florida State University, 476 pp.

Taylor, W. R., and G. C. Van Dyke. 1985. Revised procedures for staining and clearing small fishes and other vertebrates for bone and cartilage study. Cybium 9:107–119.

Uyeno, T. 1961. Osteology and phylogeny of the American cyprinid fishes allied to the genus *Gila*. PhD dissertation, University of Michigan, 174 pp.

Chapter 4: Conclusions

For the first part of this thesis, I described the osteology of *Notropis hudsonius* Clinton, 1824, emphasizing intraspecific osteological variation. While several authors have described the osteology of *Notropis* Rafinesque, 1818 and its relatives (Harrington, 1955; Buhan, 1970; Coburn, 1982; Mayden, 1989), no description of the osteology of *N. hudsonius* has previously been published nor had any authors given special focus to the intraspecific osteology of any *Notropis* species. The osteological description provided here outlines the osteology of *N. hudsonius*, documents osteological characteristics that vary among individuals, how they vary, and how these variants may differ between different populations and regions. Recent molecular studies indicate that *N. hudsonius* forms a basal relationship with most other notropin species (Mayden et al., 2006; Schönhuth et al., 2018; Stout et al., 2022). Coburn (1982) also regarded *N. hudsonius* as one of the most plesiomorphic members of *Notropis.* Thus, the first part of this thesis does not simply describe the osteology of another *Notropis* species; it also provides an osteological description of a basal, plesiomorphic species, which can, in turn, be used as a point of osteological comparison in future studies on notropin osteology and gives much needed information on what osteological characteristics vary and how they vary, which may be useful in future osteological descriptions and analyses of other notropin species. Finally, the first part of this thesis reveals key osteological differences between specimens sampled from eastern and western Canada.

The second part of this thesis compared the osteology of 11 *Notropis* species, representing four subgenera and two species of unclear placement *sensu* Mayden et al. (2006). Osteology was key for early researchers to evaluate the evolutionary relationships of North American cyprinoids, including *Notropis* (Coburn, 1982; Mayden, 1989; Cavender and Coburn, 1992; Coburn and Cavender, 1992). Molecular data has since emerged as a new way to assess the evolutionary relationships of notropin fishes (Simons and Mayden, 1999; Bielawski and Gold, 2001; Simons et al., 2003; Mayden et al., 2006; Schönhuth and Mayden, 2010; Schönhuth et al., 2018; Stout et al., 2022), leading to the reclassification of many *Notropis* species into different subgenera. Before this thesis, no work had been done to reassess *Notropis* osteology in the context of these molecular-based reclassifications. The osteological analysis provided here not only overviews what osteological characteristics vary among species, it also shows what osteological traits are shared within and between subgenera, highlighting the role of convergent evolution in notropin evolution. The results of the second chapter also raise further questions about how niche and habitat shape and are reflected in the osteology of *Notropis* and its relatives.

4.1 Summary of Results

Notropis hudsonius clearly shows a high degree of intraspecific osteological variation. Except for the pelvic girdle, all the regions I examined showed some variation. Many of the variants examined are found across multiple regions and populations, having been observed in specimens sampled from Alberta, the Northwest Territories, Manitoba and western Ontario. However, there are key regional differences with respect to the pectoral girdle, urohyal, and caudal skeleton. The cleithrum, coracoid, mesocoracoid and scapula of the pectoral girdle were fused in almost all specimens sampled from Manitoba and western Ontario. Only a small minority of *N. hudsonius* specimens from Alberta and the Northwest Territories showed complete or partial fusion of the pectoral girdle. In the caudal skeleton, it was much more common for the parhypural and hypural to either abut or fuse in specimens from Manitoba and Ontario. The urohyal is distinct between eastern and western regions. In around three quarters of specimens from Alberta and the Northwest Territories, the posterior end of the dorsal wing of the urohyal has a distinct semicircular edge when viewed laterally. In the other quarter, the dorsal wing has a triangular shape. This rounded, semicircular variant is not observed in specimens from Manitoba and Ontario at all. Future research examining the osteology of *N. hudsonius* should pay special attention to these three osteological features.

Of the eleven species examined, *Notropis atherinoides* Rafinesque, 1818, *N. blennius* Girard, 1856*, Notropis buchanani* Meek, 1896, *N. heterodon* Cope, 1865 , *N. hudsonius*, *N. percobromus* Cope, 1871, *N. stramineus* Cope, 1865, *N. texanus* Girard, 1856, and *N. volucellus* Cope, 1865 represent four subgenera, while *N. dorsalis* Agassiz, 1854 and *N. heterolepis* Eigenmann and Eigenmann, 1893 are of unclear placement (Mayden et al., 2006). Overall, I observed that osteological traits shared among species of the same subgenus were often found in species belonging to other, more distantly related subgenera, with only a few exceptions. Several shared osteological characters noted both in this thesis and by past researchers are reinterpreted as convergent characteristics instead of synapomorphies in the context of molecular phylogenetic trees. For example, Mayden (1989) placed *N. heterodon* and *N. texanus* into a "*Notropis texanus* species group" based partly on the fact that both species have serrated pharyngeal teeth. However, recent molecular studies indicate that these species are in different subgenera (Mayden et al., 2006; Schönhuth et al., 2018; Stout et al., 2022). Thus, serrated pharyngeal teeth can be reinterpreted as a convergent trait.

Similarly, *Notropis buchanani*, *Notropis heterodon* and *Notropis heterolepis* are not closely related (Mayden et al., 2006; Schönhuth et al., 2018; Stout et al., 2022). However, I, as well as Reno (1966) and Swift (1970), observed that these species all show a reduction of the sensory canals of the skull most likely as a convergent adaptation to aquatic habitats with low turbidity (Swift, 1970). Convergent evolution clearly plays a large role in notropin osteology and must be considered when osteological characteristics are examined and compared among species.

4.2. Limitations

A limitation of this thesis was the quality of the cleared and stained specimens that I used. Several of the *Notropis hudsonius* and *Notropis heterolepis* specimens that I prepared were partly disarticulated or disintegrated during the clearing and staining process, resulting in a loss of bony elements in a few instances. As a result, I could not do as comprehensive an analysis of the osteology of these two species as would be ideal. For Chapter 2, especially, this meant that my analysis of the osteological variation of *N. hudsonius* was also less comprehensive than it would ideally be. Another limitation was the cartilage stain. Past researchers have regarded the degree of ossification in the ethmoid region as an important aspect of leuciscid osteology (Buhan, 1970; Coburn, 1982; Mayden, 1989). The cartilage for the specimens prepared before this study were, for the most part, visible and well dyed. However, the cartilage stain for the specimens I prepared did not produce the expected results and left the cartilage unstained. As a result, I could not analyze and compare the ossification of the ethmoid region in the specimens. Another limitation of this thesis relates to the number of *Notropis* specimens used. For most of the species I analyzed, I had fewer than ten specimens to measure and make counts and usually only three cleared and stained specimens to examine. In the case of *Notropis texanus* and *Notropis volucellus*, I only had two cleared and stained specimens to analyze. The *N. texanus* specimens used in this thesis were also very small and immature. Ideally, I would examine mature specimens. I was also limited by the number of specimens that I was allowed to dissect. As a result, I could not analyze and compare the branchial apparatuses and the otic, occipital and basicranial regions of the upper skull as comprehensively as would be ideal. While my thesis focused only on osteology, many other characteristics, such as body and fin pigmentation, head tuberculation, breeding behaviour, scale morphology and egg size, have also been regarded as systematically important (Coburn, 1982; Mayden, 1989; Cavender and Coburn, 1992). It would be beneficial for future studies to incorporate these features into the analysis.

4.3. Future Research

Based on my results from Chapter 2, I have identified two areas that future research should focus on. My study on the osteology of *Notropis hudsonius* used specimens sampled from Alberta, Manitoba and the Northwest Territories. These provinces and territories only represent a portion of the native range of *N. hudsonius*, which extends into eastern Canada and the southeastern USA (Page and Burr, 2011). Past researchers have similarly used *N. hudsonius* specimens from a limited region of this range (Eastman and Underhill, 1973; Coburn, 1982; Mayden, 1989). Thus, further research should draw on specimens collected from throughout the entire native range to properly assess the osteological variation and overall diversity of *N. hudsonius.* Going further, I would suggest incorporating molecular data to assess the relatedness of different *N. hudsonius* populations and regions. In both cases, doing so will provide a better, more comprehensive understanding of the diversity of *N. hudsonius* and better determine if it can be reclassified into subspecies or even different species.

Building on the findings of the third chapter, I recommend that future research look at the osteology of more notropin species, both from different subgenera and those of unclear placement. Doing so would properly identify key osteological traits shared between members of different subgenera and help identify synapomorphies and convergent characteristics. In addition, future research should re-examine notropin osteology in the context of niche, diet, and habitat (i.e., pelagic versus benthic). Following Chapter 2 of this thesis, future research should also focus on describing the osteology and intraspecific osteological variation of other *Notropis* species, including but not limited to the ones assessed here. Doing so will be critical to better understand the inter and intraspecific variability of notropin fishes and determine if other species show the same degree of intraspecific variability as *Notropis hudsonius.*

4.4. Literature Cited

Agassiz, L. 1854. Notice of a collection of fishes from the southern bend of the Tennessee River, in the State of Alabama. American Journal of Science and Arts 17:297–308, 353–365.

Bielawski, J. P., and J. R. Gold. 2001. Phylogenetic relationships of cyprinid fishes in subgenus *Notropis* inferred from nucleotide sequences of the mitochondrially encoded cytochrome b gene. Copeia 2001:656–667.

Buhan, P. J. 1970. The comparative osteology and taxonomy of the North American cyprinid genera, *Richardsonius Ctinostomus* and *Semotilus*, with notes on other minnows. PhD dissertation, Virginia Polytechnic Institute, 332 pp.

Cavender, T. M., and M. M. Coburn. 1992. Interrelationships of North American Cyprinid Fishes; pp. 328–373 in Systematics, historical ecology, and North American freshwater fishes. Stanford University Press, Stanford, California.

Clinton, D. 1824. Description of a new species of fish, from the Hudson River. Annals of the Lyceum of Natural History of New York 1:49–50.

Coburn, M. M. 1982. Anatomy and relationships of *Notropis atherinoides*. PhD dissertation, Ohio State University, 384 pp.

Coburn, M. M., and T. M. Cavender. 1992. Phylogenetic relationships of North American Cyprinidae; pp. 328–373 in Systematics, historical ecology, and North American freshwater fishes. Stanford University Press, Stanford, California.

Cope, E. D. 1865. Partial catalogue of the cold-blooded Vertebrata of Michigan. Pt. I. Proceedings of the Academy of Natural Sciences of Philadelphia 16:276–285.

Cope, E. D. 1871. Recent reptiles and fishes. Report on the reptiles and fishes obtained by the naturalists of the expedition; pp. 432–442 in Preliminary report of the United States Geological Survey of Wyoming and portions of contiguous territories. vol. 4. Government Printing Office, Washington D.C.

Eastman, J. T., and J. C. Underhill. 1973. Intraspecific variation in the pharyngeal tooth formulae of some cyprinid fishes. Copeia 1973:45–53.

Eigenmann, C. H., and R. S. Eigenmann. 1893. Preliminary descriptions of new fishes from the northwest. American Naturalist 27:151–154.

Girard, C. F. 1856. Research upon the cyprinoid fishes inhabiting the fresh waters of the United States, west of the Mississippi Valley, from specimens in the museum of the Smithsonian Institution. Proceedings of the Academy of Natural Sciences of Philadelphia 2:165–213.

Harrington, R. W. 1955. The osteocranium of the American cyprinid Fish, *Notropis bifrenatus*, with an annotated synonymy of teleost skull bones. Copeia 1955:267.

Mayden, R. L. 1989. Phylogenetic studies of North American minnows, with emphasis on genus *Cyprinella*. Miscellaneous Publication University of Kansas Publications, Museum of Natural History 80:1–189.

Mayden, R. L., A. M. Simons, R. M. Wood, P. M. Harris, and B. R. Kuhajda. 2006. Molecular systematics and classification of North American notropin shiners and minnows (Cypriniformes: Cyprinidae); pp. 72–101 in Studies of North American Desert Fishes in Honor of EP (Phil) Pister, Conservationist. Universidad Autonoma de Nuevo Leon, Mexico.

Meek, S. E. 1896. A list of fishes and mollusks collected in Arkansas and Indian Territory in 1894. Bulletin of the U. S. Fish Commission 15:341–349.

Page, L. M., and B. M. Burr. 2011. A Field Guide to Freshwater Fishes: North America North of Mexico, 2nd ed. Houghton Mifflin Harcourt Publishing Company, New York, New York, 663 pp.

Rafinesque, C. S. 1818. Descriptions of two new genera of North American fishes, Opsanus and Notropis. American Monthly Magazine and Critical Review 2:203–204.

Reno, H. W. 1966. The infraorbital canal, its lateral-line ossicles and neuromasts, in the minnows *Notropis volucellus* and *N. buchanani*. Copeia 1966:403–413.

Schönhuth, S., and R. L. Mayden. 2010. Phylogenetic relationships in the genus Cyprinella (Actinopterygii: Cyprinidae) based on mitochondrial and nuclear gene sequences. Molecular Phylogenetics and Evolution 55:77–98.

Schönhuth, S., J. Vukić, R. Šanda, L. Yang, and R. L. Mayden. 2018. Phylogenetic relationships and classification of the Holarctic family Leuciscidae (Cypriniformes: Cyprinoidei). Molecular Phylogenetics and Evolution 127:781–799.

Simons, A. M., and R. L. Mayden. 1999. Phylogenetic Relationships of North American Cyprinids and Assessment of Homology of the Open Posterior Myodome. Copeia 1999:13–21.

Simons, A. M., P. B. Berendzen, and R. L. Mayden. 2003. Molecular systematics of North American phoxinin genera (Actinopterygii: Cyprinidae) inferred from mitochondrial 12S and 16S ribosomal RNA sequences. Zoological Journal of the Linnean Society 139:63–80.

Stout, C., S. Schonhuth, R. Mayden, N. L. Garrison, and J. W. Armbruster. 2022. Phylogenomics and classification of *Notropis* and related shiners (Cypriniformes: Leuciscidae) and the utility of exon capture on lower taxonomic groups. PeerJ 10:e14072.

Swift, C. C. 1970. A review of the eastern North American cyprinid fishes of the *Notropis texanus* species group (subgenus *Alburnops*), with a definition of the subgenus *Hydrophlox*, and materials for a revision of the subgenus *Alburnops*. PhD dissertation, Florida State University, 476 pp.

Bibliography

Agassiz, L. 1854. Notice of a collection of fishes from the southern bend of the Tennessee River, in the State of Alabama. American Journal of Science and Arts 17:297–308, 353–365.

Agassiz, L. 1855. Art. XXII.--Synopsis of the ichthyological fauna of the Pacific slope of North America, chiefly from the collections made by the U. S. Expl. Exped. under the command of Capt. C. Wilkes, with recent additions and comparisons with eastern types. American Journal of Science and Arts 19:215–231.

Armbruster, J. W. 2012. Standardized measurements, landmarks, and meristic counts for cypriniform fishes. Zootaxa 3586.

Bielawski, J. P. 2000. Molecular phylogenetics and evolution of subgenus *Notropis*. PhD dissertation, Texas A&M University pp.

Bielawski, J. P., and J. R. Gold. 2001. Phylogenetic relationships of cyprinid fishes in subgenus *Notropis* inferred from nucleotide sequences of the mitochondrially encoded cytochrome b gene. Copeia 2001:656–667.

Bird, N. C., and L. P. Hernandez. 2007. Morphological variation in the Weberian apparatus of Cypriniformes. Journal of Morphology 268:739–757.

Bird, N. C., J. R. Abels, and S. S. Richardson. 2020. Histology and structural integration of the major morphologies of the Cypriniform Weberian apparatus. Journal of Morphology 281:273–293.

Bonaparte, C. L. 1835. Prodromus systematis ichthyologiae. Nuovi Annali Delle Scienze Naturali Bologna 2:181-196,272-277.

Bortone, S. A. 1989. *Notropis melanostomus*, a New Species of Cyprinid Fish from the Blackwater-Yellow River Drainage of Northwest Florida. Copeia 1989:737.

Buhan, P. J. 1970. The comparative osteology and taxonomy of the North American cyprinid genera, *Richardsonius Ctinostomus* and *Semotilus*, with notes on other minnows. PhD dissertation, Virginia Polytechnic Institute, 332 pp.

Buhan, P. J. 1972. The comparative osteology of the caudal skeleton of some North American minnows (Cyprinidae). American Midland Naturalist 88:484–490.

Cashner, M. F., K. R. Piller, and H. L. Bart. 2011. Phylogenetic relationships of the North American cyprinid subgenus *Hydrophlox*. Molecular Phylogenetics and Evolution 59:725–735.

Cavender, T. M., and M. M. Coburn. 1992. Interrelationships of North American Cyprinid Fishes; pp. 328–373 in Systematics, historical ecology, and North American freshwater fishes. Stanford University Press, Stanford, California.

Chappell, L. E. 2023. Hydrology and geology as structuring mechanisms of semi-arid fish communities. Master's Thesis, Texas State University, 33 pp.

Chardon, M., and P. Vandewalle. 1996. Evolutionary trends and possible origin of the Weberian apparatus. Netherlands Journal of Zoology 47:383–403.

Chen, W.-J., and R. L. Mayden. 2009. Molecular systematics of the Cyprinoidea (Teleostei: Cypriniformes), the world's largest clade of freshwater fishes: Further evidence from six nuclear genes. Molecular Phylogenetics and Evolution 52:544–549.

Chernoff, B., and R. R. Miller. 1981. Systematics and variation of the aztec shiner, *Notropis sallei*, a cyprinid fish from central Mexico. Proceedings of the Biological Society of Washington 94:18–36.

Clinton, D. 1824. Description of a new species of fish, from the Hudson River. Annals of the Lyceum of Natural History of New York 1:49–50.

Coburn, M. M. 1982. Anatomy and relationships of *Notropis atherinoides*. PhD dissertation, Ohio State University, 384 pp.

Coburn, M. M., and T. M. Cavender. 1992. Phylogenetic relationships of North American Cyprinidae; pp. 328–373 in Systematics, historical ecology, and North American freshwater fishes. Stanford University Press, Stanford, California.

Conway, K. W. 2011. Osteology of the South Asian Genus *Psilorhynchus* McClelland, 1839 (Teleostei: Ostariophysi: Psilorhynchidae), with investigation of its phylogenetic relationships within the order Cypriniformes: Zoological Journal of the Linnean Society 163:50–154.

Conway, K. W., and D. Kim. 2015. Redescription of the Texas Shiner *Notropis amabilis* from the southwestern United States and northern Mexico with the reinstatement of *N. megalops*(Teleostei: Cyprinidae). Ichthyological Exploration of Freshwaters 26:305–340.

Cope, E. D. 1865. Partial catalogue of the cold-blooded Vertebrata of Michigan. Pt. I. Proceedings of the Academy of Natural Sciences of Philadelphia 16:276–285.

Cope, E. D. 1867. Synopsis of the Cyprinidae of Pennsylvania. Transactions of the American Philosophical Society 13:351–410.

Cope, E. D. 1870. A partial synopsis of the fishes of the fresh waters of North Carolina. Proceedings of the American Philosophical Society 84:448–495.

Cope, E. D. 1871. Recent reptiles and fishes. Report on the reptiles and fishes obtained by the naturalists of the expedition; pp. 432–442 in Preliminary report of the United States Geological Survey of Wyoming and portions of contiguous territories. vol. 4. Government Printing Office, Washington D.C.

Cubbage, C. C., and P. M. Mabee. 1996. Development of the cranium and paired fins in the zebrafish *Danio rerio* (Ostariophysi, Cyprinidae). Journal of Morphology 229:121–160.

Eastman, J. T., and J. C. Underhill. 1973. Intraspecific variation in the pharyngeal tooth formulae of some cyprinid fishes. Copeia 1973:45–53.

Edwards, S. 2024. _lemon: Freshing Up your 'ggplot2' Plots_. R package version 0.4.9. Available at https://CRAN.R-project.org/package=lemon. Accessed May 21, 2024.

Eigenmann, C. H., and R. S. Eigenmann. 1893. Preliminary descriptions of new fishes from the northwest. American Naturalist 27:151–154.

Etnier, D. A., and W. C. Starnes. 1993. The Fishes of Tennessee. The University of Tennessee Press, Knoxville, Tennessee, 689 pp.

Evans, H. E., and E. E. Deubler. 1955. Pharyngeal tooth replacement in *Semotilus atromaculatus,* and *Clinostomus elongatus*, two species of cyprinid fishes. Copeia 1955:31.

Fink, S. V., and W. L. Fink. 1981. Interrelationships of the ostariophysan fishes (Teleostei). Zoological Journal of the Linnean Society 72:297–353.

Fowler, H. W. 1904. Notes on fishes from Arkansas, Indian Territory and Texas. Proceedings of the Academy of Natural Sciences of Philadelphia 56:242–249.

Fowler, H. W. 1935. Notes on South Carolina fresh-water fishes. Contributions from the Charleston Museum 7:1–28.

Fricke, R., W. N. Eschmeyer, and J. D. Fong. 2024. Eschmeyer's Catalog of Fishes: Genera/Species By Family/Subfamily. Available at https://researcharchive.calacademy.org/research/ichthyology/catalog/SpeciesByFamily.asp. Accessed December 1, 2022.

Froese, R., and D. Pauly. 2023. FishBase.World Wide Web electronic publication. Available at www.fishbase.org. Accessed April 21, 2024.

Gidmark, N. J., and A. M. Simons. 2014. Cyprinidae: carps and minnows; pp. 334–450 in Freshwater Fishes of North America. Johns Hopkins University Press, Baltimore, Maryland.

Gilbert, C. H. 1884. Notes on the fishes from Kansas. Bulletin of the Washburn Laboratory of Natural History 1:10–16.

Gilbert, C. R. 1978. Type catalogue of the North American cyprinid fish genus *Notropis*. Bulletin of the Florida Museum of Natural History 23:1–104.

Gilbert, C. R., and R. M. Bailey. 1962. Synonymy, characters, and distribution of the American cyprinid Fish *Notropis shumardi*. Copeia 1962:807.

Gilbert, C. R., and R. M. Bailey. 1972. Systematics and zoogeography of the American cyprinid fish *Notropis (Opsopoeodus) emiliae*. Occasional Papers of the Museum of Zoology, University of Michigan 664:1–35.

Girard, C. F. 1856. Research upon the cyprinoid fishes inhabiting the fresh waters of the United States, west of the Mississippi Valley, from specimens in the museum of the Smithsonian Institution. Proceedings of the Academy of Natural Sciences of Philadelphia 2:165–213.

Girard, C. F. 1858. General report upon zoology of the several Pacific railroad routes; pp. in Reports of explorations and surveys, to ascertain the most practicable and economical route for a railroad from the Mississippi River to the Pacific Ocean. vol. 10. Beverly Tucker, Washington D.C.

Günther, A. 1868. Catalogue of the Physostomi, containing the families Heteropygii, Cyprinidæ, Gonorhynchiidæ, Hypodontidæ, Osteoglossidæ, Clupeidæ, Chirocentridæ, Alepochephalidæ, Notopteridæ, Halosauridæ, in the collection of the British Museum. Catalogue of the Fishes in the British Museum 7:1–512.

Habib, S. S., S. Naz, and R. Mehmood. 2019. Morphometric relationships of some specified species of family cyprinidae in Jinnah barrage Punjab, Pakistan. Journal of Entomology and Zoology Studies 7:155–159.

Harrington, R. W. 1955a. The Osteocranium of the American Cyprinid Fish, *Notropis bifrenatus*, with an Annotated Synonymy of Teleost Skull Bones. Copeia 1955:267–290.

Harrington, R. W. 1955b. The osteocranium of the American cyprinid Fish, *Notropis bifrenatus*, with an annotated synonymy of teleost skull bones. Copeia 1955:267.

Hay, O. P. 1881. On a collection of fishes from eastern Mississippi. Proceedings of the United States National Museum 3:488–515.

Hollingsworth, P. R., A. M. Simons, J. A. Fordyce, and C. D. Hulsey. 2013. Explosive diversification following a benthic to pelagic shift in freshwater fishes. BMC Evolutionary Biology 13:272.

Holm, E., and J. Houston. 1993. Status of the ghost shiner, *Notropis buchanani*, in Canada. Canadian Field-Naturalist 107:440–445.

Hubbs, C. L., and K. F. Lagler. 2004. Fishes of the Great Lakes Region, Revised Edition (G. R. Smith (ed.)). Ann Arbor: University of Michigan Press, 276 pp.

Illick, H. J. 1956. A Comparative Study of the Cephalic Lateral-Line System of North American Cyprinidae. American Midland Naturalist 56:204.

Jordan, D. S. 1876. Class V.--Pisces; pp. 199–362 in Manual of the vertebrates of the northern United States, including the district east of the Mississippi River and north of North Carolina and Tennessee, exclusive of marine species. Jansen, McClurg & Co, Chicago, Illinois.

Jordan, D. S. 1882. Report on the fishes of Ohio; pp. 735–1002 in Report of the Geological Survey of Ohio. vol. 4. Columbus, Nevins & Myers, state printers, Columbus,Ohio.

Jordan, D. S., and A. W. Brayton. 1878. Contributions to North American ichthyology. No. 3. A. On the distribution of the fishes of the Alleghany region of South Carolina, Georgia, and Tennessee, with descriptions of new or little known species. Bulletin of the United States National Museum 3–95.

Jordan, D. S., and C. H. Gilbert. 1883. Synopsis of the Fishes of North America. Bulletin of the United States National Museum, 1018 pp.

Jordan, D. S., and B. W. Evermann. 1896. The Fishes of North and Middle America : A Descriptive Catalogue of the Species of Fish-like Vertebrates Found in the Waters of North America, North of the Isthmus of Panama. United States National Museum, Washington, Smithsonian Institution, 1240 pp.

Kassambara, A. 2023. _ggpubr: 'ggplot2' Based Publication Ready Plots_. R package version 0.6.0. Available at https://CRAN.R-project.org/package=ggpubr. Accessed May 21, 2024

Lundberg, J. G., and J. N. Baskin. 1969. The caudal skeleton of the catfishes, order Siluriformes. American Museum Novitates 2398:1–49.

Martin, S. D., and R. M. Bonett. 2015. Biogeography and divergent patterns of body size disparification in North American minnows. Molecular Phylogenetics and Evolution 93:17–28.

Mayden, R. L. 1989. Phylogenetic studies of North American minnows, with emphasis on genus *Cyprinella*. Miscellaneous Publication University of Kansas Publications, Museum of Natural History 80:1–189.

Mayden, R. L., A. M. Simons, R. M. Wood, P. M. Harris, and B. R. Kuhajda. 2006a. Molecular systematics and classification of North American notropin shiners and minnows (Cypriniformes: Cyprinidae); pp. 72–101 in In Studies of North American Desert Fishes in Honor of EP (Phil) Pister, Conservationist. Universidad Autonoma de Nuevo Leon, Mexico.

Mayden, R. L., A. M. Simons, R. M. Wood, P. M. Harris, and B. R. Kuhajda. 2006b. Molecular systematics and classification of North American notropin shiners and minnows (Cypriniformes: Cyprinidae); pp. 72–101 in Studies of North American Desert Fishes in Honor of EP (Phil) Pister, Conservationist. Universidad Autonoma de Nuevo Leon, Mexico.

Meek, S. E. 1896. A list of fishes and mollusks collected in Arkansas and Indian Territory in 1894. Bulletin of the U. S. Fish Commission 15:341–349.

Meek, S. E. 1904. The Fresh-Water Fishes of Mexico North of the Isthmus of Tehuantepec. Field Columbian Museum, pp.

Munno, K., P. A. Helm, C. Rochman, T. George, and D. A. Jackson. 2022. Microplastic contamination in Great Lakes fish. Conservation Biology 36:e13794.

Myers, G. S. 1925. *Notropis cummingsae*, a new minnow from Wilmington, North Carolina. American Museum Novitates 164.

Nelson, J. S., and M. J. Paetz. 1992. The Fishes of Alberta. The University of Alberta Press, Edmonton, Alberta, 437 pp.

Nelson, J. S., T. C. Grande, and M. V. H. Wilson. 2016. Fishes of the World, 5th ed. John Wiley & Sons, Inc, Hoboken, New Jersey, 707 pp.

Nursall, J. R. 1963. The Hypurapophysis, an Important Element of the Caudal Skeleton. Copeia 1963:458.

Page, L. M., and E. C. Beckham. 1987. *Notropis rupestris*, A New Cyprinid from the Middle Cumberland River System, Tennessee, with Comments on Variation in *Notropis heterolepis*. Copeia 1987:659.

Page, L. M., and B. M. Burr. 2011. A Field Guide to Freshwater Fishes: North America North of Mexico, 2nd ed. Houghton Mifflin Harcourt Publishing Company, New York, New York, 663 pp.

Pasco-Viel, E., C. Charles, P. Chevret, M. Semon, P. Tafforeau, L. Viriot, and V. Laudet. 2010. Evolutionary trends of the pharyngeal dentition in Cypriniformes (Actinopterygii: Ostariophysi). PLoS ONE 5:1–15.

Peer, D. L. 1961. Aspects of the LIife History and Ecology of the SpottailL Shiner *Notropis Hudsonius* (Clinton). Master's Thesis, University of Saskatchewan, 69 pp.

Rafinesque, C. S. 1815. Analyse de La Nature, Ou Tableau de l'univers et Des Corps Organises. Aux dépens de l'auteur, Palerme, 224 pp.

Rafinesque, C. S. 1818. Descriptions of two new genera of North American fishes, Opsanus and Notropis. American Monthly Magazine and Critical Review 2:203–204.

Rafinesque, C. S. 1820. Fishes of the Ohio River. Western Review and Miscellaneous Magazine: A Monthly Publ., Devoted to Literature and Science 2:235–242.

Raley, M. E., and R. M. Wood. 2001. Molecular systematics of members of the *Notropis dorsalis* species group (Actinopterygii: Cyprinidae. Copeia 2001:638–645.

Reno, H. W. 1966. The infraorbital canal, its lateral-line ossicles and neuromasts, in the minnows *Notropis volucellus* and *N. buchanani*. Copeia 1966:403–413.

Schauberger, P., and A. Walker. 2023. _openxlsx: Read, Write and Edit xlsx Files_. R package version 4.2.5.2. Available at https://CRAN.R-project.org/package=openxlsx. Accessed May 21, 2024.

Schönhuth, S., and I. Doadrio. 2003. Phylogenetic relationships of Mexican minnows of the genus *Notropis* (Actinopterygii, Cyprinidae). Biological Journal of the Linnean Society 80:323–337.

Schönhuth, S., and R. L. Mayden. 2009. Phylogenetic relationships in the genus *Cyprinella* (Actinopterygii: Cyprinidae) based on mitochondrial and nuclear gene sequences. Molecular Phylogenetics and Evolution 55:77–98.

Schönhuth, S., and R. L. Mayden. 2010. Phylogenetic relationships in the genus Cyprinella (Actinopterygii: Cyprinidae) based on mitochondrial and nuclear gene sequences. Molecular Phylogenetics and Evolution 55:77–98.

Schönhuth, S., J. Vukić, R. Šanda, L. Yang, and R. L. Mayden. 2018. Phylogenetic relationships and classification of the Holarctic family Leuciscidae (Cypriniformes: Cyprinoidei). Molecular Phylogenetics and Evolution 127:781–799.

Schultz, L. P. 1929. Check-list of the fresh-water fishes of Oregon and Washington; pp. 43–50 in Check-list of the fresh-water fishes of Oregon and Washington. vol. 2. Publications in Fisheries, Seattle, Washington.

Scott, W. B., and E. J. Crossman. 1973. Freshwater Fishes of Canada. Fisheries Research Board of Canada, 966 pp.

Seghers, B. H. 1981. Facultative schooling behavior in the spottail shiner (*Notropis hudsonius*): possible costs and benefits. Environmental Biology of Fishes 6:21–24.

Simons, A. M., and R. L. Mayden. 1998. Phylogenetic Relationships of the Western North American Phoxinins (Actinopterygii: Cyprinidae) as Inferred from Mitochondrial 12S and 16S Ribosomal RNA Sequences. Molecular Phylogenetics and Evolution 9:308–329.

Simons, A. M., and R. L. Mayden. 1999. Phylogenetic Relationships of North American Cyprinids and Assessment of Homology of the Open Posterior Myodome. Copeia 1999:13–21.

Simons, A. M., P. B. Berendzen, and R. L. Mayden. 2003. Molecular systematics of North American phoxinin genera (Actinopterygii: Cyprinidae) inferred from mitochondrial 12S and 16S ribosomal RNA sequences. Zoological Journal of the Linnean Society 139:63–80.

Snelson, F. F. 1968. Systematics of the Cyprinid Fish *Notropis amoenus*, with Comments on the Subgenus Notropis. Copeia 1968:776.

Snelson, F. F. 1971. *Notropis mekistocholas*, a New Herbivorous Cyprinid Fish Endemic to the Cape Fear River Basin, North Carolina. Copeia 1971:449–462.

Stacklies, W., H. Redestig, M. Scholz, D. Walther, and J. Selbig. 2007. pcaMethods—a bioconductor package providing PCA methods for incomplete data. Bioinformatics 23:1164–1167.

Stout, C., S. Schonhuth, R. Mayden, N. L. Garrison, and J. W. Armbruster. 2022. Phylogenomics and classification of *Notropis* and related shiners (Cypriniformes: Leuciscidae) and the utility of exon capture on lower taxonomic groups. PeerJ 10:e14072.

Stout, C. C., M. Tan, A. R. Lemmon, E. M. Lemmon, and J. W. Armbruster. 2016. Resolving Cypriniformes relationships using an anchored enrichment approach. BMC Evolutionary Biology 16:244.

Swift, C. C. 1970. A review of the eastern North American cyprinid fishes of the *Notropis texanus* species group (subgenus *Alburnops*), with a definition of the subgenus *Hydrophlox*, and materials for a revision of the subgenus *Alburnops*. PhD dissertation, Floridaa State University, 476 pp.

Tan, M., and J. W. Armbruster. 2018. Phylogenetic classification of extant genera of fishes of the order Cypriniformes (Teleostei: Ostariophysi). Zootaxa 4476:6–39.

Taylor, W. R., and G. C. Van Dyke. 1985. Revised procedures for staining and clearing small fishes and other vertebrates for bone and cartilage study. Cybium 9:107–119.

Uyeno, T. 1961. Osteology and phylogeny of the American cyprinid fishes allied to the genus *Gila*. PhD dissertation, University of Michigan, 174 pp.

Warren, M. L., B. M. Burr, and J. M. Grady. 1994. *Notropis albizonatus*, a new cyprinid fish endemic to the Tennessee and Cumberland River drainages, with a phylogeny of the *Notropis procne* species group. Copeia 1994:868–886.

Wickham, H. 2007. Reshaping Data with the **reshape** Package. Journal of Statistical Software 21.

Wickham, H. 2011. The Split-Apply-Combine Strategy for Data Analysis. Journal of Statistical Software 40.

Wickham, H. 2016. _ggplot2: Elegant Graphics for Data Analysis_. Springer-Verlag New York. ISBN 978-3-319-24277-4. Available at https://ggplot2.tidyverse.org. Accessed May 21, 2024.

Wickham, H., M. Averick, J. Bryan, W. Chang, L. McGowan, R. François, G. Grolemund, A. Hayes, L. Henry, J. Hester, M. Kuhn, T. Pedersen, E. Miller, S. Bache, K. Müller, J. Ooms, D. Robinson, D. Seidel, V. Spinu, K. Takahashi, D. Vaughan, C. Wilke, K. Woo, and H. Yutani. 2019. Welcome to the Tidyverse. Journal of Open Source Software 4:1686.

Wickham, H., and R. Bryan . 2023. _readxl: Read Excel Files_. R package version 1.4.3, Available at https://cran.r-project.org/web/packages/readxl/index.html. Accessed May 21, 2024.

Wickham, H., R. François, L. Henry, K. Müller, and D.Vaughan. 2023. _dplyr: A Grammar of Data Manipulation_. R package version 1.1.4. Available at https://CRAN.R-project.org/package=dply. Accessed May 21, 2024.

Wickham, H., and L. Henry. 2023. _purrr: Functional Programming Tools_. R package version 1.0.2. Available at https://CRAN.R-project.org/package=purrr. Accessed May 21, 2024.

Appendix A: Summary of Samples Used in Chapters 2 and 3

Table A.1. Summary of samples used in Chapters 2 and 3.

Collection	Catalogue number	Sample site	Date collected	Species
University of Alberta	UAMZ 205	Cold Lake, AB	09/02/1952	*Notropis atherinoides*
University of Manitoba	MZF 776	Wardells creek, MB	Unknown	*Notropis atherinoides*
University of Alberta	UAMZ 3540	Red Deer River, AB	07/19/1974	*Notropis blennius*
University of Alberta	UAMZ 2852	South Saskatchewan River, AB	05/09/1971	*Notropis blennius*
University of Alberta	UAMZ F5562.1	Sturgeon River, AB	Unknown	*Notropis blennius*
University of Manitoba	MZF 1606	Sydenham river, ON	05/06/1987	*Notropis buchanani*
University of Manitoba	MZF 649	Oak Creek, MB	08/28/1984	*Notropis dorsalis*
University of Manitoba	MZF 1027	Kiche Manitoba Lake, MB	07/28/1984	*Notropis heterodon*
University of Alberta	UAMZ 208	Greenwater Lake, SK	07/13/1938	*Notropis heterolepis*
University of Manitoba	MZF 685	Kiche Manitoba Lake, MB	09/18/1982	*Notropis heterolepis*
University of Manitoba	MZF 689	ELA Lake 305, ON	09/1991	*Notropis heterolepis*
University of Manitoba	MZF 2494	Oak creek, MB	09/22/1985	*Notropis heterolepis*
University of Alberta	UAMZ 209	North Saskatchewan River, Edmonton, AB	02/19/1961	*Notropis hudsonius*
University of Alberta	UAMZ 213	Elinor Lake, AB	09/7/1950	*Notropis hudsonius*
University of Alberta	UAMZ 214	Pigeon Lake, AB	1941	*Notropis hudsonius*
University of Alberta	UAMZ 220	Cold lake, AB	1952	*Notropis hudsonius*
University of Alberta	UAMZ 221	Square Lake, AB	08/7/1952	*Notropis hudsonius*
University of Alberta	UAMZ 4950	Muriel Lake, AB	07/27/1966	*Notropis hudsonius*

University of Alberta	UAMZ 1525	Lac Ste. Anne, AB	1968	*Notropis hudsonius*
University of Alberta	UAMZ 1528	Lac Ste. Anne, AB	1968	*Notropis hudsonius*
University of Alberta	UAMZ 3060	Hay River, NWT	06/04/1967	*Notropis hudsonius*
University of Alberta	UAMZ 3215	Bocquene Lake, AB	06/24/1973	*Notropis hudsonius*
University of Alberta	UAMZ F5644.1	Buck Lake, AB	07/16/1971	*Notropis hudsonius*
University of Alberta	UAMZ F9126	Vandersteene Lake, AB	06/22/1969	*Notropis hudsonius*
University of Alberta	UAMZ F9131	Pembina River, AB	Unknown	*Notropis hudsonius*
University of Manitoba	MZF 680	Clearwater Lake, MB	07/14/1967	*Notropis hudsonius*
University of Manitoba	MZF 2506	Dummy Lake, ON	06/26/1991	*Notropis hudsonius*
University of Manitoba	MZF 2507	Fisher River, MB	06/03/1992	*Notropis hudsonius*
University of Manitoba	MZF 719	White Mouth River	10/07/1984	*Notropis percobromus*
University of Alberta	UAMZ 7418	Souris river, MB	09/25/1991	*Notropis stramineus*
University of Manitoba	MZF 719	Roseau River, MB	06/19/1990	*Notropis stramineus*
University of Manitoba	MZF 1445	Winnipeg River, MB	09/21/1991	*Notropis texanus*
University of Alberta	UAMZ 7247	Assiniboine River, MB	09/22/1990	*Notropis volucellus*
University of Alberta	UAMZ 2478	Unknown	Unknown	*Notropis volucellus*
University of Manitoba	MZF 2036	Little Vermilion River, IL	06/10/1992	*Notropis volucellus*

Appendix B: Guide of Complete Measurements and Counts

Table B.1. detailed description of measurements and meristic counts. Measurements and meristic counts generally follow Hubbs and Lagler (2004). Measurements taken according to Habib et al. (2019) are indicated with an asterix (*). Measurements and counts taken according to Armbruster (2012) are indicated with an obelisk (†).

Measurement	Description
Standard Length	Distance from anterior most part of head to caudal peduncle
Preanal Length*	Distance from tip of the snout to base of first anal ray
Predorsal Length	Distance from tip of the snout to base of first dorsal ray
Prepectoral Length*	Distance from snout to base of pectoral fin
Prepelvic Length*	Distance from snout to base of pelvic fin
Head Length	Distance from anteriormost part of snout to most distant point of opercular membrane
Snout Length	Distance from the anterior most point of the snout to the anterior margin of the eye orbit
Postorbital Length	The greatest distance between the posterior margin of the eye orbit and the membranous opercular margin
Interorbital Width	The least distance between the eye orbits
Eye Diameter	Distance between anterior and posterior margins of the eye orbit
Dorsal Fin Base	The greatest overall basal length of the dorsal fin, extending from the first ray to the point where the membrane of the last ray contacts the body

Anal Fin Base	The greatest overall basal length of the anal fin, extending from the first ray to the point where the membrane of the last ray contacts the body
Peduncle Length†	Distance between insertion of last anal fin ray and the hidden base of the middle caudal ray
Peduncle Depth	The narrowest depth of the caudal peduncle
Body Depth	The widest vertical dimension of the body, exclusive of the bony or scaly structures pertaining to the fin bases
Dorsal Fin Length	The distance from the structural base of the longest dorsal fin ray to its tip
Anal Fin Length	The distance from the structural base of the longest anal fin ray to its tip
Pectoral Fin Length	The distance from the structural base of the longest pectoral fin ray to its tip
Pelvic Fin length	The distance from the structural base of the longest pelvic fin ray to its tip
Dorsal Fin Rays	Number of rays on dorsal fin
Anal Fin Rays	Number of rays on anal fin
Pectoral Fin Rays	Number of rays on pectoral fin
Pelvic Fin Rays	Number of rays on pelvic fin
Lateral Line Scales†	Scales bearing the lateral-line canal from the head to the end of the vertebral column (hypural plate)
Predorsal Scales†	Scales in row between the supraoccipital and the origin of the dorsal fin

Postdorsal Scales†	Scales in row between posterior base of the dorsal fin and end of caudal fin
Scales Above Lateral Line†	Scales counted in a diagonal from the origin of dorsal fin posteroventrally to the lateral line, not including lateral line scale
Scales Below Lateral Line†	Scales counted from the anterior insertion of the anal fin anterodorsally to the lateral line, not including lateral line scale
Circumferential Scales†	Scales encircling the body immediately anterior to the dorsal fin
Peduncle Scales†	Scales from the ventromedial to posteromedial lines at narrowest portion of caudal peduncle continued around to other side in an anterodorsal to posteroventral direction
Gill Rakers	Total number of rakers on the first gill arch
Total Vertebrae	Total number of vertebrae
Predorsal Vertebrae	Number of vertebrae before the dorsal fin

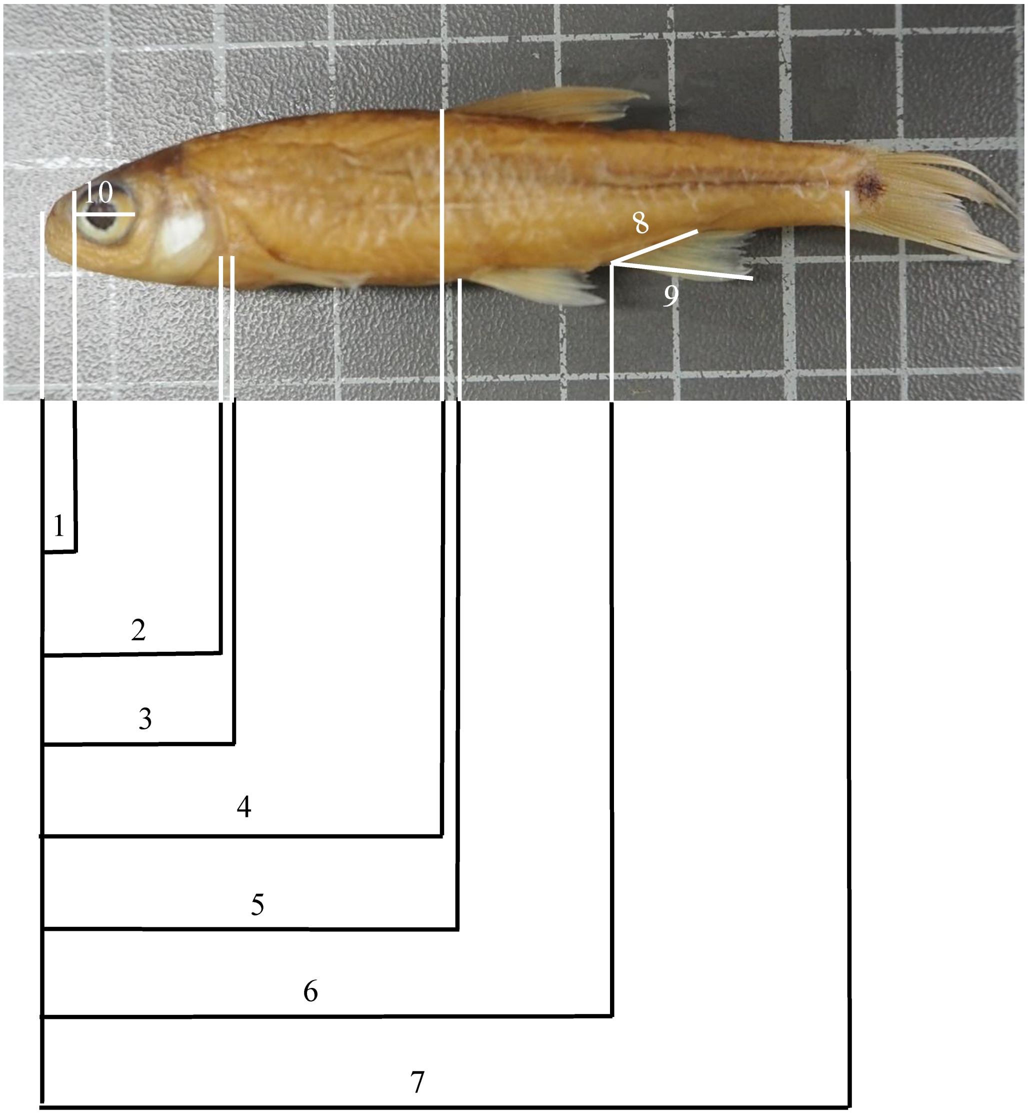

Figure B.1. Schematic of select measurements taken on specimens for this thesis. Photograph of a preserved specimen of *Notropis hudsonius*, MZF 2507, specimen 2. One square = 10 mm in width. (1) snout length, (2) head length, (3) prepectoral length, (4) predorsal length, (5) prepelvic length, (6) preanal length, (7) standard length, (8) anal fin base, (9) anal fin length, (10) eye diameter.

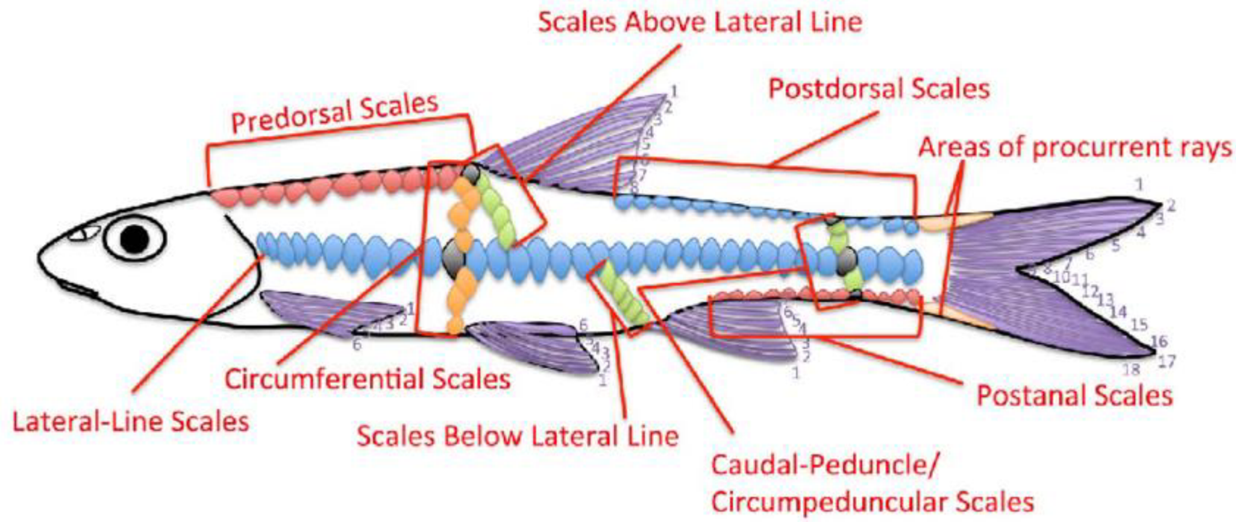

Figure B.2. Schematic illustrating standard meristic counts taken on specimens for this thesis (Armbruster, 2012, figure 4).

Appendix C: Statistical Packages Used for PCA

Table C.1. Statistical packages used for the Principal component analysis (PCA) of this thesis. The analysis was completed using R Studio version 4.2.2.

Package name	Package version	Package author(s)	Year
plyr	v.1.8.9	Hadley Wickam	2011
dplyr	v.1.1.4	Hadley Wickam, Romain François, Lionel Henry, Kirill Müller and Davis Vaughan	
tidyverse	v.2.0.0	Hadley Wickam, Mara Averick, Jennifer Bryan, winston chang, lucy McGowan, Romain François, Garrett Grolemund, Alex Hayes, Lionel Henry, Jim Hester, Max Khun, Thomas Pedersen, Evan Miller, Stephan Bache, Kirill Müller, Jeroen Ooms, David Robinson, Dana Seidel, Vitalle Spinu, Kohske Takahashi, Davis Vaughan, Claus Wilke, Kara Woo and Hiroshi Yutani	2019
readxl	v.1.4.3	Hadley Wickam and Jennifer Bryan	2023
reshape2	v.1.4.4	Hadley Wickam	2007
pcaMethods	v.1.88.0	Wolfram Stacklies,Henning Redestig, Matthias Scholz, Dirk Walther and Joachim Selbig	2007
openxlsx	v.4.2.5.2	Phillip Schauberger and Alexander Walker	2023
purrr	v.1.0.2	Hadley Wickam and Lionel Henry	2023
ggplot2	v.3.5.0	Hadley Wickam	2016
lemon	v.0.4.9	Stefan Edwards	2024